De Novo Designed Organic Donor-Acceptor Systems Featuring Inter- and Intramolecular Charge Transfer Interactions

Thesis Submitted to AcSIR for the Award of
the degree of
DOCTOR OF PHILOSOPHY
in Chemical Sciences

By
Kilingaru I. Shivakumar
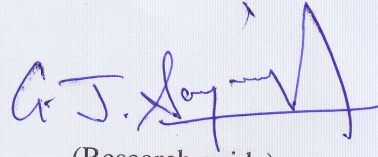10CC11J26079

Under the guidance of
Dr. Gangadhar J. Sanjayan

CSIR-National Chemical Laboratory, Pune

CERTIFICATE

This is to certify that the work incorporated in this Ph.D thesis entitled *"De Novo* **Designed Organic Donor-Acceptor Systems Featuring Inter- and Intramolecular Charge Transfer Interactions"** submitted by **Mr. K. I. Shivakumar** to Academy of Scientific and Innovative Research (AcSIR) in fulfillment of the requirements for the award of the degree of **Doctor of Philosophy**, embodies original research work carried out under my supervision. I further certify that this work has not been submitted to any other university or institution in part or full for the award of any degree or diploma. Research material obtained from other sources has been duly acknowledged in the thesis. Any text, illustration, table etc., used in the thesis from other sources, have been duly cited and acknowledged.

(Student) 28/02/2017

(Research guide)

CANDIDATE'S STATEMENT

I hereby declare that the thesis entitled **"*De Novo* Designed Organic Donor-Acceptor Systems Featuring Inter- and Intramolecular Charge Transfer Interactions"** submitted for the degree of Doctor of Philosophy in Chemical Sciences to the Academy of Scientific and Innovative Research (AcSIR) has not been submitted by me to any other university or institution. This work has been carried out at the Division of Organic Chemistry, CSIR-National Chemical Laboratory, Pune under the supervision of Dr. G. J. Sanjayan.

28/02/2017

Shivakumar K. I.

Dedicated to my beloved family

Acknowledgements

Table of Contents

CHAPTER 1

INTRODUCTION

PART A

PART B

CHAPTER 2

PART A: An Easy and Multigram Synthesis of Pillar[5]quinone

PART B: Solvent-Assisted Solid-State Self-Assembly of Pillar[5]quinone

CHAPTER 3

PART A: Room-Temperature Ferroelectric Organic CT Crystals of Pillar[5]quinone and Tetrathiafulvalene

PART B: Charge Transfer Crystals of Pillar[5]quinone and 4,4'-Bis(N-carbazoyl)-1,1'-biphenyl

CHAPTER 4

Self-Assembly of Solvatofluorochromic Phloroglucinol-Dithiolylidene-based C_3 Symmetric Molecules into One-dimensional Nanostructures

ABBREVIATIONS

A

α   alpha
Å   Angström
a.u.   arbitrary unit
A   acceptor (charge)

B

β   beta

C

calcd   calculated
$CDCl_3$ chloroform-*d*
°C   degree Celcius
CT   charge transfer
CBP   4,4'-(N-carbazolyl)-1,1'-biphenyl
CCDC   Cambridge Crystallographic
          Data Center
cw   continuous wave

D

d   doublet (NMR)
δ   delta chemical shift (NMR)
D   donor (charge)
DMF   dimethylformamide
DCM   dichloromethane
χ_D magnetic susceptibility

E

ESI   electron spray ionization
eV   electronvolt
E   electric field

G

γ   gamma
G   Gauss
g   gram

H

h   hour
H   magnetic field strength
Hz   hertz

I

I   electric current
ICT   intramolecular charge transfer

J

J   joule

K

K   kelvin

M

M   magnetization
mp   melting point
MS   mass spectrometry

P

ppm   parts per million
PFM   piezo-response
          force microscopy

S

s   singlet (NMR)
SEM   scanning electron
          microscopy

T

t   triplet (NMR)
TEM   transmission
          electron
          microscopy
TFA   trifluoroacetic
          acid
TCE   1,1,2,2-tetrachloro
          ethane

U

UV   ultraviolet

V

V   volt
Vis   visible

X

XRD   X-ray diffraction

ABSTRACT

Donor-acceptor charge transfer systems boast myriad of applications in organic electronics and photonics. The electronegativity difference between two or more molecules (intermolecular) or two or more parts of a single molecule (intramolecular) effectuates the phenomenon of charge transfer, wherein transfer of a fraction of electron occurs from less electronegative species (donor) to the more electronegative species (acceptor). In this connection, the dissertation entitled "*De Novo* **Designed Organic Donor-Acceptor Systems Featuring Inter- and Intramolecular Charge Transfer Interactions**" attempts at studying the intriguing physical properties manifested by novel electroactive organic compounds/complexes as a consequence of molecular self-assembly. Besides, an endeavor to understand the role played by charge transfer interactions in eliciting properties such as ferroelectricity and conductivity is undertaken. This thesis is divided into four chapters. The first is an introductory chapter. The second chapter describes facile and multigram-scale synthesis of a cyclic pentaquinone, pillar[5]quinone (**P5Q**), and its solvent-assisted solid-state self-assembly. The third chapter dwells upon the mixed-stacked charge transfer (CT) complexes of P5Q with tetrathiafulvalene (**TTF**) and 4,4'-bis(*N*-carbazolyl)-1,1'-biphenyl (**CBP**). The **TTF**-**P5Q** complex exhibits unprecedented room temperature ferroelectricity in TTF-quinone CT systems. Lastly, the fourth chapter chronicles the self-assembly of solvatofluorochromic phloroglucinol-dithiolylidene-based C_3 symmetric molecules into one-dimensional (1D) nanostructures.

CHAPTER 1

The first part of this introductory chapter describes the charge transfer interactions in organic system by providing a glimpse of the historical background, their types and applications. Further, it catalogues the ongoing works in this field and provides a perspective on future prospects. The second part prefaces macrocycles and their supramolecular interactions besides detailing pillararene chemistry.

CHAPTER 2

Part A: Pillar[5]quinone (Fig. 1a),[1] a potential molecule for anion recognition and supramolecular host-guest chemistry, has not so far been used for practical purposes,

presumably owing to the difficulty in accessing it in large amounts without much synthetic hassles. In this direction, we reveal an easy-to-operate and chromatography-free synthetic strategy that can furnish this valuable macrocyclic quinone in multi-gram scale. The success of this methodology relies on the utility of hypervalent iodine, generated *in situ* from oxone[®]-iodobenzene system, as an efficient oxidant. **P5Q** has been obtained in multi-gram quantities by oxidizing *per*-methylated pillar[5]arene[2] with oxone[®]-iodobenzene oxidant system and simply purifying by crystallizing from 1,1,2,2-tetrachloroethane (TCE), thus opening up the opportunity to explore the properties of this interesting macrocyclic quinone.
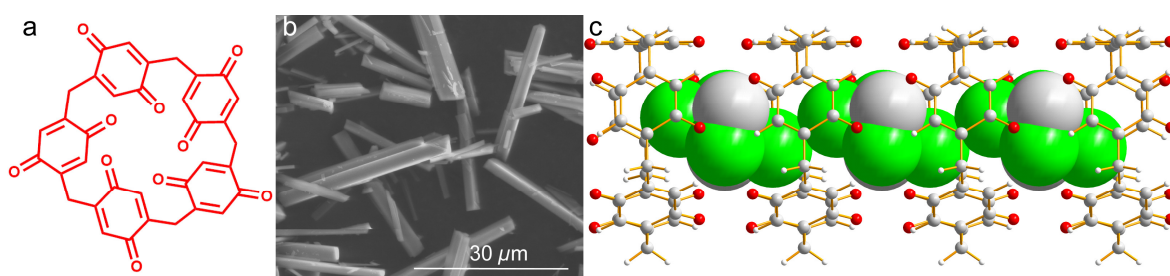
Fig. 1 (a) Molecular structure of pillar[5]quinone. (b) Representative SEM image of the self-assembled P5Q.2TCE. (c) Crystal structure of P5Q. 2TCE viewed along the *a*-axis.

Part B: This part of the work focuses on the solvent-mediated supramolecular assembly of **P5Q**.[3] The supramolecular assembly of P5Q is promoted by the solvent TCE, furnishing a microcrystalline solvate material P5Q.2TCE with a fluffy texture. Optical and electron microscopy images revealed rod-shaped morphology, extending up to several micrometers in length (Fig. 1b). The microcrystalline nature of the solvated P5Q precluded us from obtaining crystal structure from single crystal X-ray diffraction; hence we resorted to determine structure directly from powder X-ray diffraction, supplemented by high-resolution solid-state ^{13}C NMR (Fig. 1c). The two dissimilar TCE molecules occupy two types of void in the structure and possess distinct dynamic properties. P5Q was subjected to crystallization using large number common organic solvents, but only TCE facilitated the formation of a crystalline phase. Indeed, features of the crystal structure suggest that the solvent TCE plays a significant role in fostering the columnar assembly of P5Q molecules.

Chapter 3

Part A: Room-temperature ferroelectric materials have important practical applications in the fabrication of compact memory devices and ultra-sensitive multifunctional detectors. In organic CT ferroelectric materials, ordered arrangement of electron donor and acceptor molecules enables spontaneous and electrically reversible polarization, leading to tunable ferroelectricity. In this direction, we report an emerald green-colored CT complex consisting **P5Q** and **TTF** that exhibits room-temperature ferroelectricity (T_c = 329 K).[4] Single-crystal structure of **TTF-P5Q**, obtained from synchrotron X-ray diffraction, showcases alternately stacked dimers of **TTF** and **P5Q**. The CT complex exhibits ferroelectric features such as optical polarization rotation, temperature dependent phase transition and piezoelectric response in single crystals. Ferroelectric behavior observed in **P5Q**-based CT complex widens the scope for further work on this structurally intriguing and readily accessible cyclic pentaquinone (Fig. 2a).
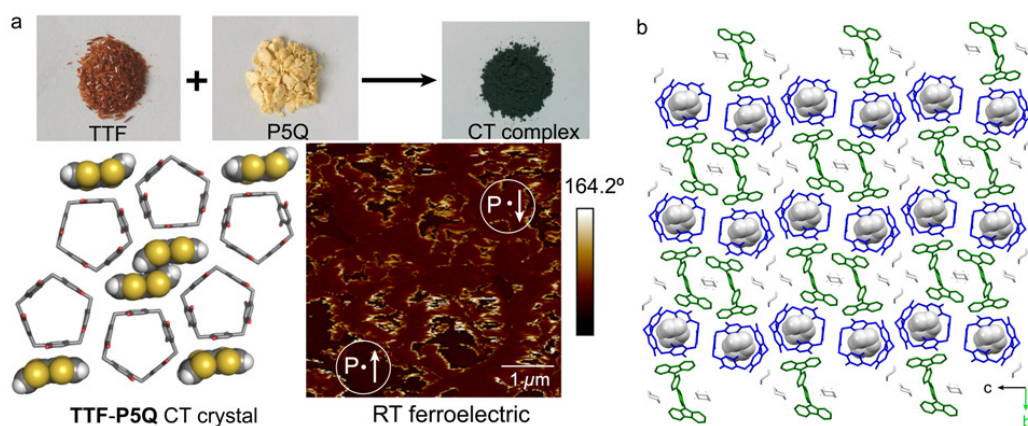
Fig. 2 (a) Graphical abstract of RT ferroelectric **TTF**-**P5Q** crystal. (b) Single-crystal structure of CBP-P5Q viewed along the *a* axis.

Part B: Ferroelectricity and ambipolar charge transport property observed recently in organic systems have reinvigorated the study of mixed-stacked CT assembly of donor and acceptor. 4,4'-bis(*N*-carbazolyl)-1,1'-biphenyl (**CBP**), possessing low triplet energy and high charge carrier mobility, has become an indispensable ingredient, in recent times, in the fabrication of white/phosphorescent organic light emitting diodes. Herein, we report a brown-CT complex of charge acceptor **P5Q** and charge donor **CBP**.[5] The π-stacking interactions coerce the donor and acceptor to form mixed-stack CT complex with **CBP** and **P5Q** π-stacking in an alternate

fashion along the *b*-axis (Fig. 2b). The mixed-stack assembly observed in **P5Q**-based CT complex beckons for further work on this cyclooligomeric quinone.[5]

Chapter 4

1D nanostructures assembled through π-stacking interactions are potent conduits of charge with built-in channels for conduction. Such nanostructures when composed of molecules bestowed with large π-surface besides push-pull groups would enhance electron delocalization and conductivity. In this direction, we report the self-assembly in two of the five *C₃* symmetric 2,4,6-tris(4,5-bis(alkylthio)-1,3-dithiol-2-ylidene)cyclohexane-1,3,5-triones, we synthesized (Fig. 3a), into elongated nanostructures. These compounds exhibited solvatofluorochromism due to intramolecular charge transfer with colors ranging from green to orange in cyclohexane and DMF, respectively (Fig. 3b). The amphoteric redox behaviour was evident from their cyclic voltammograms. Crystal structure of **2e** unveiled intramolecular S···O and intermolecular π-stacking interactions. Conductivity measured on the undoped nanofibres of **2b** (Fig. 3c) using current sensing atomic force microscopy (Cs-AFM) revealed high conductivity *ca.* 0.15 mScm^{-1}.[6]
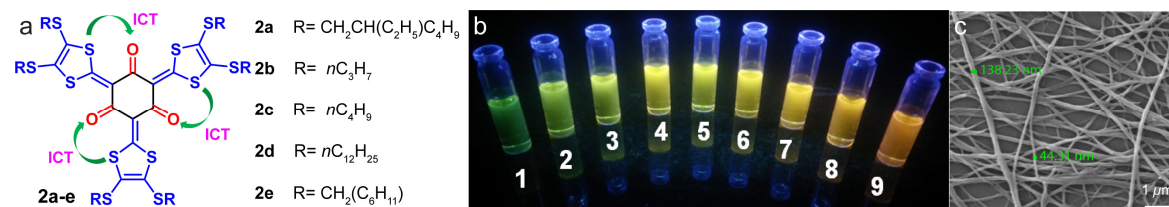
Fig. 3 (a) Molecular structures of synthesized compounds **2a-e**. (b) Positive fluorescence solvatochromism in compound **2c**: 1. cyclohexane, 2. toluene, 3. dioxane, 4. THF, 5. ethyl acetate, 6. chloroform, 7. dichloromethane, 8. acetone, and 9. DMF. (c) Representative SEM image of self-assembled nanofibres of **2b**.

References

[1]   (a) Shivakumar, K. I.; Sanjayan, G. J. *Synthesis* **2013**, *45*, 896; (b) Cao, D.; Kou, Y.; Liang, J.; Chen, Z.; Wang, L.; Meier, H. *Angew. Chem. Int. Ed.* **2009**, *48*, 9721; (c) Sanjayan, G. J.; Shivakumar, K. I. U.S. Patent 9000224 B1, **2015**.

[2]   Ogoshi, T.; Yamagishi, T.-a.; Nakamoto, Y. *Chem. Rev.* **2016**, *116*, 7937.

[3]   Shivakumar, K. I.; Yan, Y.; Hughes, C. E.; Apperley, D. C.; Harris, K. D.; Sanjayan, G. J. *Cryst. Growth Des.* **2015**, *15*, 1583.

[4]   Shivakumar, K. I.; Swathi, K.; Goudappagouda, Das, T.; Kumar, A.; Makde, R.D.; Vanka, K.; Narayan, K. S.; Babu, S.S.; Sanjayan. G. J. *Chem. Eur. J.* **2017**, Just Accepted, doi: 10.1002/chem.201702577

[5]   Shivakumar, K.I.; Gonnade, R.; Sanjayan, G.J. *Manuscript under preparation*.

[6]   Shivakumar, K. I.; Goudappagouda, Gonnade, R. Babu, S.S.; Sanjayan, G.J. *Manuscript communicated*.

GENERAL REMARKS

❖ Unless otherwise stated, all the chemicals and reagents were obtained commercially.

❖ Dry solvents and reagents were prepared by the standard procedures.

❖ Dry reactions were performed under argon atmosphere.

❖ NMR spectra were recorded in $CDCl_3$ and d-trifluoroacetic acid on AV 400/500 MHz spectrometers. Chemical shifts are reported in δ ppm downfield to TMS and peak multiplicities are mentioned as singlet (s), doublet (d), triplet (t), quartet (q) and multiplet (m).

❖ IR spectra were recorded as neat or as a solution in chloroform using Bruker alpha platinum ATR spectrophotometer.

❖ Melting points were determined on a Buchi Melting Point B-540 and are uncorrected.

❖ HRMS TOF MS (ESI) was obtained from the Waters Q-TOF Micro ESI (Time of Flight LC/MS) and MALDI-TOF/TOF measurements were carried employing ABSCIEX TOF/TOF^{TM} 5800 mass spectrometer. HRMS was also obtained using Thermo Scientific Q-Exactive, Accela 1250 pump mass spectrometer.

❖ The stereo microscope image was obtained from the Leica MZ 75 stereomicroscope.

❖ All the reactions were monitored by thin layer chromatography (TLC) on precoated silica gel plates (Kieselgel 60F$_{254}$, Merck) with UV, I_2 or anisaldehyde solution, as the developing reagents in the concerned cases.

❖ Column chromatographic purifications were performed with flash silica gel (230-400 mesh).

❖ Distilled solvents were used as eluents in the column chromatography.

❖ Ball milling was carried out using Retsch MM 400 instrument at the frequency of 25 Hz.

❖ Solid-state UV-Vis-NIR absorption spectra were recorded on PerkinElmer Lambda-950 UV-Vis spectrophotometer.

❖ Solid-state 13C CPMAS NMR spectra were obtained at ambient temperature from Jeol ECX-400 NMR spectrophotometer operating at ^{13}C Larmour frequency of 100.53 MHz with magic angle spinning at 8 KHz.

❖ The wide-angle X-ray diffraction measurements were performed using a Rigaku Micromax-007HF diffractometer operating at 40 kV and 30 mA. The samples were exposed to the X-ray beam for 3 minutes and the scattering pattern was imaged by Rigaku R-AXIS IV++ area detector. The conversion from 2D pattern to 1D was done using Rigaku 2DP software.

❖ Olympus SZX2 was used to image crystals.

❖ Electron spin resonance spectra were recorded using Bruker EMX Plus series (Germany) spectrometer. Modulation frequency of 100 KHz and modulation amplitude of 4 G and power attenuation of 22 dB were applied to collect the EPR signals. Magnetic measurements were carried out on a SQUID magnetometer (Quantum design SQUID-VSM MPMS).

❖ Single crystal X-ray data were collected on a Bruker SMART APEX CCD area diffractometer in CSIR-NCL, Pune and INDUS-2, PX-21 beamline at RRCAT, Indore

LIST OF PUBLICATIONS/PATENTS

1. An Easy and Multigram-Scale Synthesis of Pillar[5]quinone by the Hypervalent Iodine Oxidation of 1, 4-Dimethoxypillar[5]arene

Shivakumar, K. I.; Sanjayan, G. J. *Synthesis* **2013**, *45*, 896.

2. Process for the Preparation of Pillar[5]quinone

Sanjayan G. J.; **Shivakumar, K. I.** *US Patent 9000224 B1*, April 7, 2015.

3. Exploiting Powder X-ray Diffraction to Establish the Solvent-Assisted Solid-State Supramolecular Assembly of Pillar[5]quinone

Shivakumar, K. I.; Yan, Y.; Hughes, C. E.; Apperley, D. C.; Harris, K. D.; Sanjayan, G. J. *Cryst. Growth Des.* **2015**, *15*, 1583.

4. Mixed-Stack Charge Transfer Crystals of Pillar[5]quinone and Tetrathiafulvalene Exhibiting Ferroelectric Features
Shivakumar, K. I.; K. Swathi; Goudappagouda, Das, T.; Kumar, A.; Makde, R.D.; Praveenkumar, B.; Vanka, K.; Narayan, K. S.; Babu, S.S.; Sanjayan. G. J. *Chem. Eur. J.* **2017**, Just Accepted, doi: 10.1002/chem.201702577.

5. Charge Transfer Crystals of Pillar[5]quinone and 4,4'-Bis(*N*-carbazolyl)-1,1'-biphenyl (CBP)
Shivakumar, K.I.; Gonnade, R.; Sanjayan, G.J. *Manuscript under preparation.*

6. Self-Assembly of Solvatofluorochromic Phloroglucinol-Dithiolylidene-based C_3 Symmetric Molecules into One-dimensional Nanostructures
Shivakumar, K. I.; Goudappagouda; Gonnade, R.; Babu, S.S.; Sanjayan, G. J. *Manuscript submitted.*

Chapter 1

Introduction

Part-A: Introduction to charge transfer interactions

Part-B: Introduction to macrocycles

Part A

1. Charge Transfer Interactions

Electron transfer (ET) reactions between the two different molecules (intermolecular) or between the two different regions of the same molecule are some of the frequently observed photochemical phenomena.[1] Consequently, the reaction product is termed as a charge-transfer (CT) state, an intramolecular CT (ICT) state or an exciplex. The attractive forces binding the donor and acceptor molecules in intermolecular charge transfer complexes are electrostatic in nature and are much weaker than a covalent bond. These complexes possess different energy states than the parent compounds and usually undergo electronic transition from ground to excited state by absorbing the energy in the visible region of the spectrum and hence are strikingly colored (Fig. 1.1a). On the other hand, an intermediate ICT state is developed in molecules exhibiting ICT in between the ground and excited state of the molecule, which is sensitive to the polarity of the solvents resulting in solvatochromism (Fig. 1.1b). Organic CT systems have found tremendous applications as molecular devices in modern technologies, in particular - electronics.[2]
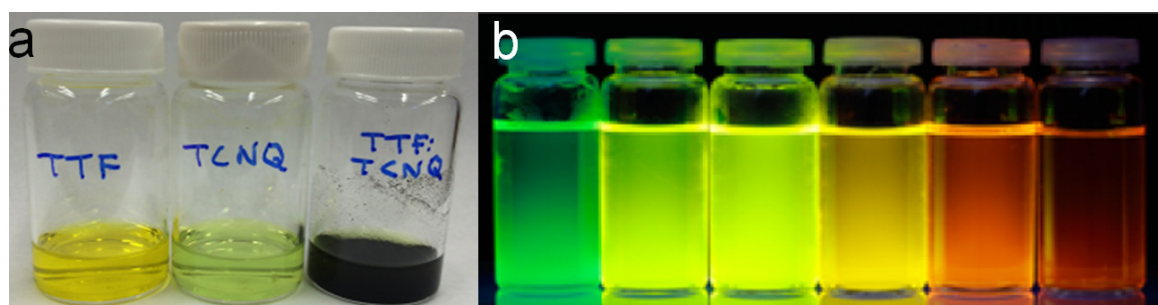
Fig. 1.1 (a) Solutions of donor TTF, acceptor TCNQ and their intermolecular CT complex in acetonitrile. (b) Fluorescence solvatochromism as observed in π-extended pyrrole as a consequence of ICT with emission shifting from green to red with increase in solvent polarity from toluene to methanol. Fig. 1.1a and b are reproduced, with permission, from ref 3 and ref 4, respectively. Copyright © 2015 and © 2016 American Chemical Society.

1.1 A historical glimpse on the conceptualization of 'molecular complex'

Hantzch, in 1905, opined that the nitrogen atom in the colored solutions of amines and iodine cannot be regarded as pentavalent, but the compounds should be considered as a salt *i.e.* $R_3N^+-X^{\cdots}X^-$.[5] Tinkler (1909), while studying the colored compounds obtained during methylation of cyclic organic bases using methyl halides, found much literature

precedence of the fact that iodides are strikingly colored; the bromides are moderately colored, while the chlorides lacked any color.[6] Furthermore, he observed that the colors were solvent dependent. Ostromisslensky, in 1911, noted that upon mixing nitrobenzene and aniline the solution turned deep orange.[7] Tinkler (1913) took this observation a step forward by generalizing that the color change occurred when nitro compounds and amines were mixed together. In addition, he studied the effect of temperature and inert solvents and concluded that their additive behavior is responsible for the color changes.[8] However, the reasons for color change in amine-nitro solutions were thought to be configuration change in the nitro group and polymerization in iodine solutions.

By the 1920's these systems became a puzzle to chemists, as the two chemically saturated entities involved contravened the existing rules of chemical bonding upon mixing, in terms of their valencies. Pfeiffer (1927) hypothesized that the weak forces of attraction could be owed to the saturation of "residual valence forces".[9] In 1929, Bennet and Willis discerned the donor-acceptor nature of interaction amongst the entities involved and justified the bonding in terms of covalent linkage.[10] However, the single-crystal X-ray diffraction revealed that the distance between the entities were larger than the typical covalent bond lengths. Briegleb (1932) furthered the idea postulated by Pfeiffer by interpreting the interaction in terms of non-covalent forces of attraction: dipole-dipole and dipole-induced-dipole.[11] Nevertheless, rationalizing the reason behind how these interactions altered the electronic balance in the two participating molecules to have an effect on absorption spectra was challenging then. In 1940, Gibson and Loeffler[12] and Hammick and Yule[13] attributed the spectroscopic changes upon complexation to the electronic interchange between the two molecules during the normal collisions. However, their isolation as stable solids ruled out this theory.

Weiss (1942) postulated that one of the interacting molecules was electron rich (donor) and the other electron poor (acceptor). In addition, he proposed that the interaction of aromatic compounds (D:) with nitro compounds and quinones (A) in terms of a single electron transfer [D: + A → D$^{+\bullet}$ + A$^{\bullet}$] affording odd electron ions which are stabilized by electrostatic forces of attraction.[14] However, their low heat of formation ruled out the possibility of distinct ion pairs. Woodward, in 1942, in a similar theory suggested that the first step involved in the formation of donor-acceptor adduct is an electron transfer.[15] He proposed that the collisions led to reversible electron transfer

resulting in the formation of dipolar aggregates which are stabilized by ionic forces. Further, he explained that their close proximity provides additional stabilization by orbital overlap. This was reported as "intermolecular semi-polar bond".

The term "complex resonance" was coined by Brackman (1949) to justify the interaction of the donor and acceptor and regarded 1:1 adduct as a resonance hybrid of a no-bond structure and a single covalent bond (D: A ⇌ D$^+$: A$^-$). Significantly, Brackman related the observed color to the adduct and not to the individual molecules.[16] While all the above theories helped chemists in understanding the molecular complexes better, it was not until Mulliken (1952) postulated his theory of the nature of these weak forces; a sound theoretical basis was established. In fact, Mulliken's quantum mechanics, in part, covered most of these concepts. He ascertained that the new absorption band ushering to characteristic color of the complex is due to the electronic transition occurring from the ground state to excited state.[17] Murrell, in 1959, rationalized the strong charge transfer absorption intensity to the interaction of charge transfer states with the donor excited states.[18] Dewar[19] (1966) expressed skepticism over the work of Mulliken and suggested that charge transfer complexes, such as hydrocarbons-tetracyanoethylene (TCNE), cannot be solely stabilized by the charge transfer forces, but classical stabilizing forces like electrostatic interactions and Heitler-London dispersion forces come into existence. Le Fevre, in 1968, noted that in π-complexes, it was polarization forces that governed the contribution to the ground state dipole and not charge transfer as previously assumed.[20] Similarly, in the same year, Hanna advocated the role of quadruple-dipole and quadruple-induced dipole, to be anywhere between 30-80%, in the formation of charge transfer complexes of benzene-halogen.[21]

1.2 Intermolecular charge transfer interactions

Combination of charge donating (D) and accepting (A) compounds bring about charge transfer complexation. The D-A complexes, although not covalently bonded, can possess entirely new properties than the individual molecules taking part in complexation. The discovery of the first conducting 'organic metal' tetrathiafulvalene (TTF)-tetracyanoquinodimethane (TCNQ) in 1973,[22] steered chemists to come up with a library of charge donor (D) and acceptor (A) molecules in pursuit of fabricating devices exhibiting metallic[23] to superconductivity.[24] In addition to conductivity, this journey over four decades has made them uncover remarkable ferroelectric,[25] photoconductive,[26]

thermoelectric,[27] and magnetic[28] properties of charge transfer (CT) complexes. Subsequent to the advent of conductive CT complex TTF-TCNQ, another complex which raised the hope of obtaining high-temperature superconducting organic CT salt was (TMSTF)$_2$-PF$_6$. This low temperature superconducting complex was obtained by Bechgaard and co-workers in 1980 with donor tetramethylselenafulavlene (TMSTF) and acceptor hexafluorphosphate (PF$_6$)$^-$.[29] Design and studies on myriads of organic CT complexes led chemists to relate two important parameters to their property: first, the choice of donor and acceptor and second, the arrangement of donor and acceptor in the crystal lattice.

Selected examples of donors

Naphthalene   Anthracene   Phenazine   Tetracene

Perylene   Coronene   Chrysene   Pyrene

Tetrathiafulvalene (TTF) Dibenzotetrathiafulvalene (DBTTF)   *Trans*-stilbene   Carbazole
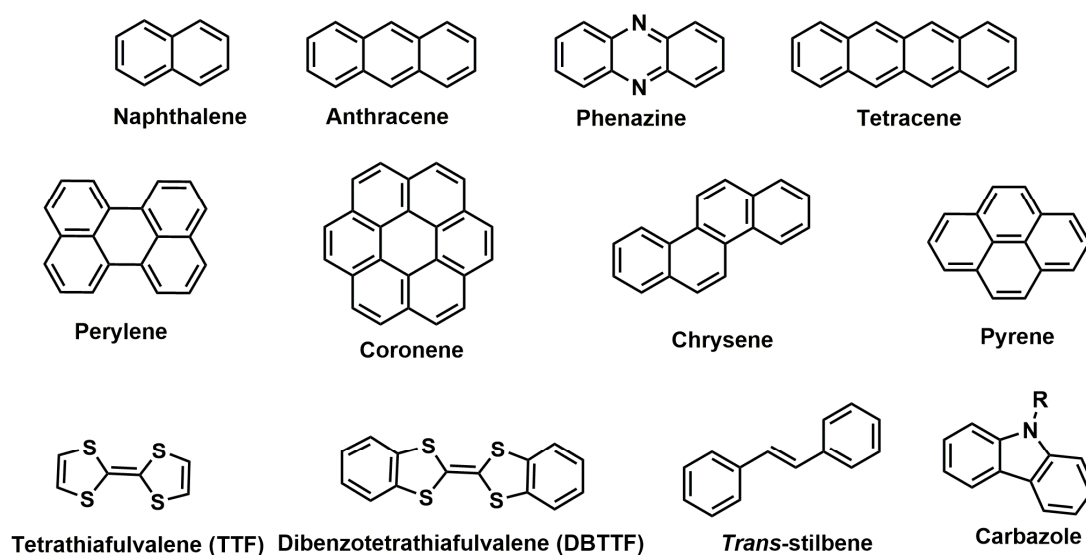
Selected examples of acceptors

R = H: Benzoquinone   Tetracyanoethylene   R = H: TCNQ
R = F: Fluoranil   (TCNE)   R = F: F$_4$TCNQ
R = Cl: Chloranil

Pyromellitic dianhydride   Fullerene
(PMDA)
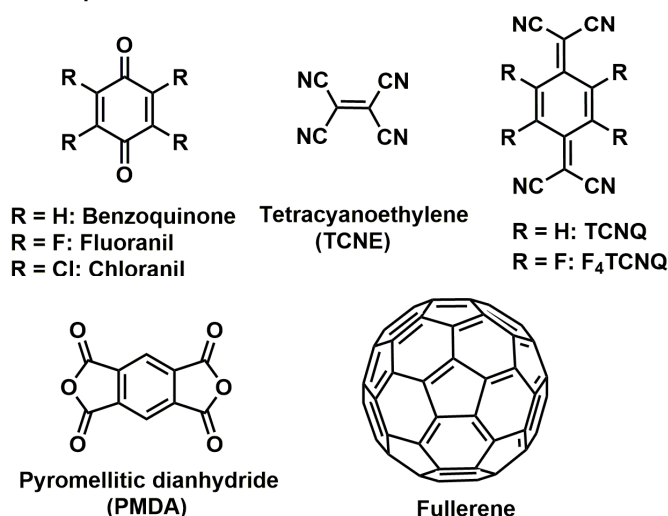
Fig. 1.2 Molecular structures of well known donors and acceptors.

1.2.1 Donors and acceptors

The property exhibited by the CT complexes relies upon the preferred donor and acceptor (Fig. 1.2) in addition to their arrangement in the crystal lattice. In general, the molecule possessing low ionization potential (I_D) which is capable of affording an electron or fraction of negative charge is a donor and the molecule with high electron affinity and capable of accepting an electron or fraction of negative charge (E_A) is an acceptor. The highest occupied molecular orbit (HOMO) of the donor and lowest unoccupied molecular orbit (LUMO) of the acceptor electronically couple leading to the partial or complete transfer of electrons from HOMO to LUMO. Remarkably, tailoring of CT complexes with desired donors and acceptors can be attempted with the knowledge of their HOMO-LUMO energy levels (Fig 1.3). The band structure of CT complex usually differs from that of its constituent compounds (depicted in yellow). The computational studies have established that the HOMO of the CT complex has predominant contribution from the HOMO of donor, and the LUMO of the CT complex from LUMO of the acceptor.[30]
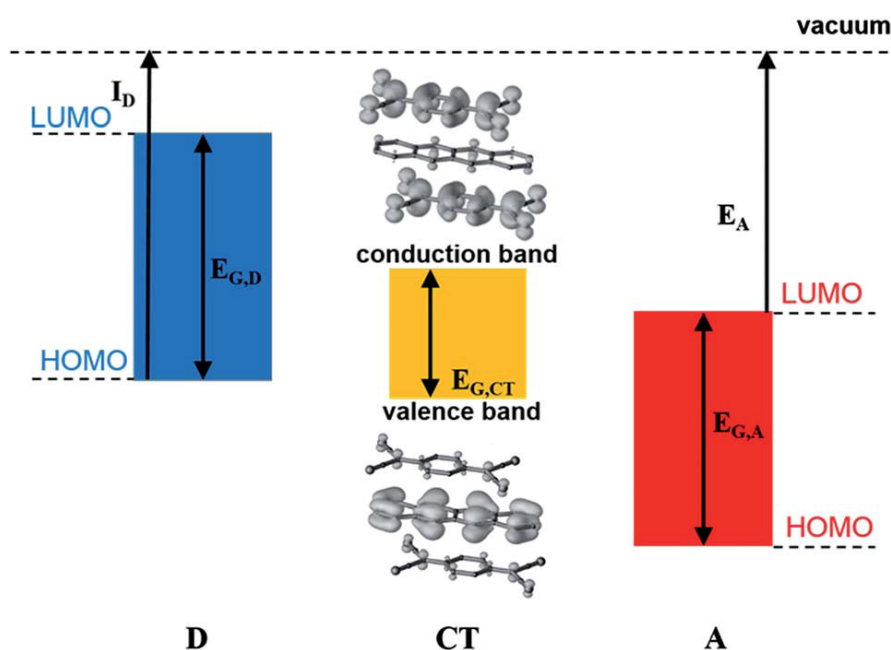
Fig 1.3 The band structures of donor tetracene (blue) and acceptor TCNQ (red) along with the approximation of their CT band structure (yellow).[2] Reproduced, with permission, from ref 31. Copyright © 2008 American Chemical Society.

The magnitude of the charge transferred is gauged by the degree of ionicity (ρ).[32] The CT complexes could be considered neutral or quasi-neutral when ρ < 0.5 with I_D - E_A

>> E_M, where E_M is the electrostatic Madelung energy of the crystal. On the other hand, when donors and acceptors are chosen so that the ρ > 0.5 with I_D - E_A << E_M, the resulting complex would be quasi-ionic or ionic.[33] Herbestein pointed out two important observations regarding the choice of donor and acceptor. First, electronic properties of resulting CT complexes are governed by the difference in the energy between the donor and acceptor. And, second, increased planarity in the constituent molecules may lead to enhanced charge transfer.[34] In addition to choice of suitable donor and acceptor molecules, other factors such as crystal packing, play significant role in determining the properties of the CT complex.
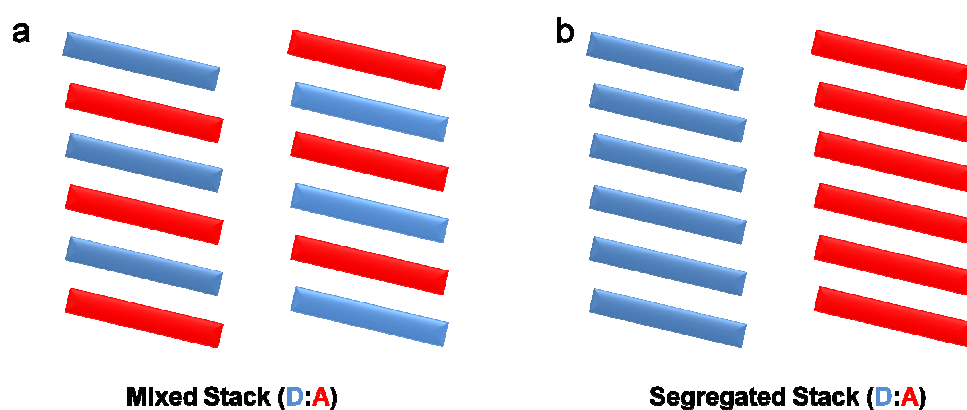
Fig. 1.4 Crystal packing of 1:1 charge transfer complexes (a) mixed and (b) segregated stacking.

1.2.2 Crystal packing in charge transfer complexes

Theoretically, the donors and acceptors may undergo crystallization in various *m:n* stoichiometries. Interestingly, 1:1 stoichiometry is generally observed with two different types of crystal packing: mixed/alternate and segregated. In mixed packing, the donors and acceptors π- stack alternately along the stacking direction as …D-A-D-A… (Fig. 1.4a) and the examples include TTF-bromanil (Fig. 1.5a),[35] pyrene-TCNQ,[36] perylene-TCNQ,[37] anthracene-PMDA,[38] DBTTF-TCNQ[39] *etc.* On the contrary, in the segregated packing the donors and acceptors π- stack among themselves separately as …D-D-D-D… and …A-A-A-A… (Fig. 1.4b); and the typical example includes TTF-TCNQ (Fig. 1.5b).[40] CT complexes with mixed stacked D-A assembly is frequently observed, while the ones with segregated stacked are rare. Remarkably, in both these stacking geometries, at least one D-A pair can be anticipated. A single CT complex can possess two different

kinds of crystal geometry with different colors and properties, for instance, in the superconducting Bechgaard's salt, TMTSF-TCNQ, the red colored mixed stack complex is semiconductive,[41] while the black segregated-stack complex is metallic.[42] Although generalities are set with the crystal geometries and their properties, such as the segregated stacking is an essentiality (but not guaranteed) of conductivity and non-centrosymmetric mixed stacking for ferroelectricity, further study is necessitated to establish any specific (crystal) structure-property relationship.
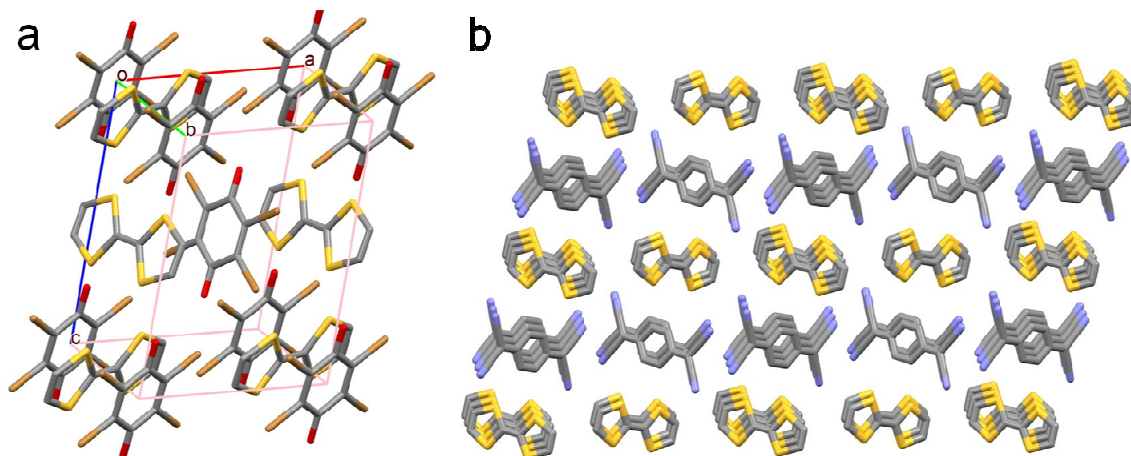
Fig. 1.5 Single crystal structure showcasing the arrangement of donors and acceptors. (a) Mixed stacking in cryo-temperature ferroelectric TTF-bromanil, and (b) Segregated stacking in metallic conductor TTF-TCNQ. Crystal structures courtesy of CCDC.

1.2.3 Ferroelectricity

Ferroelectric materials are endowed with spontaneous polarization which can be reversed by applying external electrical field.[43] In addition, these materials possess ability to manipulate light owing to the optical non-linearities and electro-optic effects, sense temperature (pyroelectricity) and respond mechanically to electrical stimulus and *vice versa* (peizoelectricity) and all these properties of ferroelectrics bear applications.[44] As a consequence of spontaneous alignment of electrical dipoles, the polarization draws a hysteresis loop as a function of applied electrical field (Fig. 1.6a). Owing to this switchable property, ferroelectrics find applications in memory storage devices.[45] Furthermore, the ferroelectric materials possess a thermal transition point, Curie temperature (T_c) wherein, the material undergoes changeover from ferroelectric to paraelectric. Whilst the temperature approaches near T_c, a sudden increase in the dielectric constant (ε) of the material is observed before it undergoes a jump

discontinuity as dictated by the Curie-Weiss law, which is exploited in developing ferroelectric condenser and capacitors with high ε.[46] The dielectric constant of a ferroelectric material as a function of applied electric field affords butterfly loop (Fig. 1.6b).
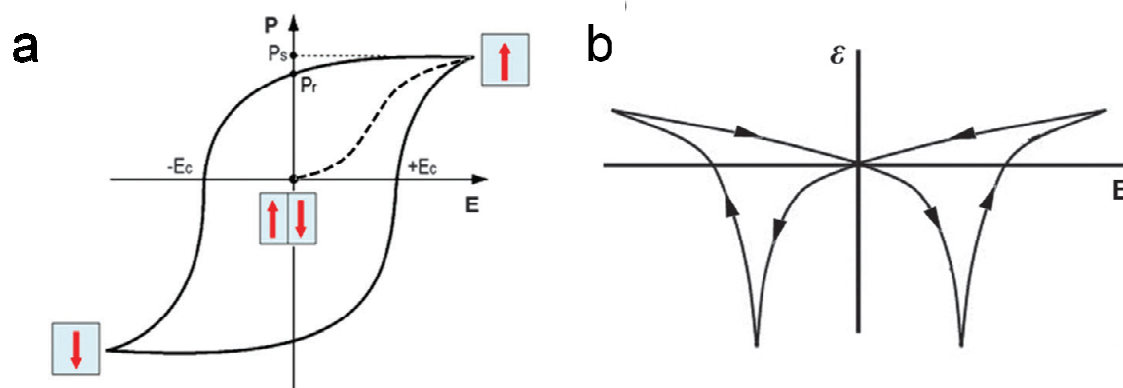
Fig. 1.6 Characteristic ferroelectric loops. (a) P(E) hysteresis and (b) butterfly. Reproduced, with permission, from ref 48. Copyright © 2015 Nature Publishing Group.

Perovskites, such as barium titanate (BTO) and lead zirconate titanate (PZT), had been dominating the field of ferroelectrics in the last quarter of 20th century.[47] However, the rigidity, heavy-weight, high temperature processing, and presence of environmentally hazardous substance such as lead, make them disadvantageous. Hence, the materials which are flexible, light-weighted, low-temperature solution processable, and environmentally benign are the need of the hour, and in this perspective, the advent of molecular ferroelectrics have slowly started to plug the gap.[46,48] The molecular ferroelectrics reported till date fall into three different kinds. First, mixed CT complexes where spontaneous polarization occurs due to collective transfer of electrons from donors to acceptors. The alternately arranged donor and acceptor undergo neutral-to-ionic transition and dimerize, thus breaking the centrosymmetry. Upon reversing the electrical field the material switches the polarization by pairing its $D^{\delta+}/A^{\delta-}$ with the next adjacent $A^{\delta-}/D^{\delta+}$ (Fig. 1.7a). Ferroelectricity as a consequence of electronic polarization is exemplified in TTF-chloranil (CA) below 81 K with large remnant polarization of 6.3 μCcm^{-2} (Fig. 1.7a).[49] However, recent works to elevate the temperature of ferroelectric ordering by implementing hydrogen-bond-augmented mixed stacked CT complexes have led to the discovery of room temperature supramolecular ferroelectrics, with remanence exceeding 1 μCcm^{-2} (Fig. 1.7b).[48,50]
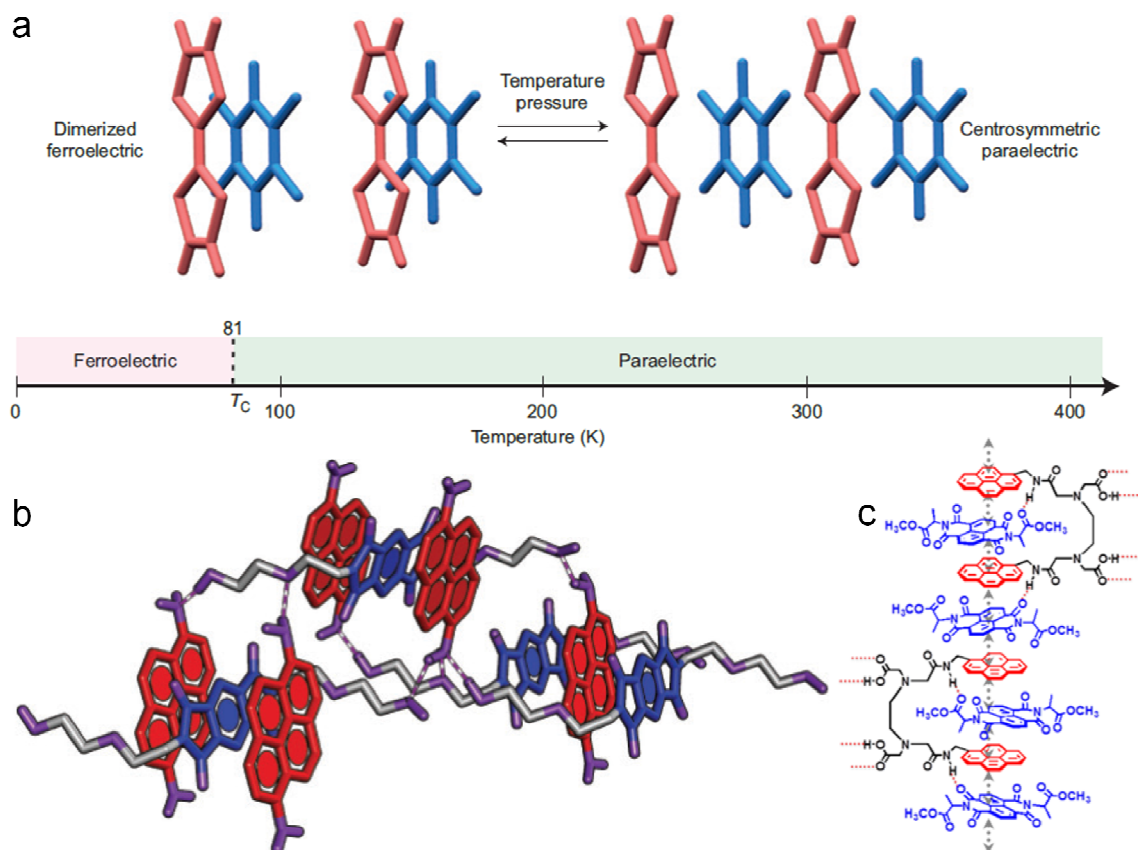
Fig. 1.7 (a) Centrosymmetric crystal of TTF-CA undergoing neutral-to-ionic transition and consequently a change over in phase from paraelectric to ferroelectric. (b) Individual stacks of room temperature ferroelectric CT co-crystal of 1,6-diaminopyrene and pyromellitic diimide derivative bound together by hydrogen bonding. (c) Proposed molecular model showcasing the extended mixed CT assembly of tweezer-inclusion sandwich (TIS) formed by dipyrene tweezer-like (DPT) and naphthalene diimide (NDI) owing to π-stacking and hydrogen bonding interactions. Reproduced, with permission, from ref 48. Copyright © 2015 Nature Publishing Group.

Second, single component organic systems permit site-to-site migration of protons involved in hydrogen bonding, thus promoting switching of polarization. Horiuchi, Tokura and co-workers demonstrated room temperature ferroelectricity with remanence of ~20 μCcm^{-2} for croconic acid, which undergoes reversal of polarization by proton transfer mechanism.[51] The crystal structure unveiled the two dimensional sheeted arrangement of croconic acid with two labile protons involved in hydrogen bonding undergoing migration (Fig. 1.8a). Further, the same group reported the ferroelectricity and antiferroelectricity in imidazole derivatives through proton tautomerization with remanence of 5-10 μCcm^{-2} at room temperature (Fig. 1.8b).[52]
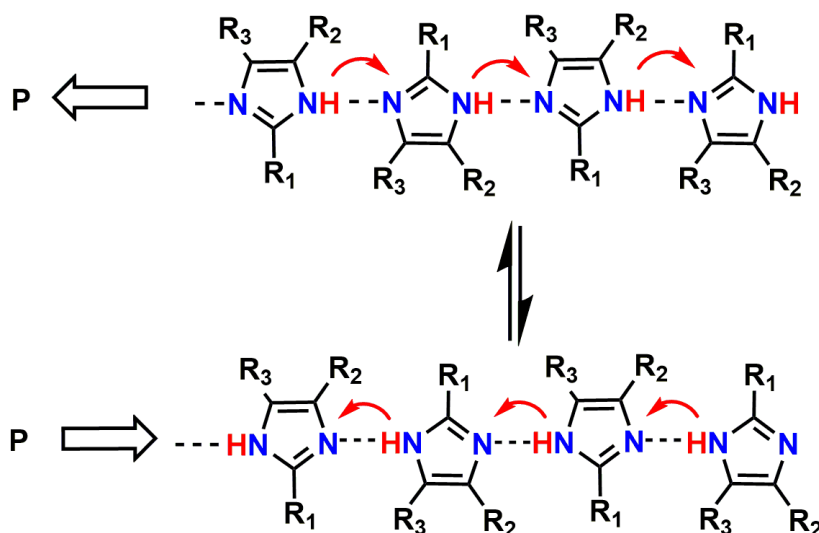
Fig. 1.8 Polarization switching employing proton transfer mechanism in molecular ferroelectrics.

The third strategy is to use the order-disorder transition of ammonium ions in the crystal. The organometallic complex, ethylammonium copper chloride [$(C_2H_5NH_3)_2CuCl_4$] bearing a perovskite-type structure undergoes paraelectric to ferroelectric phase transition below 77 K with large remanent polarization of 37 μCcm^{-2}. The ferroelectric phase is brought by order-disorder transition owing to the reorientation of alkylammonium groups within the crystal lattice.[53] Recently, two simple secondary ammonium salts have been reported to exhibit ferroelectricity: diisopropylammonium bromide (DIPAB) and diisopropylammonium chloride (DIPAC). The DIPAB with large remanence of 23 μCcm^{-2} possesses high T_c of 426 K where the nitrogen atoms enter an apparently disordered state, losing ferroelectric order.[54] Similarly, DIPAC is endowed with a T_c of 440 K and displays the remanence of 8.9 μCcm^{-2}.[55]

In spite of several recent works in the realm of ferroelectricity, this field is still in its infancy and beckons for further study in understanding the ferroelectric mechanism, relationship with the crystal structure and improving the performance.

1.3 Intramolecular charge transfer complexes

Intramolecular charge transfer (ICT) is one of the myriad deactivation phenomena taking place in excited molecules.[56] ICT occurs in molecules having push-pull groups wherein, electron transfer takes place from donor to acceptor moieties within the molecule.[1] A dyad molecule, with a π-conjugated linker between the donor and

acceptor, has its electron density shifted towards the acceptor at its excited state through the conjugated linker. The dyad molecule as a whole along with the conjugated linker can be considered as a single chromophore. The dyad molecule with the π-conjugated linker between donor and acceptor induces a significant change in the dipole moment in the excited state. Hence, the ICT phenomenon is regarded to be responsible for the large stokes shift, which is highly sensitive to the solvent polarity (Fig. 1.9).[57]
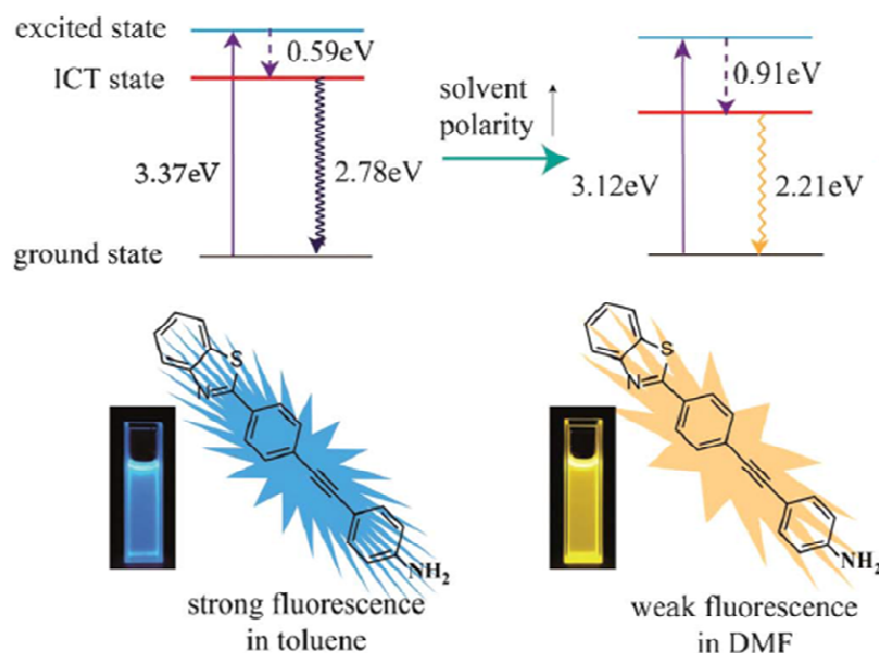
Fig. 1.9 Fluorescence solvatochromism observed in 4-((4-(benzothiazol-2-yl)phenyl)ethynyl) aniline (BA) along with its schematic energy states. Reproduced from ref. 58 with permission from the Royal Society of Chemistry.

Remarkably, tetrathiafulvalene (TTF) based donor units have been associated with myriad acceptors, within the molecule, in pursuance of materials possessing low optical band gap that can be suitably employed in organic electronics.[59] Tuning the ICT bands by adopting various linkers and by incorporating different acceptor groups have been attempted in recent years.[60] Selected examples, wherein the ICT band has through bond character with a σ-bond between the donor and acceptor, involve TTF-pyridinium,[61] TTF-benzothiadiazole,[62] TTF-oxophenalenoxyl[63] *etc*. Hauser, Avarvari and co-workers synthesized tris(TTF)-triazine exhibiting π (TTF) → π* (triazine) ICT transition with emission. However, the emission owing to the excitation of the ICT band could be quenched by oxidizing the TTF moieties.[64]

Part B

1.4 Macromolecules and their supramolecular interactions

Macrocycles, according to IUPAC definition, are the cyclic macromolecules or cyclic portion of a macrocycle.[65] Designing and synthesizing a novel macrocycle without much synthetic hassles with at least one homologue, which is bestowed with a unique shape and good solubility and versatile tailorability would be challenging, nevertheless highly rewarding. Cyclodextrins,[66] crown ethers,[67] calixarenes[68] and cucurbiturils[69] have dominated the realm of macrocyclic chemistry for over a century owing to the presence of aforementioned properties (Fig. 1.10a-d). Ogoshi and coworkers, in 2008, introduced a new macrocycle consisting of five hydroquinones with methylene linkers in their *para* positions, and named them pillar[5]arenes (**P5A**) (Fig. 1.10e).[70] **P5A**, since its advent, have caught considerable attention of chemists, which is evident from the number of publications reaching around 350 in the span of less than eight years. Pillar[*n*]arenes possess similar composition to that of calix[*n*]arene except that the methylene groups link the hydroquinones in *1,4* position, unlike *1,3* position in calixarenes. While calixarenes being metacyclophanes are vase/calyx shaped, lower homologues of pillar[*n*]arenes (*n*= 5,6) are highly symmetrical in shape which propelled the pioneer group to christen this paracyclophane after the symmetrical 'pillar's of Greek temple, Parthenon.[71] Pillar[5]quinone (**P5Q**),[72] the oxidized form of **P5A**, was synthesized in a pure form and in multigram-scale by Shivakumar and Sanjayan in 2013 (chapter 2, section I). While the five dialkoxy/dihydroxy benzenes make peralkylated-**P5A/P5A** electron rich, **P5Q**, adorned with five *p*-benzoquinones is electron deficient and forms CT complexes with electron rich donors.
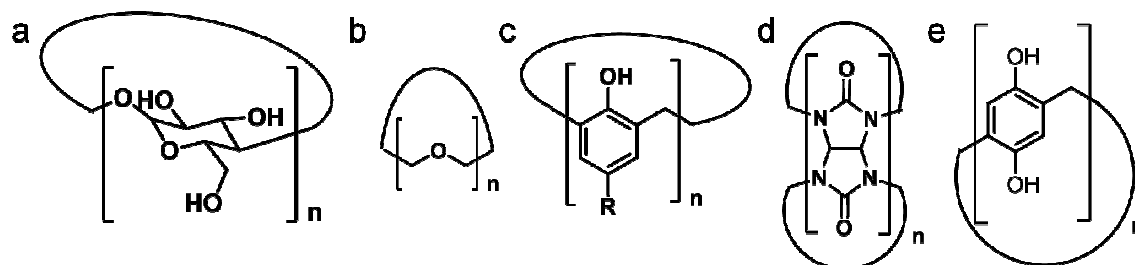

Fig. 1.10 Repeating units of macrocycles. (a) Cyclodextrin, (b) Crown ether, (c) Calixarene, (d) Cucurbituril, and (e) Pillararene.

1.5 Macrocycles: from cyclodextrins to pillararenes- a historical background

Advent of a new macrocyclic hosts with easy synthesis, unique structure, good solubility, facile functionality and capable of forming higher homologues are seldom observed. Nevertheless, their arrival opens up new avenues towards realization of their functional characteristics resulting from their unique structure, reactivity and host-guest properties. This section would describe, in brief, on the macrocycles that created a lasting impact in the realm of supramolecular chemistry with pillar[*n*]arene chemistry, in detail.

1.5.1 Cyclodextrins:

Cyclodextrins (CDs) were the first macrocycle to be discovered in 1891 by A. Villiers.[73] They are the cyclic oligosaccharides consisting glucopyranose units connected by 1,4 linkage (Fig. 1.10a, 1.11a). The homologues of CDs commonly observed are 6 (α), 7 (β) and 8 (γ). They are bucket shaped, with a large opening at one end and narrow at the other (Fig. 1. 11b). The presence of hydroxyl groups at either faces makes CD an ideal candidate for functionalization. CDs, possessing inner hydrophobic and outer hydrophilic environment, are water soluble. Their cavity sizes range from 4.9-8.0 Å and are capable of forming several host-guest complexes.[74] α-CD, the smallest among CDs possessing cavity size of 4.9 Å, encapsulates linear alkanes and small aromatic compounds. β-CD, the medium sized CD traps relatively bigger guests like bulky hydrocarbons- adamantane and cyclohexane derivatives, and polyaromatic compounds such as naphthalene and anthracene derivatives. γ-CD consisting of 8 glucopyranose units encapsulates larger guests. While a molecule of γ-CD can encapsulate two aromatic guests or polymeric chains, two molecules of γ-CD is reported to sandwich a fullerene. Host-guest property of CD is employed to construct myriads of mechanically interlocked molecules (MIMS) such as catenanes, rotaxanes, polyrotaxanes, molecular shuttles and topological gels (Fig. 1.11c).[66b,75] Commercial availability, non-toxicity, capability to form host-guest complexation in aqueous media and ability to accommodate diverse hydrophobic guests like fats, foods, medicines and coenzyme Q10 make CDs advantageous over other macrocycles. As a consequence of their host-guest complexation with various guests in aqueous environment they are also employed in drug delivery systems (DDS).[76] However, the poor solubility of CDs in non-polar solvents has made chemists to look forward to functionalize the hydroxyl groups to increase the solubility, and thereby expand the scope of utilizing CDs effectively.
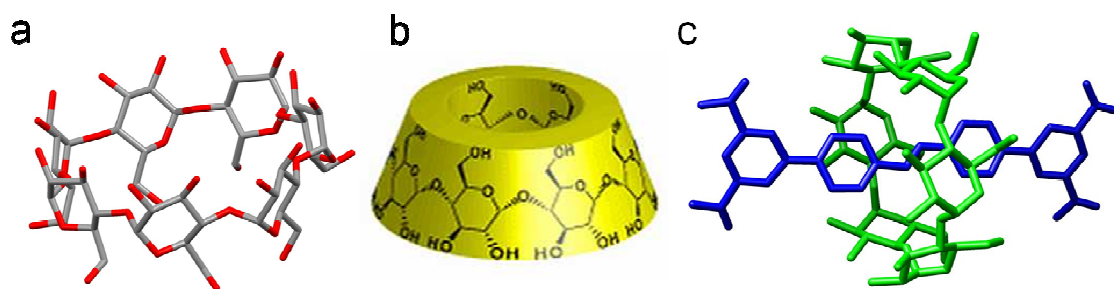
Fig. 1.11 (a) Crystal structure of β-cyclodextrin. (b) Representative 3D model showing bucket shaped β-cyclodextrin. (c) Cyclodextrin forming rotaxane with stilbene. Images courtesy: CCDC (Fig. 1.11a and 1.11c) and B. Voncina and V. Vivod (2013), InTech (Fig. 1.11b).

1.5.2 Crown ethers

Pederson, in 1967, accidentally discovered that cyclic oligomers of ethylene oxide entrap various alkali metal ions depending on their size (Fig. 1.12). They were named crown ethers as their solid-state structures resemble the 'crown'. The driving force is the chelating ability of oxygen which coordinates with the metal ion. It is noteworthy that, the ion-recognition by synthetic compounds was unprecedented till then, and thus revolutionized the realm of molecular recognition, supramolecular and biomimetic chemistry. Crown ethers possess high solubility in aqueous and organic media and hence could be easily tailored. The ion coordination ability of crown ethers is high in non-polar solvents compared to the polar solvents.[77] The conformation flexibility and organo-solubility of crown ethers make them more advantageous compared to CDs. Crown ethers have been used as phase transfer catalysts due to their amphiphilic nature in addition to selective recognition of metal cations through encapsulation.[78] As a consequence of encapsulation, the reactivity of naked counter anions get enhanced. Subsequent to the discovery of crown ethers, Lehn synthesized double-cyclic crown ethers in 1969 and named them cryptands.[79] Cryptand, analogous to the action of valinomycin, an antibacterial agent, is able to selectively and strongly bind to K^+ ions and forms cryptate.
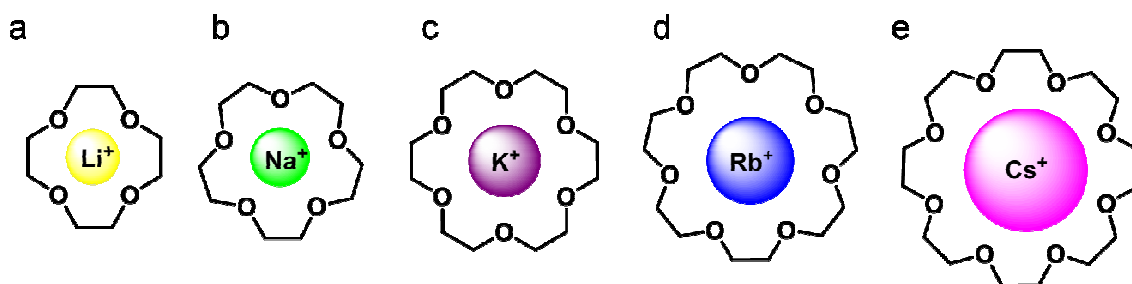
Fig. 1.12 Inclusion complexes of **c**rown ethers with various alkali metal ions (a) 12-crown-3, (b) 15-crown-5, (c) 18-crown-6, (d) 21-crown-7 and (e) 24-crown-8.

1.5.3 Calixarenes

Calixarenes, although date back to Baeyer's phenol-formaldehyde synthesis in the 1870s,[80] were popularized by Gutsche only in 1978.[81] Calix[*n*]arenes are the cyclic oligomers of phenolic moieties linked by methylene bridges at 2- and 6- positions (Fig. 1.10c). These [*n*]metacyclophanes are usually found with even number of repeating units (*n* = 4, 6, 8). However, odd-numbered calix[*n*]arenes and large calixarenes are rare due to the low yields.[82] Multiple intramolecular hydrogen bonds between the hydroxyl groups of the phenolic units make these metacyclophanes attain the shape of the vase (Fig. 1.13a). The presence of electron rich phenolic units coerce calixarenes to encapsulate electron deficient species, in particular - the cations. Calix[8]arenes selectively entrap C_{60} and have been used to isolate C_{60} from the fullerene mixture (Fig. 1.13c).[83] Water soluble calixarenes, synthesized by sulfonating the hydroxyl groups (Fig. 1. 13b), were reported to form host-guest complexation in aqueous media with cationic as well as neutral molecules.[84] It is noteworthy that, hydrophilic-hydrophobic and cation-π interactions drive sulfonated calixarenes to encapsulate guests in water. Calix[*n*]arenes possess various conformations owing to the rotation of phenolic units.[85] The four conformers of calix[4]arene are cone, partial cone, 1,2-alternate and 1,3-alternate. The conformational switching plays an important role in sensor applications.[86] Furthermore, calix[*n*]arenes have been derivatized to thiacalix[*n*]arenes,[87] where methylene bridges are replaced by sulfide, sulfinyl and sulfonyl units. Notably, the thiacalix[*n*]arenes can selectively extract metal ions and those thiacalixarenes that encapsulate lanthanide ions, particularly, have been used as fluorescent markers and MRI sensitizers.[88] Subsequently over the years, bowl-shaped resorcin[*n*]arenes,[89] pyrogallol[*n*]arenes[90] and calix[*n*]pyrroles,[91] constituting resorcinolic, pyrogallolic and pyrrolic units, respectively, have surfaced and expanded the host-guest chemistry of calix[*n*]arenes and their analogues.
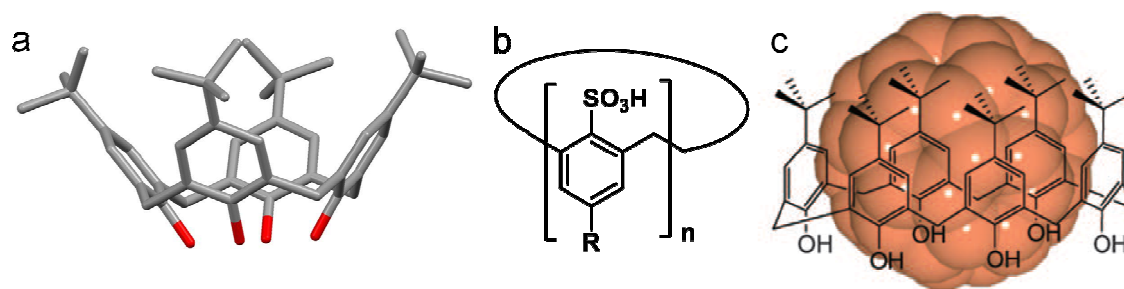
Fig. 1.13 (a) Crystal structure of *t*-butyl calix[4]arene. (b) Water soluble calixarene bearing sulfonic acid groups. (c) Host-guest complex of calix[8]arene and C_{60}. Image courtesy: CCDC (Fig. 1.13a) and ref.71 (Fig. 1.13c).

1.5.4 Cucurbit[*n*]urils

Curcurbit[*n*]urils (CB[*n*], *n* = 5-11) are pumpkin-shaped, highly symmetrical macrocycles consisting of repeating glycouril units linked by two methylene bridges (Fig. 1.14a). Although, the synthesis of CB[6] appeared in literature in 1905,[92] its complete characterization and host-guest property were reported only in 1981 by Freeman-Mock.[93] Unfortunately, the poor solubility of CB[6] led to its poor development till 2000. Nevertheless, Kim and coworkers, in 2000, were successful in synthesizing CB[*n*] (*n* = 5-11) in moderate yields by lowering the reaction temperature from >110 ^{o}C to 75-90 ^{o}C which reinvigorated the CB[*n*] chemistry.[94] The moderate water solubility of CB[5] and CB[7] in conjunction with their symmetrical hydrophobic cavities promote inclusion complexes of these macrocycles with water soluble guests like neutral diamines and cations. Notably, the guest molecules have access to the cavitand from both the faces owing to the highly symmetric entrances compared to CDs and calixarenes (Fig. 1.14b). The two methylene bridges between the glycouril units provide rigidity to the CB[*n*]s affording no conformational flexibility and thus resulting in the formation of inclusion complexes with exceptional selectivity and affinity. The cavity sizes of CB[6] (5.8 Å) and α-CD (4.7 Å) are comparable and so are CB[7] (7.3 Å) and β-CD (6.5 Å), and CB[8] (8.8 Å) and γ-CD (8.3 Å). Similar to the CD counterparts, CB[6] forms inclusion complexes with cationic linear alkanes and small aromatic compounds. On the other hand, CB[7] encapsulates cationic polyaromatic compounds and bulky hydrocarbons like bicyclooctanes and adamantanes. Interestingly, CB[8] forms 1:1:1 ternary complexes with electron donor and acceptor. The electron acceptor fails to complex with CB[8] alone in the absence of electron donor, thus necessitating the presence of CB[8] to form charge transfer complex (Fig. 1.14c).[95] Two of the hurdles

which slowed the growth of CB[*n*] chemistry are poor solubility in common organic solvents and difficulty in functionalization. Kim and coworkers addressed the issue of solubility of CB[5] and CB[6] by appending cyclohexyl moiety in each glycouril unit, upon which these cavitands became water soluble despite possessing hydrophobic cyclohexyl groups.[96] Furthermore, the same group attended to the problem of functionality by oxidizing CB[*n*] using $K_2S_2O_8$ in water to yield *per*-hydroxylated CB[*n*].[97] Subsequently, Sherman's and Isaac's groups came up with mono-hydroxylated[98] and monofunctionalized cucurbit[6]urils,[99] respectively. Till date, various derivatives of cucurbiturils have been synthesized with intriguing structures and properties which, indeed, has aided in expanding the host-guest chemistry of CB[*n*]s.[100]
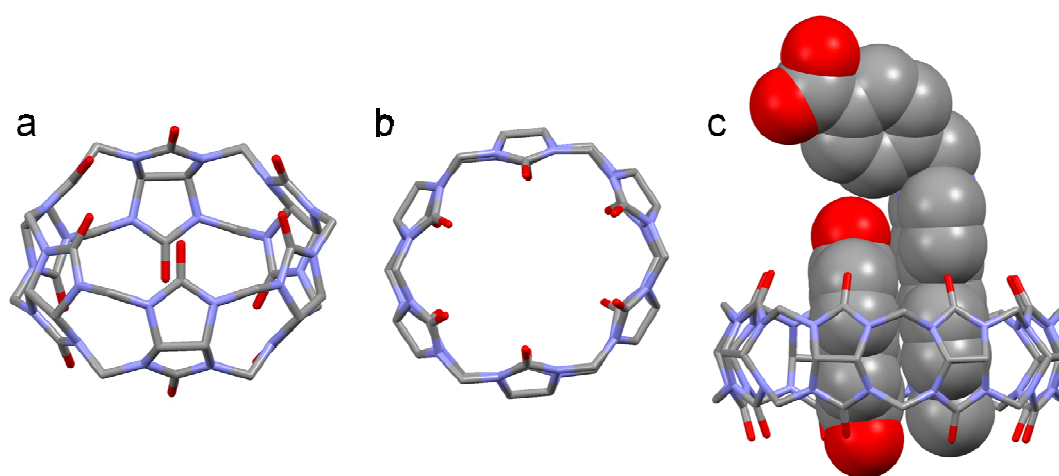
Fig. 1.14 Two different views of crystal structure of CB[6]: (a) side view, (b) top view. (c) Ternary charge transfer complex of CB[8], viologen and 2,6-dihydroxynapthalene. Crystal structures courtesy of CCDC.

1.5.5 Pillar[n]arenes

1.5.5.1 Synthesis

Ogoshi and coworkers, in 2008, accidentally discovered pillar[5]arene (**P5A**) while attempting reaction of 1,4-dimethoxybenzene with formaldehyde catalyzed by a lewis acid.[101] Phenol-formaldehyde chemistry dates back to 1870 and as a result, till date, numerous interesting products, including macrocycles like calixarenes and pillararenes, have come into existence. Synthesis of a phenolic macrocycle, as a major product, based on phenol formaldehyde chemistry could be achieved by circumventing the formation of linear and 3D polymers using suitable phenolic monomers, lewis acids, solvents, and by maintaining optimum reaction temperature and time. Phenol, the simplest monomer, with

three electron rich sites- *ortho* and *para* positions, forms extensive 3D polymer upon treating with aldehydes. However, protection of one of the reaction sites, as in calixarenes where *para* position is alkylated, restricts the formation of 3D polymer and affords linear oligomers that are intermediates for the formation of macrocycle. Calix[4]resorcinarenes are the macrocycles formed as a result of condensation of resorcinarene and formaldehyde under suitable conditions. Although in resorcinarene, 2-, 4- and 6- positions are all electron-rich, steric hindrance precludes the 2- position from reacting with formaldehyde resulting in the formation of metacyclophane.[102] Upon using veratrole for reaction with formaldehyde under appropriate conditions, cyclization occurs *via* the formation of methylene linkers across 4- and 5- positions. Again, the steric hindrance prevents 3- and 4- positions from undergoing electrophilic substitution reaction (scheme 1.1).[103]
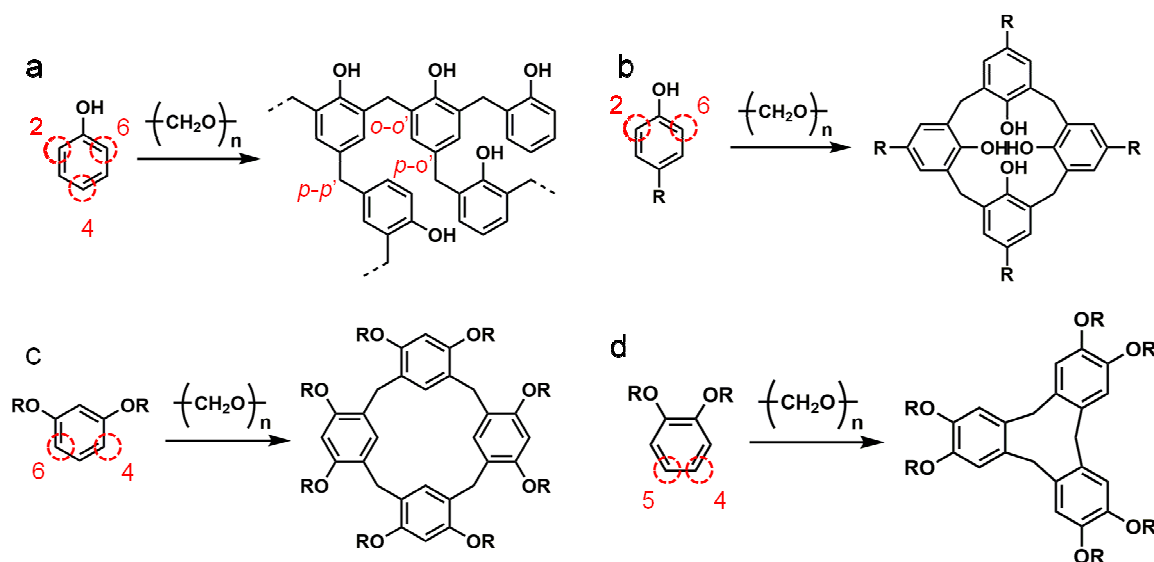
Scheme 1.1 (a) Three dimensional network structure of phenolic resin formed by the reaction of phenol and aldehydes, and macrocyclization reactions of *para* substituted phenols (b), alkylated resorcinols (c), and alkylated catechols (d) yielding calixarenes, calix[4]resorcinarenes, and cyclotriveratrylenes, respectively. *Note:* red dotted circles indicate reactive sites.

Pillar[*n*]arene, a condensation product formed by the reaction of 1,4-dimethoxybenzene and formaldehyde, is a new entrant in the field of macrocyclic hosts. Upon reacting with formaldehyde the 1,4-dimethoxybenzene, with four electron-rich sites: 2-, 3-, 5- and 6- positions, gets appended with methylol moiety in one of the reactive sites. Subsequently, the next electrophilic attack takes place at 5- position ensuing in the formation of [*n*]paracyclophane. While the steric hindrances from the 4-methoxy and

methylene groups prevent the reactive site in 3- position from undergoing reaction, 1-methoxy poses hurdle to the 6-position (scheme 1.2).
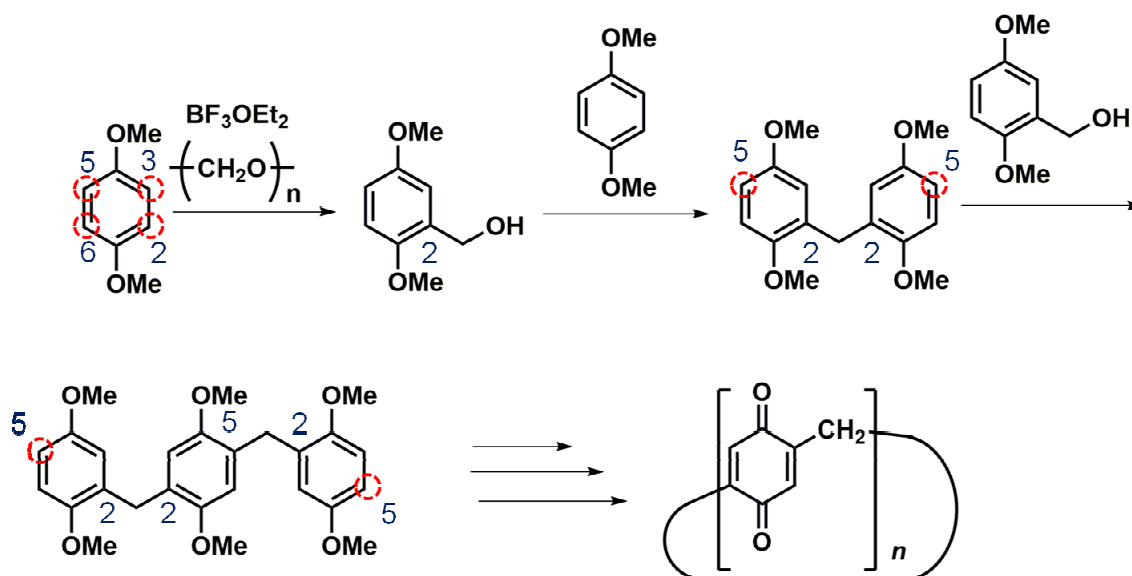
Scheme 1.2 Proposed mechanism of pillar[*n*]arene macrocyclization by the reaction of 1,4-dimethoxybenzene and paraformaldehyde catalyzed by boron trifluoride etherate.

Ogoshi *et al.* initially observed that among the lewis acids BF₃OEt₂ afforded *per*-methylated **P5A** without the formation of polymers, while FeCl₃ and SnCl₄ yielded *per*-methylated **P5A** along with the polymer.[101] Subsequently, the same group improved the yield to 71% by increasing the equivalence of paraformaldehyde from one to three.[104] In fact, the kinetically controlled reactions yielding macrocycles are largely effected by reaction time and temperature and afford homologues with the macrocycle having least strain as a major product and rest in minor amounts.[69d] However, in the thermodynamically controlled reactions additives act as a template and ensure a single macrocycle as product, and thus are attractive over the kinetically controlled ones. In fact, the desired crown ether is obtained by employing suitable metal ion as template.[67b] Although, Ogoshi *et al.* predicted that BF₃OEt₂, could be responsible for the formation of *per*-methylated **P5A** as single product by acting as a template, Boinski and Szumna proved otherwise by reporting 1,2-dichloroethane as the template solvent. In addition, they reported that the synthesis of *per*-methylated **P5A** is moisture-insensitive and improved the yield up to 81% using trifluoroacetic acid as the catalyst.[105] Alternatively, *per*-methylated **P5A** can also be obtained, although on a lengthy route, as a major product along with *per*-methylated **P6A** in minor amounts from 2,5-bis(alkoxymethyl)-

1,4-diethoxybenzene and from 2,5-dialkoxybenzyl bromide using *para*-toluenesulfonic acid and lewis acid, respectively.[72b,106]
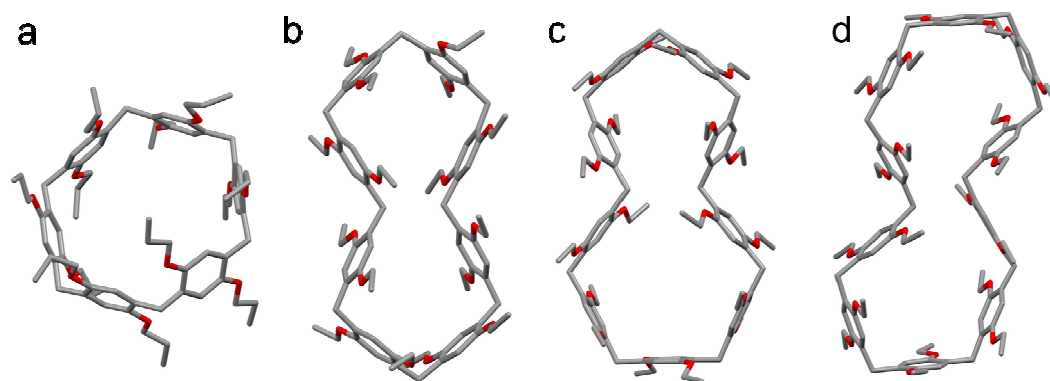
Fig. 1.15 Crystal structures of higher homologues of pillararenes: (a) *per*-propylated pillar[6]arene, (b) *per*-ethylated pillar[8]arene, (c) *per*-ethylated pillar[9]arene, and (d) *per*-ethylated pillar[10]arene. Crystal structures courtesy of CCDC.

1.5.5.2 Homologues of pillar[*n*]arenes (*n* = 5 to 13)

Higher oligomers of pillararenes are usually obtained under kinetic control. Pillar[6]arene was obtained in poor to moderate yields by using $FeCl_3$ as lewis acid under kinetic control by couple of groups.[107] However, Ogoshi *et al.* thermodynamically controlled the reaction by using chlorocyclohexane, a bigger solvent molecule relative to 1,2-DCE, as a template solvent to obtain pillar[6]arene in 87% along with pillar[5]arene in 3% by employing BF_3OEt_2 as a lewis acid. Interestingly, the pillar[6]arene can be converted to pillar[5]arene and *vice-versa* using 1,2-DCE and chlorocyclohexane as solvents, respectively.[108] This experiment justified the observation made by Neirengarten and coworkers that macrocyclization occurred by dynamic covalent chemistry.[109] Recently, mechanochemical synthesis of pillar[6]arene was carried out by grinding 1,4-dialkyloxybenzene and paraformaldehyde in the presence of catalytic amount of con. H_2SO_4 in 81% yield.[110] Larger homologues of pillar[*n*]arenes are usually obtained under kinetic control using a solvent, in particular- chloroform, which fails to template the formation of any homologue. Hou and coworkers synthesized pillar[*n*]arene homologues in chloroform using BF_3OEt_2 in 20 min with *n* = 5 in 20% yield, *n* = 6 in 6% yield, *n* = 7 in 3% yield, *n* = 8 in 1% yield, *n* = 9 in 2% yield and *n* = 10 in 2% yield.[111] The larger macrocycles (*n* = 8, 9, 10) possess two cavities as evident from their crystal structures (Fig. 1.15). Ogoshi *et al.* synthesized higher homologues pillar[*n*]arene (*n* = 5-15) by 'ring-opening' pillar[5]arene in chloroform at 50 $^{\circ}$C in 1 h.[112]
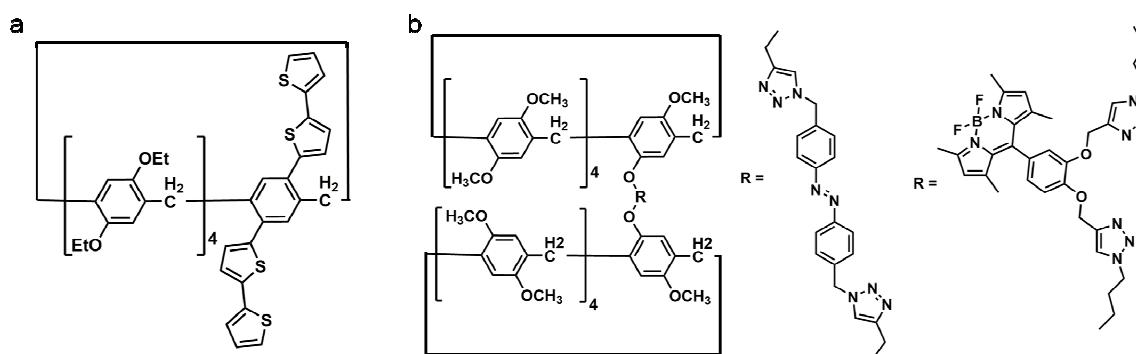
Fig. 1.16 (a) Pillar[5]arene incorporated with extended π-conjugated units at A1/A2 using Suzuki coupling reaction. (b) Pillar[5]arene dimers linked by click reaction possessing photoresponsive azobenzene and BODIPY.

1.5.5.3 Functionalization of pillar[5]arenes

Functionalization of pillararenes on both the rims would influence its solubility along with the conformational and host-guest properties. In fact, functionalizing pillararenes having hydroxyl groups on the rims can be extremely facile. Deprotection of *per*-methylated pillar[5]arene to obtain *per*-hydroxylated pillar[5]arene by treating with excess BBr₃ was reported by Ogoshi *et al.*[101] Subsequent optimization of reaction condition by tuning the feed ratio of BBr₃ and reaction temperature resulted in selective deprotection.[113] Alternatively, deprotection can be performed by selective oxidative dearomatization of preformed *per*-alkylated pillar[5]arene to obtain pillar[4]arene[1]quinone and pillar[3]arene[2]quinone using phenyliodine bis(trifluoroacetate) (PIFA) or ceric ammonium nitrate (CAN) followed by reduction of the benzoquinone units employing sodium dithionite or sodium borohydride as reductant.[114] Pan and Xue were able to oxidize selectively the alkoxy group in the pillar[5]arene protected by ester and alkyl groups to pillar[2]arene[3]quinones and reduce them to corresponding hydroquinones.[115]

Macrocyclization of functionalized monomer[116] or cocylization[117] of two different types of 1,4-dialkoxylated monomers resulted in the formation of mono-,[118] di-[119] and tetra-[120] functionalized pillar[5]arene. Synthesis of *per*-functionalized pillar[5]arenes by etherification or esterification of *per*-hydroxylated pillar[5]arene are reported. The sodium salt of decacarboxylate pillar[5]arene,[121] obtained by the hydrolysis of decaester, and amphiphilic *per*-triethylene oxide appended pillar[5]arene,[122] obtained by etherification, are found to be water soluble. Palladium catalyzed coupling reaction

attempted on the A1/A2 ditriflate afforded π-conjugated pillar[5]arenes (Fig. 1.16a).[123] The copper(I) catalyzed Huisgen alkyne-azide 1,3-dipolar cycloaddition reactions (CuAAC) carried out on pillar[5]arenes to append various functional groups have manifested in intriguing physical properties of functionalized pillar[5]arenes (Fig. 1.16b).[124]
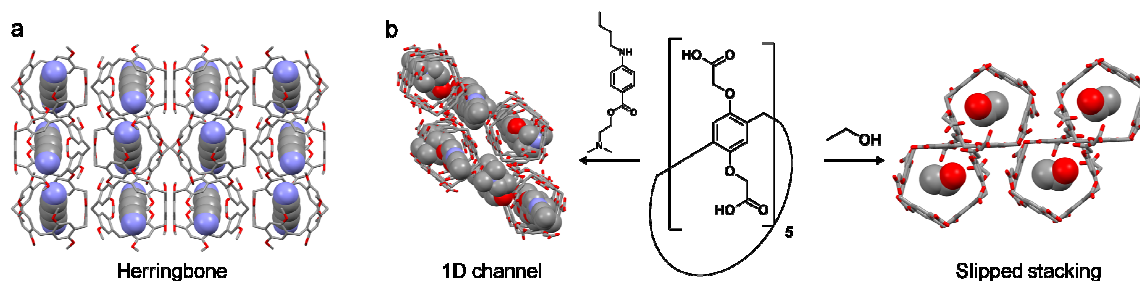
Fig. 1.17 (a) Herringbone crystal packing observed in *per*-methylated pillar[5]arene crystallized from acetonitrile. (b) Two different crystal packing of *per*-carboxylated pillar[5]arene depending on solvent and guest inclusion. Crystal structures courtesy of CCDC.

1.5.5.4 Solid-state assembly of pillar[5]arenes

The solid-state assembly of pillar[5]arenes with various guests and in presence of different solvents is an interesting field of study as this would shed light on the way the host may interact with the guests. Pillar[5]arenes assemble in three different ways: herringbone,[101,114b,125] slipped-stacks[104,115,126] and one-dimensional channels.[114a,125a,127] The solvents and guests play a pivotal role in assembling the pillar[5]arene units in the crystal lattice. Ogoshi *et al.* reported that *per*-ethylated pillar[5]arene forms two different types of crystal packing - herringbone in acetone and 1D channels in chloroform under hexane vapor.[128] Pillar[5]arenes appended with ten carboxylic acids crystallized with slipped-stacking arrangement in 1:1 ethanol-water mixture, but upon encapsulation of the guest tetracaine hydrochloride the macrocycles crystallized as 1D channels (Fig. 1.17).[129]

1.5.5.5 Host-guest chemistry of pillar[5]arenes

Noncovalent interactions such as electrostatic force of attraction, charge transfer, van der Waals, π-π and hydrogen bonding bring about molecular recognition between the host and guest. Pillar[5]arenes bestowed with a symmetrical pentagonal shape and possessing five electron rich *per*-alkylated/hydroxylated benzene units make them exceptional donors that would form inclusion complexes with electron acceptors. Cations

such as viologen,[101] pyridinium[130] and imidazolium[131] interact with the pillar[5]arene owing to cation-π interactions as evident from spectroscopic studies and crystal structures. Pillar[5]arene adorned with ten ethylene oxides on the rims encapsulates viologen[126a] and a vinylogous viologen salt[132] with the aid of noncovalent interactions *viz.* CH/O, CH/π and face-to-face π-stacking. Furthermore, cation-π interactions play a pivotal role in the complexation of *per*-butylated pillar[5]arenes with quarternary ammonium salt octatrimethylammonium hexafluorophosphate.[117] Similarly, *per*-methylated pillar[5]arene encapsulates the secondary ammonium salt *n*-octylethylammonium hexafluorophosphate (Fig. 1.19a).[133] In these cases, in addition to cation-π interactions, host-guest complexation is reinforced by multiple NH-π interactions. The nature of counteranions tremendously influences the strength of association between the host and guest. The *n*-octylethylammonium chloride being a strong ion pair in chloroform relative to *n*-octylethylammonium hexafluorophosphate reduces the ability of cation to bind with pillar[5]arene. Water soluble pillar[5]arenes, appended with carboxylate anions at the rims, by virtue of having five substituted benzene moieties, possess hydrophobic cavity capable of accommodating hydrophobic guests in aqueous environment. Amino acids containing two or more basic nitrogen containing groups, such as arginine, lysine and histidine, form inclusion complexes with water soluble pillar[5]arenes.[134] Furthermore, long chain diacids[135] and alkyl diamines[136] (Fig. 1.19b) get encapsulated inside the cavity of pillar[5]arene ascribed to electrostatic interactions and CH/π interactions. Interestingly, *per*-butylated pillar[5]arenes form inclusion complexes with neutral linear alkane, in particular - *n*-hexane in solid-state with CH/π and CH/O interactions playing the role (Fig. 1.19c).[117]
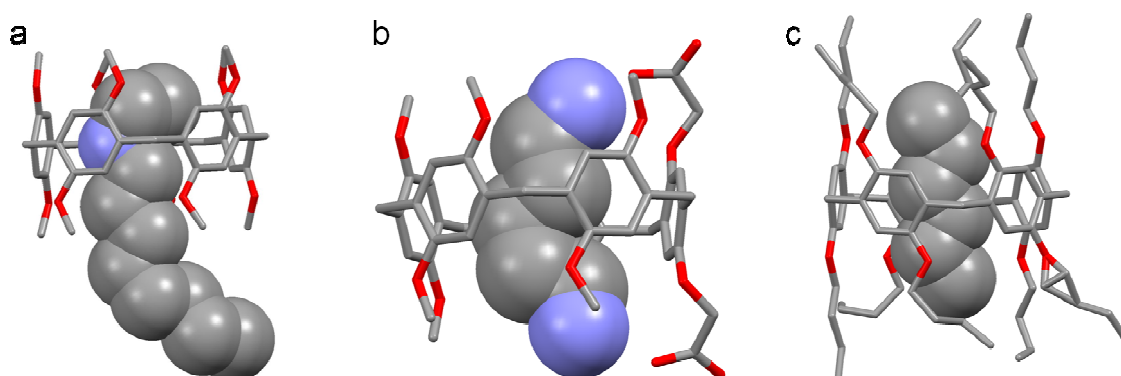

Fig. 1.19 Host-guest complexation of pillar[5]arenes: inclusion complexes of (a) *per*-methylated pillar[5]arene and *n*-octylethylammonium cation, (b) diacid pillar[5]arene and *n*-pentyldiamine, and (c) *per*-butylated pillar[5]arene and *n*-hexane. Crystal structures courtesy of CCDC.

Li and coworkers reported regioselective inclusion complex of nonsymmetric pillar[5]arene with non-symmetric guest bearing cyano and bromide groups.[137] The same group introduced pH responsive host-guest complexation of *per*-hydroxylated pillar[5]arene and 1,4-bis(imidazolium)butane, wherein the complexation is driven by cation-π interactions.[138] Ogoshi *et al.* studied the rate of complexation/decomplexation in a photoresponsive inclusion complex of *per*-hydroxylated pillar[5]arene and an axle having photoreversible azobenzene at one end and adamantyl in the other. The exchange rate observed in *trans* was much faster than in *cis* as a result of increased free energy of activation.[139] Cohen's group employed water soluble pillar[5]arene, appended with ten carboxylate ions on the rims, to encapsulate the hydrophobic xenon and studied the change in the microenvironment around the element by ^{129}Xe NMR. The xenon, otherwise insoluble, readily dissolved in the aqueous medium. The downfield shift in the NMR signal was observed upon addition of hydrophobic *n*-hexane.[140] Yaun and coworkers were successful in using pillar[5]arenes possessing ten phosphine oxides or diglycolamide on its rims to selectively entrap *f*-block elements.[141]

1.5.6 Pillar[5]quinone

Pillar[5]quinone (P5Q) is a fascinating cyclic pentaquinone adorned with five benzoquinones linked by a methylene bridge at 2,5-positions (Fig. 1.20a). P5Q could be obtained by completely oxidizing the *per*-hydroxylated pillar[5]arene. Cao and Meier reported for the first time the synthesis of P5Q using ceric ammonium nitrate in 62% yield. However, the reported compound was likely to be contaminated with metal impurities which gave P5Q a red coloration.[72b] Subsequently, Shivakumar and Sanjayan synthesized highly pure, yellow colored P5Q by employing hypervalent iodine reaction and thus circumventing contamination by metal impurities.[72a,142] The reaction was facile and possessed the advantage of easily scaling up to several grams. Further, the same group reported the formation of self-assembled rod-shaped structures of P5Q mediated by solvent 1,1,2,2-tetrachloroethane. The crystal structure of microcrystalline P5Q obtained by the combination of synchrotron X-ray diffraction and ^{13}C high resolution solid-state NMR revealed pentagonal shape of molecule with a single enantiomer (details in chapter II).[143]
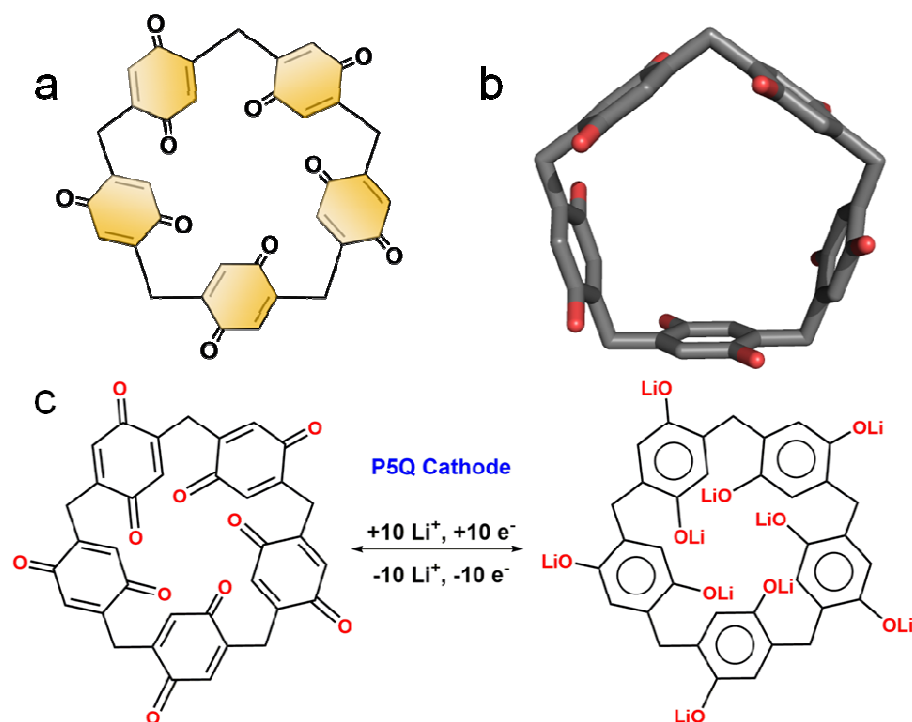
Fig. 1.20 (a) Molecular structure of pillar[5]quinone (P5Q). (b) Crystal structure of P5Q. (c) Schematic representation of P5Q as cathode in lithium ion battery applications.

Consequently, several groups successfully brought out the applications of P5Q, particularly, in the field of material science using the hypervalent iodine reaction. Chen and coworkers fabricated an all-solid-state lithium ion battery comprising P5Q as cathode and obtained a high initial capacity of 418 mAh g^{-1} with a stable cyclability.[144] The presence of ten carbonyl groups symmetrically placed above and below the rim uptook the lithium ions (Fig. 1.20b). Cheng and Kaifer studied the cathodic voltammetric behavior of P5Q and observed that only eight among ten electrons could be fed into the molecule in a 2-1-2 pattern.[145] Recently, Ogoshi *et al.* employed pentagonal P5Q along with hexagonal pillar[6]arene in 12:20 feed ratio to obtain spherical vesicles.[146] Shivakumar *et al.* employed electron deficient P5Q as acceptor and complexed with charge donor molecules like tetrathiafulvalene (TTF) and 4,4'-Bis(N-carbazolyl)-1,1'-biphenyl (CBP) to obtain green and brown charge transfer crystals, respectively. Both the CT complexes showcased mixed stacking with former in dimers of donors and acceptors while the latter as single donor and acceptor. The TTF-P5Q complex exhibited unprecedented 'room temperature ferroelectricity in TTF-quinone system' (details in chapter III).[147]

1.6 References

(1) Grabowski, Z. R.; Rotkiewicz, K.; Rettig, W. *Chem. Rev.* **2003**, *103*, 3899.

(2) Goetz, K. P.; Vermeulen, D.; Payne, M. E.; Kloc, C.; McNeil, L. E.; Jurchescu, O. D. *J. Mater. Chem. C* **2014**, *2*, 3065.

(3) van de Wouw, H. L.; Chamorro, J.; Quintero, M.; Klausen, R. S. *J. Chem. Educ.* **2015**, *92*, 2134.

(4) Zhylitskaya, H.; Cybińska, J.; Chmielewski, P.; Lis, T.; Stępień, M. *J. Am. Chem. Soc.* **2016**, *138*, 11390.

(5) Hantzsch, A. *Chem. Ber.* **1905**, *38*, 2161.

(6) Tinkler, C. K. *J. Chem. Soc., Trans.* **1909**, *95*, 921.

(7) Ostromisslensky, I. *Chem.Ber.* **1911**, *44*, 268.

(8) Tinkler, C. K. *J. Chem. Soc., Trans.* **1913**, *103*, 2171.

(9) Pfeiffer, P.; Schmidt, J. *Organische molekulverbindungen*; Ferdinand Enke, 1927.

(10) Bennett, G. M.; Willis, G. H. *J. Chem. Soc.* **1929**, 256.

(11) Briegleb, G. *Z. Phys. Chem.* **1932**, *B16*, 249.

(12) Gibson, R. E.; Loeffler, O. *J. Am. Chem. Soc.* **1940**, *62*, 1324.

(13) Hammick, D. L.; Yule, R. *J. Chem. Soc.* **1940**, 1539.

(14) Weiss, J. *J. Chem. Soc.* **1942**, 245.

(15) Woodward, R. *J.Am.Chem.Soc.* **1942**, *64*, 3058.

(16) Brackman, W. *Rec. trav. chim.* **1949**, *68*, 147.

(17) a) Mulliken, R. S. *J. Phys. Chem.* **1952**, *56*, 801; b) Mulliken, R. S. *J. Am. Chem. Soc.* **1952**, *74*, 811.

(18) Murrell, J. N. *J. Am. Chem. Soc.* **1959**, *81*, 5037.

(19) Dewar, M. J. S.; Thompson, C. C. *Tetrahedron Suppl.* **1966**, *7*, 97.

(20) Le Fevre, R. J. W.; Radford, D.; Stiles, P. *J. Chem. Soc. (B)* **1968**, 1297.

(21) Hanna, M. W. *J. Am. Chem. Soc.* **1968**, *90*, 285.

(22) Ferraris, J.; Cowan, D.; Walatka, V. t.; Perlstein, J. *J. Am. Chem. Soc.* **1973**, *95*, 948.

(23) Alves, H.; Molinari, A. S.; Xie, H.; Morpurgo, A. F. *Nat. Mater.* **2008**, *7*, 574.

(24) Ishiguro, T.; Yamaji, K.; Saito, G. *Organic superconductors*; Springer Science & Business Media, 2012; Vol. 88.

(25) Tayi, A. S.; Kaeser, A.; Matsumoto, M.; Aida, T.; Stupp, S. I. *Nat. Chem.* **2015**, *7*, 281.

(26) a) Dogru, M.; Handloser, M.; Auras, F.; Kunz, T.; Medina, D.; Hartschuh, A.; Knochel, P.; Bein, T. *Angew. Chem. Int. Ed.* **2013**, *52*, 2920; b) Dogru, M.; Handloser, M.; Auras, F.; Kunz, T.; Medina, D.; Hartschuh, A.; Knochel, P.; Bein, T. *Angew. Chem.* **2013**, *125*, 2992; c) Alves, H.; Pinto, R. M.; Maçôas, E. S. *Nat. Commun.* **2013**, *4*, 1842.

(27) Itahara, H.; Maesato, M.; Asahi, R.; Yamochi, H.; Saito, G. *J. Electron. Mater.* **2009**, *38*, 1171.

(28) a) Shil, S.; Paul, S.; Misra, A. *J.Phys. Chem. C* **2013**, *117*, 2016; b) Qin, W.; Chen, X.; Li, H.; Gong, M.; Yuan, G.; Grossman, J. C.; Wuttig, M.; Ren, S. *ACS Nano* **2015**, *9*, 9373.

(29) Jerome, D.; Mazaud, A.; Ribault, M.; Bechgaard, K. *J. Phys. Lett.* **1980**, *41*, 95.

(30) Zhu, L.; Yi, Y.; Li, Y.; Kim, E.-G.; Coropceanu, V.; Brédas, J.-L. *J. Am. Chem. Soc.* **2012**, *134*, 2340.

(31) Shokaryev, I.; Buurma, A.; Jurchescu, O.; Uijttewaal, M.; de Wijs, G.; Palstra, T.; de Groot, R. *J. Phys. Chem. A* **2008**, *112*, 2497.

(32) Soos, Z.; Keller, H.; Moroni, W.; Nöthe, D. *Ann. N.Y. Acad. Sci.* **1978**, *313*, 442.

(33) a) Mori, T.; Kawamoto, T. *Annu. Rep. Prog., Sect. C Phys. Chem.* **2007**, *103*, 134; b) Torrance, J. B. *Mol. Cryst. Liq. Cryst.* **1985**, *126*, 55.

(34) Herbstein, F. H. *Crystalline molecular complexes and compounds: structures and principles*; Oxford University Press: New York, 2005.

(35) García, P.; Dahaoui, S.; Fertey, P.; Wenger, E.; Lecomte, C. *Phys. Rev. B* **2005**, *72*, 104115.

(36) Prout, C. K.; Tickle, I. J.; Wright, J. D. *J. Chem. Soc., Perkin Trans. 2* **1973**, 528.

(37) Tickle, I. J.; Prout, C. K. *J. Chem. Soc., Perkin Trans. 2* **1973**, 720.

(38) Boeyens, J.; Herbstein, F. *J. Phys. Chem.* **1965**, *69*, 2153.

(39) Kistenmacher, T.; Emge, T.; Wiygul, F.; Bryden, W.; Chappell, J.; Stokes, J.; Chiang, L.; Cowan, D.; Bloch, A. *Solid State Commun.* **1981**, *39*, 415.

(40) Kistenmacher, T. J.; Phillips, T. E.; Cowan, D. O. *Acta Cryst. B* **1974**, *30*, 763.

(41) Kistenmacher, T. J.; Emge, T. J.; Bloch, A.; Cowan, D. *Acta Crystallogr., Sect. B: Struct. Crystallogr. Cryst. Chem.* **1982**, *38*, 1193.

(42) Bechgaard, K.; Kistenmacher, T. J.; Bloch, A. N.; Cowan, D. O. *Acta Crystallogr. Sect. B: Struct. Crystallogr. .Cryst. Chem.* **1977**, *33*, 417.

(43) a) Li, J.; Liu, Y.; Zhang, Y.; Cai, H.-L.; Xiong, R.-G. *Phys. Chem. Chem. Phys.* **2013**, *15*, 20786; b) Lines, M. E.; Glass, A. M. *Principles and applications of ferroelectrics and related materials*; Oxford university press, 1977.

(44) a) Scott, J. *Science* **2007**, *315*, 954; b) James, S.; Arujo, P.; Carlos, A. *Science* **1989**, *246*, 1400.

(45) Scott, J. F. *Ferroelectric memories*; Springer Science & Business Media: Heidelberg, 2013; Vol. 3.

(46) Horiuchi, S.; Tokura, Y. *Nat. Mater.* **2008**, *7*, 357.

(47) Cohen, R. E. *Nature* **1992**, *358*, 136.

(48) Tayi, A. S.; Kaeser, A.; Matsumoto, M.; Aida, T.; Stupp, S. I. *Nat. Chem.* **2015**, *7*, 281.

(49) Kobayashi, K.; Horiuchi, S.; Kumai, R.; Kagawa, F.; Murakami, Y.; Tokura, Y. *Phys. Rev. Lett.* **2012**, *108*, 237601.

(50) Pandeeswar, M.; Senanayak, S. P.; Narayan, K. S.; Govindaraju, T. *J. Am. Chem. Soc.* **2016**, *138*, 8259.

(51) Horiuchi, S.; Tokunaga, Y.; Giovannetti, G.; Picozzi, S.; Itoh, H.; Shimano, R.; Kumai, R.; Tokura, Y. *Nature* **2010**, *463*, 789.

(52) Horiuchi, S.; Kagawa, F.; Hatahara, K.; Kobayashi, K.; Kumai, R.; Murakami, Y.; Tokura, Y. *Nat. Commun.* **2012**, *3*, 1308.

(53) Kundys, B.; Lappas, A.; Viret, M.; Kapustianyk, V.; Rudyk, V.; Semak, S.; Simon, C.; Bakaimi, I. *Phys. Rev. B* **2010**, *81*, 224434.

(54) a) Piecha, A.; Gągor, A.; Jakubas, R.; Szklarz, P. *CrystEngComm* **2013**, *15*, 940; b) Fu, D.-W.; Cai, H.-L.; Liu, Y.; Ye, Q.; Zhang, W.; Zhang, Y.; Chen, X.-Y.; Giovannetti, G.; Capone, M.; Li, J. *Science* **2013**, *339*, 425.

(55) Fu, D. W.; Zhang, W.; Cai, H. L.; Ge, J. Z.; Zhang, Y.; Xiong, R. G. *Adv. Mater.* **2011**, *23*, 5658.

(56) Lippert, E.; Lüder, W.; Boos, H. *Advances in molecular spectroscopy* Oxford, Pergamon, 1962.

(57) Valeur, B.; Berberan-Santos, M. N. *Molecular fluorescence: principles and applications*; John Wiley & Sons: Singapore, 2012.

(58) Tan, Y.; Yu, J.; Gao, J.; Cui, Y.; Wang, Z.; Yang, Y.; Qian, G. *RSC Adv.* **2013**, *3*, 4872.

(59) Brédas, J.-L.; Beljonne, D.; Coropceanu, V.; Cornil, J. *Chem. Rev.* **2004**, *104*, 4971.

(60) a) Jia, C.; Liu, S. X.; Tanner, C.; Leiggener, C.; Neels, A.; Sanguinet, L.; Levillain, E.; Leutwyler, S.; Hauser, A.; Decurtins, S. *Chem. Eur. J.* **2007**, *13*, 3804; b) Otón, F.;

Lloveras, V.; Mas-Torrent, M.; Vidal-Gancedo, J.; Veciana, J.; Rovira, C. *Angew. Chem. Int. Ed.* **2011**, *50*, 10902.

(61) Paz-Tal Levi, O.; Becker, J. Y.; Ellern, A.; Khodorkovsky, V. *Tetrahedron Lett.* **2001**, *42*, 1571.

(62) Pop, F.; Amacher, A.; Avarvari, N.; Ding, J.; Daku, L. M. L.; Hauser, A.; Koch, M.; Hauser, J.; Liu, S. X.; Decurtins, S. *Chem. Eur. J.* **2013**, *19*, 2504.

(63) Nishida, S.; Morita, Y.; Fukui, K.; Sato, K.; Shiomi, D.; Takui, T.; Nakasuji, K. *Angew. Chem.* **2005**, *117*, 7443.

(64) Pop, F.; Riobé, F. o.; Seifert, S.; Cauchy, T.; Ding, J.; Dupont, N.; Hauser, A.; Koch, M.; Avarvari, N. *Inorg. Chem.* **2013**, *52*, 5023.

(65) McNaught, A. D.; Wilkinson, A. *Compendium of chemical terminology. IUPAC recommendations*; Blackwell Scientific Publications: Oxford (United Kingdom), 1997.

(66) a) Crini, G. *Chem. Rev.* **2014**, *114*, 10940; b) Wenz, G.; Han, B.-H.; Müller, A. *Chem. Rev.* **2006**, *106*, 782; c) Khan, A. R.; Forgo, P.; Stine, K. J.; D'Souza, V. T. *Chem. Rev.* **1998**, *98*, 1977.

(67) a) Pedersen, C. J. *J. Am. Chem. Soc.* **1967**, *89*, 2495; b) Pedersen, C. J. *J. Am. Chem. Soc.* **1967**, *89*, 7017.

(68) a) Gutsche, C. D. *Calixarenes: an introduction*; Royal Society of Chemistry, 2008; b) Gutsche, C. D. *Acc. Chem. Res.* **1983**, *16*, 161.

(69) a) Kaifer, A. E. *Acc. Chem. Res.* **2014**, *47*, 2160; b) Isaacs, L. *Acc. Chem. Res.* **2014**, *47*, 2052; c) Lagona, J.; Mukhopadhyay, P.; Chakrabarti, S.; Isaacs, L. *Angew. Chem. Int. Ed.* **2005**, *44*, 4844; d) Lee, J. W.; Samal, S.; Selvapalam, N.; Kim, H.-J.; Kim, K. *Acc. Chem. Res.* **2003**, *36*, 621.

(70) Ogoshi, T.; Kanai, S.; Fujinami, S.; Yamagishi, T.-a.; Nakamoto, Y. *J. Am. Chem. Soc.* **2008**, *130*, 5022.

(71) Ogoshi, T.; Yamagishi, T.-a.; Nakamoto, Y. *Chem. Rev.* **2016**, *116*, 7937.

(72) a) Shivakumar, K. I.; Sanjayan, G. J. *Synthesis* **2013**, *45*, 896; b) Cao, D.; Kou, Y.; Liang, J.; Chen, Z.; Wang, L.; Meier, H. *Angew. Chem. Int. Ed.* **2009**, *48*, 9721.

(73) Villiers, A. *Compt. Rend. Fr. Acad. Sci* **1891**, *112*, 435.

(74) Rekharsky, M. V.; Inoue, Y. *Chem. Rev.* **1998**, *98*, 1875.

(75) a) Harada, A.; Hashidzume, A.; Yamaguchi, H.; Takashima, Y. *Chem. Rev.* **2009**, *109*, 5974; b) Nepogodiev, S. A.; Stoddart, J. F. *Chem. Rev.* **1998**, *98*, 1959.

(76) Uekama, K.; Hirayama, F.; Irie, T. *Chem. Rev.* **1998**, *98*, 2045.

(77) Strasser, B. O.; Popov, A. I. *J. Am. Chem. Soc.* **1985**, *107*, 7921.

(78) Lee, D. G.; Chang, V. S. *J. Org. Chem.* **1978**, *43*, 1532.

(79) Dietrich, B.; Lehn, J.; Sauvage, J. *Tetrahedron Lett.* **1969**, *10*, 2889.

(80) Baeyer, A. v. *Ber. Dtsh. Chem. Ges.* **1872**, *5*, 280.

(81) Gutsche, C. D.; Muthukrishnan, R. *J. Org. Chem.* **1978**, *43*, 4905.

(82) Stewart, D. R.; Gutsche, C. D. *J. Am. Chem. Soc.* **1999**, *121*, 4136.

(83) Atwood, J. L.; Koutsantonis, G. A.; Raston, C. L. *Nature* **1994**, *368*, 229.

(84) a) Shinkai, S.; Mori, S.; Koreishi, H.; Tsubaki, T.; Manabe, O. *J. Am. Chem. Soc.* **1986**, *108*, 2409; b) Shinkai, S.; Mori, S.; Tsubaki, T.; Sone, T.; Manabe, O. *Tetrahedron Lett.* **1984**, *25*, 5315.

(85) Ikeda, A.; Shinkai, S. *Chem. Rev.* **1997**, *97*, 1713.

(86) Schazmann, B.; Alhashimy, N.; Diamond, D. *J. Am. Chem. Soc.* **2006**, *128*, 8607.

(87) Morohashi, N.; Narumi, F.; Iki, N.; Hattori, T.; Miyano, S. *Chem. Rev.* **2006**, *106*, 5291.

(88) Schühle, D. T.; Schatz, J.; Laurent, S.; Vander Elst, L.; Muller, R. N.; Stuart, M. C. A.; Peters, J. A. *Chem. Eur. J.* **2009**, *15*, 3290.

(89) MacGillivray, L. R.; Atwood, J. L. *Nature* **1997**, *389*, 469.

(90) Cram, D. J.; Karbach, S.; Kim, Y. H.; Baczynskyj, L.; Kallemeyn, G. W. *J. Am. Chem. Soc.* **1985**, *107*, 2575.

(91) a) Kim, S. K.; Sessler, J. L. *Acc. Chem. Res.* **2014**, *47*, 2525; b) Gale, P. A.; Sessler, J. L.; Král, V.; Lynch, V. *J. Am. Chem. Soc.* **1996**, *118*, 5140.

(92) Behrend, R.; Meyer, E.; Rusche, F. *Justus Liebigs Ann. Chem.* **1905**, *339*, 1.

(93) Freeman, W.; Mock, W.; Shih, N. *J. Am. Chem. Soc.* **1981**, *103*, 7367.

(94) Kim, J.; Jung, I.-S.; Kim, S.-Y.; Lee, E.; Kang, J.-K.; Sakamoto, S.; Yamaguchi, K.; Kim, K. *J. Am. Chem. Soc.* **2000**, *122*, 540.

(95) Ko, Y. H.; Kim, E.; Hwang, I.; Kim, K. *Chem. Commun.* **2007**, 1305.

(96) Zhao, J.; Kim, H. J.; Oh, J.; Kim, S. Y.; Lee, J. W.; Sakamoto, S.; Yamaguchi, K.; Kim, K. *Angew. Chem. Int. Ed.* **2001**, *40*, 4233.

(97) Jon, S. Y.; Selvapalam, N.; Oh, D. H.; Kang, J.-K.; Kim, S.-Y.; Jeon, Y. J.; Lee, J. W.; Kim, K. *J. Am. Chem. Soc.* **2003**, *125*, 10186.

(98) Zhao, N.; Lloyd, G. O.; Scherman, O. A. *Chem. Commun.* **2012**, *48*, 3070.

(99) Lucas, D.; Minami, T.; Iannuzzi, G.; Cao, L.; Wittenberg, J. B.; Anzenbacher Jr, P.; Isaacs, L. *J. Am. Chem. Soc.* **2011**, *133*, 17966.

(100) a) Svec, J.; Necas, M.; Sindelar, V. *Angew. Chem.* **2010**, *122*, 2428; b) Miyahara, Y.; Goto, K.; Oka, M.; Inazu, T. *Angew. Chem. Int. Ed.* **2004**, *43*, 5019.

(101) Ogoshi, T.; Kanai, S.; Fujinami, S.; Yamagishi, T.-a.; Nakamoto, Y. *J. Am. Chem. Soc.* **2008**, *130*, 5022.

(102) Ogoshi, T.; Kitajima, K.; Umeda, K.; Hiramitsu, S.; Kanai, S.; Fujinami, S.; Yamagishi, T.-a.; Nakamoto, Y. *Tetrahedron* **2009**, *65*, 10644.

(103) Brotin, T.; Dutasta, J.-P. *Chem. Rev.* **2008**, *109*, 88.

(104) Ogoshi, T.; Aoki, T.; Kitajima, K.; Fujinami, S.; Yamagishi, T.-a.; Nakamoto, Y. *J. Org. Chem.* **2011**, *76*, 328.

(105) Boinski, T.; Szumna, A. *Tetrahedron* **2012**, *68*, 9419.

(106) Ma, Y.; Zhang, Z.; Ji, X.; Han, C.; He, J.; Abliz, Z.; Chen, W.; Huang, F. *Eur. J. Org. Chem.* **2011**, *2011*, 5331.

(107) a) Cao, J.; Shang, Y.; Qi, B.; Sun, X.; Zhang, L.; Liu, H.; Zhang, H.; Zhou, X. *RSC Adv.* **2015**, *5*, 9993; b) Tao, H.; Cao, D.; Liu, L.; Kou, Y.; Wang, L.; Meier, H. *Sci.China Chem.* **2012**, *55*, 223.

(108) Ogoshi, T.; Ueshima, N.; Akutsu, T.; Yamafuji, D.; Furuta, T.; Sakakibara, F.; Yamagishi, T.-a. *Chem. Commun.* **2014**, *50*, 5774.

(109) Holler, M.; Allenbach, N.; Sonet, J.; Nierengarten, J.-F. *Chem. Commun.* **2012**, *48*, 2576.

(110) Santra, S.; Kopchuk, D.; Kovalev, I.; Zyryanov, G.; Majee, A.; Charushin, V.; Chupakhin, O. *Green Chem.* **2016**, *18*, 423.

(111) Hu, X.-B.; Chen, Z.; Chen, L.; Zhang, L.; Hou, J.-L.; Li, Z.-T. *Chem. Commun.* **2012**, *48*, 10999.

(112) Ogoshi, T.; Ueshima, N.; Sakakibara, F.; Yamagishi, T.-a.; Haino, T. *Org. Lett.* **2014**, *16*, 2896.

(113) a) Han, J.; Hou, X.; Ke, C.; Zhang, H.; Strutt, N. L.; Stern, C. L.; Stoddart, J. F. *Org. Lett.* **2015**, *17*, 3260; b) Chen, Y.; He, M.; Li, B.; Wang, L.; Meier, H.; Cao, D. *RSC Adv* **2013**, *3*, 21405; c) Ogoshi, T.; Demachi, K.; Kitajima, K.; Yamagishi, T.-a. *Chem. Commun.* **2011**, *47*, 7164.

(114) a) Ogoshi, T.; Yamafuji, D.; Kotera, D.; Aoki, T.; Fujinami, S.; Yamagishi, T.-a. *J. Org. Chem.* **2012**, *77*, 11146; b) Han, C.; Zhang, Z.; Yu, G.; Huang, F. *Chem. Commun.* **2012**, *48*, 9876.

(115) Pan, M.; Xue, M. *Eur. J. Org. Chem.* **2013**, *2013*, 4787.

(116) a) Nierengarten, I.; Guerra, S.; Holler, M.; Karmazin-Brelot, L.; Barberá, J.; Deschenaux, R.; Nierengarten, J. F. *Eur. J. Org. Chem.* **2013**, *2013*, 3675; b) Deng, H.; Shu, X.; Hu, X.; Li, J.; Jia, X.; Li, C. *Tetrahedron Lett.* **2012**, *53*, 4609.

(117) Zhang, Z.; Xia, B.; Han, C.; Yu, Y.; Huang, F. *Org. Lett.* **2010**, *12*, 3285.

(118) a) Strutt, N. L.; Forgan, R. S.; Spruell, J. M.; Botros, Y. Y.; Stoddart, J. F. *J. Am. Chem. Soc.* **2011**, *133*, 5668; b) Liu, L.; Cao, D.; Jin, Y.; Tao, H.; Kou, Y.; Meier, H. *Org. Biomol. Chem.* **2011**, *9*, 7007.

(119) Duan, Q.; Xia, W.; Hu, X.; Ni, M.; Jiang, J.; Lin, C.; Pan, Y.; Wang, L. *Chem. Commun.* **2012**, *48*, 8532.

(120) Wei, P.; Yan, X.; Li, J.; Ma, Y.; Huang, F. *Chem. Commun.* **2013**, *49*, 1070.

(121) Ogoshi, T.; Hashizume, M.; Yamagishi, T.-a.; Nakamoto, Y. *Chem. Commun.* **2010**, *46*, 3708.

(122) Ogoshi, T.; Shiga, R.; Yamagishi, T.-a. *J. Am. Chem. Soc.* **2012**, *134*, 4577.

(123) Ogoshi, T.; Yamafuji, D.; Akutsu, T.; Naito, M.; Yamagishi, T.-a. *Chem. Commun.* **2013**, *49*, 8782.

(124) Strutt, N. L.; Zhang, H.; Schneebeli, S. T.; Stoddart, J. F. *Acc. Chem. Res.* **2014**, *47*, 2631.

(125) a) Strutt, N. L.; Fairen-Jimenez, D.; Lehl, J.; Lalonde, M. B.; Snurr, R. Q.; Farha, O. K.; Hupp, J. T.; Stoddart, J. F. *J. Am. Chem. Soc.* **2012**, *134*, 17436; b) Shu, X.; Fan, J.; Li, J.; Wang, X.; Chen, W.; Jia, X.; Li, C. *Org. Biomol. Chem.* **2012**, *10*, 3393.

(126) a) Chi, X.; Xue, M.; Yao, Y.; Huang, F. *Org. Lett.* **2013**, *15*, 4722; b) Ogoshi, T.; Kitajima, K.; Aoki, T.; Fujinami, S.; Yamagishi, T.-a.; Nakamoto, Y. *J. Org. Chem.* **2010**, *75*, 3268; c) Han, C.; Ma, F.; Zhang, Z.; Xia, B.; Yu, Y.; Huang, F. *Org. Lett.* **2010**, *12*, 4360.

(127) a) Yao, Y.; Xue, M.; Chen, J.; Zhang, M.; Huang, F. *J. Am. Chem. Soc.* **2012**, *134*, 15712; b) Zhang, Z.; Luo, Y.; Xia, B.; Han, C.; Yu, Y.; Chen, X.; Huang, F. *Chem. Commun.* **2011**, *47*, 2417; c) Si, W.; Hu, X.-B.; Liu, X.-H.; Fan, R.; Chen, Z.; Weng, L.; Hou, J.-L. *Tetrahedron Lett.* **2011**, *52*, 2484.

(128) Ogoshi, T.; Sueto, R.; Yoshikoshi, K.; Sakata, Y.; Akine, S.; Yamagishi, T. *Angew. Chem. Int. Ed.* **2015**, *54*, 9849.

(129) Danylyuk, O.; Sashuk, V. *CrystEngComm* **2015**, *17*, 719.

(130) Li, C.; Xu, Q.; Li, J.; Yao, F.; Jia, X. *Org. Biomol. Chem.* **2010**, *8*, 1568.

(131) Ogoshi, T.; Tanaka, S.; Yamagishi, T.-a.; Nakamoto, Y. *Chem. Lett.* **2011**, *40*, 96.

(132) Chi, X.; Xue, M. *RSC Adv.* **2014**, *4*, 365.

(133) Han, C.; Yu, G.; Zheng, B.; Huang, F. *Org. Lett.* **2012**, *14*, 1712.

(134) Li, C.; Ma, J.; Zhao, L.; Zhang, Y.; Yu, Y.; Shu, X.; Li, J.; Jia, X. *Chem. Commun.* **2013**, *49*, 1924.

(135) Hu, X.-B.; Chen, L.; Si, W.; Yu, Y.; Hou, J.-L. *Chem. Commun.* **2011**, *47*, 4694.

(136) Yu, G.; Hua, B.; Han, C. *Org. Lett.* **2014**, *16*, 2486.

(137) Shu, X.; Chen, W.; Hou, D.; Meng, Q.; Zheng, R.; Li, C. *Chem. Commun.* **2014**, *50*, 4820.

(138) Li, C.; Zhao, L.; Li, J.; Ding, X.; Chen, S.; Zhang, Q.; Yu, Y.; Jia, X. *Chem. Commun.* **2010**, *46*, 9016.

(139) Ogoshi, T.; Yamafuji, D.; Aoki, T.; Yamagishi, T.-a. *J. Org. Chem* **2011**, *76*, 9497.

(140) Adiri, T.; Marciano, D.; Cohen, Y. *Chem. Commun.* **2013**, *49*, 7082.

(141) Wu, L.; Fang, Y.; Jia, Y.; Yang, Y.; Liao, J.; Liu, N.; Yang, X.; Feng, W.; Ming, J.; Yuan, L. *Dalton Trans.* **2014**, *43*, 3835.

(142) Sanjayan, G. J.; Shivakumar, K. I. (CSIR, India). Process for the preparation of pillar[5]quinone. US Patent 9000224, April 7, 2015.

(143) Shivakumar, K. I.; Yan, Y.; Hughes, C. E.; Apperley, D. C.; Harris, K. D.; Sanjayan, G. J. *Cryst. Growth Des.* **2015**, *15*, 1583.

(144) Zhu, Z.; Hong, M.; Guo, D.; Shi, J.; Tao, Z.; Chen, J. *J. Am. Chem. Soc.* 2014, *136*, 16461.

(145) Cheng, B.; Kaifer, A. E. *J. Am. Chem. Soc.* 2015, *137*, 9788.

(146) Ogoshi, T.; Sueto, R.; Yoshikoshi, K.; Yasuhara, K.; Yamagishi, T.-a. *J. Am. Chem. Soc.* 2016, *138*, 8064.

(147) a) Shivakumar, K. I.; Swathi, K.; Goudappagouda, T.; Das, T.; Kumar, A.; Makde, R. D.; Vanka, K.; Narayan, K. S.; Babu, S. S.; Sanjayan, G. J. *Unpublished manuscript* **2017**;   b) Shivakumar, K. I.; Gonnade, R.; Sanjayan, G. J. *Unpublished manuscript* **2017**.

Chapter 2

Part A: An easy and multigram synthesis of pillar[5]quinone

*Part B: Solvent-assisted solid-state self-assembly of pillar[5]quinone*

Part A: *An Easy and Multigram Synthesis of Pillar[5]quinone*

2.1 Introduction

Pillar[5]arenes,[1] a novel class of fascinating cyclophanes, continuous to attract the attention of chemists and the interest in this class of macrocycles continues unabated essentially due to their enormous application potential in diverse areas.[2] The most notable feature of pillar[5]arenes is their deep π-encircled internal cavity – capable of accommodating guest molecules through diverse non-covalent interactions, thereby raising the hope of developing molecular sensors.[3] It is noteworthy that by virtue of their structural architecture, cycloquinones adorned with deep internal cavity - indispensable for molecular sensing, are also being increasingly explored for the development of molecular sensors exhibiting redox active properties.[4] A recently reported quinone-based, redox-active resorcin[4]arene cavitand is one such candidate which is capable of forming kinetically stable host–guest complexes whose binding affinity can be modulated by altering the redox state of the cavitand.[5] However, the quinone rings in the aforementioned system do not form part of the cyclamer backbone.
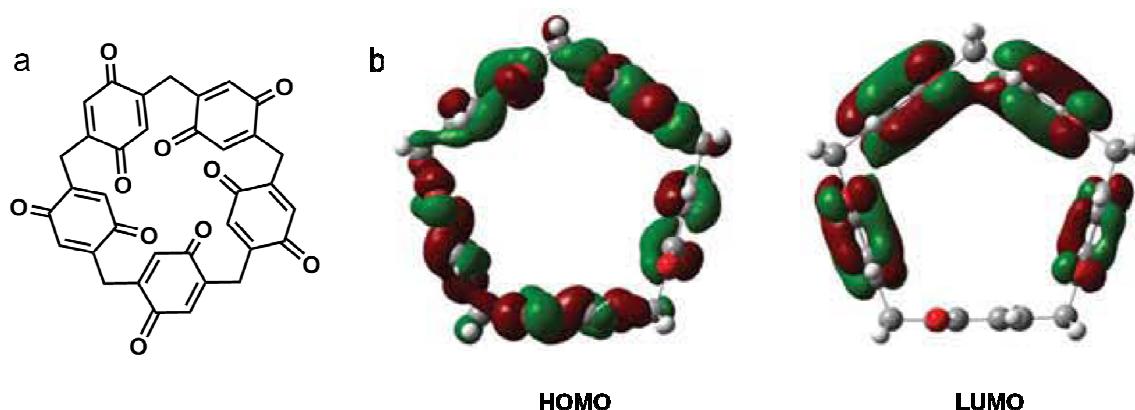
Fig. 2.1 (a) Molecular structure of P5Q, (b) Frontier orbitals of HOMO and LUMO of P5Q.[6] Fig. 2.1b is reproduced, with permission, from ref 6. Copyright © 2011 John Wiley and Sons.

2.2 Objective of the present work

Envisaging the importance of the P5Q in the domain of materials chemistry, we sought to obtain P5Q in a facile way and in significant amounts using inexpensive and environmentally benign starting materials.

2.3 Methods

This work describes a facile and multi-gram scale synthesis of P5Q – a lemon yellow microcrystalline fibrous material, by the oxone®-iodobenzene-mediated oxidative *de-aromatization* of the readily available *per*-methylated pillar[5]arene.[7] Employing this easy-to-operate methodology, without any involvement of tedious isolation and chromatographic procedures, we have been able to synthesize P5Q in amounts – up to seven grams. Purification was simply effected by an efficient single crystallization protocol (Scheme 2.1).

P5Q had earlier been obtained by the cerium(IV)ammonium nitrate-mediated oxidation of 1,4-diethoxypillar[5]arene, which in turn was obtained by the acid-catalyzed rearrangement of 2,5-bis(benzyloxymethyl)-1,4-diethoxybenzene. The one-step ready availability of *per*-methylated pillar[5]arene[7] in huge amounts from commercially available and inexpensive 1,4-dimethoxybenzene triggered us to exploit it as the starting material and the highly efficient oxone®-iodobenzene oxidant system[8] as the environmentally benign reagent for effecting oxidative demethylation – avoiding the generation of heavy metal waste, particularly when the reaction is done in a large scale.

Pillar[5]quinone (P5Q) (Fig. 2.1a) is structurally unique in this aspect not only because of the fact that all the five quinone rings are part of the cyclamer backbone, but also due to the symmetrical crowning of the periphery by ten carbonyl oxygen atoms. Indeed, computational studies have suggested that P5Q could exhibit intramolecular charge transfer upon excitation of electrons from HOMO to LUMO, ascribed to the large difference in the electron distribution between them (Fig. 2.1b).[6] Moreover, P5Q-derived systems have been predicted to be promising candidates for trapping anionic halogens.[6] All these properties and their potential applications make P5Q a highly beneficial building block for researchers. In this direction, ready access to P5Q in significant quantities would clearly be of considerable importance.

**Scheme 2.1** Synthesis of pillar[5]quinone (P5Q)
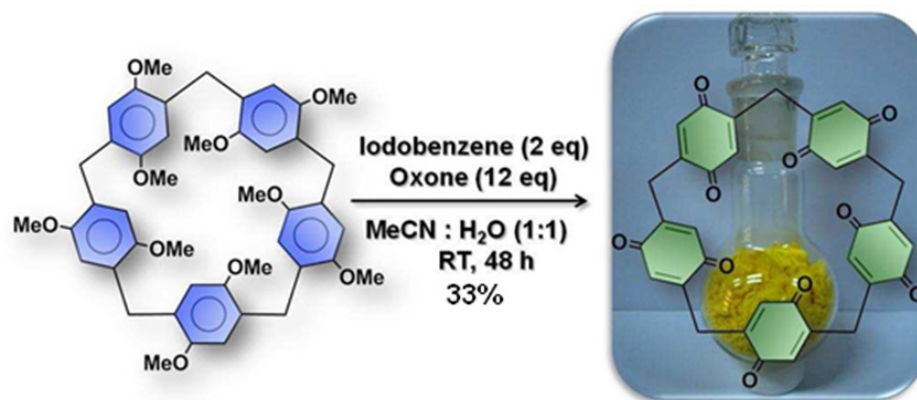
2.4 Results and discussion

One of the best reaction media recommended for performing the oxone[®]-iodobenzene-mediated oxidative *de-aromatization* of *p*-dialkoxybenzenes to *p*-quinones is acetonitrile-water (1:1).[8b] Although catalytic amount of iodobenzene has been suggested to be sufficient for bringing out exceptional product conversion, the poor solubility of *per*-methylated pillar[5]arene in aqueous acetonitrile prompted us to utilize at least 2 equivalents of iodobenzene and 12 equivalents of oxone[®] ($2KHSO_5 \cdot KHSO_4 \cdot K_2SO_4$) to guarantee maximum yield of the product (Scheme 2.1). Isolation of the product was remarkably simple. After stirring for 48 h, the reaction mixture was poured into water, filtered and washed sequentially with hot water (to completely remove oxone[®]), and methanol (to completely remove iodobenzene, and its oxidized species), and finally crystallizing the dried material from hot 1,1,2,2-tetrachloroethane (TCE). Evaporation of the TCE mother liquor and trituration of the residue with methanol afforded unreacted starting material. By following this procedure (Scheme 2.1), we have been able to synthesize P5Q in large amounts. It is our observation that during dissolution of the crude P5Q in hot TCE while crystallization, there remains some small amounts of insoluble brownish-colored material, which has not yet been characterized owing to its insolubility in common organic solvents. Fortunately, this insoluble impurity could be readily eliminated by filtration of the crude P5Q in hot TCE.

It is noteworthy that, the *per*-methylated pillar[5]arene we employed in the reaction was crystallized from boiling chlorobenzene. We have found that chlorobenzene is a very good solvent for crystallizing large quantities of *per*-methylated pillar[5]arene, since substantial amount of *per*-methylated pillar[5]arene can be dissloved in boiling chlorobenzene, from which it crystallizes out upon cooling. Furthermore, it is our

observation that efficient stirring is critical for the success of the oxidative de-aromatization reaction, since the starting material have always been found to remain as a suspension due to its poor solubility in the reaction solvent. In fact, trials using 1 equiv of iodobenzene on a smaller scale with 1 day reaction time did not have considerable effect on the product yield.
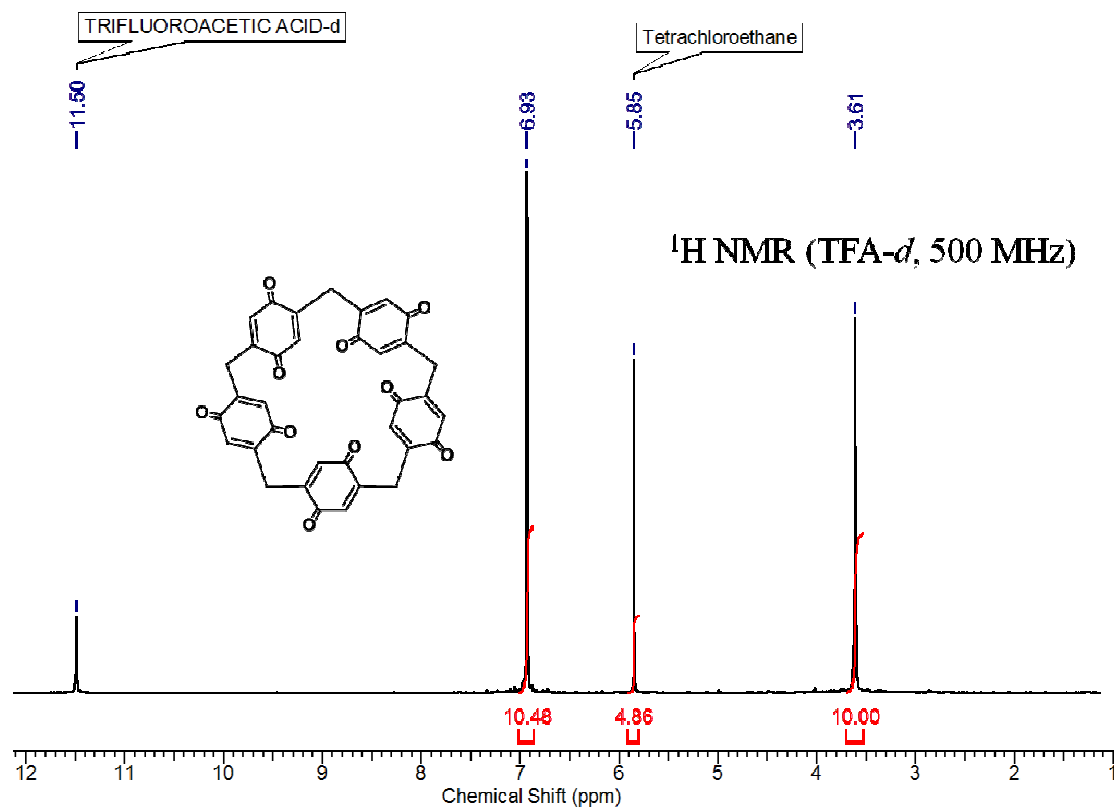

Fig. 2.2 ^{1}H NMR spectrum of pillar[5]quinone crystallized from 1,1,2,2-tetrachloroethane showing the presence of around two molecules of solvent.
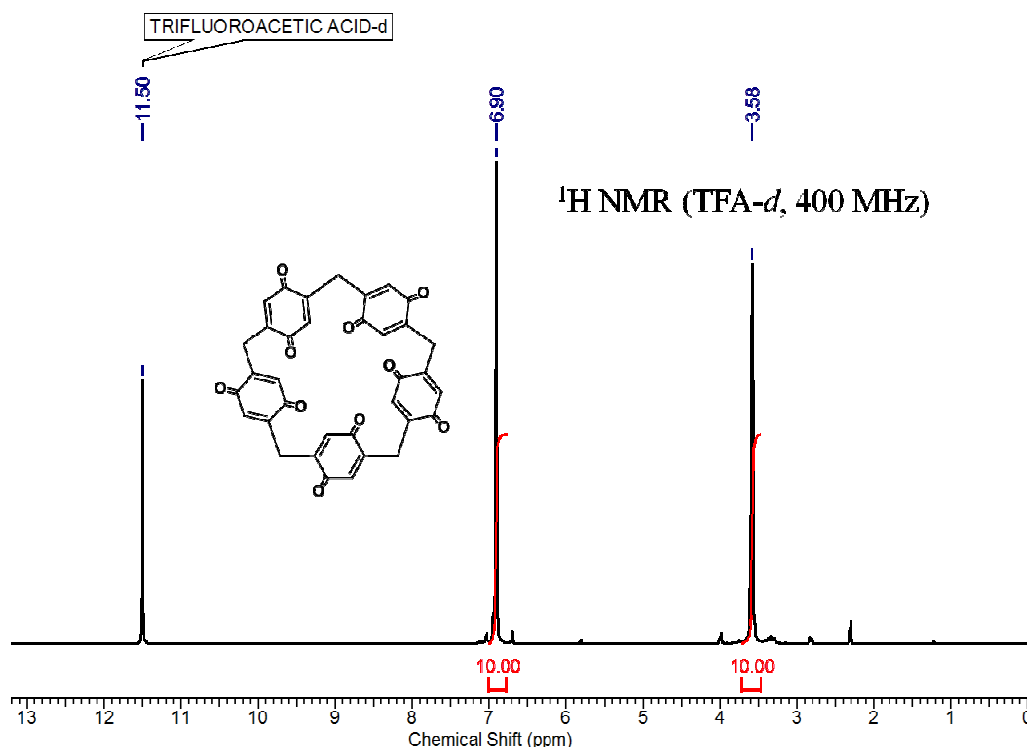
Fig. 2.3 ^{1}H NMR spectrum of pillar[5]quinone crystallized from 1,1,2,2-tetrachloroethane after methanol wash.

We explored several solvents to dissolve P5Q in an effort to grow crystals suitable for single crystal X-ray diffraction studies, but in vain. The major problem is its poor solubility in most of the organic solvents, except hexafluoroisopropanol (HFIP) and trifluoroacetic acid (TFA) in which it is readily soluble at room temperature, although good quality crystals, suitable for crystal structure studies, could not be obtained. P5Q has been found to be sparingly soluble in most of the chlorinated solvents. However, P5Q could be crystallized from hot TCE, affording lemon-yellow fibrous and fluffy microcrystals – retaining 2.5 equivalents of TCE in the crystal lattice, as evident from its ^{1}H NMR (Fig. 2.2). The associated TCE can be readily removed by washing the TCE-crystallized fibrous mass, before drying, with methanol, followed by prolonged drying under vacuum affording yellowish P5Q (Fig. 2.3). It has been found that hot acidic solvents like acetic and formic acids too, interestingly though, solubilize P5Q apparently by protonation of the outer rim carbonyl oxygens, although it precipitates upon cooling. The fine crystallinity of freshly crystallized P5Q, although not suitable for single crystal X-ray studies, is clearly evident from its microscopy images (Fig. 2.4).
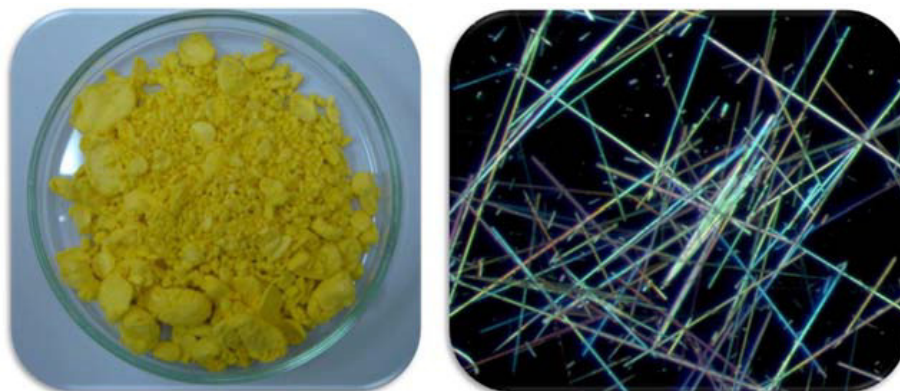
Fig. 2.4 Freshly crystallized P5Q from 1,1,2,2-tetrachloroethane (left) and its stereo microscope image (right).

2.5 Conclusions

In summary, this work unveils an easy-to-operate and chromatography-free synthetic strategy that can afford the valuable macrocyclic quinone P5Q in multi-gram quantities, as demonstrated herein (see experimental details, *vide infra*). The use of environmentally benign hypervalent-iodine oxidant system derived from iodobenzene-oxone®, which allows quick scale up, is further noteworthy. The remarkable ease with which P5Q has been synthesized in multi-gram quantity is expected to steer supramolecular host-guest chemistry and material property investigations of this unique cyclooligomeric quinone.
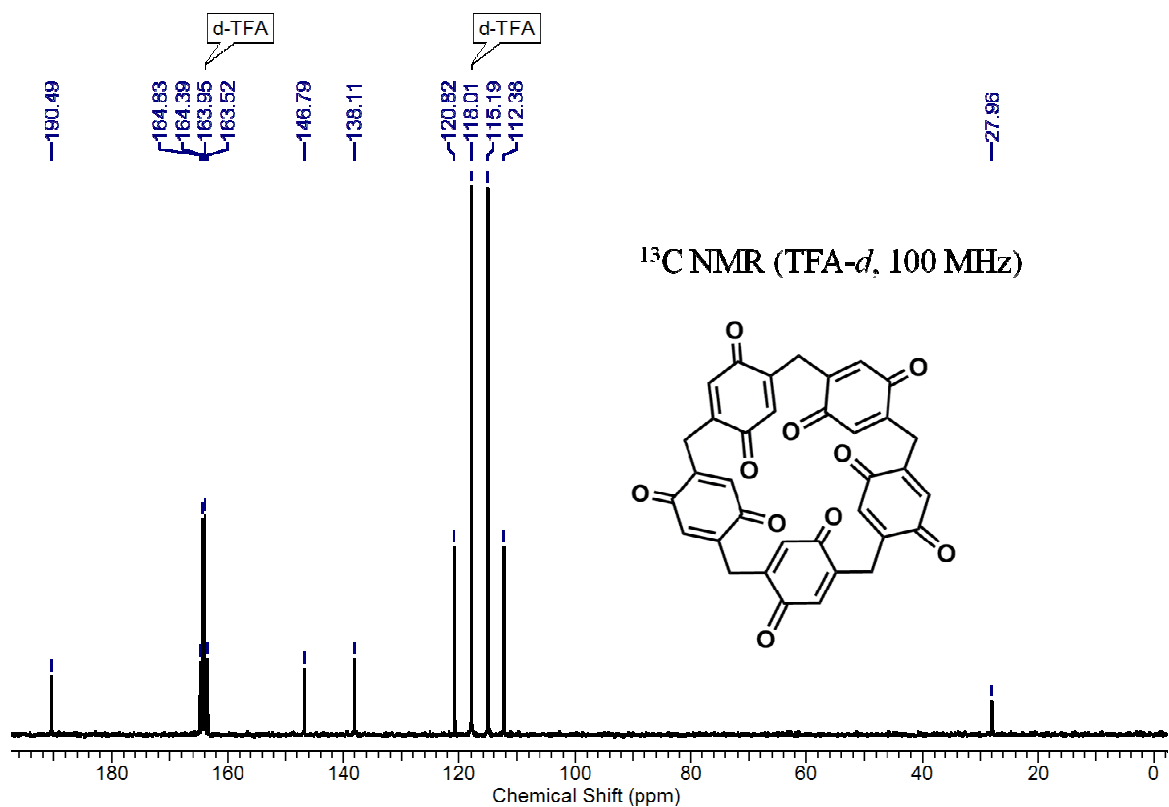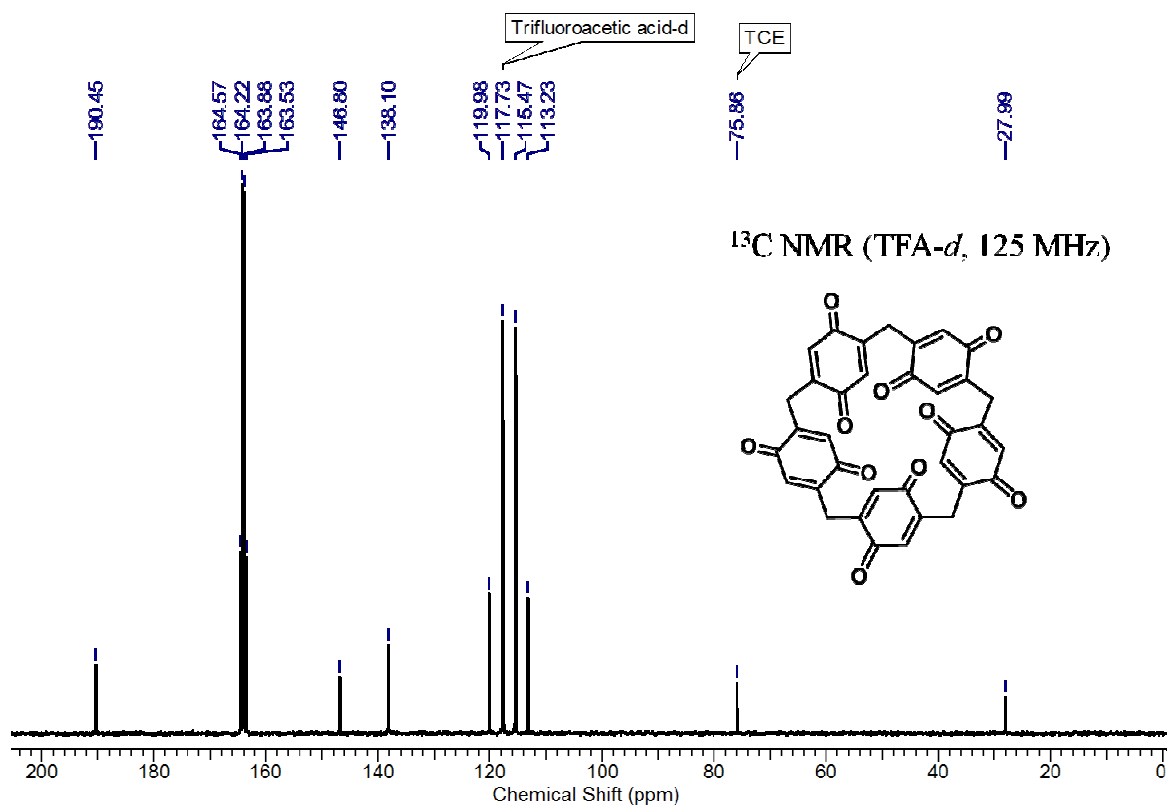
2.6 Experimental Section

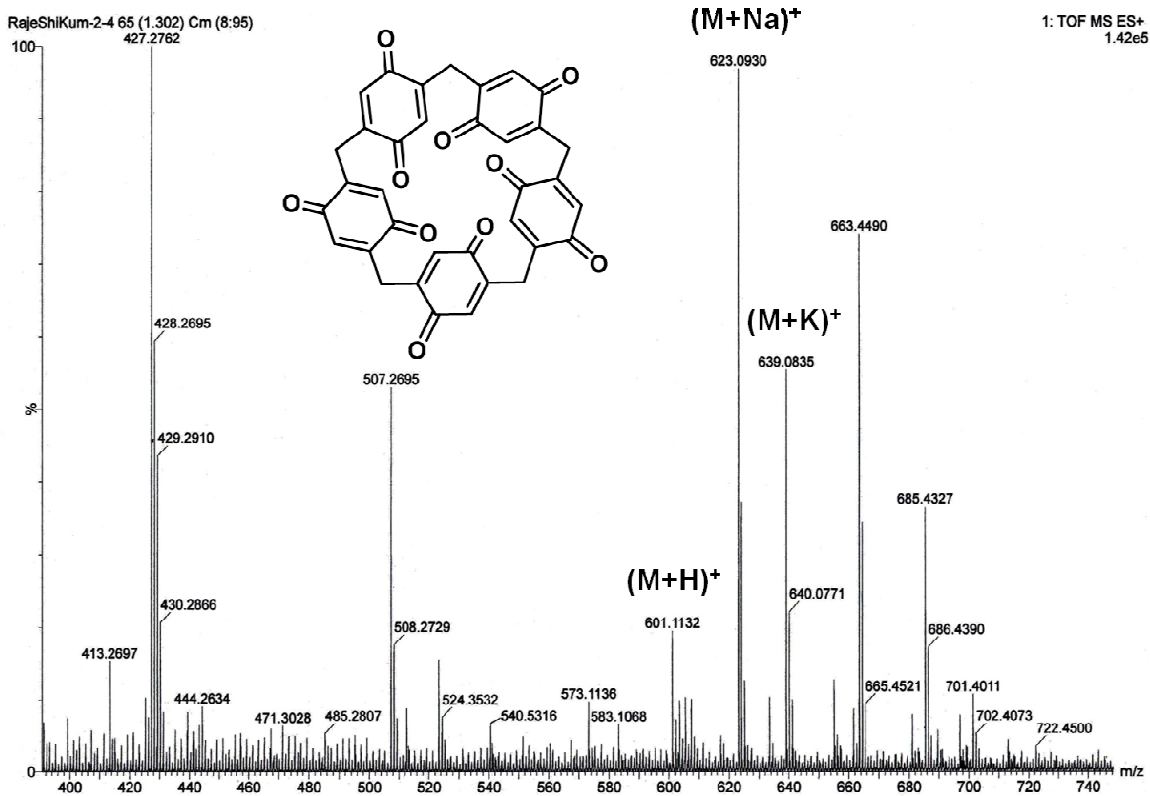**Synthesis of Pillar[5]quinone**

A single-necked 2 L round bottom flask was charged with finely ground 1,4-dimethoxypillar[5]arene[7] (25.0 g, 33.3 mmol), acetonitrile (350 mL) and a solution of oxone ($2KHSO_5 \cdot KHSO_4 \cdot K_2SO_4$, 122.9 g, 400.0 mmol) in water (350 mL). To the above mixture, iodobenzene (7.5 mL, 66.6 mmol) was added. The reaction mixture, after vigorously stirring at room temperature for 48 hours, was poured into water and filtered under suction. The yellow colored residue was repeatedly washed with plenty of water followed by methanol and dried. Purification was carried out by the following crystallization procedure: The crude compound (18.264 g) was first dissolved in boiling 1,1,2,2-tetrachloroethane (TCE, 350 mL), and filtered under suction to remove some undissolved brownish material (0.813 g), which was discarded. The reddish-colored clear

filtrate was left at room temperature for 6 h (substantial amount of P5Q crystallized out during this period), and later maintained at ~ 6-10 ^{o}C for 8 h. The microcrystalline mass was filtered under suction, washed with small portions of chilled TCE (3 x 10 mL) and methanol (3 x 15 mL), and dried over P_2O_5, to afford P5Q as a lemon-yellow colored light-weight solid (6.66 g, 33%) without the associated TCE molecules. mp: compound does not melt, but decomposes above 250 ^{o}C; IR (Nujol mull, ν (cm^{-1})): 1654 (m), 1610 (m), 1461 (s), 1377 (s), 1286 (m), 1250 (m), 1125 (m), 921 (m), 722 (m); ^{1}H NMR (trifluoroacetic acid-*d*, 500 MHz, ppm): δ 6.93 (s, 10H, quinone CH), δ 3.61 (s, 10H, methylene protons); ^{13}C NMR (trifluoroacetic acid-*d*, 125 MHz, ppm) δ 190.5 (C of carbonyl), δ 146.8 (C of quinone ring attached to methylene group), δ 138.1 (tertiary C of quinone ring), δ 28.0 (methylene C); HRMS (TOF MS ES+): calcd for $C_{35}H_{21}O_{10}$ (M+H)$^+$: 601.1129, found: 601.1132; calcd for $C_{35}H_{20}O_{10}Na$ (M+Na)$^+$: 623.0949, found: 623.0930.

The TCE filtrate was evaporated under reduced pressure and the reddish residue was triturated with hot methanol (100 mL), and filtered (while hot) and dried to afford an off-white residue which was found to be the starting material (8.371 g). Thus, yield of crystallized P5Q based on recovered starting material is 50%.

Note: ¹H NMR spectra of P5Q with (top) and without (bottom) associated TCE molecules.

RajeShiKum-2-4 65 (1.302) Cm (8:95)

1: TOF MS ES+
1.42e5

100

%

0

(M+Na)+

(M+K)+

(M+H)+

427.2762
428.2695
429.2910
430.2866
413.2697
444.2634
471.3028
485.2807
507.2695
508.2729
524.3532
540.5316
573.1136
583.1068
601.1132
623.0930
639.0835
640.0771
663.4490
665.4521
685.4327
686.4390
701.4011
702.4073
722.4500

400 420 440 460 480 500 520 540 560 580 600 620 640 660 680 700 720 740   m/z

Part B: Solvent-Assisted Solid-State Self-Assembly of Pillar[5]quinone

2.7 Introduction

Self-assembly of organic molecules driven by non-covalent interactions has acquired widespread attention in recent years, as the intriguing supramolecular architectures that result have applications in several areas such as optoelectronics, biomimetics, catalysis and medicine.[9] Self-organization of molecules due to supramolecular interactions encompassing hydrogen bonding, π-stacking, van der Waals interactions and electrostatic forces have been studied extensively.[10] In some cases, solvents can play a pivotal role in dictating the supramolecular assembly. The shape, size and polarity of solvents along with solvophobic interactions may organize molecules resulting in supramolecular chirogenesis,[11] chirality inversion,[12] gelation,[13] host-guest complexation[14] and oligomer folding.[15]

Pillar[5]arene[16] is an electron-rich symmetrical cavitand, which joined the family of macrocyclic hosts[17] in 2008. In addition to showing promise in sensing applications,[18] pillar[*n*]arene analogues are also reported to self-assemble and form supramolecular polymers,[19] polyrotaxanes,[20] polypseudo-rotaxanes[21] and other nanoscale architectures,[2g,22] aided by hydrogen bonding and cation-π interactions. In contrast to pillar[*n*]arenes, which have electron-rich cavities, pillar[*n*]quinones[23] have electron-deficient cavities and are expected to be potential candidates for anion sensing.[23b] Lately, organic compounds such as calixquinones have been explored increasingly as cathodes in lithium battery applications.[24] It is noteworthy that P5Q, which encloses two additional carbonyl groups compared to calix[4]quinone, is potentially also a promising candidate for lithium-ion battery applications.
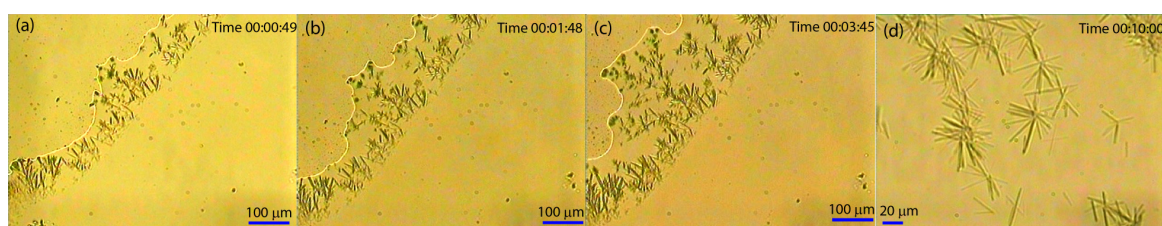

Fig. 2.5 Polarizing optical microscopy images (a, b, c, d) captured on time-scale showcasing the growth of self-assembly of pillar[5]quinone in 1,1,2,2-tetrachloroethane.

2.8 Solid-State Self-Assembly of P5Q

Isolation of P5Q from the oxidative mixture containing oxone/iodobenzene used for oxidative dearomatization of dimethoxypillar[5]arene proved to be highly challenging.[23c]

The poor solubility of P5Q in almost all common organic solvents prompted us to explore other solvents. Serendipitously, P5Q was found to dissolve readily in boiling 1,1,2,2-tetrachloroethane (TCE). Cooling this solution led to precipitation of a microcrystalline, fibrous, fluffy yellow solid. The presence of two molecules of TCE per molecule of P5Q in the crystal structure was evident from the solution-state ^{1}H NMR spectrum of the dissolved material (Fig. 2.2). The TCE solvate of P5Q is formed swiftly (in *ca*. 10mins) on cooling, growing as rod-shaped crystallites (Figure 2.5) of length *ca*. 20 – 40 µm as observed from polarizing optical microscopy. In fact, these rods agglomerate in solution on attaining the room temperature, giving a feather-weighted polycrystalline material.
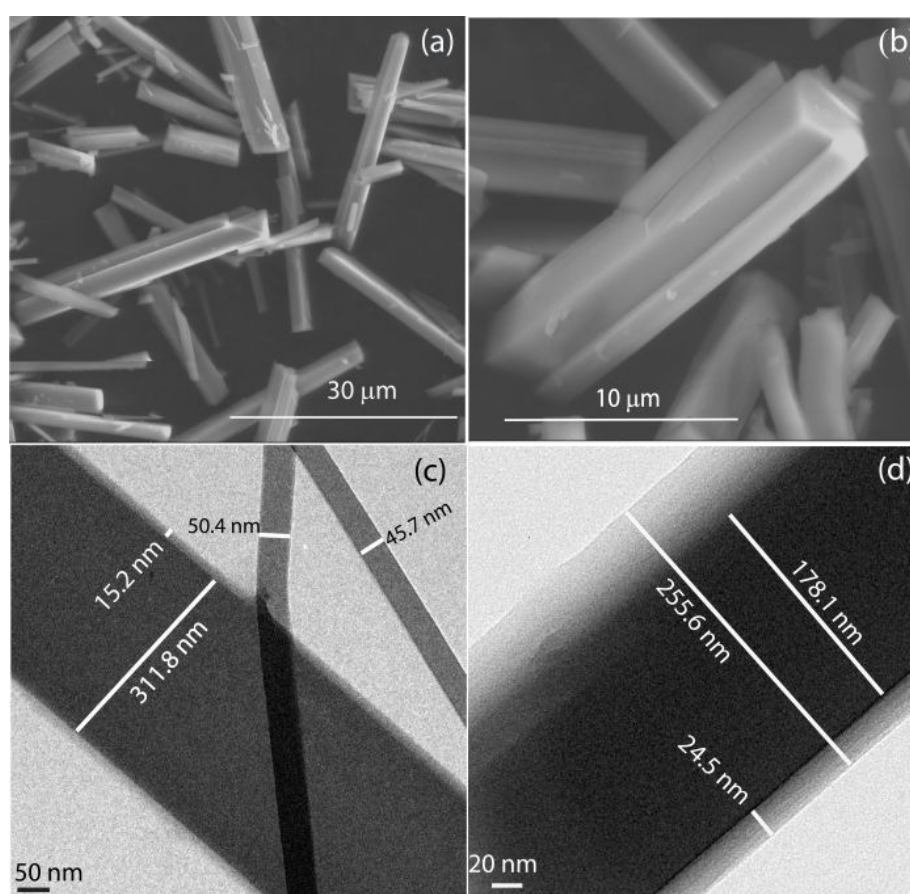
Fig. 2.6 Representative images of crystallites of P5Q.2TCE recorded using: (a,b) SEM, (c,d) TEM.

The surface topography of P5Q.2TCE investigated (Fig. 2.6a-d) by scanning electron microscopy (SEM) and transmission electron microscopy (TEM) revealed rod-shaped structures which extended to few µm in length and *ca*. 200 – 300 nm in width. The rod-shaped morphology was not retained when the solvent TCE was stripped off[23c] using methanol (Fig. 2.7), demonstrating that the presence of TCE is essential for the formation

of supramolecular assembly. Apparently, the rod shaped architectures are bundled nano-tubular structures formed by columnar stacking of P5Q, as observed from the SEM images of P5Q obtained subsequent to removal of TCE, which shows unbundling of the stacked nanotubes.
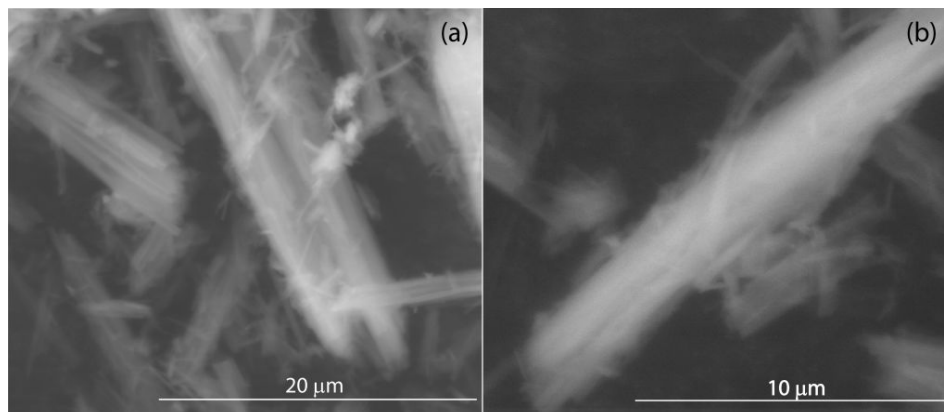
Fig. 2.7 (a, b) Representative SEM images of the P5Q obtained following removal of the solvent TCE from the P5Q. 2TCE.

2.9 Structure determination of P5Q. 2TCE from powder X-ray diffraction data

While single-crystal X-ray diffraction (XRD) is the most powerful experimental technique for ascertaining crystal structures, the requirement for a suitable single-crystal specimen enforces a limitation on the applicability of this technique. When a suitable single crystal cannot be obtained, as in the case of P5Q.2TCE, structure determination becomes challenging and must be tackled instead from powder XRD data. However, the task of carrying out structure determination by powder XRD is considerably more challenging than by single-crystal XRD, particularly in the case of organic materials. Nevertheless, the opportunities for structure determination of organic materials from powder XRD data have advanced considerably in recent years,[25] particularly through the development of the direct-space strategy for structure solution.

The powder XRD pattern of P5Q.2TCE was recorded at room temperature in transmission mode on a Bruker D8 instrument using Ge-monochromated CuKα_1 radiation (2θ range, 4 – 50°; total time, 48 h). The powder XRD pattern was indexed using the TREOR code[26] in the program CRYSFIRE,[27] giving the following unit cell with orthorhombic metric symmetry: a = 18.29 Å, b = 15.26 Å, c = 6.91 Å (V = 1929.9 Å^3). The high-resolution solid-state ^{13}C NMR spectrum showcases two crystallographically distinct TCE molecules, supporting an asymmetric unit with stoichiometry P5Q.2TCE.

Considering the volume of the unit cell and density, the number of formula units P5Q.2TCE in the unit cell was assigned as Z = 2.

Initial profile fitting performed using the Le Bail method[28] in the GSAS program[29] did not yield an acceptable quality of fit. However, by reducing the symmetry to monoclinic and allowing one angle in the above unit cell to relax, an improved fit was realized (Fig. 2.8 R_{wp} = 1.13%; R_p = 0.87%) for the following unit cell: a = 18.7709(4) Å, b = 15.2498(4) Å, c = 6.90511(17) Å, β = 89.7359(15)°. The correct space group could not be assigned unequivocally on the basis of systematic absences alone and structure solution was attempted for each of the space groups P2, P2$_1$, Pm, P2$_1$/n P2/m, P2/n and P2$_1$/m. The refined unit cell and profile parameters obtained from the Le Bail fit were employed in the subsequent structure-solution calculations.
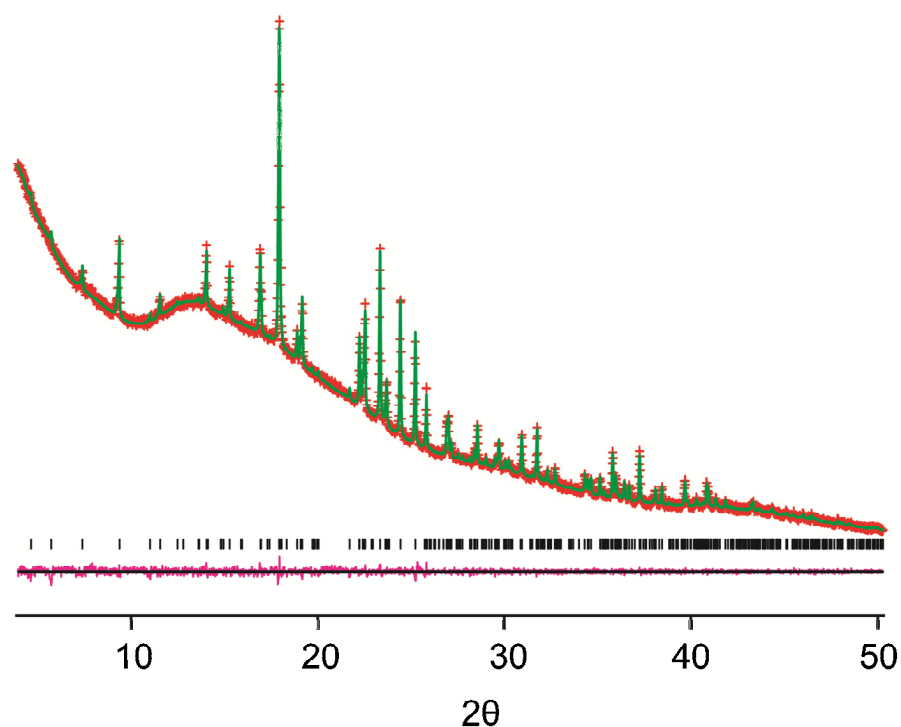

Fig. 2.8 Le Bail fit of the powder XRD pattern of P5Q.2TCE for space group P2$_1$ (red + marks, experimental data; green line, calculated data; purple line, difference plot; black tick marks, predicted peak positions).

Structure solution was executed using the direct-space genetic algorithm (GA) technique[30] incorporated in the program EAGER.[31] Initial calculations were carried out on a number of monoclinic space groups: P2, P2$_1$, Pm, P2$_1$/n P2/m, P2/n and P2$_1$/m. The model constituted one P5Q molecule and two TCE molecules for the order 2 space groups and half P5Q molecule and one TCE molecule for the order 4 space groups. The best fit to

the experimental powder XRD data was found for space group $P2_1$. However, the model failed to provide an adequate description of one TCE molecule in the crystal structure, with considerable features in the difference Fourier map in the vicinity of this molecule. For this reason, a revised model was considered in which disorder of this TCE molecule was introduced as two distinct components each with occupancy of 0.5. The GA structure-solution calculation was repeated for this model in space group $P2_1$. Each trial structure was defined by a total of 26 variables (11 positional, 12 rotational and 3 torsional variables). The P5Q molecule was treated as rigid while varying one torsional angle for each TCE molecule. One positional variable (on the P5Q molecule) was fixed as the origin may be freely defined along the *b*-axis in space group $P2_1$.

In total, 16 independent GA structure-solution calculations were performed. Each calculation involved the evolution of 1000 generations for a population of 100 structures, with 10 mating operations and 50 mutation operations carried out per generation. All 16 calculations congregated essentially on the same structure solution, corresponding to the lowest value of R_{wp}.

The best structure solution (i.e., the structure with lowest R_{wp} attained in the GA calculations) was used as the initial structural model for Rietveld refinement,[32] which was performed using the GSAS program. However, positioning the disordered TCE molecule was found to be unreasonable. Accordingly, the disordered TCE molecules were eliminated and Rietveld refinement was performed. The Fourier difference map calculated following this refinement showcased two strong positions of electron deficiency and chlorine atoms were positioned at each of these positions. Rietveld refinement was again performed, followed by calculation of another Fourier difference map. Again, two chlorine atoms were placed at the positions of largest electron deficiency and Rietveld refinement was executed, followed by Fourier difference calculation. In the end, two carbon atoms were added to the structural model at the positions of highest electron deficiency and a final Rietveld refinement was performed.
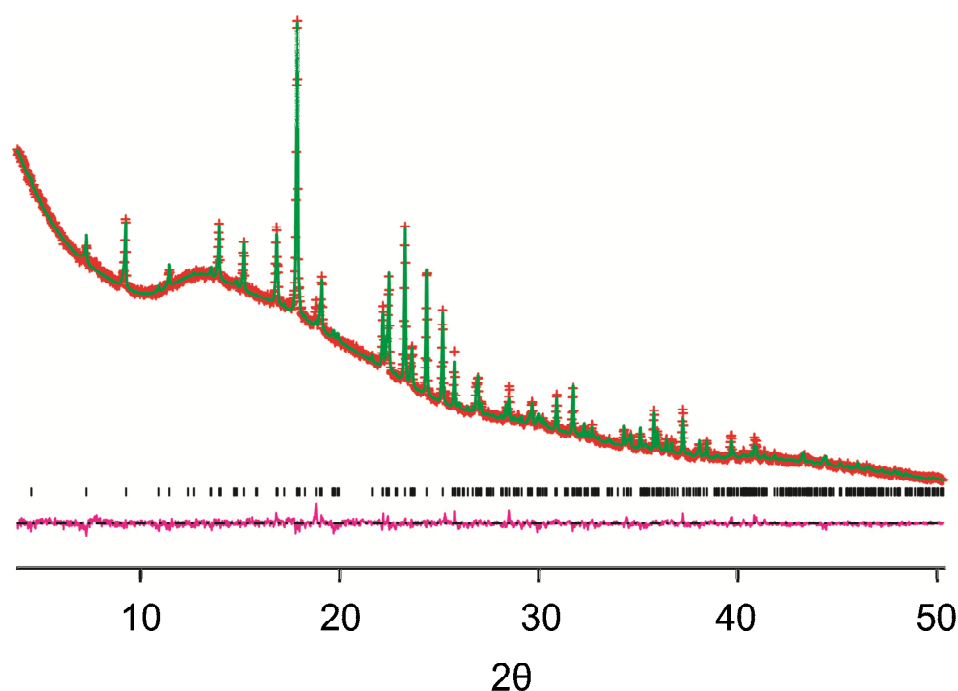
Fig. 2.9 Final Rietveld refinement for P5Q.2TCE.

In the final Rietveld refinement, planar restraints were applied to the quinone groups and standard restraints were applied to bond lengths and bond angles. The positions of the atoms representing the disordered TCE molecule were not restrained in any case. Separate common isotropic displacement parameters (U_{iso}) were refined for the non-hydrogen atoms of the P5Q molecule, the ordered TCE molecule and the disordered TCE molecule. In each case, U_{iso} for the hydrogen atoms in a given molecule was set to 1.2 times the common value for the non-hydrogen atoms in the same molecule. Refinement of preferred orientation parameters allowed the effects of a small extent of preferred orientation in the experimental data to be taken into account [March-Dollase preferential orientation plane (001); ratio, 86.5%]. The final Rietveld refinement (2θ range, 4 – 50°; 2703 profile points; 271 refined variables) afforded a good fit to the powder XRD data ($R_{wp} = 1.55\%$, $R_p = 1.09\%$; Fig. 2.9), with the following refined parameters: a = 18.7686(6)Å, b = 15.2482(5)Å, c = 6.90544(25) Å, β = 89.7367(22)°, V = 1976.23(18) Å^3.

Powder XRD data were also recorded at low temperature (250, 200, 150, 100 and 90 K) on beam-line I11 at Diamond Light Source, UK to explore the effects of temperature on the crystal structure. No noteworthy changes were observed within the temperature range investigated (except for minor peak shifts due to unit cell contraction), signifying that no solid-state phase transition occurs at low temperature and suggesting

that there is no considerable change in the extent of disorder in the space/time averaged crystal structure. Clearly, the latter conclusion considers the possibility that the dynamic disorder of one TCE molecule at room temperature may become static positional disorder at sufficiently low temperature.
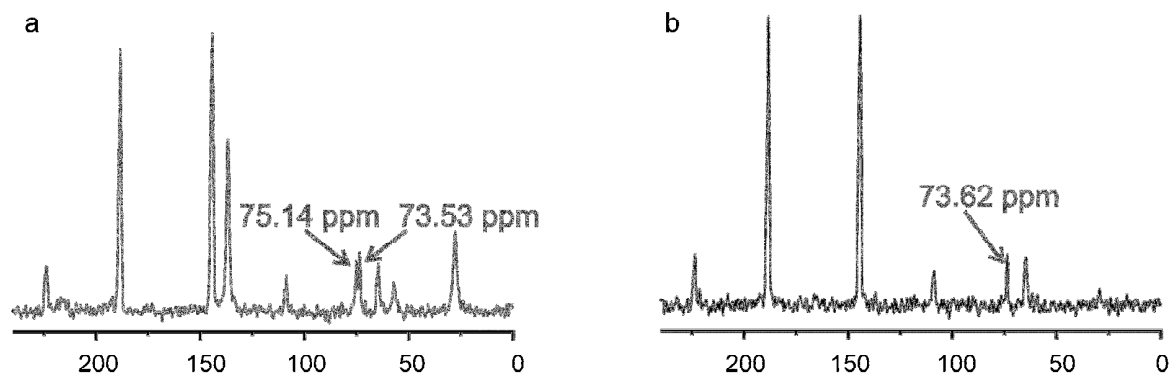

Fig. 2.10 High-resolution solid-state ^{13}C NMR spectra recorded for P5Q·2TCE (a) without a dephasing delay and (b) with a dephasing delay of 50 μs. The isotropic peaks at 75.14 ppm and 73.53 ppm in (a) are assigned to the carbon atoms of TCE and are consistent with the assignment that there are two different TCE environments in the crystal structure. In the spectrum recorded with a dephasing delay in (b), and peak at 75.14 ppm is missing, but the peak at 73.62 ppm remains. On this basis, the peak at 75.14 ppm can be assigned as a static TCE molecule and the peak at 73.53 ppm can be assigned as a dynamic TCE molecule.

2.10 High-resolution solid-state ^{13}C NMR of P5Q.2TCE

High-resolution solid-state ^{13}C NMR spectra of P5Q.2TCE were recorded at room temperature on a Varian VNMRS spectrometer operating at ^{13}C Larmor frequency 100.562 MHz with magic angle spinning at 8 kHz. Spectra were recorded both using the standard ^{1}H→^{13}C cross polarization magic angle spin (CPMAS) pulse sequence and using the ^{1}H→^{13}C CPMAS pulse sequence with a dipolar dephasing delay of 50 μs between the ^{1}H excitation pulse and cross polarization (Fig. 2.10). In the spectra recorded with the dipolar dephasing pulse sequence, signals corresponding to static ^{13}C nuclei bonded to at least one ^{1}H nucleus are suppressed; thus, the spectrum only possesses signals from dynamic ^{13}C nuclei bonded to at least one ^{1}H nucleus or from ^{13}C nuclei that are not bonded to ^{1}H. The dipolar dephasing spectrum for P5Q·2TCE contains ^{13}C signals for one TCE molecule, but the ^{13}C signals for the other TCE molecule are suppressed, leading to the conclusion that one TCE molecule endures rapid dynamics whereas the other TCE molecule is static. This conclusion is fully consistent with the crystal structure established from powder XRD data, in which one TCE molecule in the asymmetric unit showcases

disorder (ascribed from the NMR data as dynamic disorder) whereas the other TCE molecule has a single well-defined position, orientation and conformation in the crystal structure.
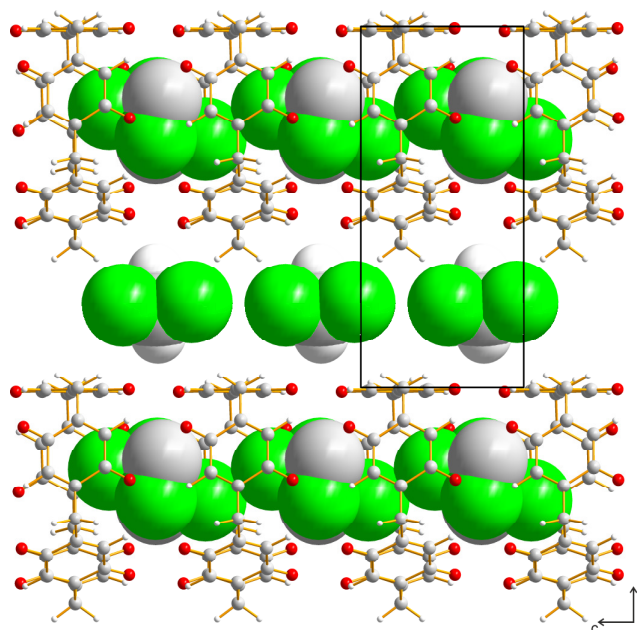
Fig. 2.11 Crystal structure of P5Q.2TCE determined directly from powder XRD data, viewed perpendicular to the columnar arrays (which run in the horizontal direction). The TCE molecules are shown in space-filling representation. For the disordered TCE site (within the columnar array), the atom positions in the refined structural model represent the optimal description of the resultant "smeared-out" electron density distribution, rather than representing atom positions in a discrete TCE molecule. The ordered TCE site is located between adjacent columnar arrays.

2.11 Crystal structure of P5Q.2TCE

The crystal structure is described in terms of columnar arrays in which the disordered TCE molecules and P5Q molecules alternate along the *c*-axis. As shown in Fig. 2.11, the TCE molecules within these columnar arrays penetrate inside the macrocyclic rings of both adjacent P5Q molecules, effectively threading the P5Q molecules such that they assemble along the one-dimensional array. The ordered TCE molecule is located in the region between adjacent columnar arrays of this type and plausibly acts to bundle adjacent columns together. The distinct environments of the two types of TCE molecule in the crystal structure are clearly evident from Fig. 2.12.
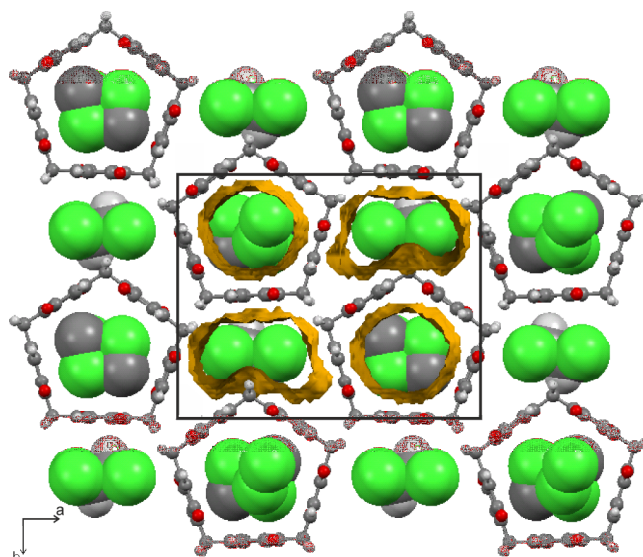
Fig. 2.12 Crystal structure of P5Q.2TCE viewed along the *c*-axis, parallel to the columnar arrays. The two types of TCE molecule in the crystal structure are shown in space-filling mode, together with the Connolly surfaces for the voids occupied by these molecules.

To obtain further insights into the observation that one TCE molecule is disordered and the other is ordered, the van der Waals surfaces of the voids containing the two distinct TCE molecules in the crystal structure were computed. The results reveal that the van der Waals cavity occupied by the disordered TCE molecule is significantly larger and more isotropic than that for the ordered TCE molecule.

2.12 Powder XRD of P5Q.2TCE and P5Q

The powder XRD patterns of P5Q.2TCE and the material obtained on removing the associated TCE component from this structure are considerably different (Fig. 2.13) indicating that the two solids are present in different crystalline phases.
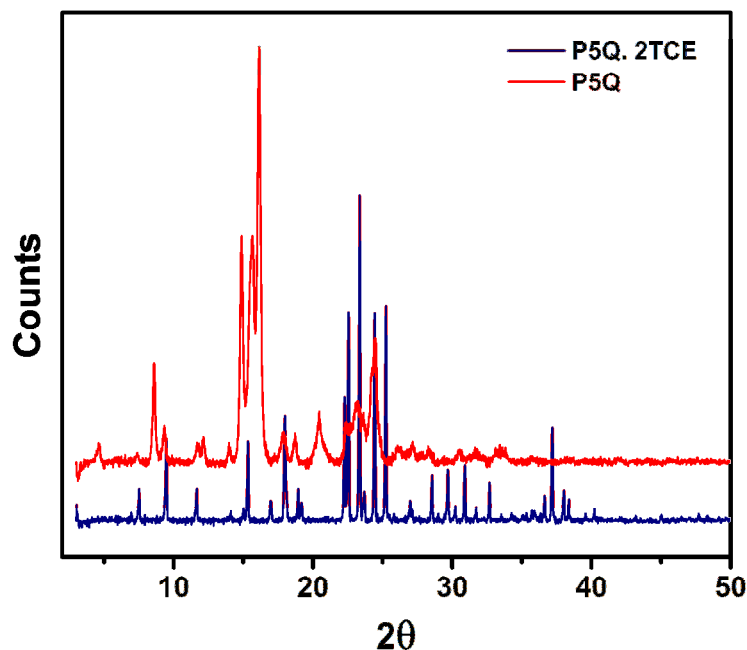
Fig. 2.13 Experimental powder XRD patterns recorded for P5Q·2TCE and for the material obtained by removal of the associated solvent TCE.

2.13 Thermal studies

Thermogravimetric analysis on P5Q.2TCE signifies that a mass loss of 35.85% occurs on increasing temperature at constant rate (Fig. 2.14a), which is clearly attributed to loss of the two TCE molecules from the crystal structure (calculated mass loss, 35.87%). Differential thermogravimetry from 80 $^{\circ}$C to 200 $^{\circ}$C (heating rate 1 $^{\circ}$C/min) exhibited a single minima, implying that the energies of association of the two types of TCE molecule are not considerably different (Fig. 2.14b).
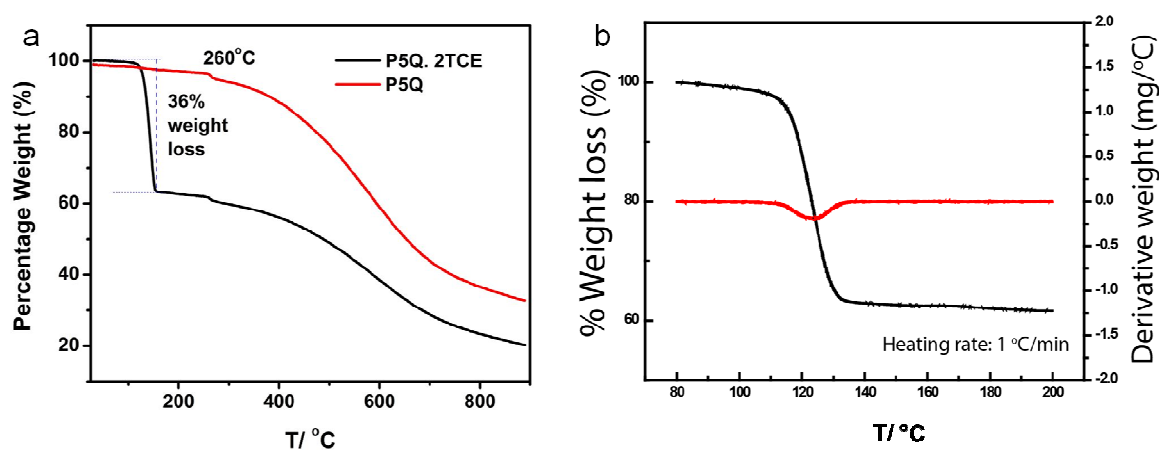
Fig. 2.14 (a) TGA data (heating rate 10 °C/min; nitrogen atmosphere) for P5Q.2TCE and for the material obtained following removal of the TCE component; (b) TGA and DTG data (heating rate 1 °C/min; nitrogen atmosphere) for P5Q.2TCE.

2.14 Conclusions

In conclusion, we report the crystal structure of the P5Q.2TCE solvate material, determined directly from powder XRD data, and augmented by structural insights revealed from high-resolution solid-state ^{13}C NMR. The assembly of the P5Q molecules is aided by the TCE component, resulting in columnar supramolecular ensembles of alternating P5Q and TCE molecules. The columnar character of the supramolecular assembly is consistent with the rod-like morphology observed in electron microscopy images. The solvent molecules play a critical role in assembling the columnar arrays of P5Q molecules, as well as bundling adjoining columns together. This observation may shed more light on understanding solvent-substrate interactions using various non-covalent forces leading to the formation of diverse supramolecular architectures. Finally, we emphasize that this work further highlights the real opportunities that now exist for determining the crystal structures of organic materials directly from powder XRD data.

2.15 References

(1) (a) Ogoshi, T.; Yamagishi, T.-a.; Nakamoto, Y. *Chem. Rev.* **2016**, *116*, 7937; (b) Ogoshi, T. *Pillararenes*; Royal Society of Chemistry, 2015; (c) Xue, M.; Yang, Y.; Chi, X.; Zhang, Z.; Huang, F. *Acc. Chem. Res.* **2012**, *45*, 1294; (d) Cragg, P. J.; Sharma, K. *Chem. Soc. Rev.* **2012**, *41*, 597.

(2) (a) Yu, G.; Zhang, Z.; Han, C.; Xue, M.; Zhou, Q.; Huang, F. *Chem. Commun.* **2012**, *48*, 2958; (b) Strutt, N. L.; Zhang, H.; Giesener, M. A.; Lei, J.; Stoddart, J. F. *Chem. Commun.* **2012**, *48*, 1647; (c) Ogoshi, T.; Shiga, R.; Yamagishi, T.-a. *J. Am. Chem. Soc.* **2012**, *134*, 4577; (d) Strutt, N. L.; Forgan, R. S.; Spruell, J. M.; Botros, Y. Y.; Stoddart, J. F. *J. Am. Chem. Soc.* **2011**, *133*, 5668; (e) Si, W.; Hu, X.-B.; Liu, X.-H.; Fan, R.; Chen, Z.; Weng, L.; Hou, J.-L. *Tetrahedron Lett.* **2011**, *52*, 2484; (f) Ogoshi, T.; Shiga, R.; Hashizume, M.; Yamagishi, T.-a. *Chem. Commun.* **2011**, *47*, 6927; (g) Aoki, T.; Ogoshi, T.; Yamagishi, T.-a. *Chem. Lett.* **2011**, *40*, 795.

(3) (a) Yu, G.; Han, C.; Zhang, Z.; Chen, J.; Yan, X.; Zheng, B.; Liu, S.; Huang, F. *J. Am. Chem. Soc.* **2012**, *134*, 8711; (b) Zhang, Z.; Luo, Y.; Chen, J.; Dong, S.; Yu, Y.; Ma, Z.; Huang, F. *Angew. Chem.* **2011**, *123*, 1433; (c) Zhang, Z.; Xia, B.; Han, C.; Yu, Y.; Huang, F. *Org. Lett.* **2010**, *12*, 3285; (d) Li, C.; Zhao, L.; Li, J.; Ding, X.; Chen, S.; Zhang, Q.; Yu, Y.; Jia, X. *Chem. Commun.* **2010**, *46*, 9016; (e) Kim, C.; Agasti, S. S.; Zhu, Z.; Isaacs, L.; Rotello, V. M. *Nat. Chem.* **2010**, *2*, 962; (f) Han, C.; Ma, F.; Zhang, Z.; Xia, B.; Yu, Y.; Huang, F. *Org. Lett.* **2010**, *12*, 4360; (g) Lagona, J.; Mukhopadhyay, P.; Chakrabarti, S.; Isaacs, L. *Angew. Chem. Int. Ed.* **2005**, *44*, 4844.

(4) Gomez-Kaifer, M.; Reddy, P. A.; Gutsche, C. D.; Echegoyen, L. *J. Am. Chem. Soc.* **1994**, *116*, 3580.

(5) Pochorovski, I.; Boudon, C.; Gisselbrecht, J. P.; Ebert, M. O.; Schweizer, W. B.; Diederich, F. *Angew. Chem. Int. Ed.* **2012**, *51*, 262.

(6) Lao, K.-u.; Yu, C.-h. *J. Comput. Chem.* **2011**, *32*, 2716.

(7) Ogoshi, T.; Aoki, T.; Kitajima, K.; Fujinami, S.; Yamagishi, T.-a.; Nakamoto, Y. *J. Org. Chem.* **2011**, *76*, 328.

(8) (a) Yusubov, M. S.; Nemykin, V. N.; Zhdankin, V. V. *Tetrahedron* **2010**, *66*, 5745; (b) Yakura, T.; Yamauchi, Y.; Tian, Y.; Omoto, M. *Chem. Pharm. Bull.* **2008**, *56*, 1632; (c) Yakura, T.; Konishi, T. *Synlett* **2007**, *2007*, 0765.

(9) (a) Lehn, J.-M. *Science* **2002**, *295*, 2400; (b) Schenning, A. P. H. J.; Meijer, E. W. *Chem.Commun.* **2005**, 3245; (c) Palmer, L. C.; Stupp, S. I. *Acc.Chem.Res.* **2008**, *41*,

1674; (d) Chen, Z.; Lohr, A.; Saha-Moller, C. R.; Wurthner, F. *Chem.Soc.Rev.* **2009**, *38*, 564; (e) Pepe-Mooney, B. J.; Fairman, R. *Curr. Opin. Struct. Bio.* **2009**, *19*, 483; (f) Zhao, Y. S.; Fu, H.; Peng, A.; Ma, Y.; Liao, Q.; Yao, J. *Acc. Chem. Res.* **2010**, *43*, 409; (g) Luo, Z.; Zhang, S. *Chem. Soc. Rev.* **2012**, *41*, 4736; (h) Matson, J. B.; Stupp, S. I. *Chem. Comm.* **2012**, *48*, 26; (i) Prabhakaran, P.; Priya, G.; Sanjayan, G. J. *Angew. Chem. Int. Ed.* **2012**, *51*, 4006; (j) Hosseinkhani, H.; Hong, P.-D.; Yu, D.-S. *Chem. Rev.* **2013**, *113*, 4837; (k) Li, H.; Choi, J.; Nakanishi, T. *Langmuir* **2013**, *29*, 5394; (l) Ogoshi, T.; Ueshima, N.; Yamagishi, T.-a. *Org.Lett.* **2013**, *15*, 3742; (m) Tovar, J. D. *Acc. Chem. Res.* **2013**, *46*, 1527; (n) Yao, Y.; Xue, M.; Zhang, Z.; Zhang, M.; Wang, Y.; Huang, F. *Chem. Sci.* **2013**, *4*, 3667.

(10) (a) Whitesides, G.; Mathias, J.; Seto, C. *Science* **1991**, *254*, 1312; (b) Conn, M. M.; Rebek, J. *Chem. Rev.* **1997**, *97*, 1647; (c) Hartgerink, J. D.; Beniash, E.; Stupp, S. I. *Science* **2001**, *294*, 1684; (d) Reinhoudt, D. N.; Crego-Calama, M. *Science* **2002**, *295*, 2403; (e) Moore, J. S.; Kraft, M. L. *Science* **2008**, *320*, 620; (f) Yashima, E.; Maeda, K.; Iida, H.; Furusho, Y.; Nagai, K. *Chem. Rev.* **2009**, *109*, 6102; (g) Blight, B. A.; Hunter, C. A.; Leigh, D. A.; McNab, H.; Thomson, P. I. *Nat. Chem.* **2011**, *3*, 244; (h) Jelfs, K. E.; Wu, X.; Schmidtmann, M.; Jones, J. T.; Warren, J. E.; Adams, D. J.; Cooper, A. I. *Angew. Chem. Int. Ed.* **2011**, *50*, 10653; (i) Salonen, L. M.; Ellermann, M.; Diederich, F. *Angew. Chem. Int. Ed.* **2011**, *50*, 4808; (j) Aida, T.; Meijer, E.; Stupp, S. *Science* **2012**, *335*, 813; (k) Cooper, A. I. *Angew. Chem. Int. Ed.* **2012**, *51*, 7892.

(11) Borovkov, V. V.; Hembury, G. A.; Inoue, Y. *Acc. Chem. Res.* **2004**, *37*, 449.

(12) Cantekin, S.; Nakano, Y.; Everts, J. C.; van der Schoot, P.; Meijer, E. W.; Palmans, A. R. A. *Chem. Commun.* **2012**, *48*, 3803.

(13) (a) van Esch, J. H.; Schoonbeek, F.; de Loos, M.; Kooijman, H.; Spek, A. L.; Kellogg, R. M.; Feringa, B. L. *Chem. Eur. J.* **1999**, *5*, 937; (b) Jeong, Y.; Hanabusa, K.; Masunaga, H.; Akiba, I.; Miyoshi, K.; Sakurai, S.; Sakurai, K. *Langmuir* **2005**, *21*, 586; (c) Edwards, W.; Lagadec, C. A.; Smith, D. K. *Soft Matter* **2011**, *7*, 110.

(14) (a) Juwarker, H.; Suk, J.-m.; Jeong, K.-S. *Chem. Soc. Rev.* **2009**, *38*, 3316; (b) Dsouza, R. N.; Pischel, U.; Nau, W. M. *Chem. Rev.* **2011**, *111*, 7941.

(15) (a) Nelson, J. C.; Saven, J. G.; Moore, J. S.; Wolynes, P. G. *Science* **1997**, *277*, 1793; (b) Lahiri, S.; Thompson, J. L.; Moore, J. S. *J. Am. Chem. Soc.* **2000**, *122*, 11315.

(16) (a) Ogoshi, T.; Kanai, S.; Fujinami, S.; Yamagishi, T.-a.; Nakamoto, Y. *J. Am. Chem. Soc.* **2008**, *130*, 5022; (b) Xue, M.; Yang, Y.; Chi, X.; Zhang, Z.; Huang, F. *Acc. Chem. Res.* **2012**, *45*, 1294; (c) Cragg, P. J.; Sharma, K. *Chem. Soc. Rev.* **2012**, *41*, 597;

(d) Ogoshi, T. *J. Incl. Phenom. Macrocycl. Chem.* **2012**, *72*, 247; (e) Ogoshi, T.; Yamagishi, T.-a. *Eur. J. Org. Chem.* **2013**, *2013*, 2961; (f) Ogoshi, T.; Yamagishi, T.-a. *Bull. Chem. Soc. Jpn.* **2013**, *86*, 312; (g) Cao, D.; Meier, H. *Asian. J. Org. Chem* **2014**, *3*, 244.

(17) (a) Casnati, A.; Pochini, A.; Ungaro, R.; Ugozzoli, F.; Arnaud, F.; Fanni, S.; Schwing, M.-J.; Egberink, R. J.; de Jong, F.; Reinhoudt, D. N. *J. Am. Chem. Soc.* **1995**, *117*, 2767; (b) Bradshaw, J. S.; Izatt, R. M. *Acc. Chem. Res.* **1997**, *30*, 338; (c) Ikeda, A.; Shinkai, S. *Chem. Rev.* **1997**, *97*, 1713; (d) Szejtli, J. *Chem. Rev.* **1998**, *98*, 1743; (e) Lee, J. W.; Samal, S.; Selvapalam, N.; Kim, H.-J.; Kim, K. *Acc. Chem. Res.* **2003**, *36*, 621; (f) Gokel, G. W.; Negin, S. *Acc. Chem. Res.* **2013**, *46*, 2824; (g) Harada, A.; Takashima, Y.; Nakahata, M. *Acc. Chem. Res.* **2014**, *47*, 2128; (h) Isaacs, L. *Acc. Chem. Res.* **2014**, *47*, 2052.

(18) (a) Strutt, N. L.; Forgan, R. S.; Spruell, J. M.; Botros, Y. Y.; Stoddart, J. F. *J. Am. Chem. Soc.* **2011**, *133*, 5668; (b) Zhang, H.; Strutt, N. L.; Stoll, R. S.; Li, H.; Zhu, Z.; Stoddart, J. F. *Chem. Commun.* **2011**, *47*, 11420; (c) Li, H.; Chen, D.-X.; Sun, Y.-L.; Zheng, Y. B.; Tan, L.-L.; Weiss, P. S.; Yang, Y.-W. *J. Am. Chem. Soc.* **2013**, *135*, 1570; (d) Yu, G.; Han, C.; Zhang, Z.; Chen, J.; Yan, X.; Zheng, B.; Liu, S.; Huang, F. *J. Am. Chem. Soc.* **2012**, *134*, 8711; (e) Li, C.; Ma, J.; Zhao, L.; Zhang, Y.; Yu, Y.; Shu, X.; Li, J.; Jia, X. *Chem. Commun.* **2013**, *49*, 1924; (f) Zhang, H.; Ma, X.; Guo, J.; Nguyen, K. T.; Zhang, Q.; Wang, X.-J.; Yan, H.; Zhu, L.; Zhao, Y. *RSC Adv.* **2013**, *3*, 368; (g) Kothur, R. R.; Hall, J.; Patel, B. A.; Leong, C. L.; Boutelle, M. G.; Cragg, P. J. *Chem. Commun.* **2014**, *50*, 852.

(19) (a) Zhang, Z.; Luo, Y.; Chen, J.; Dong, S.; Yu, Y.; Ma, Z.; Huang, F. *Angew. Chem. Int. Ed.* **2011**, *50*, 1397; (b) Guan, Y.; Ni, M.; Hu, X.; Xiao, T.; Xiong, S.; Lin, C.; Wang, L. *Chem. Commun.* **2012**, *48*, 8529; (c) Ogoshi, T.; Kayama, H.; Yamafuji, D.; Aoki, T.; Yamagishi, T.-a. *Chem. Sci.* **2012**, *3*, 3221; (d) Strutt, N. L.; Zhang, H.; Giesener, M. A.; Lei, J.; Stoddart, J. F. *Chem. Commun.* **2012**, *48*, 1647; (e) Ogoshi, T.; Yoshikoshi, K.; Aoki, T.; Yamagishi, T.-a. *Chem. Commun.* **2013**, *49*, 8785; (f) Wang, K.; Wang, C.-Y.; Wang, Y.; Li, H.; Bao, C.-Y.; Liu, J.-Y.; Zhang, S. X.-A.; Yang, Y.-W. *Chem. Commun.* **2013**, *49*, 10528; (g) Li, C.; Han, K.; Li, J.; Zhang, Y.; Chen, W.; Yu, Y.; Jia, X. *Chem. Eur. J.* **2013**, *19*, 11892; (h) Han, C.; Xia, B.; Chen, J.; Yu, G.; Zhang, Z.; Dong, S.; Hu, B.; Yu, Y.; Xue, M. *RSC Adv.* **2013**, *3*, 16089.

(20) Ogoshi, T.; Aoki, T.; Ueda, S.; Tamura, Y.; Yamagishi, T.-a. *Chem. Commun.* **2014**, *50*, 6607.

(21) (a) Ogoshi, T.; Hasegawa, Y.; Aoki, T.; Ishimori, Y.; Inagi, S.; Yamagishi, T.-a. *Macromolecules* **2011**, *44*, 7639; (b) Hu, X.-Y.; Wu, X.; Wang, S.; Chen, D.; Xia, W.; Lin, C.; Pan, Y.; Wang, L. *Polym. Chem.* **2013**, *4*, 4292.

(22) (a) Si, W.; Chen, L.; Hu, X.-B.; Tang, G.; Chen, Z.; Hou, J.-L.; Li, Z.-T. *Angew. Chem. Int. Ed.* **2011**, *50*, 12564; (b) Sun, Y.-L.; Yang, Y.-W.; Chen, D.-X.; Wang, G.; Zhou, Y.; Wang, C.-Y.; Stoddart, J. F. *Small* **2013**, *9*, 3224; (c) Yu, G.; Ma, Y.; Han, C.; Yao, Y.; Tang, G.; Mao, Z.; Gao, C.; Huang, F. *J. Am. Chem. Soc.* **2013**, *135*, 10310.

(23) (a) Cao, D.; Kou, Y.; Liang, J.; Chen, Z.; Wang, L.; Meier, H. *Angew. Chem. Int. Ed.* **2009**, *48*, 9721; (b) Lao, K.-u.; Yu, C.-h. *J. Comput. Chem.* **2011**, *32*, 2716; (c) Shivakumar, K. I.; Sanjayan, G. J. *Synthesis* **2013**, *45*, 896.

(24) (a) Genorio, B.; Pirnat, K.; Cerc-Korosec, R.; Dominko, R.; Gaberscek, M. *Angew. Chem. Int. Ed.* **2010**, *49*, 7222; (b) Huang, W.; Zhu, Z.; Wang, L.; Wang, S.; Li, H.; Tao, Z.; Shi, J.; Guan, L.; Chen, J. *Angew. Chem. Int. Ed.* **2013**, *52*, 9162.

(25) (a) Lightfoot, P.; Tremayne, M.; Harris, K. D. M.; Bruce, P. G. *J. Chem. Soc., Chem. Commun.* **1992**, 1012; (b) Harris, K. D.; Tremayne, M.; Lightfoot, P.; Bruce, P. G. *J. Am. Chem. Soc.* **1994**, *116*, 3543; (c) Kariuki, B. M.; Zin, D. M.; Tremayne, M.; Harris, K. D. *Chem. Mater.* **1996**, *8*, 565; (d) Dinnebier, R. E. *Mater. Sci. Forum* **2000**, *321-3*, 1; (e) Chernyshev, V. V. *Russ. Chem. Bull.* **2001**, *50*, 2273; (f) *Structure Determination from Powder Diffraction Data*; David, W. I. F.; Shankland, K.; McCusker, L. B.; Baerlocher, C., Eds.; IUCr/OUP, 2002; (g) Harris, K. D. *Cryst. Growth des.* **2003**, *3*, 887; (h) Huq, A.; Stephens, P. W. *J. Pharm. Sci.* **2003**, *92*, 244; (i) Harris, K. D.; Cheung, E. Y. *Chem. Soc. Rev.* **2004**, *33*, 526; (j) Favre-Nicolin, V.; Černý, R. *Kris.* **2004**, *219*, 847; (k) Tremayne, M. *Phil. Trans. Roy. Soc. A* **2004**, *362*, 2691; (l) Brodski, V.; Peschar, R.; Schenk, H. *J. Appl. Cryst.* **2005**, *38*, 688; (m) David, W. I. F.; Shankland, K. *Acta Cryst. A* **2008**, *64*, 52; (n)Tsue, H.; Horiguchi, M.; Tamura, R.; Fujii, K.; Uekusa, H. *J. Synth. Org. Chem Jpn.* **2007**, *65*, 1203.

(26) Visser, J. *J. Appl. Crystallogr.* **1969**, *2*, 89.

(27) Shirley, R. *The CRYSFIRE system for automatic powder indexing: user's manual*; The Lattice Press: Guildford, U.K., 2000.

(28) Le Bail, A.; Duroy, H.; Fourquet, J. *Mater. Res. Bull.* **1988**, *23*, 447.

(29) Larson, A.; Von Dreele, R. *Los Alamos Natl. Lab. Rep*, 2004; Vol. 86.

(30) (a) Harris, K. D.; Habershon, S.; Cheung, E. Y.; Johnston, R. L. *Z. Krist.* **2004**, *219*, 838; (b) Habershon, S.; Harris, K. D.; Johnston, R. L. *J. Comput. Chem.* **2003**, *24*, 1766; (c) Turner, G. W.; Tedesco, E.; Harris, K. D.; Johnston, R. L.; Kariuki, B. M. *Chem.*

Phys. Lett. **2000**, *321*, 183; (d) Harris, K. D.; Johnston, R. L.; Kariuki, B. M. *Acta Cryst. A* **1998**, *54*, 632; (e) Kariuki, B. M.; Serrano-Gonzalez, H.; Johnston, R. L.; Harris, K. D. *Chem. Phys. Lett.* **1997**, *280*, 189.

(31) (a) Fujii, K.; Young, M. T.; Harris, K. D. *J. Struct. Biol.* **2011**, *174*, 461; (b) Cheung, E. Y.; Fujii, K.; Guo, F.; Harris, K. D.; Hasebe, S.; Kuroda, R. *Cryst. Growth Des.* **2011**, *11*, 3313; (c) Guo, F.; Martí-Rujas, J.; Pan, Z.; Hughes, C. E.; Harris, K. D. *J. Phys. Chem. C* **2008**, *112*, 19793; (d) Pan, Z.; Xu, M.; Cheung, E. Y.; Harris, K. D.; Constable, E. C.; Housecroft, C. E. *J. Phys. Chem. B* **2006**, *110*, 11620; (e) Guo, F.; Harris, K. D. *J. Am. Chem. Soc.* **2005**, *127*, 7314; (f) Albesa-Jové, D.; Kariuki, B. M.; Kitchin, S. J.; Grice, L.; Cheung, E. Y.; Harris, K. D. *ChemPhysChem* **2004**, *5*, 414; (g) Tedesco, E.; Turner, G. W.; Harris, K. D.; Johnston, R. L.; Kariuki, B. M. *Angew. Chem. Int. Ed.* **2000**, *39*, 4488.

(32) (a) McCusker, L.; Von Dreele, R.; Cox, D.; Louer, D.; Scardi, P. *J. Appl. Crystallogr.* **1999**, *32*, 36;   (b) Rietveld, H. *J. Appl. Crystallogr.* **1969**, *2*, 65.

Chapter 3

Part A: Room-temperature ferroelectric organic CT crystals of pillar[5]quinone and tetrathiafulvalene

Part B: Charge transfer crystals of pillar[5]quinone and 4,4'-bis(N-carbazolyl)-1,1'-biphenyl

Part A: *Room Temperature Ferroelectric Organic CT Crystals of Pillar[5]quinone and Tetrathiafulvalene*

3.1 Introduction

Ferroelectric materials,[1] endowed with spontaneous and electrically reversible polarization, are ushering into prominence owing to their wide applications in data storage and optoelectronics, and in developing sensors and actuators.[2] These materials possess the ability to store and invert the polarities, manipulate light, sense temperature and respond mechanically to change in electrical stimuli and *vice versa*. Although rare, organic ferroelectrics[3] are advantageous owing to their low-temperature solution processing, light-weightedness, and mechanical flexibility, in addition to being economical and environmentally benign. Centrosymmetric mixed stack CT complexes of TTF and halogenated *p*-benzoquinones (TTF-QBr$_x$Cl$_{4-x}$) have earlier been reported to exhibit ferroelectricity by undergoing symmetry breaking transition - albeit at cryogenic temperature with Curie temperatures (T_c) 53, 67 and 81 K for TTF-bromanil (x=4),[4] TTF-2-bromo-3,5,6-trichloroquinone (x=1)[5] and TTF-chloranil (x=0),[6] respectively. Ferroelectric transition at room-temperature has been realized in TTF-2,5-dibromo-3,6-diiodoquinone (QBr$_2$I$_2$) by applying hydrostatic pressure - four orders above the atmospheric pressure.[7] Recent efforts to elevate the temperature of ferroelectric ordering by implementing hydrogen-bond-augmented mixed stacked CT complexes have led to the discovery of room-temperature supramolecular ferroelectrics[8]. Notably, in these systems, hydrogen bonds play pivotal role in severing the conventional centrosymmetric lattice of TTF-quinone to bring about room-temperature ferroelectric ordering.[3c] However, theoretical studies suggest that ferroelectricity in hydrogen-bonded CT systems, although at elevated temperature, comes at the expense of magnitude of polarization owing to the low degree of charge transfer.[9] In this perspective, pursuit towards finding a novel TTF-quinone complex which could showcase room-temperature ferroelectric behavior, apart from high polarization, would be of significant importance.

Pillar[5]quinone (P5Q),[10] obtained recently by the oxidative dearomatization of pillar[5]arene,[11] is a fascinating cyclic pentaquinone adorned with five *p*-benzoquinones sequentially bridged at 2,5- positions by methylene linkers. The arrangement of five electron deficient *p*-benzoquinone units in a robust pentagon shape[12] could render P5Q a unique charge transfer acceptor capability. On the other hand, the π-enriched tetrathiafulvalene (TTF) has found wide utility because of its low ionization potential and

versatile electron donor capability; rendering easy fabrication of diverse electronic materials – in particular organic (semi)conductors.[13]

3.2 Objective of the present work

We envisaged that the charge donor TTF and charge acceptor P5Q (Fig. 3.1a) could form a CT complex akin to **TTF**-**TCNQ** and aimed at studying the supramolecular interactions playing the role in complexation besides understanding the magnetic and electric properties of the complex.
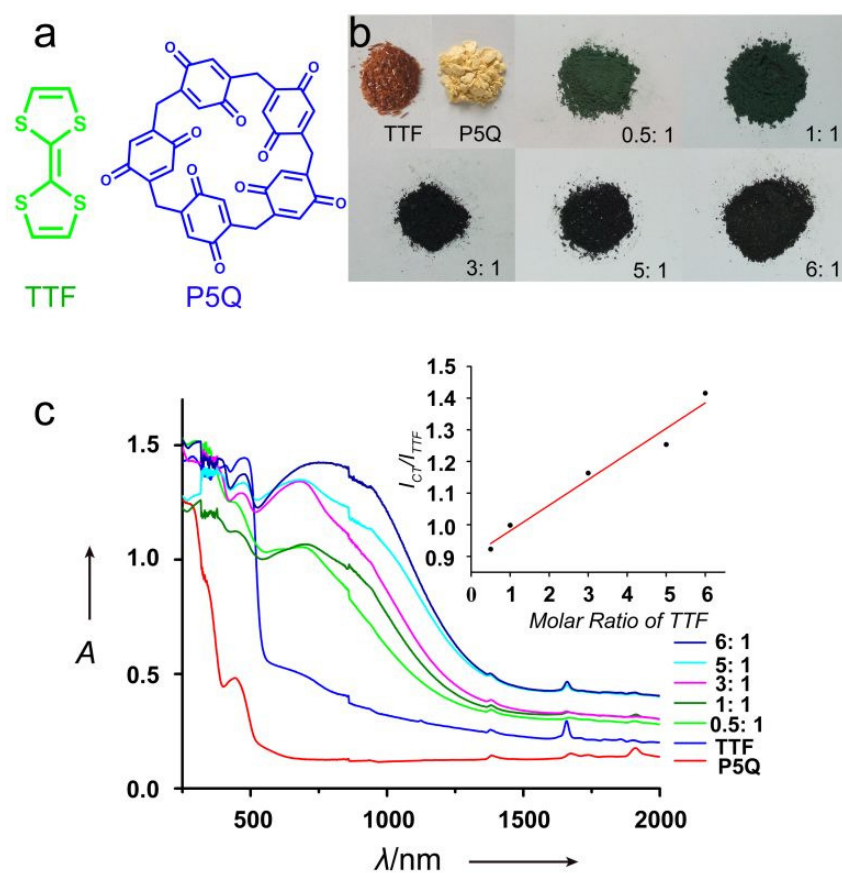

Fig. 3.1 (a) Molecular structure of TTF and P5Q. (b) Photographs of TTF, P5Q and CT complexes with varying concentration of TTF prepared by ball milling for 30 min. (c) Solid-state absorption spectra of CT complexes of **TTF**-**P5Q** with varying concentration of TTF prepared by ball milling for 30 min [inset: ratio of charge transfer intensity (812 nm) to TTF monomer intensity (479 nm) as a function of molar ratio of TTF].
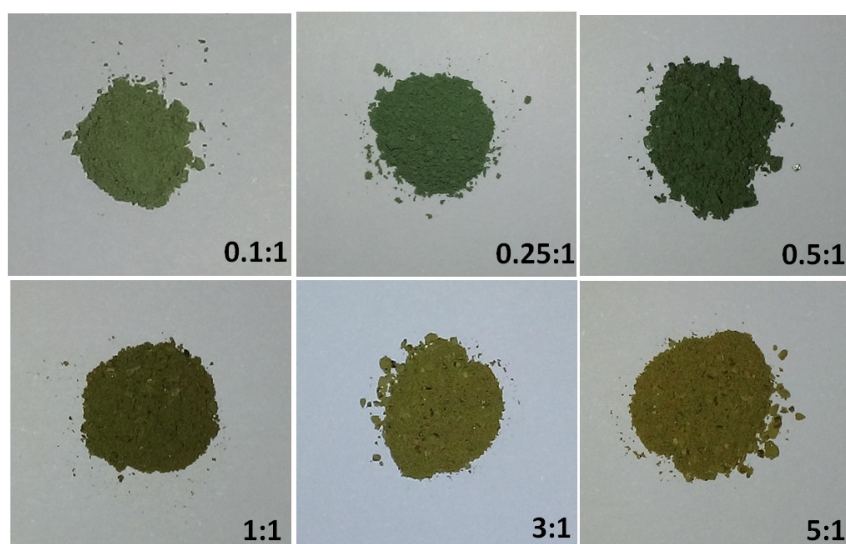
Fig. 3.2 Photographs of TTF, P5Q, and ground complexes of **TTF-P5Q** at various ratios obtained by grinding using agate mortar and pestle.

3.3 Mechanochemistry and solid-state absorption spectra

Considering the limited solubility of P5Q, readily obtained by following our reported procedure,[10b] we ground the orange TTF (Fig. 3.1b) and yellow P5Q (Fig. 3.1c) in an agate mortar without addition of any solvent, whereupon a quick change in color to green was observed which is attributable to CT complexation (Fig. 3.2). In order to achieve reproducible results, we subjected the constituent (D-A) compounds, in varying molar ratios of TTF, to ball-milling. We presumed that increasing the molar ratio of TTF up to six would ensure maximum complexation with each *p*-benzoquinone unit in P5Q, eventually establishing CT interaction with at least one TTF. The green complex turned darker with every increase in the ratio of TTF to that of P5Q, upon ball-milling (Fig. 3.1b). The broad peak extending from 520 nm to 1375 nm in the solid-state UV-Vis-NIR spectra is characteristic of a CT band (Fig. 3.1c). The plot of the ratio of CT (812 nm) and TTF (479 nm) band intensities clearly demonstrates that as more TTF molecules are incorporated, the monomer peak intensity decreases with a concomitant increase in the CT band intensity (inset, Fig. 3.1c).
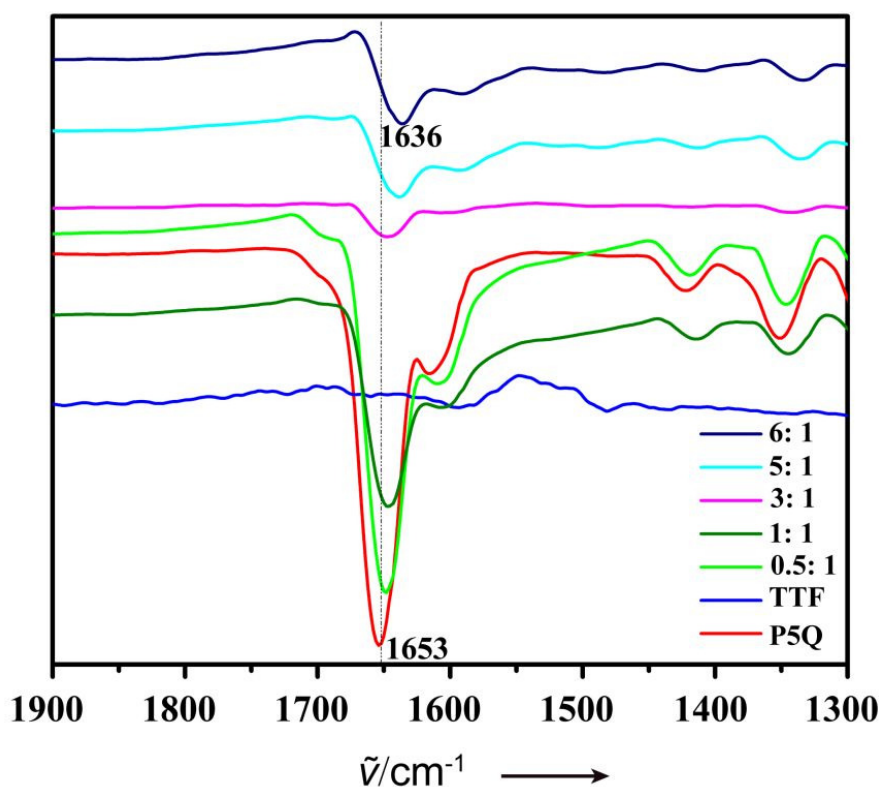
Fig. 3.3 ATR-FTIR spectra of P5Q, TTF and their ball-milled CT complexes (**TTF-P5Q**) indicating change in the carbonyl region.

3.4 Spectroscopic studies and powder XRD

The ATR-FTIR of the ball-milled solids unveiled lowering of carbonyl bond order in the CT complexes with increasing molar ratio of TTF (Fig. 3.3). The carbonyl stretching of 6:1 **TTF-P5Q** CT complex red-shifted by 17 cm^{-1}, as compared to P5Q indicating increased electron density in the antibonding orbitals of P5Q. The accumulation of partial positive and negative charges on the donor-TTF and acceptor-P5Q molecules, respectively, is reflected by shifts in solid-state high resolution ^{13}C cross polarization magic angle spin (CP/MAS) NMR spectrum. The peripheral interactions in the ground **TTF**-**P5Q** complexes manifested in small isotropic shifts in their NMR spectra (Fig. 3.4). Although we found new reflexes appearing for the **TTF**-**P5Q** complexes in the PXRD pattern, deciphering them to obtain D-A packing information appeared highly challenging (Fig. 3.5).
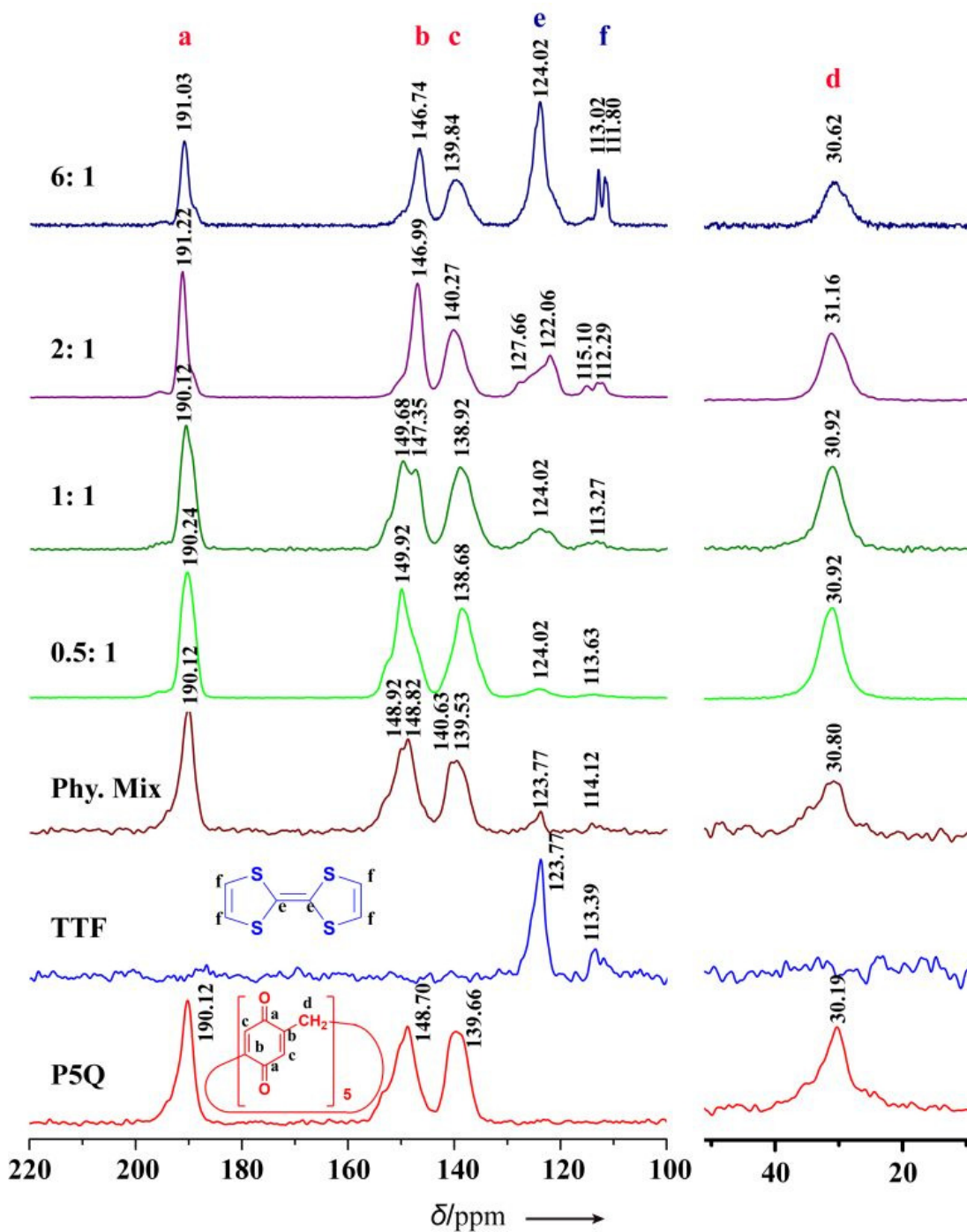
Fig. 3.4 Comparison of the 100.53 MHz ^{13}C CPMAS spectra obtained with a contact time of 3.5 ms of P5Q, TTF, a physical mixture of P5Q with TTF and ball milled **TTF-P5Q** CT complexes.
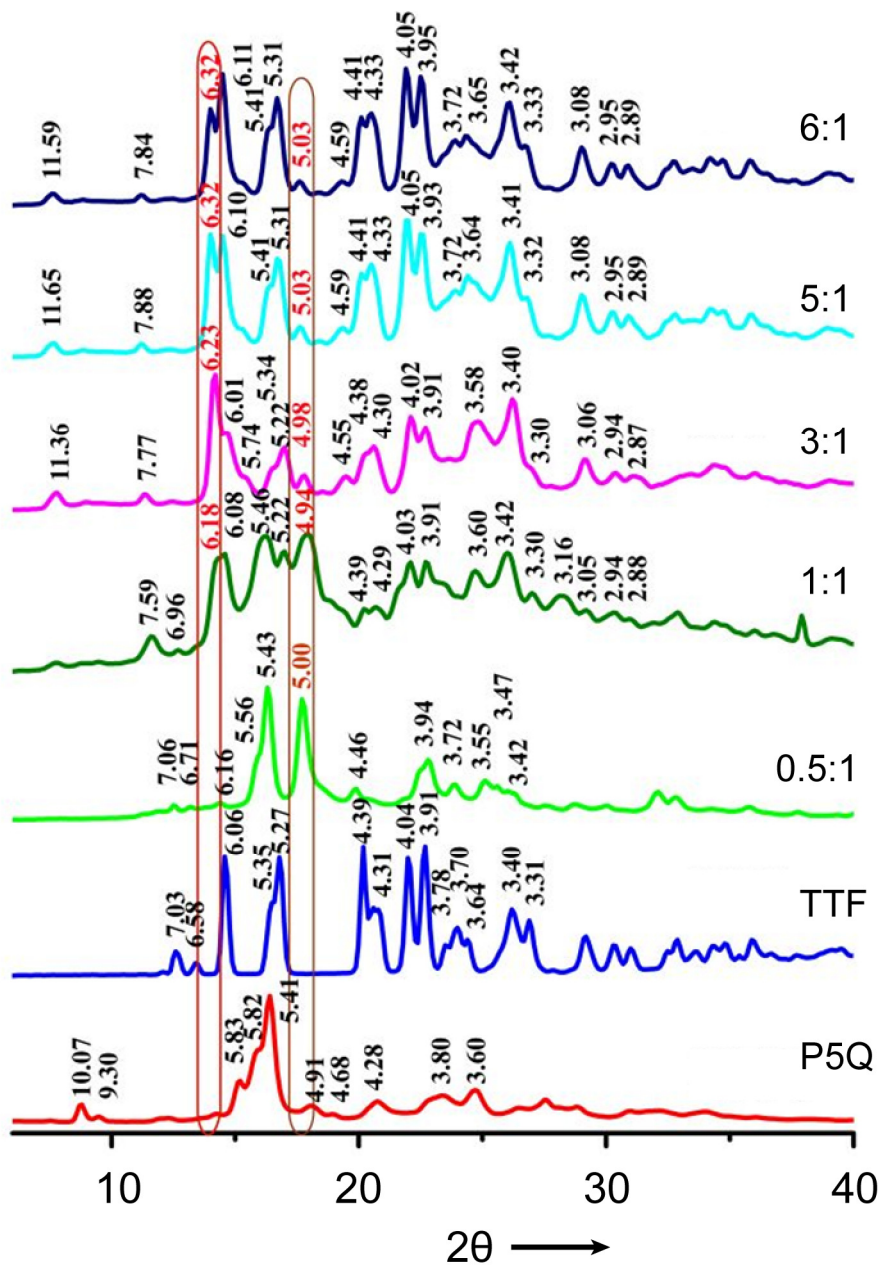
Fig. 3.5 Powder XRD profiles of P5Q, TTF and ball-milled **TTF-P5Q** CT assemblies. *Note-1*: The numbers above the reflexes are the corresponding interplanar *d* spacing distances in Angstroms. *Note-2*: The PXRD profile of 6:1 **TTF-P5Q** overwhelmed by the TTF signature peaks made us to limit the molar ratio of TTF to six.
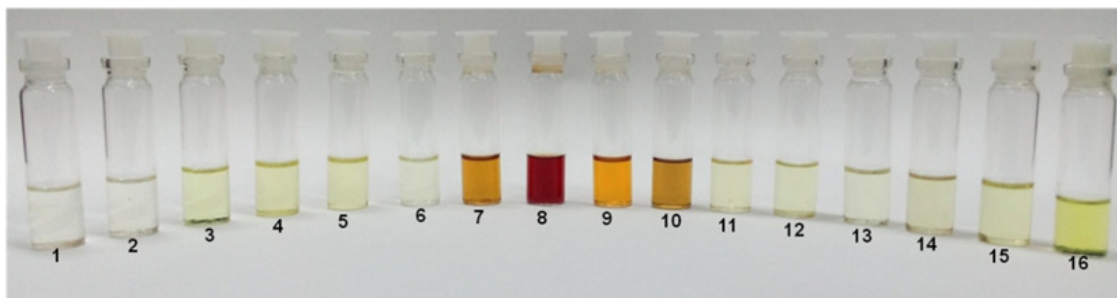
Fig. 3.6 Photograph of 1:1 **TTF**-**P5Q** in various solvents, 1. isopropanol, 2. *n*-hexane, 3. toluene, 4. xylene, 5. chlorobenzene, 6. acetonitrile, 7. dimethylformamide, 8. hexafluoroisopropanol, 9. dimethylsulphoxide, 10. tetrachloroethane, 11. dichloromethane, 12. methanol, 13. cyclohexane, 14. chloroform, 15. 1, 2-dichlorobenzene, 16. pentane.

3.5 CT complex in solution-state

Except 1,4-dioxane, most of the common organic solvents failed to retain the characteristic green color upon addition of ground **TTF**-**P5Q** complex (Fig. 3.6). This is plausibly because of the poor solubility of the CT complex in common organic solvents, other than 1,4-dioxane. The ground complexes dissolved completely in 1,4-dioxane and gave the solution a green tinge that intensified in solutions with higher mole ratios of TTF. Furthermore, the yellow P5Q solution in 1,4-dioxane turned to green when solid TTF or its solution in 1,4-dioxane was added with 1:1 **TTF**-**P5Q**, showcasing greenish-yellow color, while 6:1 ratio exhibiting emerald green color (Fig. 3.7a). However, the CT complex colors of 1:1 and 6:1 **TTF**-**P5Q** pellets looked similar (Fig. 3.7b), presumably because application of pressure to pelletize the solids would have brought the D-A molecules into close proximity. These observations clearly suggest that the more closer the TTF and P5Q get juxtaposed, better is the green color intensity. The emerald green single crystals (Fig. 3.7c) of 1:1 **TTF**-**P5Q** complex, grown from 1,4-dioxane by slow evaporation, diffracted the Indus-2 synchrotron beamline.[14]
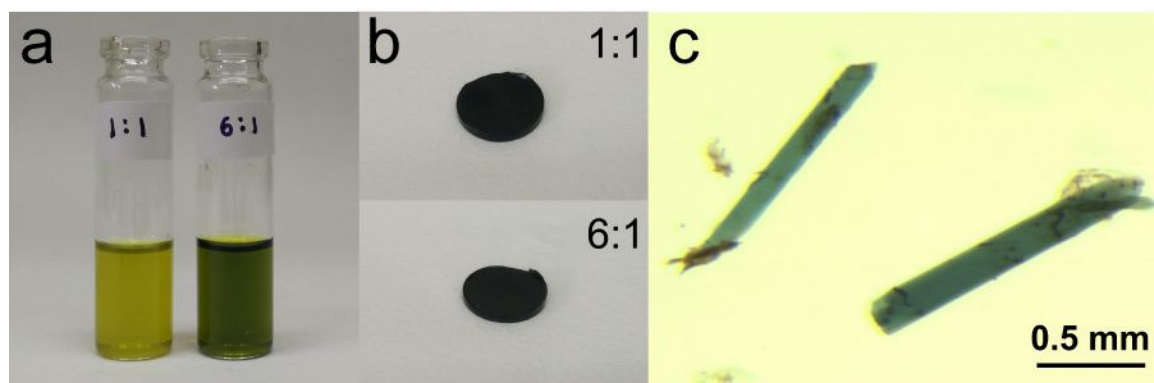
Fig. 3.7 (a) Photograph of 1,4-dioxane solutions of 1:1 and 6:1 **TTF-P5Q** prepared by addition of TTF solution to P5Q solution. (b) Photograph of 1:1 and 6:1 **TTF-P5Q** pellets obtained by stripping off 1,4-dioxane (c) Optical microscopy image of the emarald green **TTF-P5Q** crystal grown from 1,4-dioxane solution.

3.6 Single-crystal synchrotron X-ray diffraction

Single-crystal synchrotron X-ray diffraction study of the **TTF-P5Q** complex (CCDC 1482229) clearly unveiled the pivotal role of π-stacking interactions in the solid-state. Remarkably, among the five *p*-benzoquinones of P5Q, four are involved in π-stacking interactions: one with a TTF at a distance of 3.523(2) Å, and three others with the neighboring P5Qs at distances of 3.588(2) Å, 3.702(2) Å and 3.713(2) Å. On the other hand, the TTFs dimerize with the centroid-to-centroid π-stacking distance of 3.445(3) Å (Fig. 3.8a). P5Q assembly is effectuated by the corrugated sheets: one set running approximately along the *c* axis and the other in diagonal *bc* plane (Fig. 3.8a). The layers of TTF dimers intercalate these corrugated sheets, and by doing so, each TTF dimer gets encapsulated within the six hexagonally π-stacked P5Qs (Fig. 3.8a, e). Although the dimerized TTFs appear isolated from rest of the dimers along the view (010), they are part of the continuous, segregatedly arrayed channels of **TTF**-**P5Q** extending along (011) (Fig. 3.8b). This view reveals the mixed stacking of TTF and P5Q dimers with stacking axis perpendicular to the viewing axis. The TTF dimer stacks in an unprecedented 'ring-eclipsed' configuration, unlike the two types typically found: fully eclipsed and bond-over-ring (Fig. 3.8c).[15] The centroid-to-centroid π-stacking distance between the two eclipsed dithiole rings of TTFs is in agreement with the interplanar distance observed in fully eclipsed radical-cation $(TTF^{+\bullet})_2$ dimer,[16] suggesting σ-bond formation between the π-systems of dithiole rings. The sliding of the TTF dimers from the fully eclipsed or bond-over-ring conformation affording the novel 'ring-eclipsed' conformation could be ascribed to the most favorable thermodynamic arrangement that the TTF dimer could adopt by stacking with P5Qs through π-π interactions (Fig. 3.8a). Consequently, the dithiole rings of TTF showcase strong asymmetric distortion - making them to bend and twist (Fig. 3.8d).
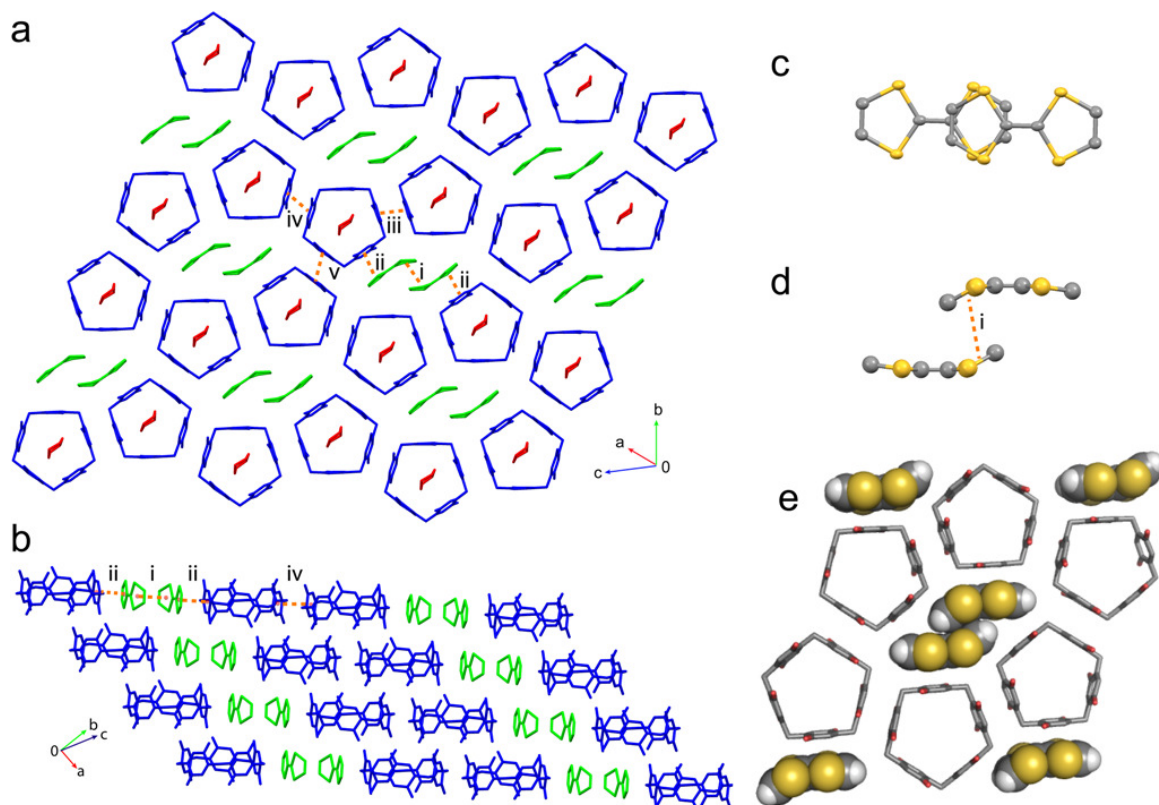
Fig. 3.8 a) Single crystal structure of 1:1 **TTF**-**P5Q** CT complex (P5Q-blue, TTF-green, and 1,4-dioxane-red) viewed perpendicular to the plane (-111) showing segregated arrangement of TTF and P5Q. b) View of the diagonal *bc* plane (0-1-1). c, d) Two perspective views of ′ring-eclipsed′ TTF dimers. e) Close-up view of hexagonally π-stacked P5Q encapsulating a TTF dimer. *Note 1*: dashed orange lines (Fig. 2a,b,d) indicate the centroid-to-centroid π-stacking distances (i) 3.445(3) Å, (ii) 3.523(2) Å, (iii) 3.586(2) Å, (iv) 3.702(2) Å and (v) 3.713(2) Å. *Note 2*: solvent molecules are excluded for clarity in 3.8b, e.
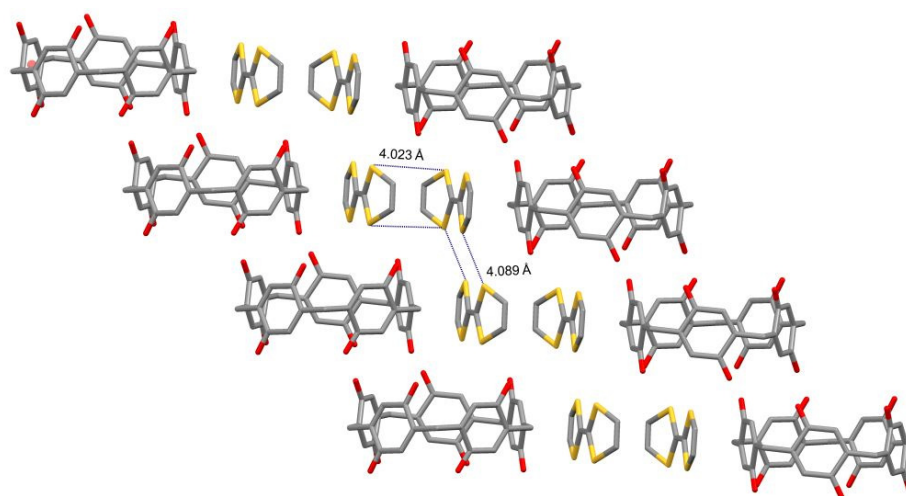
Fig. 3.9 Crystal structure packing of **TTF-P5Q** viewed along (011) showcasing intrasheet (β) and intersheet (γ) S···S interactions.

The segregatedly aligned donors and acceptors stack among themselves approximately along the *c*-axis and along the diagonal *bc* plane (Fig. 3.8a). The conducting D-A CT complexes are usually segregatedly stacked.[17] However, conductivity in the **TTF**-**P5Q** complex was elusive: the dimerized TTFs situated faraway from one another fail to π-stack with the TTFs of next dimer, thus cutting off hole conduction along the stacking axis. Similarly, the P5Qs, although stacked continuously, forbid the conduction of electrons owing to the incomplete conjugation between the stacked *p*-benzoquinone units of P5Q. Organic superconductors based on TTF and their derivatives rely largely upon the short S···S interactions to uphold high electronic dimensionality.[18] However, the S···S interactions observed in the crystal structure of **TTF**-**P5Q** are greater than their sum of van der Waals' radii with *β*-type intrasheet interaction[18] discernible at a distance of 4.023 Å and *γ*-type intersheet interaction at a distance of 4.089 Å (Fig. 3.9). Further to S···S interactions, multiple non-classical C-H···X (X= O, S) hydrogen bonding interactions[19] also reinforce the crystal packing (Figs. 3.10a, b).
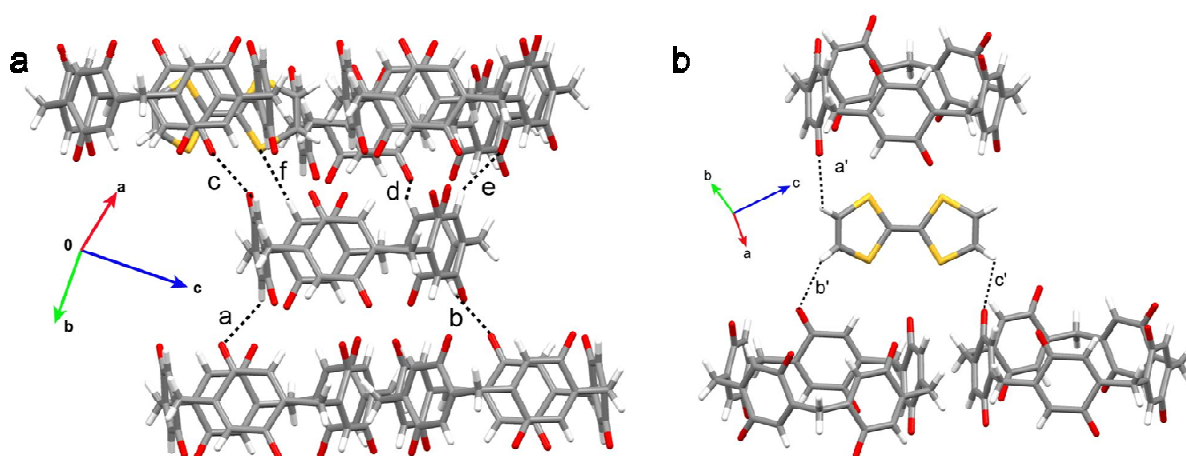
Fig. 3.10 C-H···O/S hydrogen bonding interactions observed for (a) P5Q and (b) TTF molecules in TTF-P5Q crystal (hydrogen bond parameters are enlisted in Table 3.1).

Table 3.1 Parameters corresponding to C-H···O/S hydrogen bonding interactions observed for P5Q and TTF molecules in the TTF-P5Q crystal.

Hydrogen bond	Type of hydrogen bond	d= C-H···X (X= O, S) distance (Å)	D= C···O distance (Å)	θ= C-H···X angle
a	C-H···O	2.608	3.376	138.14
b	C-H···O	2.401	3.232	145.88
c	C-H···O	2.674	3.438	137.86
d	C-H···O	2.697	3.408	132.18
e	C-H···O	2.471	3.309	147.19
f	C-H···S	2.875	3.627	136.91

a'	C-H⋯O	2.497	3.090	120.48
b'	C-H⋯O	2.543	3.373	146.09
c'	C-H⋯O	2.579	3.087	113.70

3.7 Theoretical studies

Geometry optimization of the **TTF**-**P5Q** was carried out by density function theory (DFT) at PBE/TZVP level of theory. The position and geometry of TTF and P5Q determined by solving single crystal X-ray diffraction data are in agreement with the DFT optimized structure (Fig. 3.11). The π-stacking energies (ΔE) calculated for P5Q-P5Q interaction within the unit cell, TTF-TTF and **TTF-P5Q** interactions were found to be 7.2 kcalmol^{-1}, 11.1 kcalmol^{-1} and 1.4 kcalmol^{-1}, respectively (Fig. 3.12a-c). Furthermore, the DFT calculations suggested that the energy gap between the HOMO of TTF and LUMO of P5Q is extremely small - being 0.14 eV (Fig. 3.12d, e).
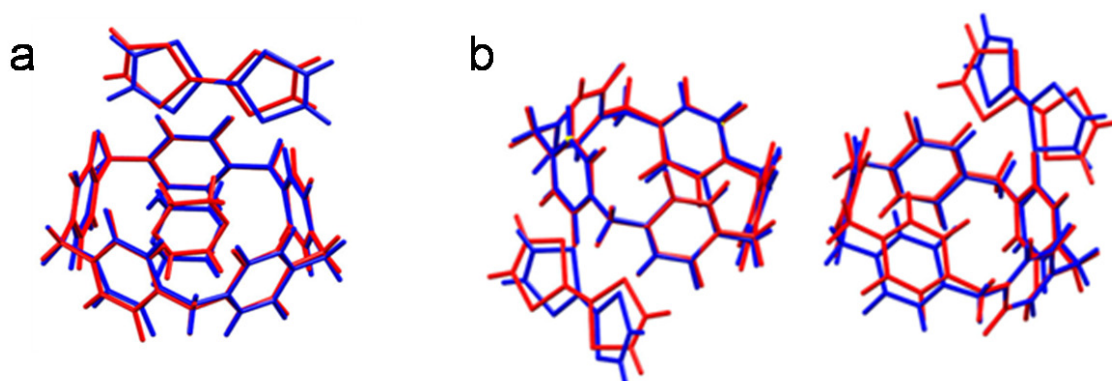
Fig. 3.11 Superposition of the X-ray structure (red) of **TTF-P5Q** with DFT optimized structures (blue). (a) **P5Q-TTF-dioxane**. (b) Two P5Qs and two TTFs as observed in a unit cell of **TTF-P5Q** crystal.
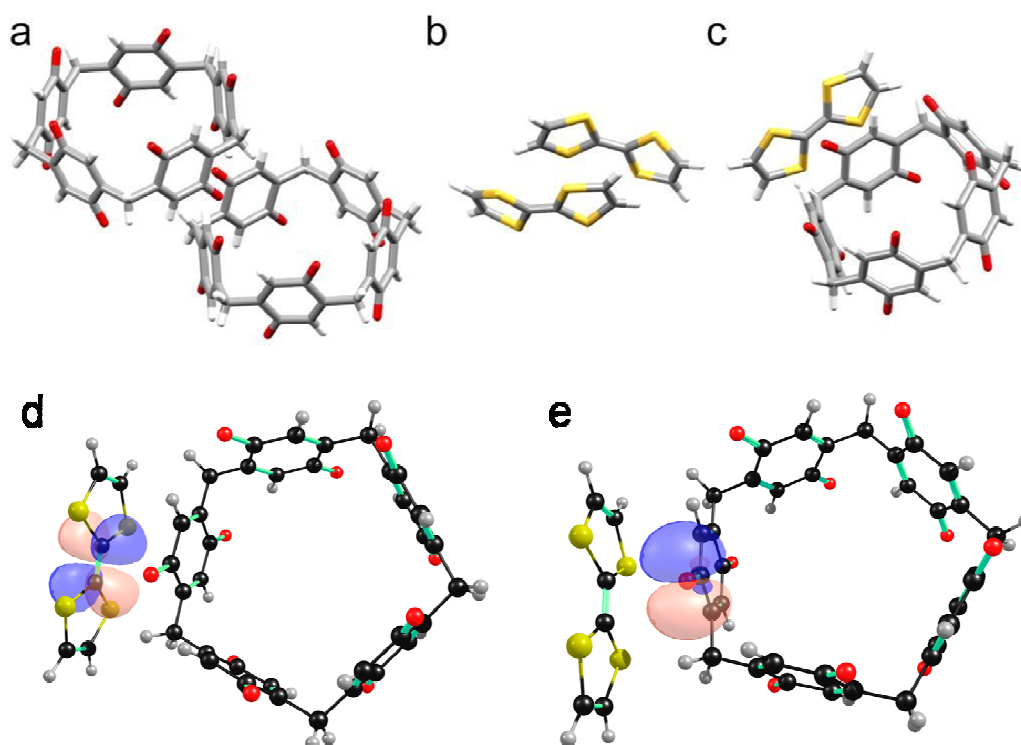
Fig. 3.12 Stacking interactions observed in the DFT optimized structure. a) P5Q-P5Q interaction within the unit cell (ΔE= 7.2 kcalmol-1). b) TTF-TTF interaction (ΔE= 11.1 kcalmol-1). c) **TTF-P5Q** interaction (ΔE= 1.4 kcalmol-1). Representative molecular orbitals of **TTF-P5Q**. (d) HOMO of TTF. (e) LUMO of P5Q.

3.8 Magnetic properties

Electron paramagnetic resonance (EPR) obtained at 300 K for the polycrystalline 1:1 and 6:1 **TTF-P5Q** suggested the presence of free radicals (Fig. 3.13). In order to determine the types of radical species involved in CT complex, the area under the curve or EPR absorption curve was plotted. Single peak fitting to accomodate lorenztian and gaussian curves within the absorption curve was initially attempted for 1:1 and 6:1 **TTF-P5Q** (Fig. 3.14 a,c). The gaussian peak showed better fitting than the lorenztian. Failure to accomodate single peak made us to attempt two gaussian peaks, which could neatly fit. This indicates the presence of two types of radicals, *i.e.*, TTF$^{+\bullet}$ and P5Q$^{-\bullet}$ (Fig. 3.14). Paramagnetism in 6:1 **TTF-P5Q** is well supported by the *M* vs *H* measurements carried out at 300 K with paramagnetic susceptibility (χ_p) of 6.14 emumol^{-1} obtained after Pascal diamagnetic correction. However, relatively lesser number of TTF$^{+\bullet}$ in 1:1 **TTF-P5Q** contributing to the paramagnetism is overwhelmed by large diamagnetic contribution from non-participating *p*-benzoquinone units in P5Q, affording negative magnetic susceptibility of -3.139 x 10^{-3} emumol^{-1} (Fig. 3.15).
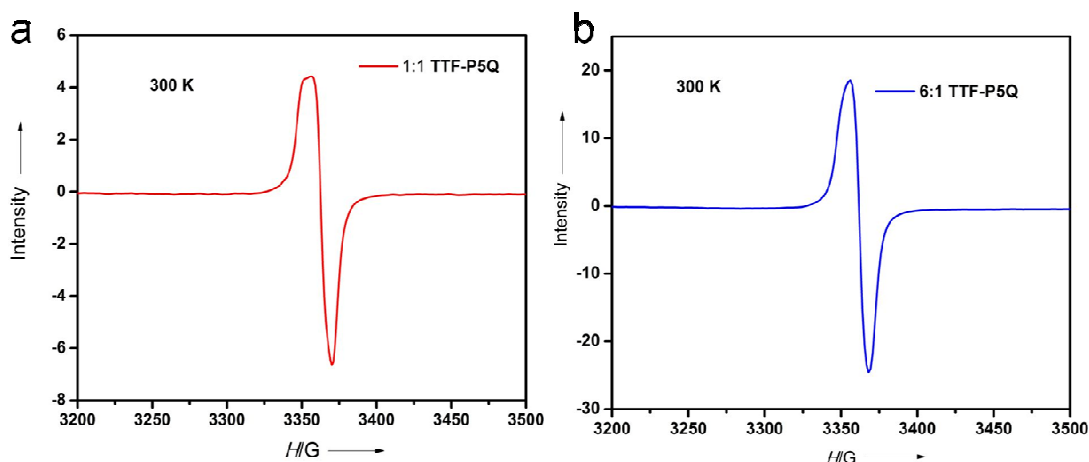
Fig. 3.13 Electron spin resonance (ESR) spectra obtained for CT complexes at room temperature. (a) 1:1 **TTF-P5Q**. (b) 6:1 **TTF-P5Q**.
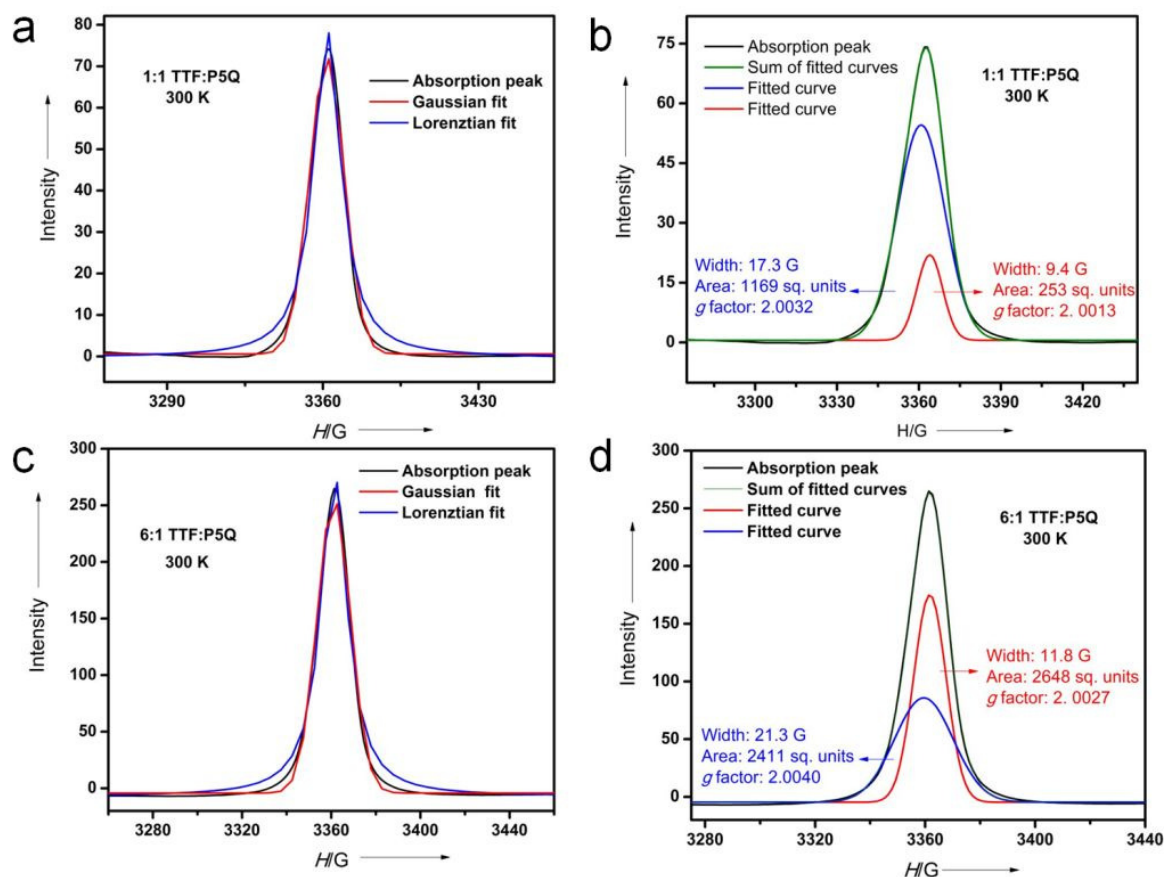
Fig. 3.14 Electron spin resonance absorption peak fitting. (a, c) Lorentzian and gaussian peaks accommodated with the latter fitting better than former; two gaussian peaks fitted with their full width at half maxima (FWHM), area and *g*-factor values. (b) 1:1 **TTF**-**P5Q** and (c) 6:1 **TTF**-**P5Q**. *Note*: *g*-factor value was calculated using the equation, $g = h\nu/\mu B$ ($\nu = 9.422843$ GHz).
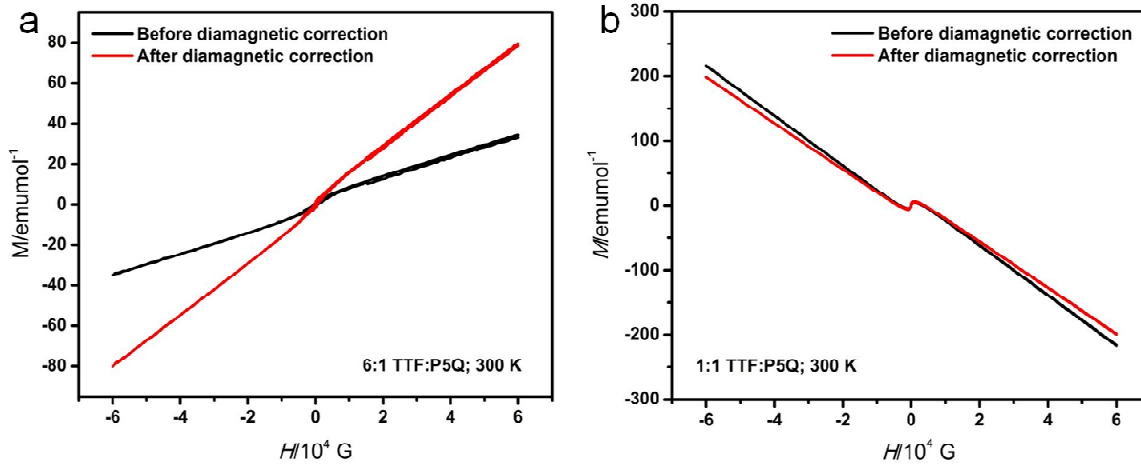
Fig. 3.15 M vs H measurements carried out for CT complexes at 300 K showing plots before and after Pascal diamagnetic correction. (a) 6:1 **TTF-P5Q**. (b) 1:1 **TTF-P5Q**.

<u>Pascal diamagnetic correction[20]:</u>

1) 6:1 **TTF-P5Q**

χ_{meas} = Slope = 6.13912 (obtained by linear-fit)

χ_D = {5[6 χ_D (C_{ring}) + 1 χ_D (C) + 4 χ_D (H) + 2 χ_D (O)] + 6[6 χ_D (C_{ring}) + 4 χ_D (S) + 4 χ_D (H)] + 5[2λ_d (C=C) + 2 λ_d (C=O)] + 6[3 λ_d (C=C)] + λ_d dioxane} – 10^{-6} emumol^{-1}

= {5[6(-6.24) + (-6) + 4 (-2.93) + 2 (-4.6)] + 6[6 (-6.24) + 4 (-15.0) + 4 (-2.93)] + 5[2(5.5) + 2 (6.3)] + 6[3 (5.5)] + 5.5} 10^{-6} emumol^{-1}

= {5[-37.44 -6 – 11.72 – 9.2] + 6[-37.44 – 60 -11.72] + 5[11+12.6] + 6[16.5] + 5.5}10^{-6} emumol^{-1}

= {5[-64.36] + 6[-109.16] + 5[23.6] + 99 + 5.5}10^{-6} emumol^{-1}

= {– 321.8 – 654.96 + 118 + 99 + 5.5} 10^{-6} emumol^{-1}

= – 754.26 * 10^{-6} emumol^{-1}

χ_P = χmeas – χ_D

  = 6.13912 – (– 0.00075426) emumol^{-1}

= 6.13987 emumol^{-1}

2) 1:1 **TTF-P5Q**

χ_{meas} = Slope = -0.00343 (obtained after linear-fit)

χ_D = {5[6 χ_D (C_{ring}) + 1 χ_D (C) + 4 χ_D (H) + 2 χ_D (O)] + 1[6 χ_D (C_{ring}) + 4 χ_D (S) + 4 χ_D (H)] + 5[2λ_d (C=C) + 2 λ_d (C=O)] + 1[3 λ_d (C=C) +] + λ_d dioxane} 10^{-6} emumol^{-1}

= {5[6(-6.24) + (-6) + 4 (-2.93) + 2 (-4.6)] + 1[6 (-6.24) + 4 (-15.0) + 4 (-2.93)] + 5[2(5.5) + 2 (6.3)] + 1[3 (5.5)] + 5.5} 10^{-6} emumol^{-1}

= {5[-37.44 -6 – 11.72 – 9.2] + 1[-37.44 – 60 -11.72] + 5[11+12.6] + 1[16.5] + 5.5}90^{-6} emumol^{-1}

= {5[-64.36] + 1[-109.16] + 5[23.6] + 16.5 + 5.5}10^{-6} emumol^{-1}

= {-321.8 – 109.16 + 118 + 16.5 + 5.5} 10^{-6} emumol^{-1}

= -290.96 * 10^{-6} emumol^{-1}

χ = χmeas – χ_D

= -0.00343-(-0.00029096) emumol^{-1}

= -0.003139 emumol^{-1}
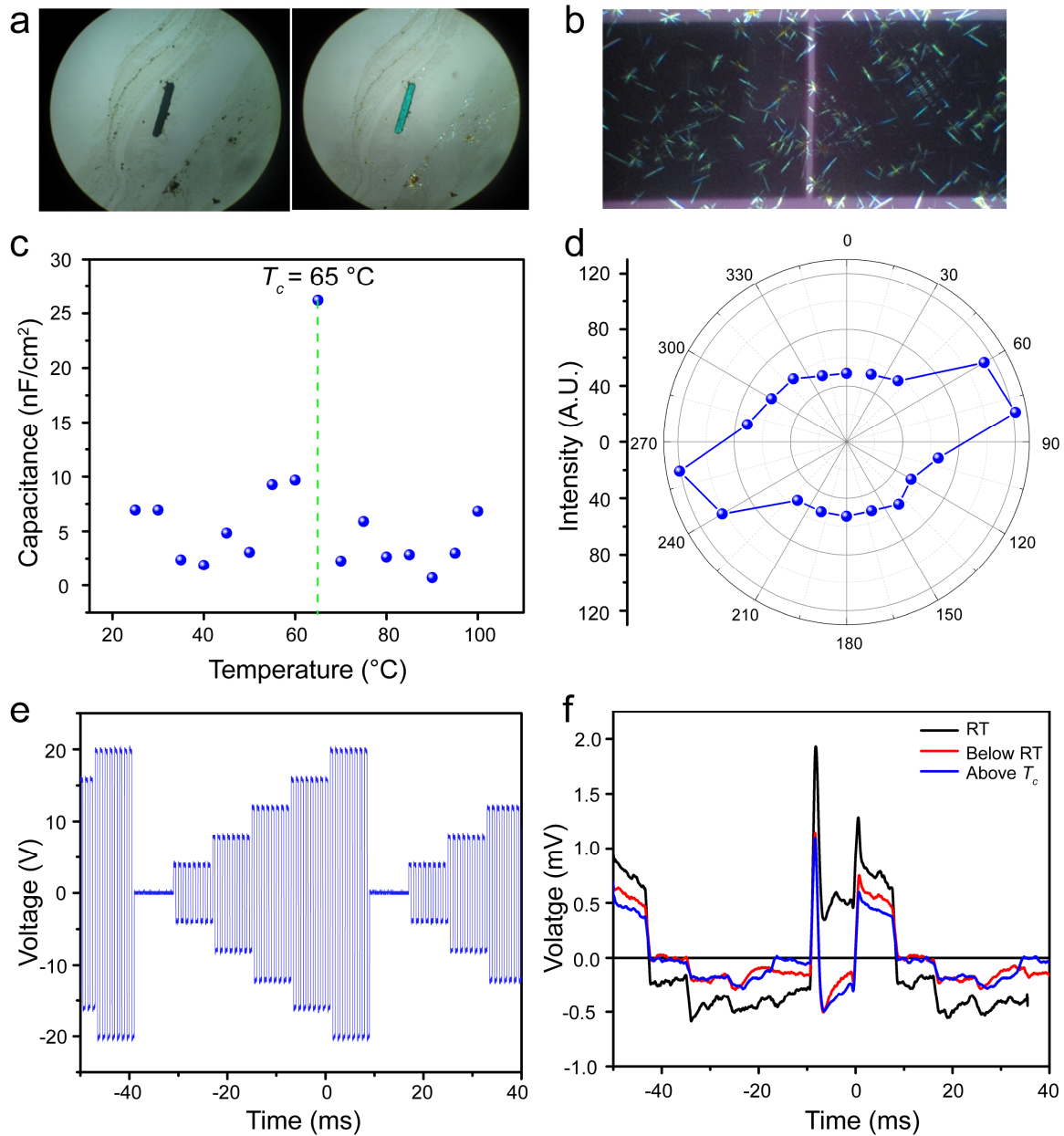
Fig 3.16 a) Optical images of a single crystal for null (left) and maximum light transmission (right) under crossed linear polarizers. b) Optical image of the fabricated capacitor with a few crystals in the channel. c) Temperature dependence of capacitance showing T_c at 65°C. d) Relative intensity of emitted light with reference to null emission for rotation of the analyzer. e) Input bias to the liquid-crystal electro-optic modulator (LCEM) which rotates the plane of polarization of incoming light (cw 532 nm) in steps. f) Photodetector response of light transmission through sample to the modulation steps shown in 3.16e.

3.9 Optical polarization and crystal anisotropy

Polarized optical microscopy was performed to ascertain the asymmetry in the **TTF**-**P5Q** crystal. Subsequent to the calibration of crossed polarizers for null transmission the **TTF-P5Q** crystal was placed in the path of incoming polarized visible light and change in the intensity of transmission was monitored upon rotating the analyzer from 0 to 360˚ (Figs 3.16a,d). Temperature-dependent capacitance measurement executed along the needle axis (*a* axis) of the crystal placed between two coplanar electrodes unveiled an anomaly at 65 ˚C (T_c) ascribed to the ferroelectric transition with a sharp increase in the capacitance to 27 nF/cm^2 before undergoing a jump discontinuity, which is characteristic of materials obeying the Curie-Weiss law. Furthermore, optical rotation was measured as a function of temperature by modulating the polarization of incoming light (Fig. 3.17). By rotating the polarization of the incoming light in steps with the aid of liquid crystal electro-optic modulator (LCEM), the optical anisotropy in the crystal was studied from the intensity of the transmitted light which is recorded as output current from the silicon photodetector (Fig. 3.16e, f). The ferroelectric phase transition in the CT crystal is accompanied by an increase in the magnitude of rotation below T_c.
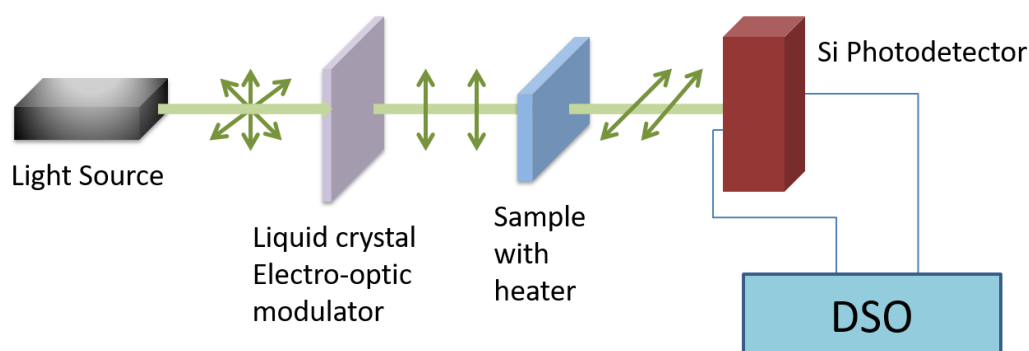
Fig. 3.17 Experimental setup for polarization dependent emission measurements.
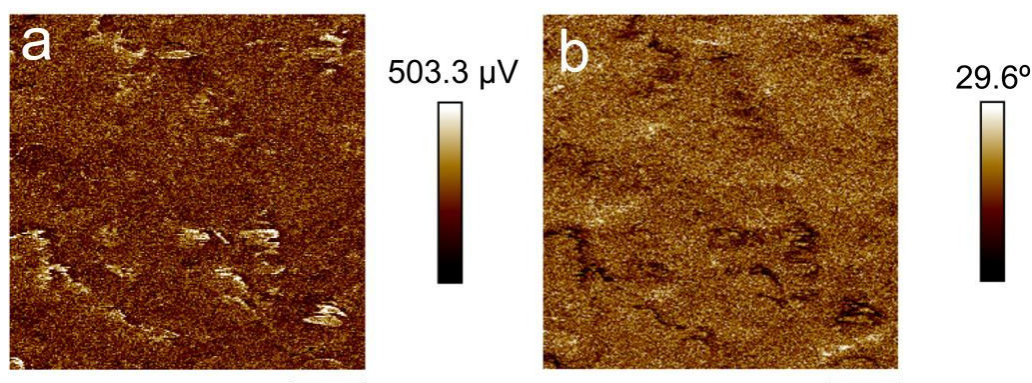
Fig. 3.18 (a) Lateral amplitude of the needle axis of the crystal. (b) lateral phase of the long axis response of the crystal. *Note*: The scale bars are 1 μm.
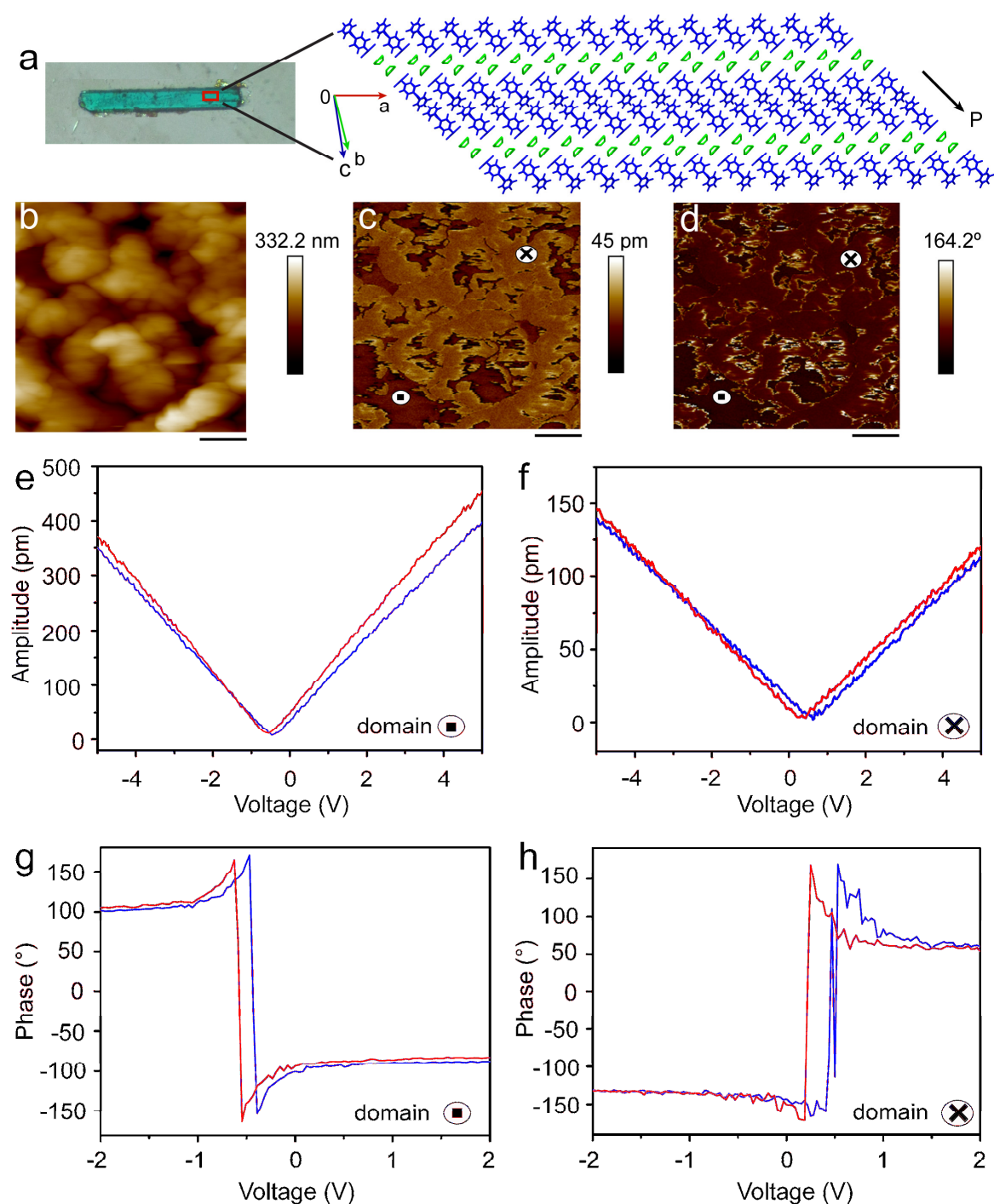
Fig. 3.19. a) Optical microscopy image (left) and molecular arrangement in the (0-1-1) plane showing alignment of spontaneous polarization (right). b) Topography of the **TTF-P5Q** crystal. c) Vertical amplitude of the needle axis of the crystal. d) Vertical phase of the long axis response of the crystal. e, f) Vertical amplitude measurements as a function of tip bias at two opposite domains, shown in 3.19c, of the crystal. g, h) Vertical phase measurements as a function of tip bias at two opposite domains, shown in 3.19d, of the crystal. *Note*: The scale bars (Fig. 3.19b-d) are 1 μm.

3.10 Piezoresponse and ferroelectric measurements

Piezoresponse Force Microscopy (PFM) was performed on a single crystal placed on a conductive substrate. A triangular voltage pulse was applied to a conductive cantilever to obtain the local electromechanical response while concomitantly mapping the topographical features of the crystal.[21] The amplitude image provides an estimate of the magnitude of the response whilst the phase image can unravel the piezo/ferroelectric domains along with the polarization orientation in the crystal. Subsequent to validation of asymmetry in the **TTF**-**P5Q** crystal with ferroelectric to paraelectric transition taking place above the room-temperature, PFM was performed at ambient temperature to ascertain the ferroelectric behavior of the CT crystal. The lateral PFM performed along the needle axis (approximately along *a* axis) (Fig. 3.19a) of **TTF**-**P5Q** crystal unveiled weak in-plane polarization (Fig. 3.18), while the out-of-plane polarization elicited by vertical PFM was strong (Figs 3.19c, d). The strong electromechanical response perpendicular to the needle axis could be attributed to the CT axis running in the diagonal *bc* plane, along which the spontaneous polarization vector aligns. The vertical PFM phase images showcase contrasting domains with their piezoresponses in-phase (0°) and out-of-phase (164.2°) to the driving voltage (Fig. 3.19d). In principle, the phase of the measured piezoresponse is directly proportional to the direction of polarization vector in the domain. Further, application of external electric field greater than the local coercive field resulted in inversion of the vertical peizoresponse in the two ferroelectric domains, unfolding the amplitude butterfly (Figs 3.19e, f) and phase hysteresis loops (Figs 3.19g, h) characteristic of polarization reversal.

3.11 Conclusions

In summary, this work resulted in the discovery of an emerald green **TTF**-**P5Q** charge transfer complex exhibiting room-temperature ferroelectric ordering (T_c = 338 ˚C). Single-crystal structure, obtained from synchrotron X-ray diffraction, revealed the fine structural characteristics of the CT complex. π-π interactions drive the P5Qs to arrange as corrugated sheets and TTFs as individual 'ring eclipsed' dimers, which intercalate the P5Q sheets. Although the crystal structure obtained at 100 K places the **TTF**-**P5Q** crystal in a non-polar space group *P-1*, the asymmetry obtained at room-temperature suggests that the crystal must have undergone a symmetry-breaking transition. In general, the centrosymmetric TTF-quinone complexes (···D-A-D-A-D-A···) undergo Peierls'

transition by dimerizing the donors and acceptors (D.AD.AD.A) resulting in macroscopic polarization, which upon applying external field undergoes inversion of polarization by exchanging their donor acceptor partners (DA.DA.DA). The mixed stacked dimers of TTF and P5Q stack along the (0-1-1) plane in an alternate fashion ($\cdots$DD-AA-DD-AA$\cdots$). The distortion in the periodic arrangement of TTF and P5Q could plausibly be due to Peierls' transition with donor and acceptor or their dimers getting exchanged. The ferroelectric property observed in **TTF**-**P5Q** CT crystal prompted us to employ this in fabrication of capacitor exhibiting high specific capacitance below Curie temperature. The profile of C(T) above T_c is indicative of the temperature dependence of the dielectric while below T_c, C(T) is governed by the relaxation dynamics of the ferroelectric domains. These observations are consistent with the optical response at different temperatures.

3.12 Experimental methods

Ball milling

Weighed amounts of P5Q and TTF were taken in stoichiometric ratios and were subjected to ball-milling for 30 min at a frequency of 25 Hz.

Crystal growth and single-crystal X-ray diffraction

Crystals were grown from 1,4-dioxane by slow evaporation. The tiny emerald green crystals were picked from the mother liquor under the microscope and cryo-soaked and cryo-frozen before mounting for collection of diffraction data. Crystals were grown from solutions containing varying molar ratios of TTF and few of them (1:1, 5:1 and 6:1 **TTF-P5Q** complexes) were mounted to obtain the lattice parameters. All the mounted crystals possessed the same lattice parameters indicating that crystals formed were all 1:1 CT complex, presumably the thermodynamically most stable arrangement. 1:1 and 5:1 were grown by adding TTF solution to P5Q solution in 1,4-dioxane, whereas 6:1 was grown by dissolving the ground green solid. Green crystals formed quickly and more in number in solutions that contained higher molar ratios of TTF. The crystal structure shown in the text was obtained from 1,4-dioxane solution of 6:1 ground complex.

Magnetic measurements

7.50 mg of 1:1 **TTF-P5Q** and 8.75 mg of 6:1 **TTF-P5Q** obtained by powdering the pellets of CT complex were taken in a sample refiller and introduced into the magnetometer for recording the magnetization as a function of magnetic field. The empty refiller measurements were obtained prior to that of the sample. The pellets of the CT complexes were prepared from the solids obtained after stripping off 1,4-dioxane.

Polarization rotation and capacitance measurements

For the polarization measurements, a crystal of the CT complex was placed on a glass slide in the path of crossed polarizers under a microscope. The analyzer was rotated with respect to the polarizer to observe the change in intensity of transmitted light. In order to see the temperature dependence of polarization rotation, incident light polarization was rotated in pre-defined steps by a LC electro-optic modulator and the transmittance of the modulated light was detected by a silicon photo-detector at three different temperatures. The three temperature regimes ($\sim$ error of 5 K expected in the peltier stage indicator and sample temperature), were maintained sufficiently away from the Curie temperature ($> T_c$ and $< T_c$) to highlight the differences in the response. Capacitance measurements were

performed using SCS-4200 semiconductor parameter analyzer. Temperature was varied by using a Linkam temperature-controlled stage positioned on a microscope.

Piezoresponse force microscopy (PFM) and piezoelectric measurements

PFM was performed using a Bruker Dimension IconSys1 Atomic Force Microscope operated in piezo mode.

Crystal data and structure refinement

Identification code	shelx
Empirical formula	$C_{45}H_{31}O_{12}S_4$
Formula weight	891.94
Temperature/K	100(2)
Crystal system	triclinic
Space group	*P-1*
a/Å	8.650(2)
b/Å	12.350(6)
c/Å	18.600(2)
α/°	86.07
β/°	77.630(10)
γ/°	83.81
Volume/Å^3	1927.4(11)
Z	2
ρ_{calc} (g/cm^3)	1.537
μ/mm^{-1}	0.401
F(000)	922.0
Crystal size/mm^3	$0.23 \times 0.03 \times 0.05$
Radiation	Synchrotron λ= 0.77488 Å
2Θ range for data collection/°	3.62 to 57.934
Index ranges	$-10 \leq h \leq 10$, $-15 \leq k \leq 15$, $-23 \leq l \leq 23$

|	
Reflections collected	59882
Independent reflections	7753 [R_{int} = 0.0421, R_{sigma} = 0.0292]
Data/restraints/parameters	7753/0/597
Completeness to theta=28.967	98.3%
Goodness-of-fit on F^2	1.061
Final R indexes [I>=2σ (I)]	R_1 = 0.0409, wR_2 = 0.1052
Final R indexes [all data]	R_1 = 0.0417, wR_2 = 0.1058
Largest diff. peak/hole / e $Å^{-3}$	0.46/-0.40

Part B: Charge Transfer Crystals of Pillar[5]quinone and 4,4'-Bis(N-carbazolyl)-1,1'-Biphenyl

3.13 Introduction

Carbazoles adorned with rigid and planar aromatic core have drawn considerable attention in the realm of optoelectronic devices embracing organic light emitting diodes (OLEDs), organic photovoltaics (OPVs), organic field effect transitors (OFETs), *etc*.[22] Charge donor molecules, like carbazoles, possessing high charge (hole) transport ability bear significant importance in organic semiconductors, especially in OLEDs. The high charge carrier ability reduces the resistance, thus enhancing the power efficiency. 4,4'-bis(N-carbazolyl)-1,1'-biphenyl (CBP) (Fig. 3.20a), a biphenyl molecule appended with two carbazoles, possesses low triplet state energy and pronounced thermal stability, in addition to the high charge mobility, ushering in their use in phosphorescent organic light emitting diodes (PHOLEDs) and white organic light emitting diodes (WOLEDs).[22c] Remarkably, the WOLEDs overcome the serious stability concerns in PHOLEDs,[22a] and promise to be highly efficient source for large-area lighting with good-color rendering properties.[22b] CBP possesses triplet energy of 2.56 eV and thus has been employed as efficient hosts in WOLEDs with red, green or blue (RGB) emitters.[23]
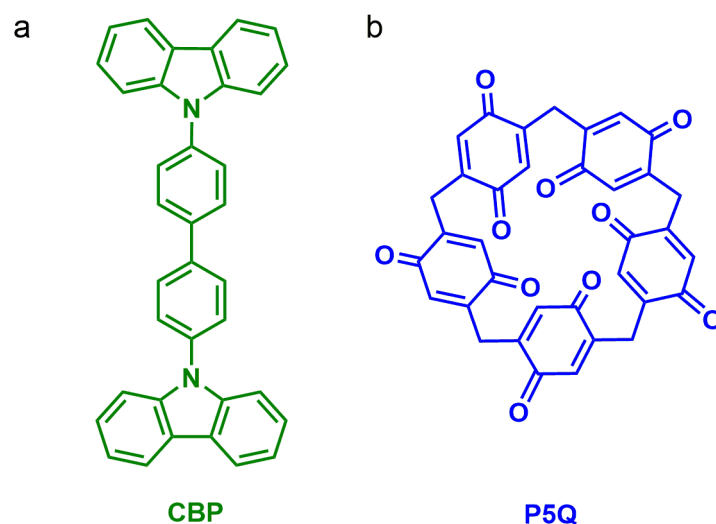
Fig. 3.20 Molecular structures of donor and acceptor. (a) 4,4'-bis(N-carbazolyl)-1,1'-biphenyl (CBP). (b) pillar[5]quinone.

Three polymorphs of luminescent CBP are reported in the literature: the *α*-CBP, *β*-CBP and *γ*-CBP.[23] While the *α*-CBP and *γ*-CBP possess almost similar geometrical structure and physical electro-optic properties, the *β*-CBP exhibits different geometrical conformation and different physical properties (Fig. 3.21).
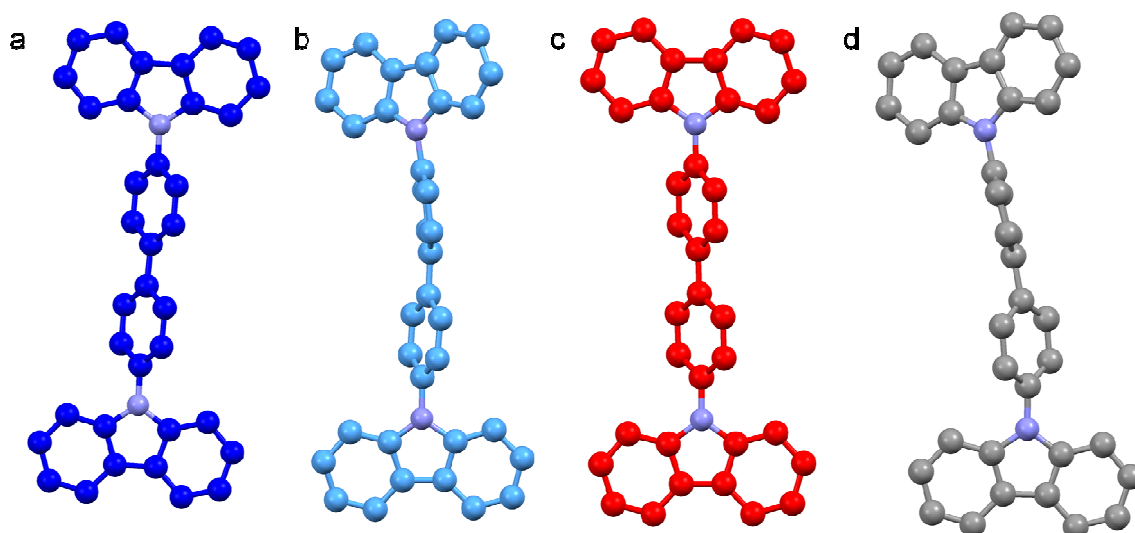
Fig. 3.21 Crystal structures of CBP polymorphism: a) *α*-CBP; b) *β*-CBP; c) *γ*-CBP; and d) CBP structure in the **CBP**-**P5Q** crystal. Crystal structures (Fig. 3.21a, b and c) courtesy of CCDC.

3.14 Objective of the present work

We envisioned that CBP could be a potential donor owing to the presence of two electron rich carbazoles with planar geometry. On the other hand, as described in section 3.1, P5Q bestowed with five electron deficient *p*-benzoquinone units is an exceptional acceptor. Similar to the charge transfer complex of **TTF**-**P5Q,** we attempted the complexation of **CBP**-**P5Q** to obtain the CT crystals and study its crystal structure besides its optophysical properties.

3.15 Results and discussion

Brown colored single crystals were grown in dioxane from the 1:1 solution of P5Q and CBP. Unlike **TTF-P5Q** crystal, the 1:1 **CBP-P5Q** crystals formed quickly- within couple of days and were relatively bigger in size. The **CBP**-**P5Q** crystal crystallized in a centrosymmetric *P-1* lattice. A unit cell of **CBP**-**P5Q** consists of two molecules each of CBP and P5Q besides seven molecules of dioxane. The presence of significant number of solvent molecules in the unit cell makes the crystal unstable outside the mother liquor and eventually leads to its crumbling. Again, π-stacking interactions play a significant role, in bringing about the CT complexation between the π-donor CBP and the π-acceptor P5Q (Fig. 3.22). Clearly, the **CBP-P5Q** unveiled mixed stacking down the *b*-axis with alternating donor and acceptor, a striking difference observed in packing compared to **TTF-P5Q** crystal wherein, the dimers of TTF and P5Q stack in alternate way. Among the

five *p*-benzoquinones of P5Q three are involved in π-stacking interactions: two with the CBPs present at top and bottom as viewed along the *a* axis at mean centroid-centroid distances of 3.509 Å and 3.585 Å, respectively and one with the *p*-benzoquinone of P5Q that is present outside the unit cell at the distance of 3.599 Å between their centroids. The P5Qs in the crystal **TTF**-**P5Q** align segregatedly as corrugated sheets with continuous staking approximately along the *c* axis. However, the P5Qs organize themselves as dimer in the *ab* plane along the *c*-axis, with π-π interaction observed only with the P5Q situated outside the unit cell and not with the one situated inside.

The CBP molecule in the crystal structure is twisted and is asymmetric, and resembles the *β*-CBP. The mean planes of biphenyl are 37.81° apart from being parallel. Similarly, the mean planes of carbazoles aren't parallel and lie 32.93° distant from each other. Twisting of the aromatic rings of the biphenyl group is observed to a significant extent with the angles between the mean planes of the nearest carbazole and the benzene in the biphenyl being 50.23° and 62.95° for the two crystallographically distinct groups.
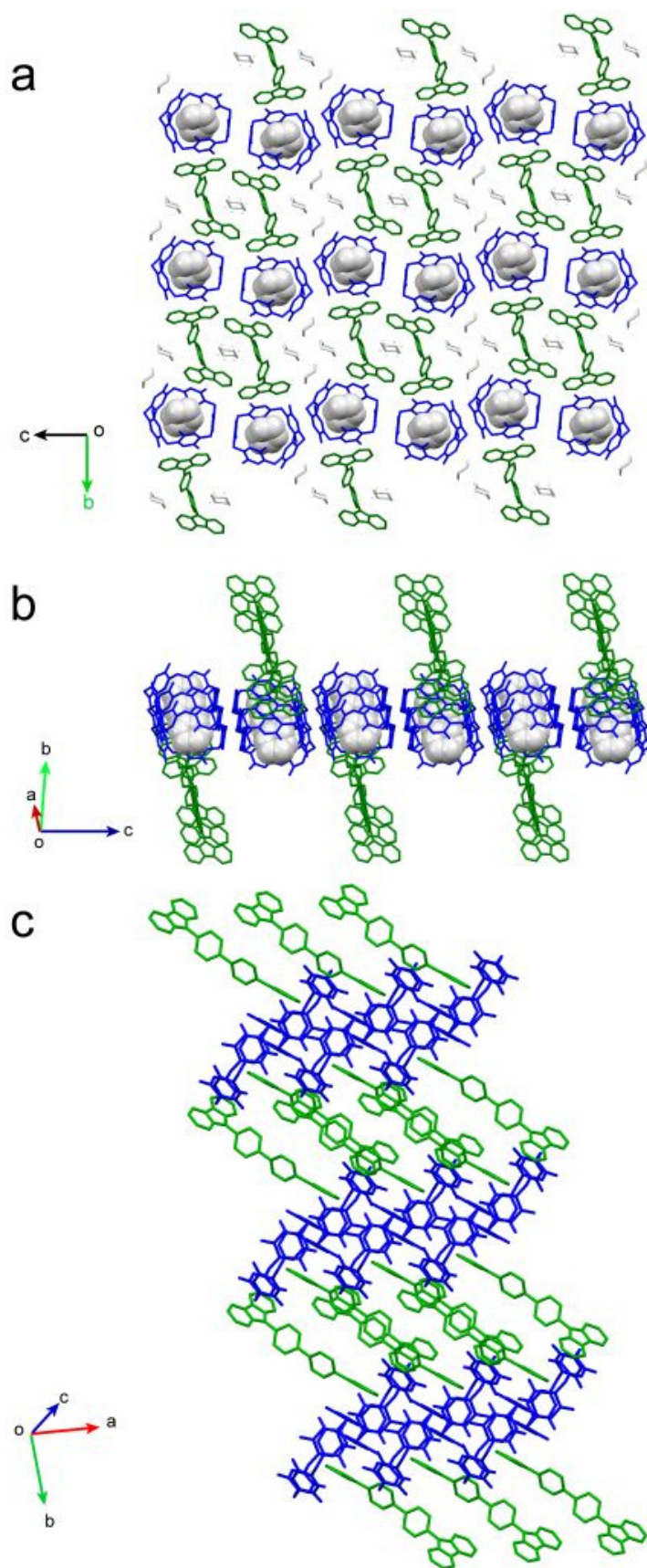
Fig. 3.22 (a) Single crystal structure of the 1:1 CT complex of **CBP-TTF** viewed along *a* axis displaying mixed stacking of donor and acceptor molecules. (b) Another view of the

plane (100) approximately along the *a*-axis. (c) View perpendicular to the plane (001) showcasing mixed stacking interaction down the *b*-axis.

3.16 Conclusions

In summary, brown millimeter sized CT crystals of P5Q and CBP were grown in dioxane which crystallized in centrosymmetric *P-1* space group. The solvent dioxane plays pivotal role in organizing P5Qs as corrugated sheets within which the donor molecule stack with the macrocycle. Mixed stacking of donor and acceptor molecules is clearly evident along the *b* axis. Further attempts in understanding the effect of complexation on the photophysical properties of CBPs will be carried out in future besides zeroing in on intriguing physical properties that would emerge due to CT complexation of P5Q and CBP.

3.17 Experimental Section

Crystal data: X-ray intensity data measurements of complex **CBP-TTF** was carried out on a Bruker D8 VENTURE Kappa Duo PHOTON II CPAD diffractometer equipped with Incoatech multilayer mirrors optics. The intensity measurements were carried out with Cu micro-focus sealed tube diffraction source (Mo K_α= 0.71073 Å) at 100(2) K temperature. The X-ray generator was operated at 50 kV and 1.4 mA. A preliminary set of cell constants and an orientation matrix were calculated from three sets of 36 frames. Data were collected with ω scan width of 0.5° at different settings of φ and *2θ* with a frame time of 10 secs keeping the sample-to-detector distance fixed at 5.00 cm. The X-ray data collection was monitored by APEX3 program (Bruker, 2016). All the data were corrected for Lorentzian, polarization and absorption effects using SAINT and SADABS programs (Bruker, 2016). SHELX-97 was used for structure solution and full matrix least-squares refinement on F^2. All the hydrogen atoms were placed in a geometrically idealized position and constrained to ride on its parent atom.

Table 3.2 Crystal data and structure refinement of CBP-P5Q

Identification code	mo_P5QBISCRB2_0m
Empirical formula	$C_{85}H_{72}N_2O_{17}$
Formula weight	1393.44

Temperature/K	100
Crystal system	triclinic
Space group	P-1
a/Å	8.2783(4)
b/Å	19.5477(9)
c/Å	21.4581(9)
α/°	85.456(2)
β/°	89.852(2)
γ/°	85.087(2)
Volume/Å^3	3448.7(3)
Z	2
ρ_{calc} (g/cm^3)	1.342
μ/mm^{-1}	0.094
F(000)	1464.0
Crystal size/mm^3	0.23 × 0.03 × 0.05
Radiation	MoK$_\alpha$ λ=0.71073 Å
2Θ max/°	55.998
Index ranges	$-10 \leq h \leq 10$, $-25 \leq k \leq 25$, $-28 \leq l \leq 28$
Independent reflections	16472
Completeness to theta=27.999	99.1%
Goodness-of-fit on F^2	1.057
Final R indexes [I>=2σ (I)]	$R_1 = 0.0684$, $wR_2 = 0.1813$

3.18 References

(1) a) Li, J.; Liu, Y.; Zhang, Y.; Cai, H.-L.; Xiong, R.-G. *Phys. Chem. Chem. Phys.* **2013**, *15*, 20786; b) Lines, M. E.; Glass, A. M. *Principles and applications of ferroelectrics and related materials*; Oxford university press, 1977.

(2) a) Scott, J. *Science* **2007**, *315*, 954; b) Han, S. T.; Zhou, Y.; Roy, V. *Adv. Mater.* **2013**, *25*, 5425.

(3) a) Horiuchi, S.; Tokura, Y. *Nat. Mater.* **2008**, *7*, 357; b) Miyajima, D.; Araoka, F.; Takezoe, H.; Kim, J.; Kato, K.; Takata, M.; Aida, T. *Science* **2012**, *336*, 209; c) Tayi, A. S.; Kaeser, A.; Matsumoto, M.; Aida, T.; Stupp, S. I. *Nat. Chem.* **2015**, *7*, 281; d) Owczarek, M.; Hujsak, K. A.; Ferris, D. P.; Prokofjevs, A.; Majerz, I.; Szklarz, P.; Zhang, H.; Sarjeant, A. A.; Stern, C. L.; Jakubas, R.; Hong, S.; Dravid, V. P.; Stoddart, J. F. *Nat. Commun.* **2016**, *7*, 13108.

(4) Kagawa, F.; Horiuchi, S.; Tokunaga, M.; Fujioka, J.; Tokura, Y. *Nat. Phys.* **2010**, *6*, 169.

(5) Kagawa, F.; Horiuchi, S.; Matsui, H.; Kumai, R.; Onose, Y.; Hasegawa, T.; Tokura, Y. *Phys. Rev. Lett.* **2010**, *104*, 227602.

(6) Kobayashi, K.; Horiuchi, S.; Kumai, R.; Kagawa, F.; Murakami, Y.; Tokura, Y. *Phys. Rev. Lett.* **2012**, *108*, 237601.

(7) Horiuchi, S.; Kobayashi, K.; Kumai, R.; Minami, N.; Kagawa, F.; Tokura, Y. *Nat. Commun.* **2015**, *6*, 7469.

8) a) Tayi, A. S.; Shveyd, A. K.; Sue, A. C.-H.; Szarko, J. M.; Rolczynski, B. S.; Cao, D.; Kennedy, T. J.; Sarjeant, A. A.; Stern, C. L.; Paxton, W. F. *Nature* **2012**, *488*, 485; b) Makam, P.; Senanayak, S. P.; Narayan, K. S.; Govindaraju, T. *J. Am. Chem. Soc.* **2016**, *138*, 8259.

(9) D'Avino, G.; Verstraete, M. J. *Phys. Rev. Lett.* **2014**, *113*, 237602.

(10) a) Cao, D.; Kou, Y.; Liang, J.; Chen, Z.; Wang, L.; Meier, H. *Angew. Chem. Int. Ed.* **2009**, *48*, 9721; b) Shivakumar, K. I.; Sanjayan, G. J. *Synthesis* **2013**, *45*, 896.

(11) Ogoshi, T.; Yamagishi, T.-a.; Nakamoto, Y. *Chem. Rev.* **2016**, *116*, 7937.

(12) Shivakumar, K. I.; Yan, Y.; Hughes, C. E.; Apperley, D. C.; Harris, K. D.; Sanjayan, G. J. *Cryst. Growth Des.* **2015**, *15*, 1583.

(13) a) Martín, N. *Chem. Commun.* **2013**, *49*, 7025; b) Bryce, M. R. *J. Mater. Chem.* **1995**, *5*, 1481; c) Bryce, M. R. *Chem. Soc. Rev.* **1991**, *20*, 355.

(14) Kumar, A.; Ghosh, B.; Poswal, H.; Pandey, K.; Hosur, M.; Dwivedi, A.; Makde, R.; Sharma, S. *J. Synchrotron Rad.* **2016**, *23*, 629.

(15) Fourmigué, M.; Batail, P. *Chem. Rev.* **2004**, *104*, 5379.

(16) a) Mohamud, S.; Phuoc, V. T.; del Campo, L.; Massa, N. E.; Pagola, S. *Synth. Met.* **2016**, *214*, 71; b) Mayerle, J. J.; Torrance, J. B. *Bull. Chem. Soc. Jpn.* **1981**, *54*, 3170; c) Kistenmacher, T. J.; Phillips, T. E.; Cowan, D. O. *Acta Cryst. B* **1974**, *30*, 763; d) Spruell, J. M.; Coskun, A.; Friedman, D. C.; Forgan, R. S.; Sarjeant, A. A.; Trabolsi, A.; Fahrenbach, A. C.; Barin, G.; Paxton, W. F.; Dey, S. K.; Olson, M. A.; Benítez, D.; Tkatchouk, E.; Colvin, M. T.; Carmielli, R.; Caldwell, S. T.; Rosair, G. M.; Hewage, S. G.; Duclairoir, F.; Seymour, J. L.; Slawin, A. M. Z.; Goddard, W. A.; Wasielewski, M. R.; Cooke, G.; Stoddart, J. F. *Nat. Chem.* **2010**, *2*, 870.

(17) Ferraris, J.; Cowan, D.; Walatka, V. t.; Perlstein, J. *J. Am. Chem. Soc.* **1973**, *95*, 948.

(18) Novoa, J. J.; Rovira, M. C.; Rovira, C.; Veciana, J.; Tarrés, J. *Adv. Mater.* **1995**, *7*, 233.

(19) Desiraju, G. R.; Steiner, T. *The weak hydrogen bond: in structural chemistry and biology*; Oxford University Press, New York: New York, 1999.

(20) Bain, G. A.; Berry, J. F. *J. Chem. Educ.* **2008**, *85*, 532.

(21) a) Hong, S.; Woo, J.; Shin, H.; Jeon, J. U.; Pak, Y. E.; Colla, E. L.; Setter, N.; Kim, E.; No, K. *J. Appl. Phys.* **2001**, *89*, 1377; b) Gruverman, A.; Auciello, O.; Tokumoto, H. *Appl. Phys. Lett.* **1996**, *69*, 3191.

(22) a) Rosenow, T. C.; Furno, M.; Reineke, S.; Olthof, S.; Lüssem, B.; Leo, K. *J. Appl. Phys.* **2010**, *108*, 113113; b) Reineke, S.; Lindner, F.; Schwartz, G.; Seidler, N.; Walzer, K.; Lüssem, B.; Leo, K. *Nature* **2009**, *459*, 234; c) Kido, J.; Kimura, M.; Nagai, K. *Science* **1995**, *267*, 1332; d) Uoyama, H.; Goushi, K.; Shizu, K.; Nomura, H.; Adachi, C. *Nature* **2012**, *492*, 234; e) Ye, J.; Chen, Z.; Fung, M.-K.; Zheng, C.; Ou, X.; Zhang, X.; Yuan, Y.; Lee, C.-S. *Chem. Mater.* **2013**, *25*, 2630; f) Nishimoto, T.; Yasuda, T.; Lee, S. Y.; Kondo, R.; Adachi, C. *Mater. Horiz.* **2014**, *1*, 264; g) Blouin, N.; Michaud, A.; Leclerc, M. *Adv. Mater.* **2007**, *19*, 2295; h) Li, J.; Grimsdale, A. C. *Chem. Soc. Rev.* **2010**, *39*, 2399; i) Tang, J.; Hua, J.; Wu, W.; Li, J.; Jin, Z.; Long, Y.; Tian, H. *Energy Environ. Sci.* **2010**, *3*, 1736; j) Ho, C.-L.; Chi, L.-C.; Hung, W.-Y.; Chen, W.-J.; Lin, Y.-C.; Wu, H.; Mondal, E.; Zhou, G.-J.; Wong, K.-T.; Wong, W.-Y. *J. Mater. Chem.* **2012**, *22*, 215.

(23) Gleason, C. J.; Cox, J. M.; Walton, I. M.; Benedict, J. B. *CrystEngComm* **2014**, *16*, 7621.

Chapter 4

Self-assembly of solvatofluorochromic phloroglucinol-dithiolylidene-based C₃ symmetric molecules into one-dimensional nanostructures

Self-Assembly of Solvatofluorochromic Phloroglucinol-Dithiolylidene-based C₃ Symmetric Molecules into One-dimensional Nanostructures

4.1 Introduction

One-dimensional supramolecular self-assembly of compounds possessing charge-transfer interactions has garnered significant attention, over past couple of decades, owing to their potential applications in organic electronics.[1] The observation of high conductivity in the single crystals of charge transfer complexes has spurred considerable interest in self-assembled functional nanoarchitectures, particularly nanofibres/rods.[2] Supramolecular interactions such as charge transfer, hydrogen bonding, van der Waals and π-stacking aid molecules to aggregate and form self-assembled ensembles on 2D susbtrate and in some cases, single crystals.[3] Nanofibres/rods usually become (semi)conducting upon doping the π-donors/acceptors with suitable oxidant/reductant. Nevertheless, few nanofibres are reported to be semiconductive without any doping.[4] Derivatives of amphiphilic hexabenzocoronene (HBC),[5] tetrathiafulvalene (TTF),[6] oligo(thiophene)[7] and perylene-3,4,9,10-tetracarboxylic diimide (PTCDI)[8] are reported to form elongated nanoarchitectures (Fig. 4.1). Conductivity in the nanostructures of TTF derivatives is typically induced by doping with iodine.[1a] However, few TTF face-to-face stacked nanofibres are conductive in an undoped state attributed to fastener effect with effective packing.[4] TTF derivatives adorned with long alkyl chains are known to self-assemble into 1D columnar architectures due to π-stacking, van der Waals, and S···S interactions. The amphiphilic diester (Fig. 4.1d) derived from TTF exhibited gelation comprising entangled nanofibres which showed conductivity upon doping with iodine.[9] The amino acid appended TTF derivatives (Fig. 4.1e) formed nanofibres owing to hydrogen bonding and showcased conductivity when exposed to iodine vapors.[10] Annulenes (Fig. 4.1f) consisting of oligomeric units of TTF possess large π-surface which effectively delocalizes the electrons, upon doping, in mixed valence state.[11] Columnar arrangement facilitated by π-stacking interactions in star-shaped TTF hexamer (Fig. 4.1g) afforded high conductivity upon oxidation with iron perchlorate.[12]
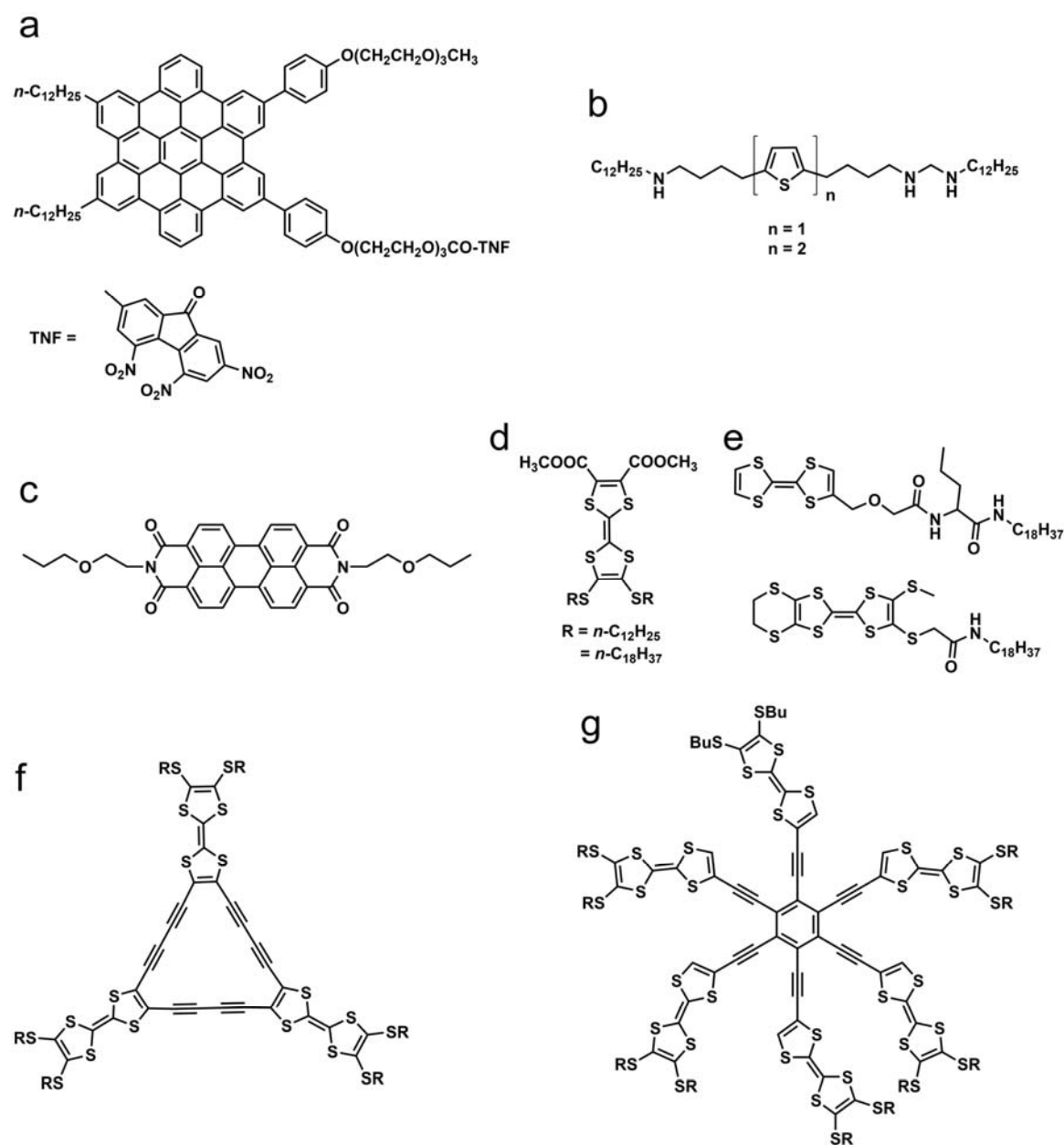
Fig. 4.1 Molecular structure of compounds reported to exhibit self-assembled elongated nanostructures.

On the other hand, compounds appended with push-pull groups and exhibiting intramolecular charge transfer (ICT) have demonstrated to be potential organic functional materials with versatile applications. ICT occurs as a consequence of shift in the electron density from the charge donor region of the molecule to the charge acceptor region. π-Extended tetrathiafulvalenes (ex-TTF) having two dithiole rings separated by a conjugated spacer have found immense applications in the field of nonlinear optics and semiconductors. The increased conjugation results in stabilized oxidation states and provides access to various polycationic species owing to reduced columbic repulsion

besides narrower energy gap. Furthermore, organic systems showcasing multi-stage amphoteric redox properties (*i.e.,* the ability to get oxidized and reduced within small range of potential) are rare. Such molecules which exhibit the aforementioned property possess enhanced π-donor and π-acceptor ability attributed to the aromatic stabilization of the charged species. Bryce and co-workers reported the crystal structure and amphoteric redox behaviour of 2,4,6-tris(4,5-diisopropyl-1,3-dithiol-2-ylidene).[13] This compound was synthesized in 30% yield by reacting phloroglucinol with 2-methylthio-4,5-di-*n*-propyl-1,3-dithiolium iodide. The iodide salt of 2-methylthio-4,5-di-*n*-propyl-1,3-dithiole was obtained in 11% yield starting from butanal in six steps.[14] Herein, we appended thioalkyl groups in place of propyl group in two steps and studied their photophysical, electrochemical and self-assembling properties.

4.2 Objective of the present work

We envisioned that the reaction of readily accessible 4,5-bis(alkylthio)-1,3-dithiole-2-thione with active methylene group, particularly phloroglucinol, would be interesting owing to the extended π-conjugation and *C₃* symmetry. Further, appending various alkyl groups would help in obtaining desired properties besides addressing the solubility issue.

4.3 Results and discussion

We report the synthesis of novel class of fluorescent compounds 2,4,6-tris(4,5-bis(alkylthio)-1,3-dithiol-2-ylidene)cyclohexane-1,3,5-triones **2a-e** (Fig. 4.2) besides their intriguing properties such as intramolecular charge transfer, self-assembly, amphoteric redox behavior in addition to the crystal structure.
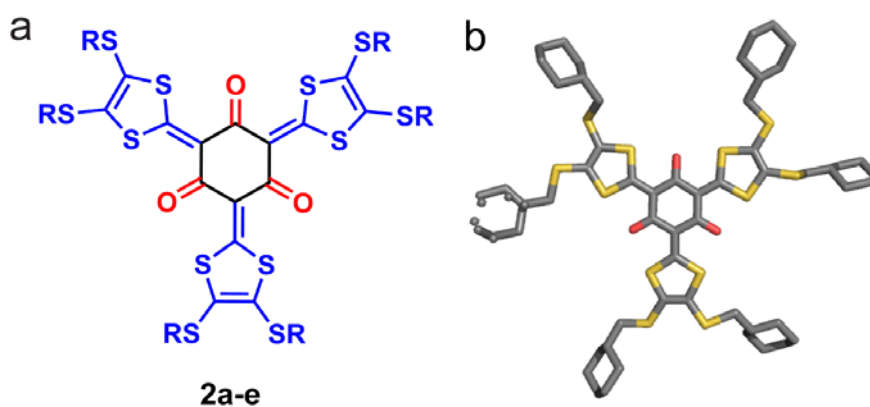
Fig. 4.2 (a) General molecular structure of 2,4,6-tris(4,5-bis(alkylthio)-1,3-dithiol-2-ylidene)cyclohexane-1,3,5-triones **2a-e**. (b) Crystal structure of compound **2e**.

4.3.1 Synthesis

The synthesis of cyclic $-(D-A)_3-$ triadic system was carried out as illustrated in the Scheme **4.1**. The precursor 4,5-bis(alkylthio)-1,3-dithiole-2-thione **1a-e** were obtained in excellent yields (>95%) *via* nucleophilic substitution by refluxing the complex bis(tetraethylammonium)bis(1,3-dithiole-2-thione-4,5-dithiolato)zincate with alkyl bromides in acetonitrile.[15] Subsequently, base-mediated electrophilic substitution afforded the target compounds **2a-e** by enabling the compounds **1a-e** to react with phloroglucinol in presence of silver nitrate in poor to fair yields (30-60%).

Scheme 4.1 Synthesis of 2,4,6-tris(4,5-bis(alkylthio)-1,3-dithiol-2-ylidene)cyclohexane-1,3,5-triones (**2a-e**)

1a: R= 2-ethylhexyl
1b: R= *n*-propyl
1c: R= *n*-butyl
1d: R= *n*-dodecyl
1e: R= cyclohexyl methyl

2a: R= 2-ethylhexyl
2b: R= *n*-propyl
2c: R= *n*-butyl
2d: R= *n*-dodecyl
2e: R= cyclohexyl methyl
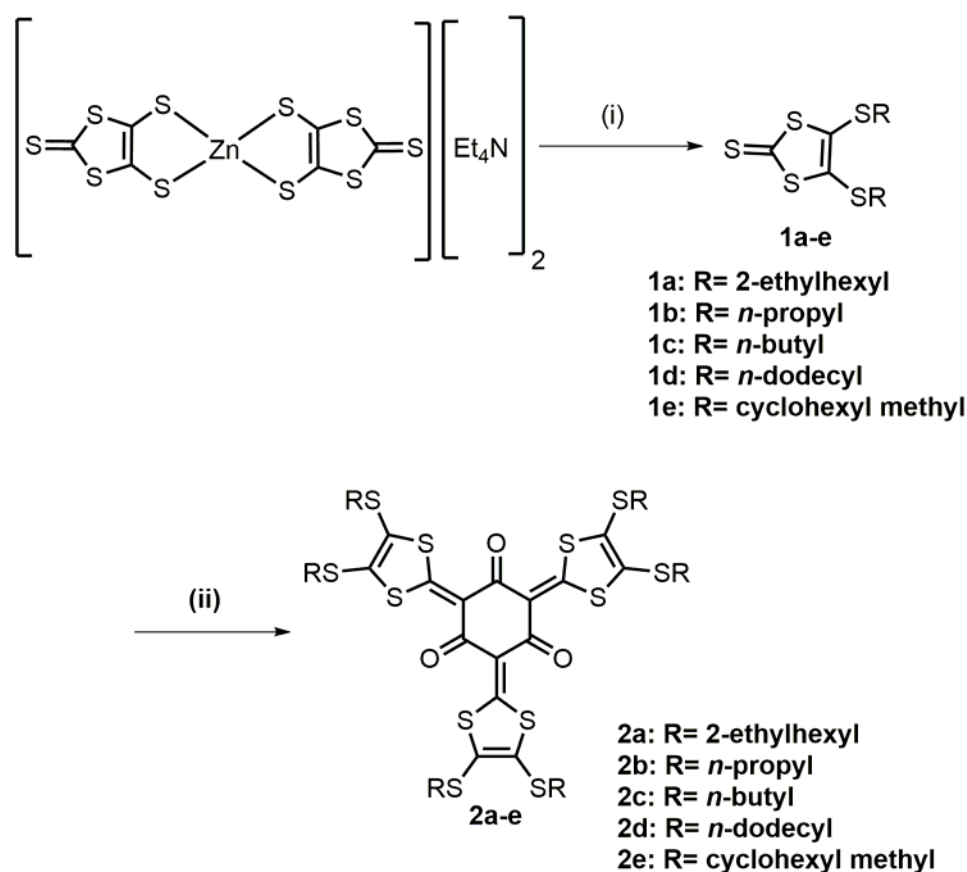
Reagents and conditions: (i) RBr, MeCN, reflux, 2 h; (ii) Phloroglucinol, **1a-e**, Et₃N, AgNO₃, MeCN, 75 °C, 12 h.
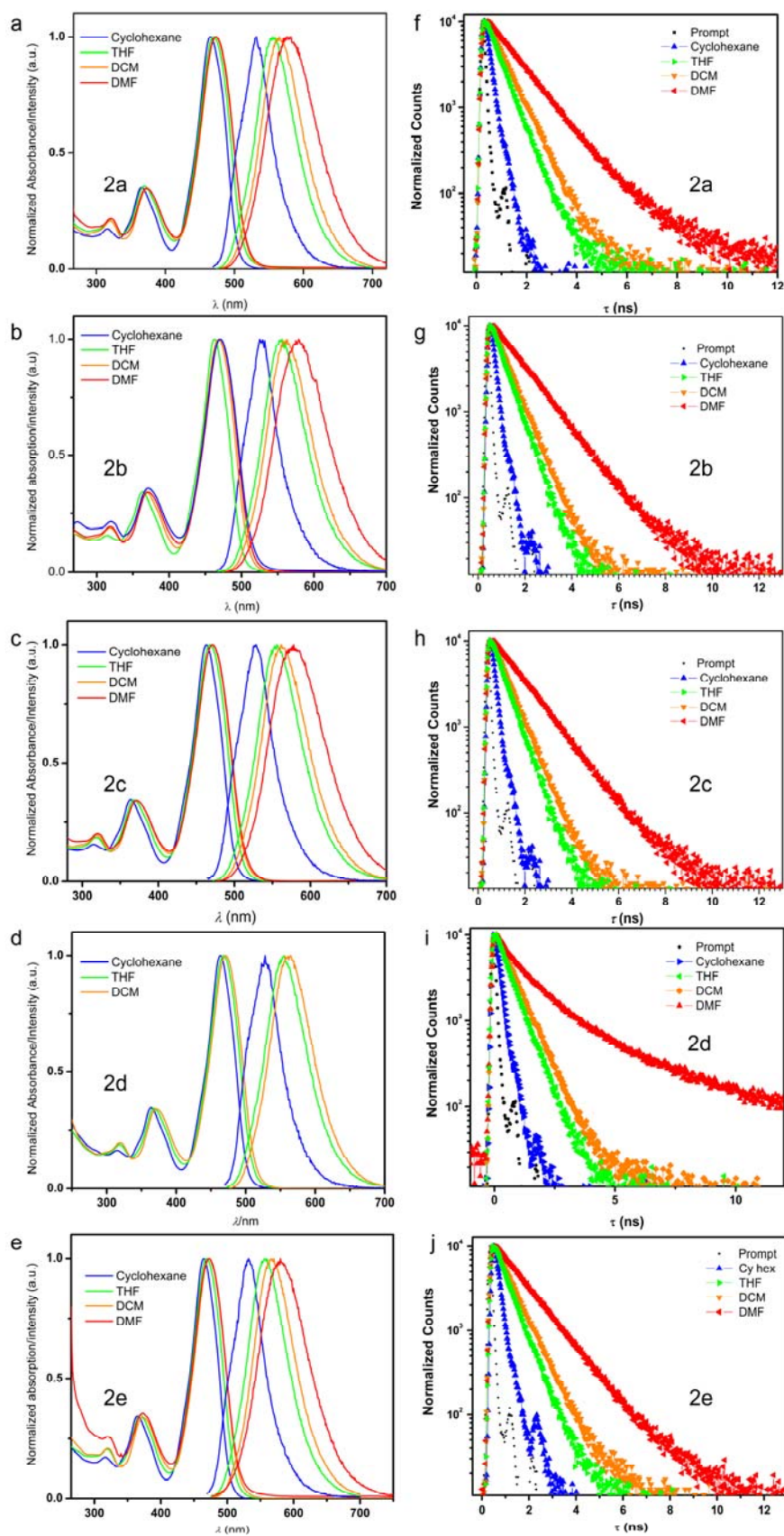
Fig. 4.3 (a-e) Absorption and emission spectra of compound **2a-e** (8 *μ*M) in cyclohexane, THF, DCM and DMF. (f-j) Fluorescence decay of compound **2a-e** (8 *μ*M) in cyclohexane, THF, DCM and DMF.

4.3.2 Photophysical studies

The different thioalkyl substitution on 1,3-dithiol-2-ylidene did not have a marked influence on the absorption and emission spectra of compounds **2a-e.** The electronic absorption spectra of compound **2a-e** unveiled small positive solvatochromic shift with their ICT bands appearing in the visible region at ≈ 463 nm in cyclohexane shifting bathochromically to ≈ 472 nm in DMF. However, the photoluminescence obtained upon exciting the ICT band of **2a-e** showcased significant positive solvatofluorochromism with shift in the emission band from ≈ 530 nm (green) in cyclohexane to ≈ 580 nm (orange) in DMF, yielding stokes' shift of ≈ 108 nm in polar solvent DMF (Figs 4.3a-e, 4.4). Furthermore, mean lifetime (τ) of the excited species of compounds **2a-e** were found to be increasing with the increase in the polarity of solvent with highest in DMF. The compound adorned with short alkyl chains - propyl (**2b**) and butyl (**2c**) exhibited monoexponential decay with τ of 1.25 and 1.31 ns, respectively. However, the compounds with alkyl C-2 substitution - 2-ethylhexyl (**2a**) and cyclohexyl methyl (**2e**) groups displayed biexponential fluorescence decay with τ of 0.50 and 0.88 ns, respectively in DMF. On the other hand, compound possessing long alkyl chain - dodecyl (**2d**) exhibited triexponential fluorescence decay with τ of 0.81 ns (Fig. 4.3f-j). The photophysical measurements are summarized in Table 4.1 (p. 109).
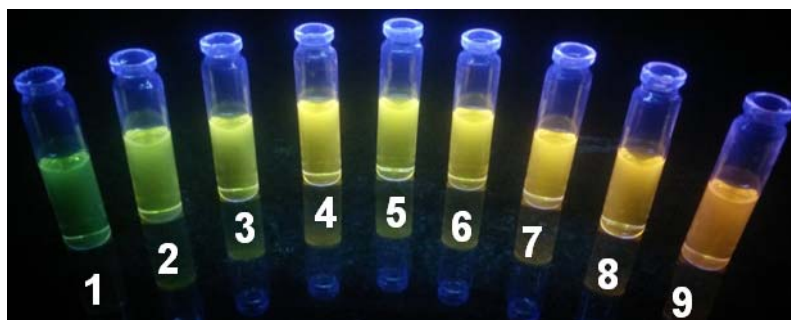
Fig. 4.4 Positive solvent solvatoflurochromism in compound **2a**, 1. cyclohexane, 2. toluene, 3. dioxane, 4. THF, 5. ethyl acetate, 6. chloroform, 7. dichloromethane, 8. acetone, and 9. DMF.
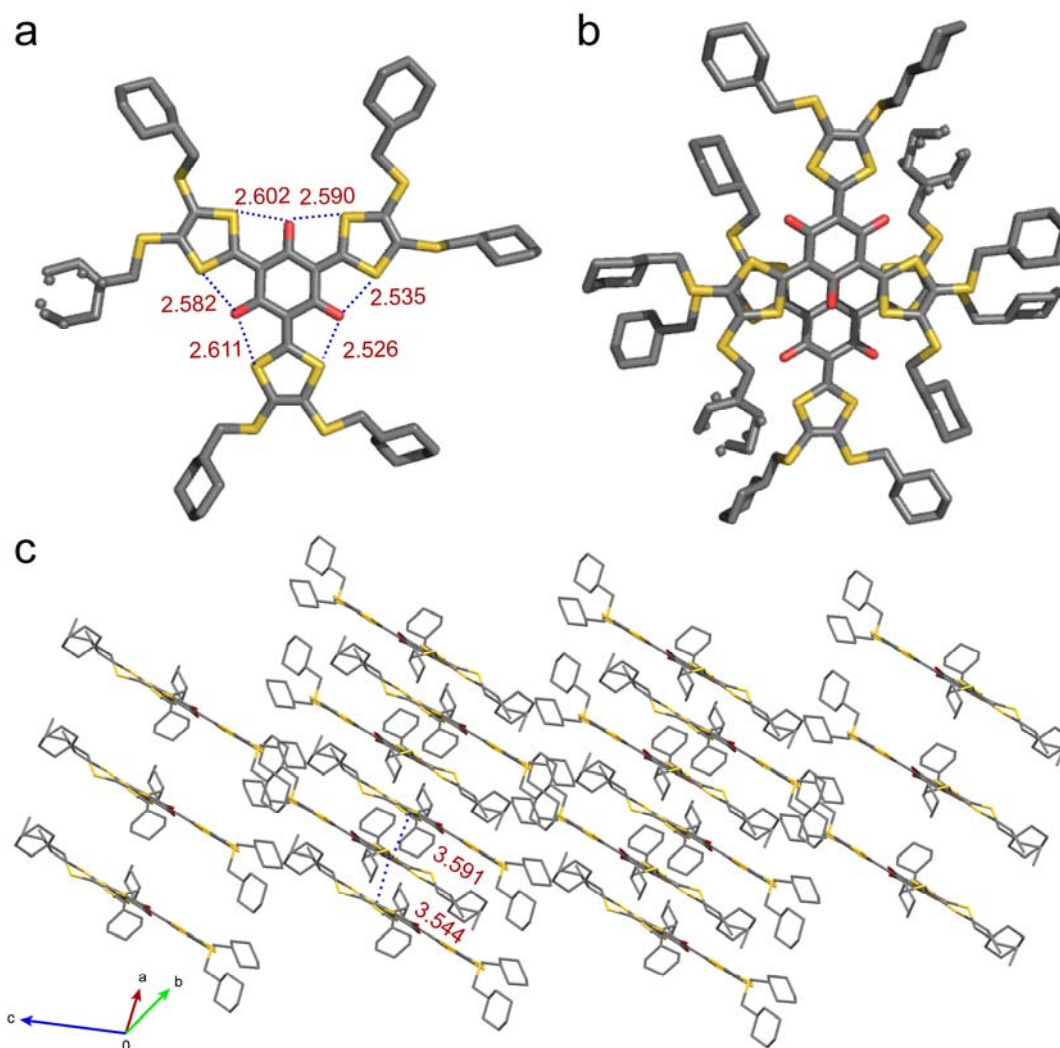
Fig. 4.5 (a) Crystal structure of **2e** showing short S···O contacts. (b) Crystallographically inequivalent dimers of **2e** showcasing π-stacking interactions. (c) Crystal packing observed approximately along the *b* axis.

4.3.3 Crystal structure

The compound **2e** crystallized in *P-1* space group upon slow evaporation of its solution in the mixture of chloroform and methanol. The crystal structure of compound **2e** showcases slight deviation of the molecule from D_{3h} symmetry, except for the cyclohexyl methyl groups. The mean planes of three dithiole rings deviated by *ca.* 1°, 5° and 9° from the mean plane of the cyclohexanetrione. The short intramolecular S···O contacts operating at the distances of 2.52-2.61 Å are considerably shorter than the sum of van der Waals' radii of the two atoms (3.25 Å) and try to induce planarity in the molecule (Fig. 4.5a). The two dithiole rings of the three in **2e** π-stack in a face-to-face manner with the mean planes bearing the two dithiole rings 10.31° apart from being parallel to each other

(Fig. 4.5b). The crystal packing of trisubstituted cyclohexanetrione **2e** viewed approximately along the *b* axis unveils diametrically opposed dimers (Fig. 4.5c) stacking continuously in a head-to-tail fashion along the *a* axis. The π-stacking distances of the molecule with the two molecules which are diametrically opposite and sandwiching are 3.544 Å and 3.591 Å (Fig. 4.5c).
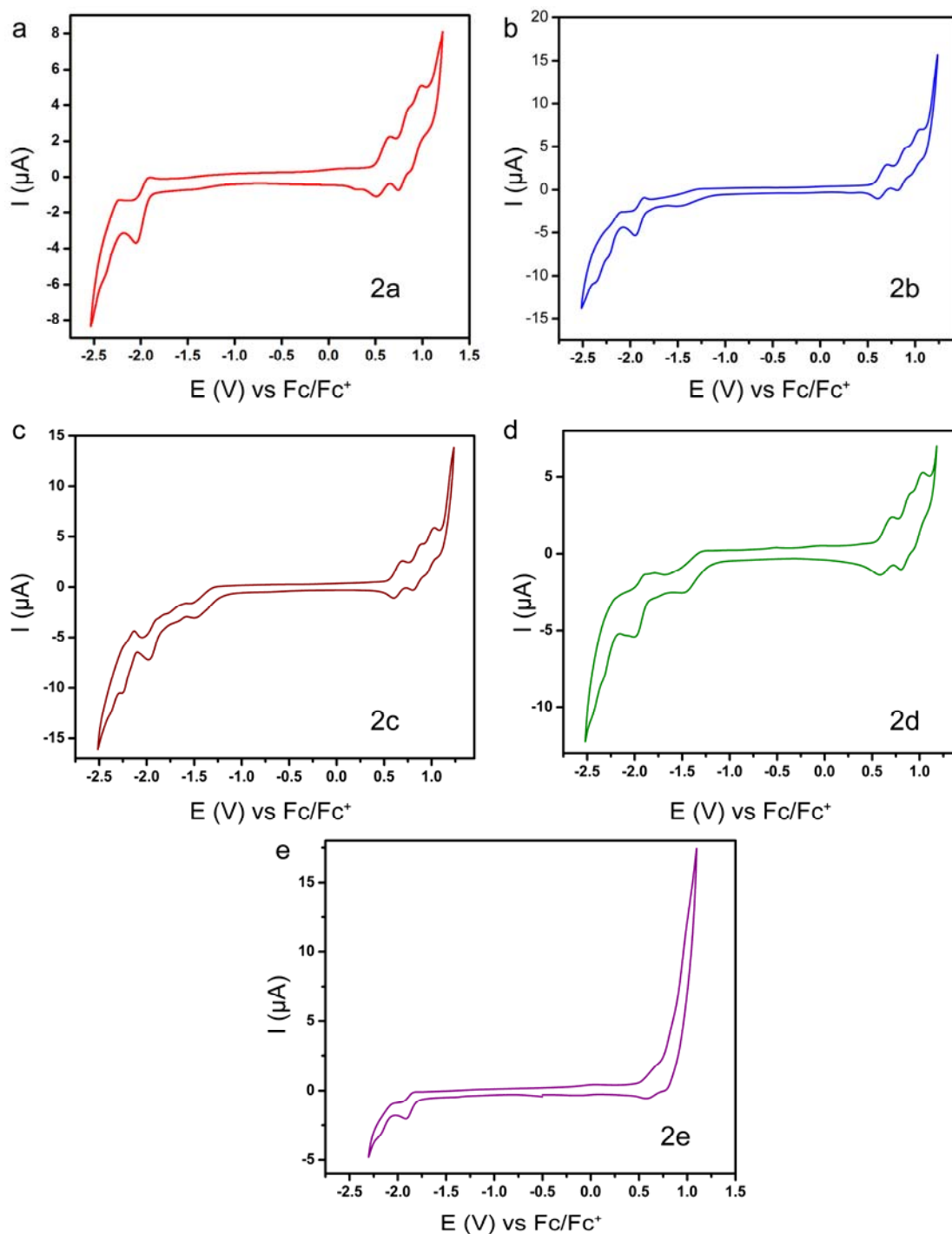
Fig. 4.6 Cyclic voltammetry of compounds **2a-e** in dichloromethane (2×10^{-4} M) at 50 mVs^{-1} using Bu$_4$NPF$_6$ (0.02 M) as supporting electrolyte, glassy carbon as working, platinum wire as counter and Ag/AgCl as reference electrodes.

4.3.4 Cyclic voltammetric studies

Cyclic voltammetry revealed amphoteric redox behaviour of compounds **2a-e** with four sets of reversible peaks: three oxidation and one reduction (Fig. 4.6a-e). The three one-electron oxidation peaks ($E_{1/2ox}$) appearing *ca.* at 0.65, 0.85 and 1.00 V lead to the formation of radical cations. The highly delocalized system bearing 24 π-electrons stabilizes the radical cations forming canonical structures- with cations being stabilized by the dithiole rings. On the other hand, the compound showcases one prominent reduction peak with half-wave potential at around -1.94 V. Again, the negative charge is being stabilized by the electronegative oxygen atoms. The reduction wave appearing close to -2 V suggests that the columbic repulsion in the electron rich system doesn't let the system to undergo reduction easily. The difference between the half-wave onset potentials afforded the electrochemical band gap for compound **2a-e** in between 2.3-2.6 eV which was in agreement with the optical bandgap of 2.4 eV. The cyclic voltammetry measurements of **2a-e** along with their HOMO-LUMO energies are summarized in Table 4.1.

Table 4.1 Photophysical and electrochemical properties of **2a-e**

Entry	λ_{max}	λ_{em}	Stokes Shift (nm)	E_g (eV) (Optical)	τ (ns)[a]	$E_{1/2ox}$	$E_{1/2red}$	HOMO	LUMO	E_g^b (CV)
2a	472[a]	578[e]	106[a]	2.40[b]	1.140 (bi)	0.58, 0.80, 0.99	-1.96	-4.89	-2.48	2.41
2b	470[a]	579[e]	109[a]	2.42[b]	1.188 (mono)	0.65, 0.85, 1.00	-1.90	-5.09	-2.55	2.55
2c	471[a]	578[e]	107[a]	2.42[b]	1.187 (mono)	0.64, 0.84, 0.98	-1.94	-4.95	-2.55	2.40
2d	471[b]	561[b]	90[b]	2.41[b]	1.294 (tri)	0.64, 0.85, 0.99	-1.94	-5.09	-2.53	2.56
2e	473[a]	580[e]	107[a]	2.40[b]	1.193 (bi)	0.60, n.d, n.d	-1.87	-4.89	-2.60	2.29

Note: The superscript *a* and *b* indicate the experiments carried out in DMF and DCM, respectively; optical band gap was calculated using the formula $E_g = 1240/\lambda_{onset}$ eV; Fluorescence lifetimes were calculated using the formulae τ (biexponential) = τ_1 (B_1/B_1+B_2) + τ_2 (B_2/B_1+B_2)   and τ (triexponential) = τ_1 ($B_1/B_1+B_2+B_3$) + τ_2

$(B_2/B_1+B_2+B_3) + \tau_3 (B_3/B_1+B_2+B_3)$; $E_{1/2}$ values obtained are the mean of anodic and cathodic peak potentials *vs* Fc/Fc⁺; HOMO and LUMO energy levels are calculated from the onset of first oxidation and reduction waves using the formulae HOMO = -(E_{ox} +4.4) and LUMO = -(E_{red} +4.4); *n.d* = not determined.

4.3.5 Self-assembly

The trisubstituted cyclohexanetrione **2** that are adorned with short alkyl chains – propyl (**2b**) and butyl (**2c**) self-assembled into fibres on a 2D substrate. The compound **2b** formed nanofibres in DMF, cyclohexane and THF (Figs 4.7a-f, 4.8a-f) while **2c** self-assembled only in DMF (Fig. 4.9a-d). The fibres in DMF had high aspect ratio and grew several micrometres in length and up to around 100-150 nm in width. The compound with branched and long alkyl chains *i.e.*, **2a**, **2d** and **2e** failed to form self-assembled structures. Self-assembly on a 2D substrate takes place in short duration of time. The shorter alkyl chains, presumably, has the advantage of building planar tri-substituted cyclohexanetrione molecules one over the other by π-stacking over large distances without much hindrance from alkyl groups, thus forming self-assembled elongated nanostructures.
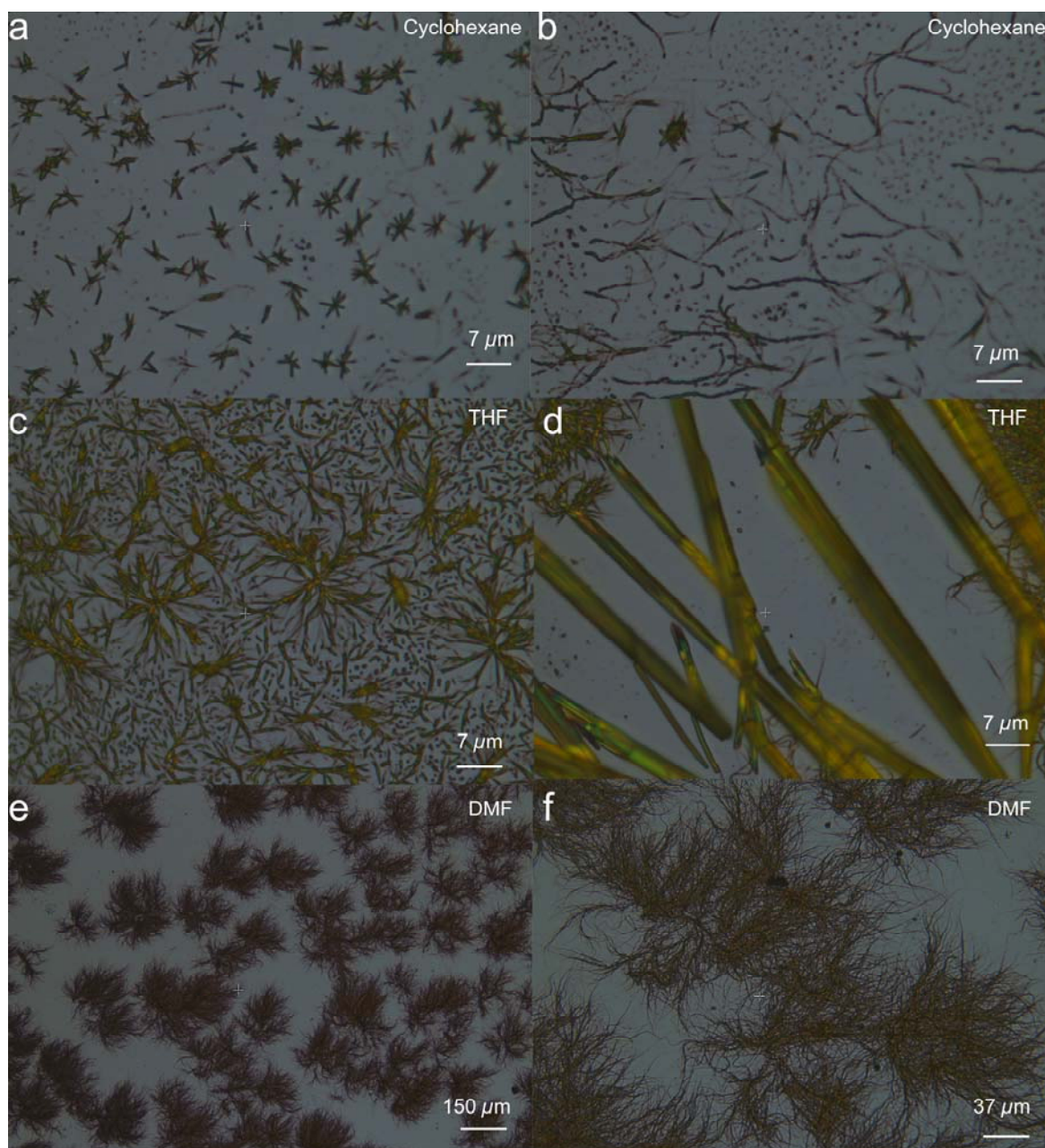
Fig. 4.7 Representative optical microscopy images of **2b** dropcasted on a silicon substrate using cyclohexane (a,b), THF (c,d) and DMF (e,f).
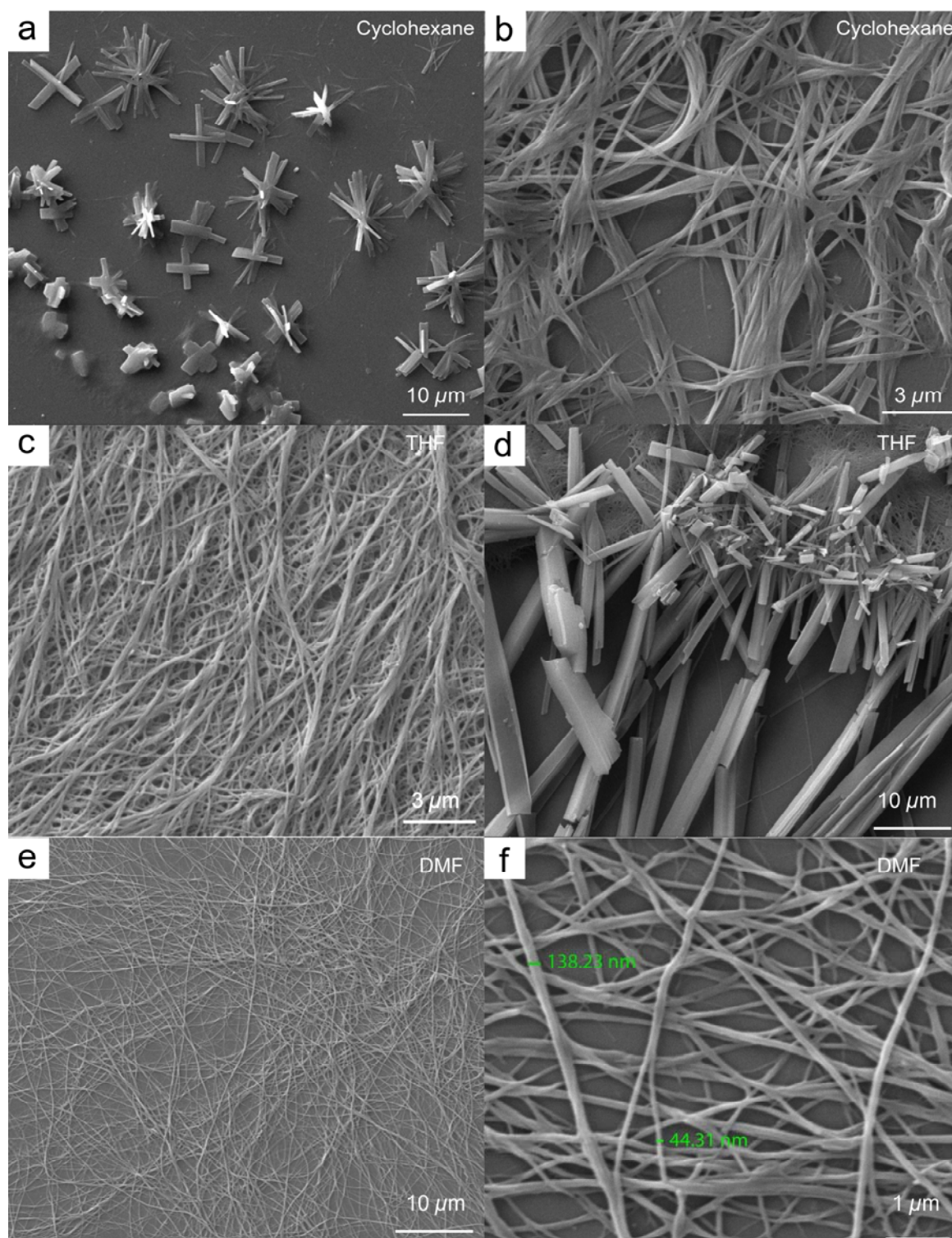
Fig. 4.8 Representative scanning electron microscopy images of compound **2b** dropcasted on a silicon substrate using cyclohexane (a,b), THF (c,d) and DMF (e.f).
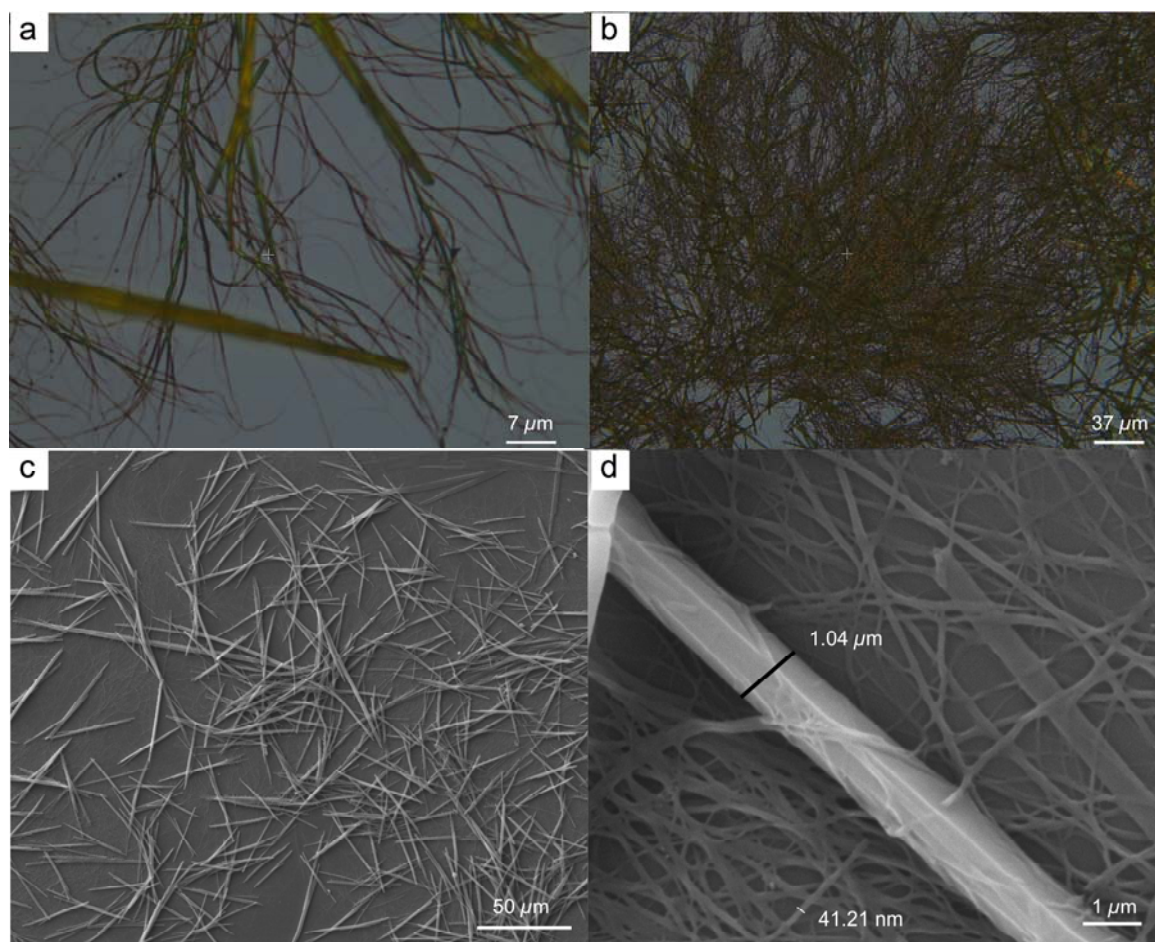
Fig. 4.9 Representative microscopy images of compound **2c** dropcasted on a silicon substrate using DMF as solvent. Optical microscopy (a,b) and SEM images (c,d).

4.3.6 Current-sensing Atomic Force Microscopy (Cs-AFM)

The highly delocalized π-electron system appended with push-pull groups is a potential (semi)conductor. In order to obtain insights into the conductivity exhibited by compound 2, we subjected compound **2b** for current sensing atomic force microscopy (Cs-AFM). The conductivity was measured along the 1D nanofibres grown on a monocrystalline silicon wafer using DMF as solvent. The compound **2b** exhibited average conductivity of 0.146 ± 0.003 mScm^{-1} at 298 K in undoped state (Fig. 4. 10, details in ESI†). The compound **2b** possessing short and linear propyl chains would pack closely, reducing the intermolecular noncovalent S···S and π-stacking distance compared to **2e**. This proximity would enhance the overlap of the $3p_z$ orbitals of sulfur, which play a key role in electron transport,[16] resulting in high conductivity.
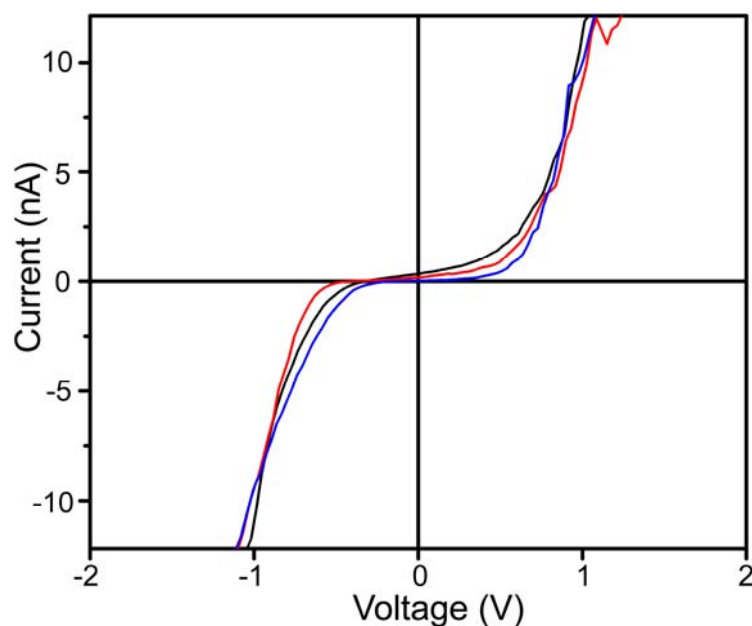
Fig. 4.10 Representative *I-V* spectroscopic curves of 2b nanofibres obtained by drop casting its DMF solution (0.1 mM) on a monocrystalline silicon wafer. The measurements obtained at three different regions using current-sensing atomic force microscopy (Cs-AFM) are shown in the plot.

4.4 Conclusions

In summary, we synthesized C_3 symmetric molecules with π-extended core comprising of alternating donor dithiolylidene and carbonyl groups. ICT interaction between the donor and acceptor groups of the core is substantiated by solvatofluorochromism with large stokes' shift up to 108 nm and extended lifetime of the excited species in polar solvent DMF. Although few nanostructure forming TTF derivatives are reported to be solvatochromic due to aggregation,[11b,17] luminescent and solvatofluorochromic TTF analogues that self-organize to nanofibres are unprecedented in literature to the best of our knowledge. The donor and acceptor groups stabilize the radical cations and anion affording amphoteric redox behaviour. Intermolecular π-stacking, S⋯S along with intramolecular S⋯O interactions, as discerned from single crystal structure, facilitate the formation of self-assembled one-dimensional structures in proypl and butyl appended core. High conductivity of ~ 0.15 mScm^{-1} in the undoped state was observed in the former, ascribed to the strong intermolecular interactions. The easy functionalization of the C_3 symmetric core with various alkyl chains allows obtaining the desired properties towards achieving a multifunctional π-extended core.

4.5 Experimental section

Crystal data: X-ray intensity data measurements of compound **2e** were carried out on a Bruker D8 VENTURE Kappa Duo PHOTON II CPAD diffractometer equipped with Incoatech multilayer mirrors optics. The intensity measurements were carried out with Cu micro-focus sealed tube diffraction source (MoK_α= 0.71073 Å) at 100(2) K temperature. The X-ray generator was operated at 50 kV and 1.4 mA. A preliminary set of cell constants and an orientation matrix were calculated from three sets of 36 frames. Data were collected with ω scan width of 0.5° at different settings of φ and 2θ with a frame time of 10 secs keeping the sample-to-detector distance fixed at 5.00 cm. The X-ray data collection was monitored by APEX3 program (Bruker, 2016). All the data were corrected for Lorentzian, polarization and absorption effects using SAINT and SADABS programs (Bruker, 2016). SHELX-97 was used for structure solution and full matrix least-squares refinement on F^2. All the hydrogen atoms were placed in a geometrically idealized position and constrained to ride on its parent atom.

Identification code	LCCYHEX_0m
Crystal Color and shape	Orange, needle
Empirical formula	$C_{57}H_{78}O_3S_{12}$, $CHCl_3$
Formula weight	1315.28
Temperature/K	100(2)
Crystal system	triclinic
Space group	*P-1*
a/Å	9.9099(6)
b/Å	17.0949(11)
c/Å	19.8240(13)
α/°	111.1910(10)
β/°	99.8140(10)
γ/°	94.4630(11)
Volume/Å³	3049.7(3)
Z	2
ρ_{calc} (g/cm³)	1.432
μ/mm⁻¹	0.605
F(000)	1388.0

Crystal size/cm^3	0.4 x 0.14 x 0.14
Radiation	MoK$_\alpha$ λ=0.71073 Å
2Θ max/°	50.000
Index ranges	-11 ≤ h ≤ 11, -20 ≤ k ≤ 20, -23 ≤ l ≤ 23
Independent reflections	9623
Completeness to theta=25.000	100%
Goodness-of-fit on F^2	1.015
Final R indexes [I>=2σ (I)]	R$_1$ = 0.0297, wR$_2$ = 0.0685

Synthesis of bis(tetraethylammonium)bis(1,3-dithiole-2-thione-4,5-dithiolato) zincate TEA₂[Zn(DMIT)₂]

The deep red organometallic complex TEA$_2$[Zn(DMIT)$_2$] was synthesized according to the reported procedure.[15]

Synthesis of compounds 4,5-bis(alkylthio)-1,3-dithiole-2-thiones (1a-1e)

Representative procedure for **4,5-bis((2-ethylhexyl)thio)-1,3-dithiole-2-thione (1a)**
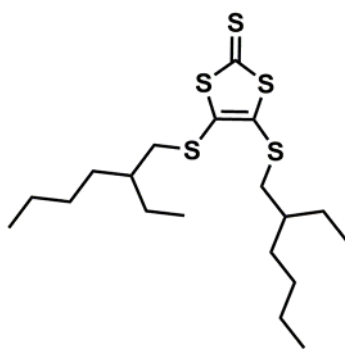
To the solution of TEA$_2$[Zn(DMIT)$_2$] (300 mg, 0.42 mmol) in acetonitrile (10 mL), 2-ethylhexyl bromide (297 mg, 1.67 mmol) was added and the reaction mixture was refluxed for 2 h. The reaction mixture, after being cooled to room temperature, was filtered. The filtrate was concentrated *in vacuo* and purified by column chromatography (eluent: petroleum ether, R$_f$ = 0.2) to furnish **1a** as brown oil (240 mg, 94%); IR (CHCl$_3$) ν (cm^{-1}): 2962, 2930, 2861, 1601, 1522, 1464, 1426, 1064, 929, 851; ^{1}H NMR (400 MHz, chloroform-*d*) δ = 2.88 (d, *J* = 6.1 Hz, 4H), 1.64 - 1.53 (m, 2H), 1.52 - 1.36 (m, 8H), 1.36 - 1.20 (m, 8H), 0.98 - 0.81 (m, 12H); ^{13}C NMR (100 MHz, chloroform -*d*) δ = 211.5, 136.5, 41.2, 39.4, 32.0, 28.6, 25.3, 22.9, 14.0, 10.7; HRMS: C$_{19}$H$_{34}$NaS$_5$ (M+Na)$^+$ Calcd: 445.1156, found: 445.1176
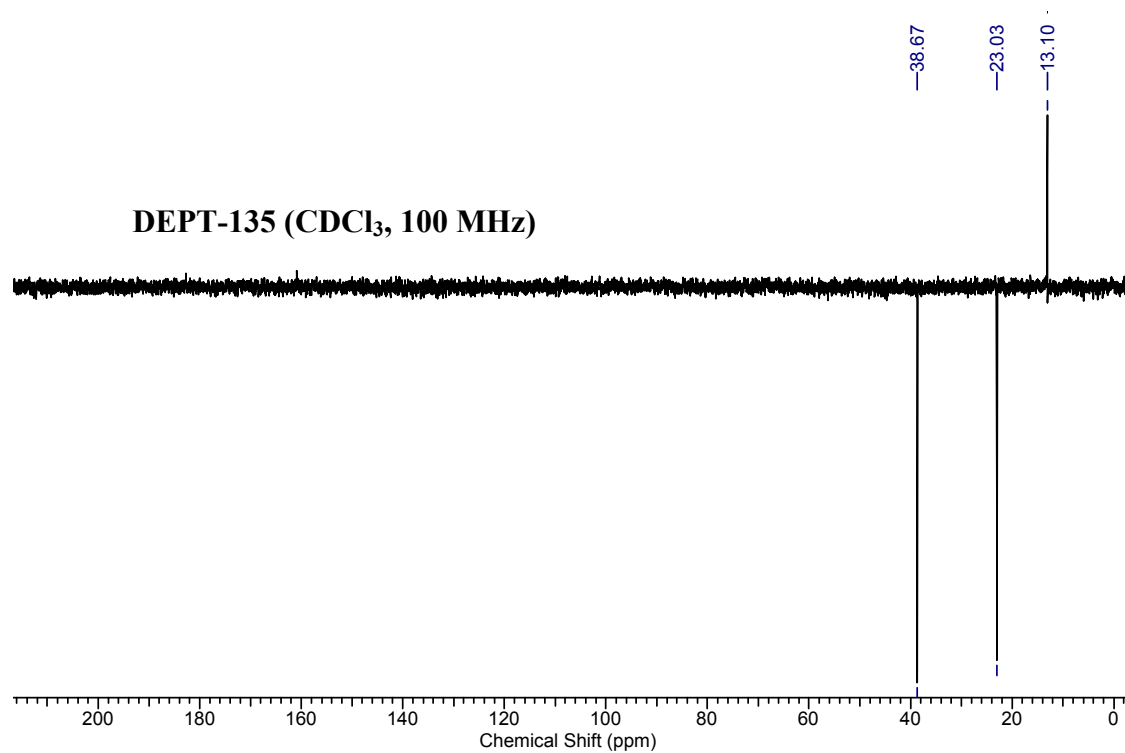
¹H NMR (CDCl₃, 400 MHz)

DEPT-135 (CDCl₃, 100 MHz)

CHLOROFORM-d

—211.50

—136.48

77.32
77.00
76.69

41.18
39.41
31.98
28.63
25.26
22.92
14.05
10.65

¹³C NMR (CDCl₃, 100 MHz)

Chemical Shift (ppm)
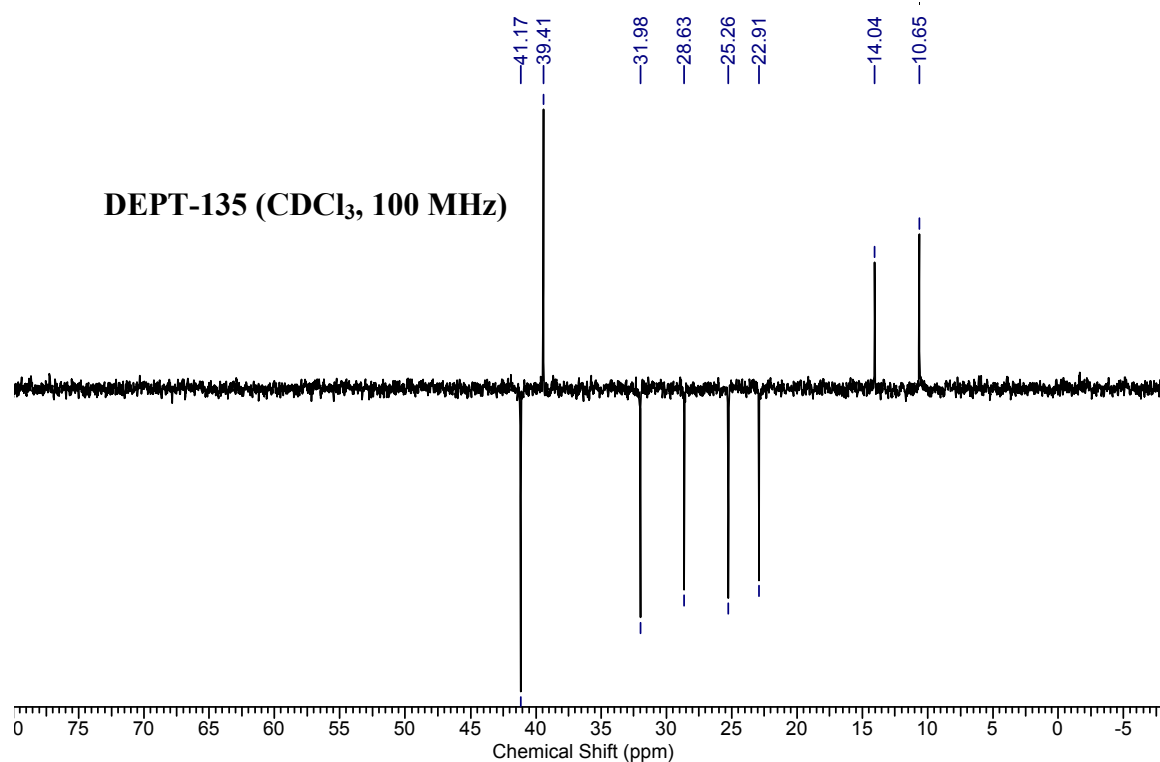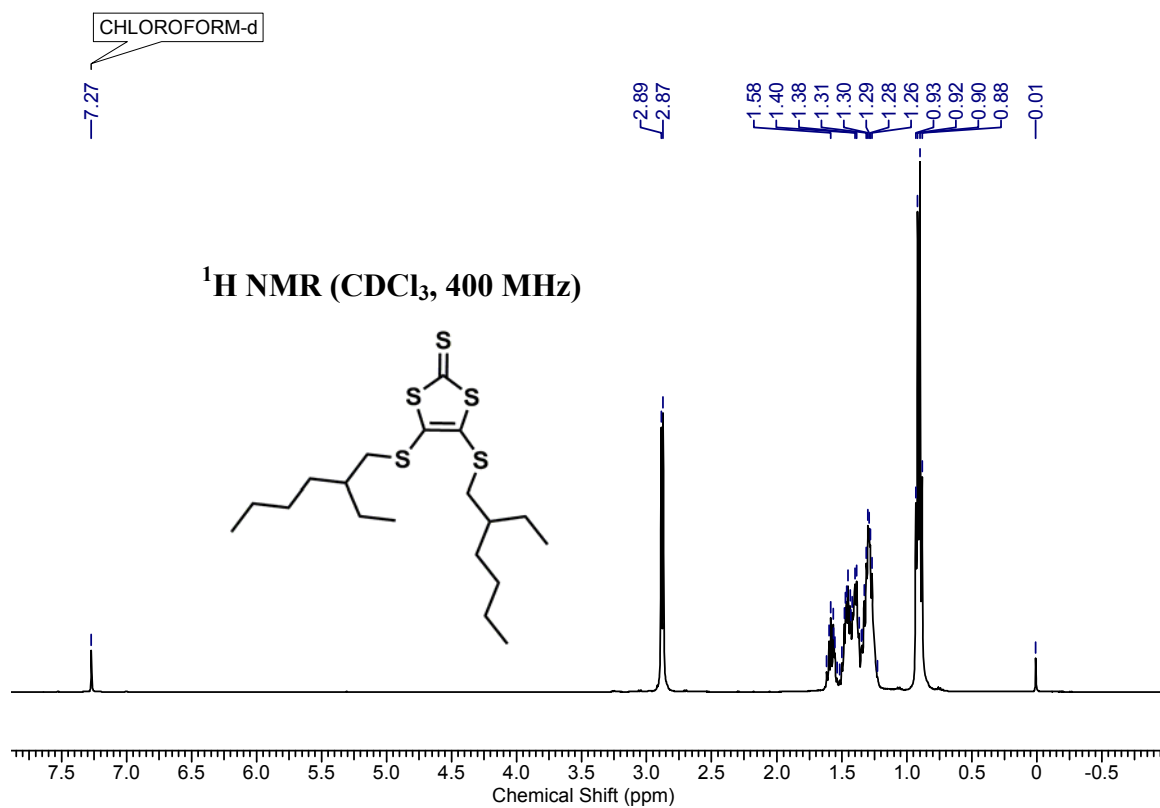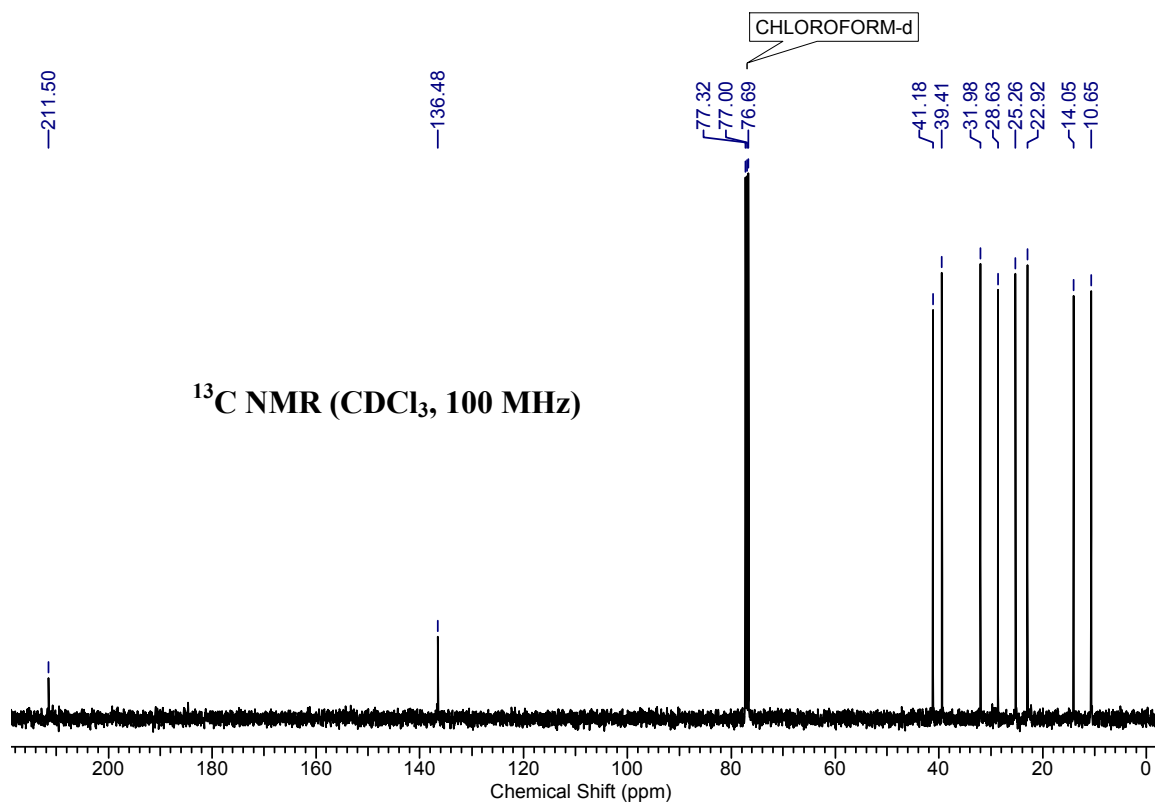
2-ET-HEXYL-THIONE #291 RT: 1.30 AV: 1 NL: 3.23E4
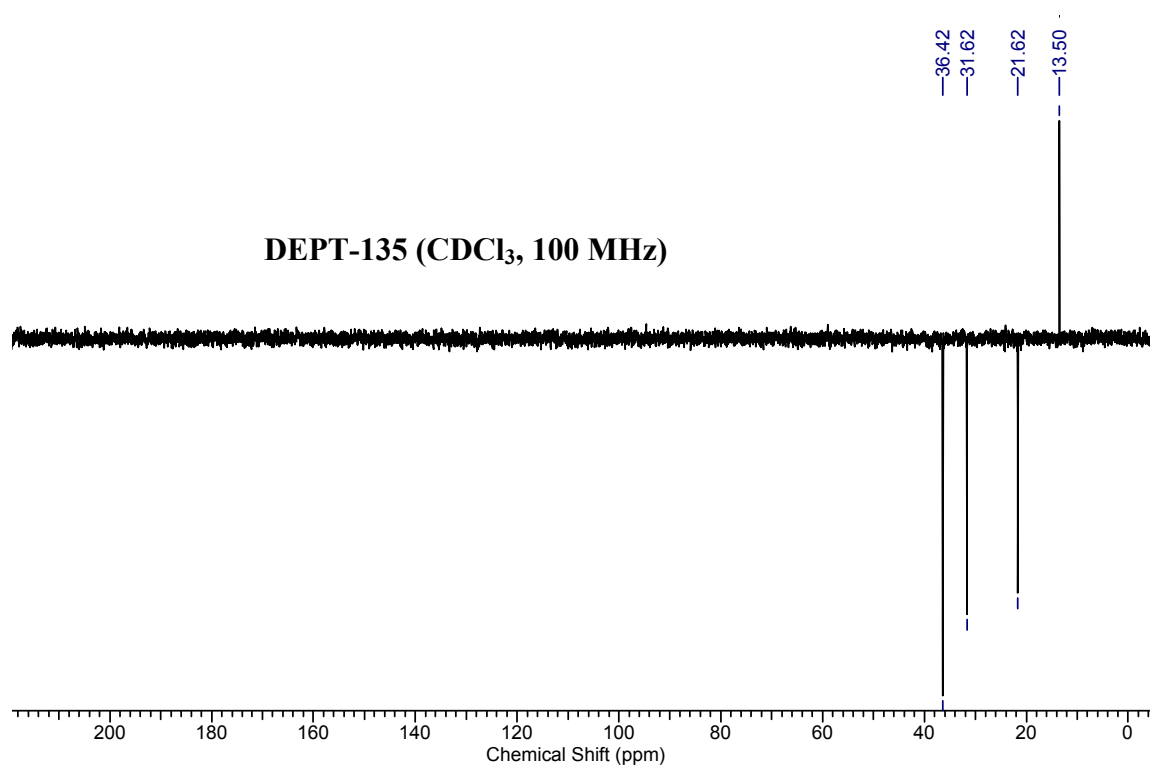T: FTMS + p ESI Full ms [100.00-1500.00]

HRMS-ESI

M+Na⁺

441.2963
R=31200

445.1176
R=34500
$C_{19}H_{34}NaS_5 = 445.1156$
4.4683 ppm

447.7637
R=36700

448.7664
R=35800
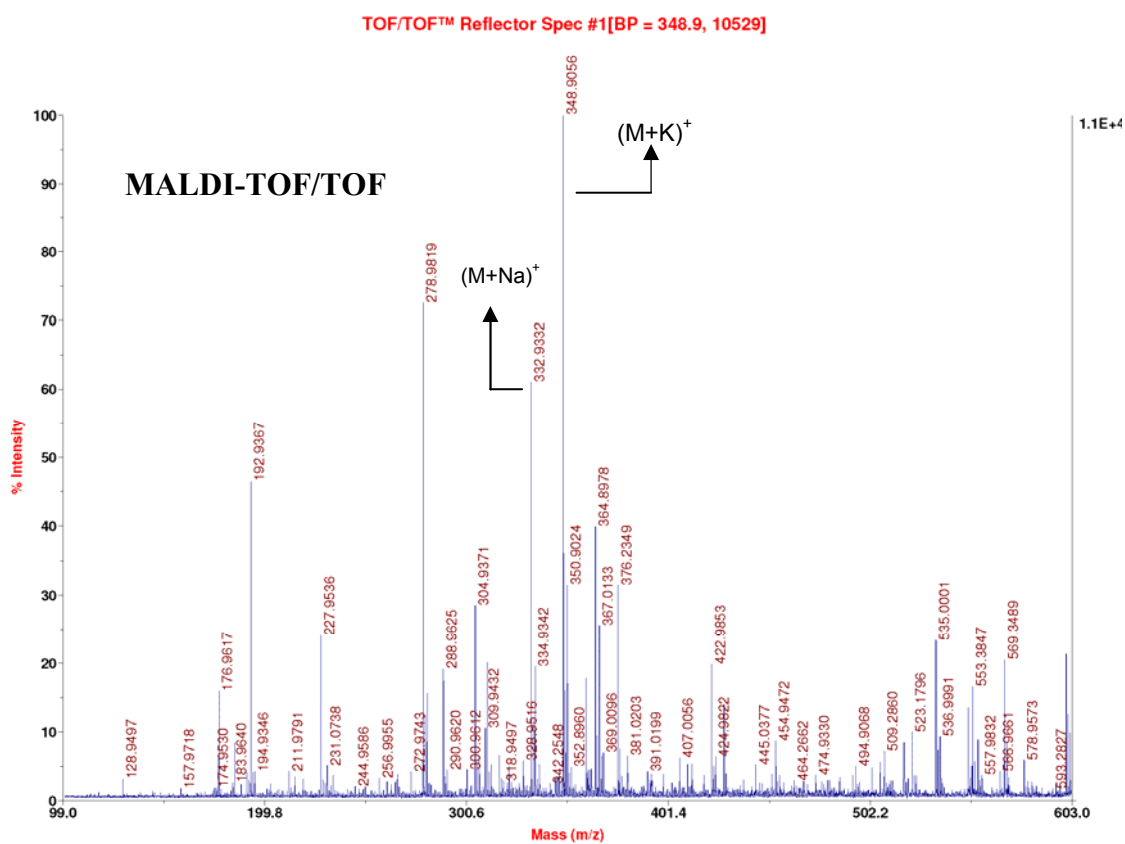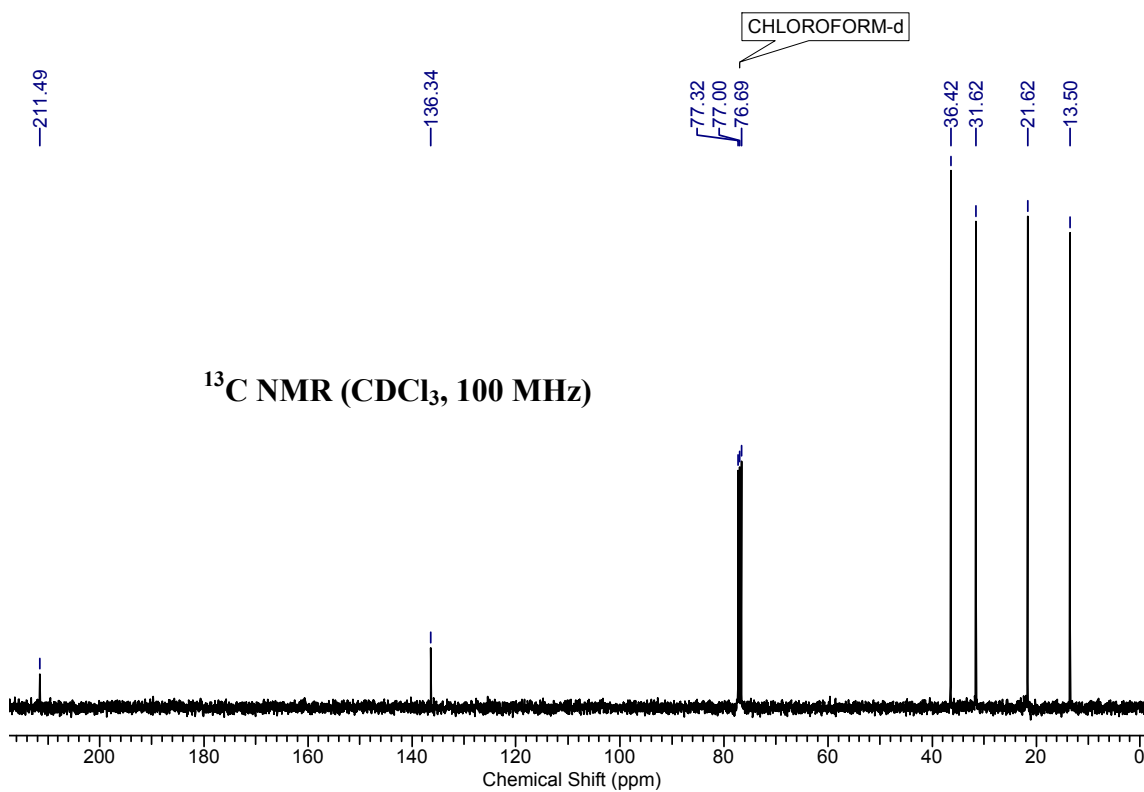
450.2731
R=37600

454.2924
R=36500

Relative Abundance

m/z
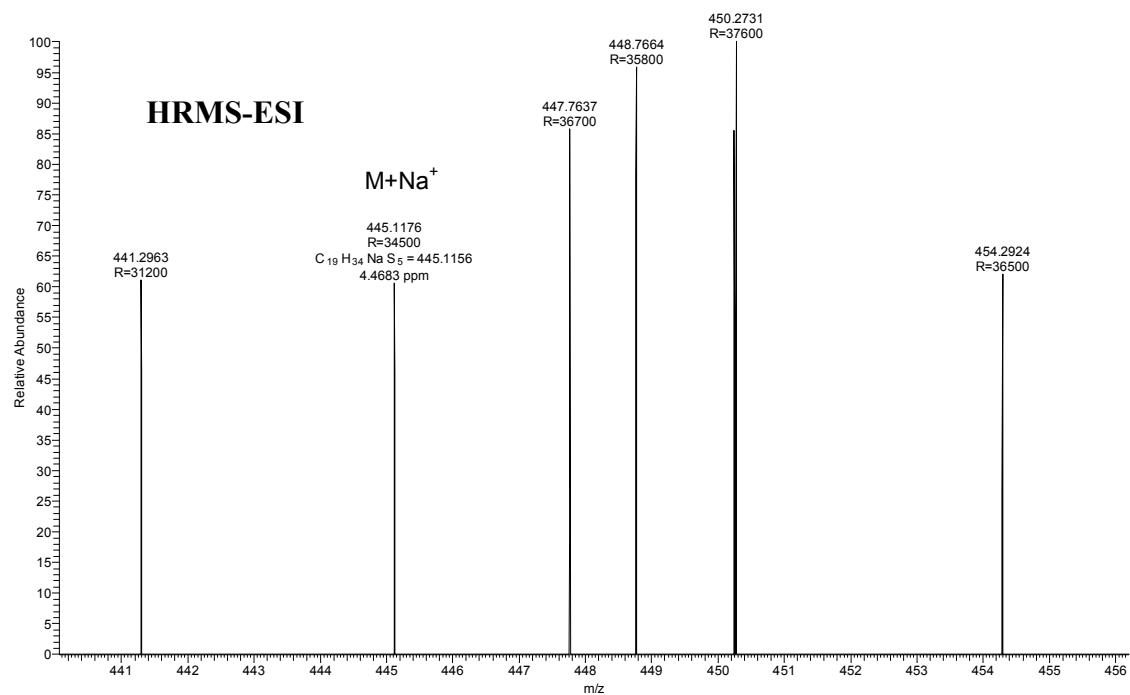
4,5-bis(propylthio)-1,3-dithiole-2-thione (1b)
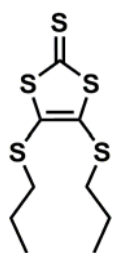
The compound **1b** was obtained following the same procedure employed for **1a** using TEA$_2$[Zn(DMIT)$_2$] (200 mg, 0.28 mmol) and propyl bromide (127 μL, 1.4 mmol). Column chromatography (eluent: petroleum ether, R$_f$ = 0.35) furnished compound **1b** as brown oil (105 mg, 67%); IR (CHCl$_3$) v (cm^{-1}): 1601, 1524, 1424, 1064, 928, 909; ^{1}H NMR (400MHz, chloroform-d) δ = 2.86 (t, J = 7.3 Hz, 4H), 1.87 - 1.63 (m, 4H), 1.04 (t, J = 7.3 Hz, 6H); ^{13}C NMR (100 MHz, chloroform -d) δ = 211.5, 136.4, 38.7, 23.0, 13.1; HRMS: C$_9$H$_{15}$S$_5$ (M+H)$^+$ calcd: 282.9772, found: 282.9785.

^{1}**H NMR (CDCl$_3$, 400 MHz)**

DEPT-135 (CDCl₃, 100 MHz)

—38.67
—23.03
—13.10

Chemical Shift (ppm)

CHLOROFORM-d

—211.50
—136.37
77.32
77.00
76.69
—38.67
—23.04
—13.10

¹³C NMR (CDCl₃, 100 MHz)

Chemical Shift (ppm)
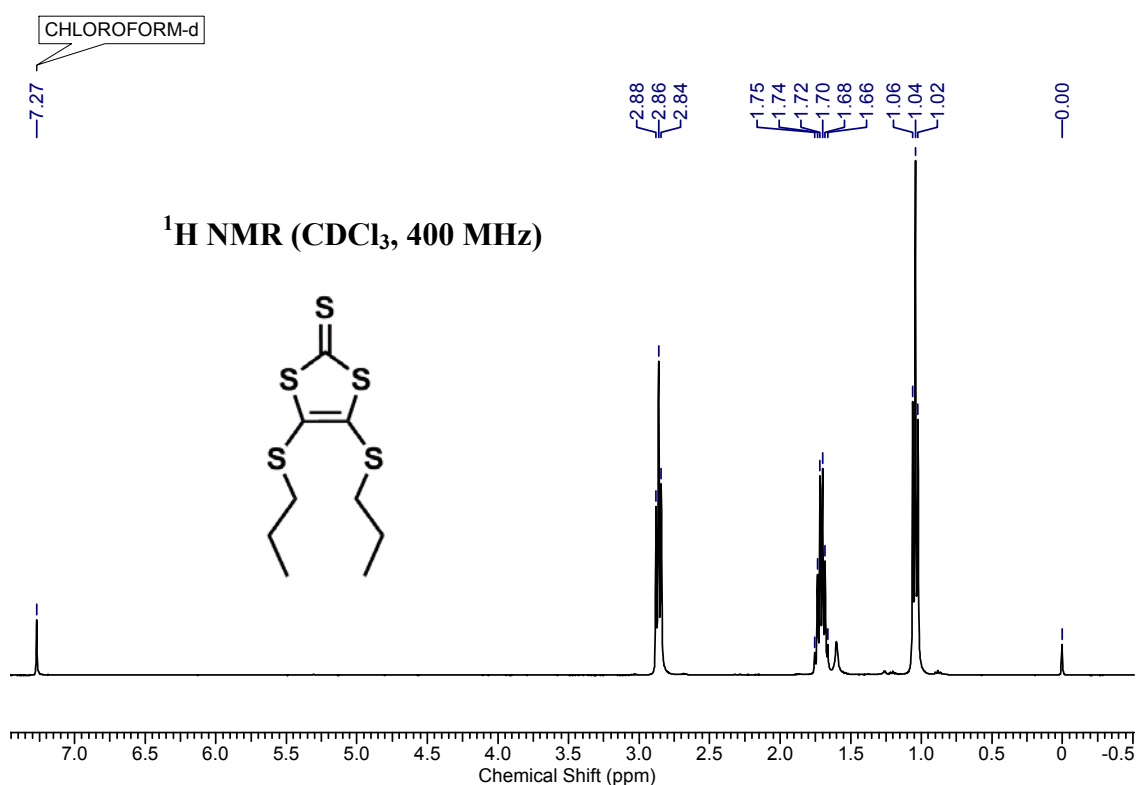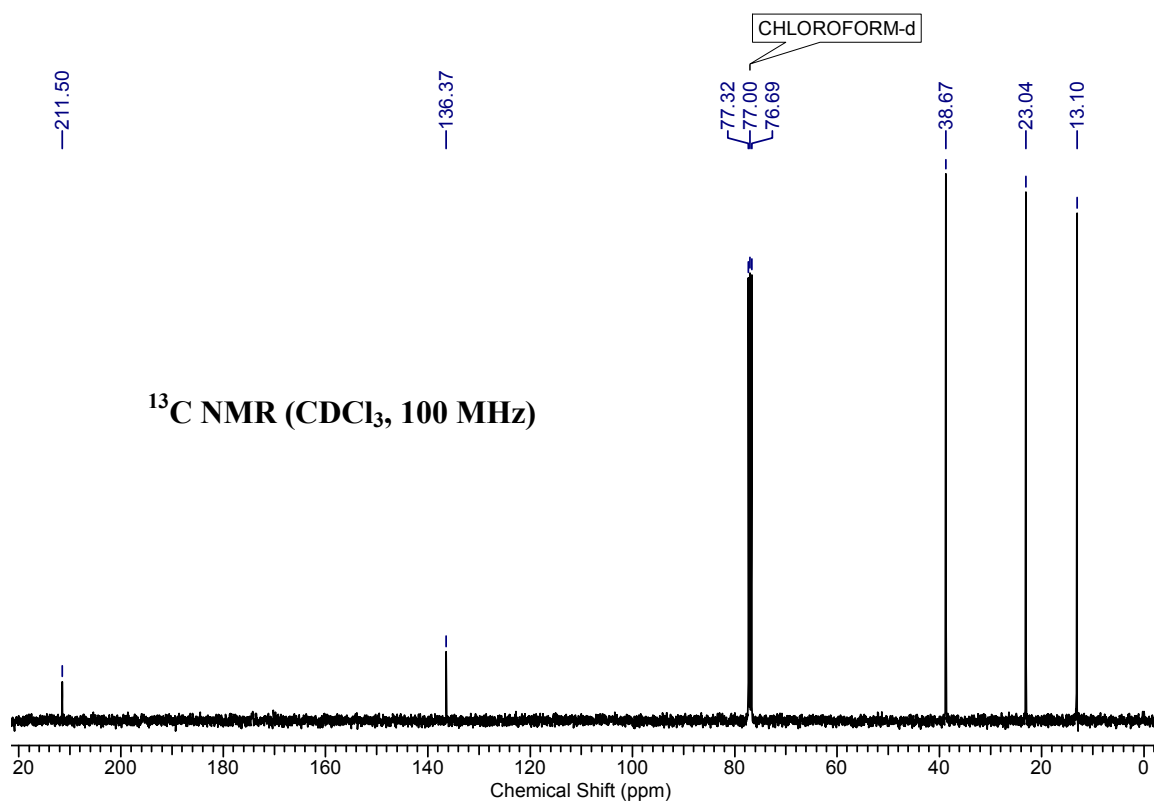
PROPYL-THIONE #146 RT: 0.65 AV: 1 NL: 5.44E4
T: FTMS + p ESI Full ms [100.00-1500.00]
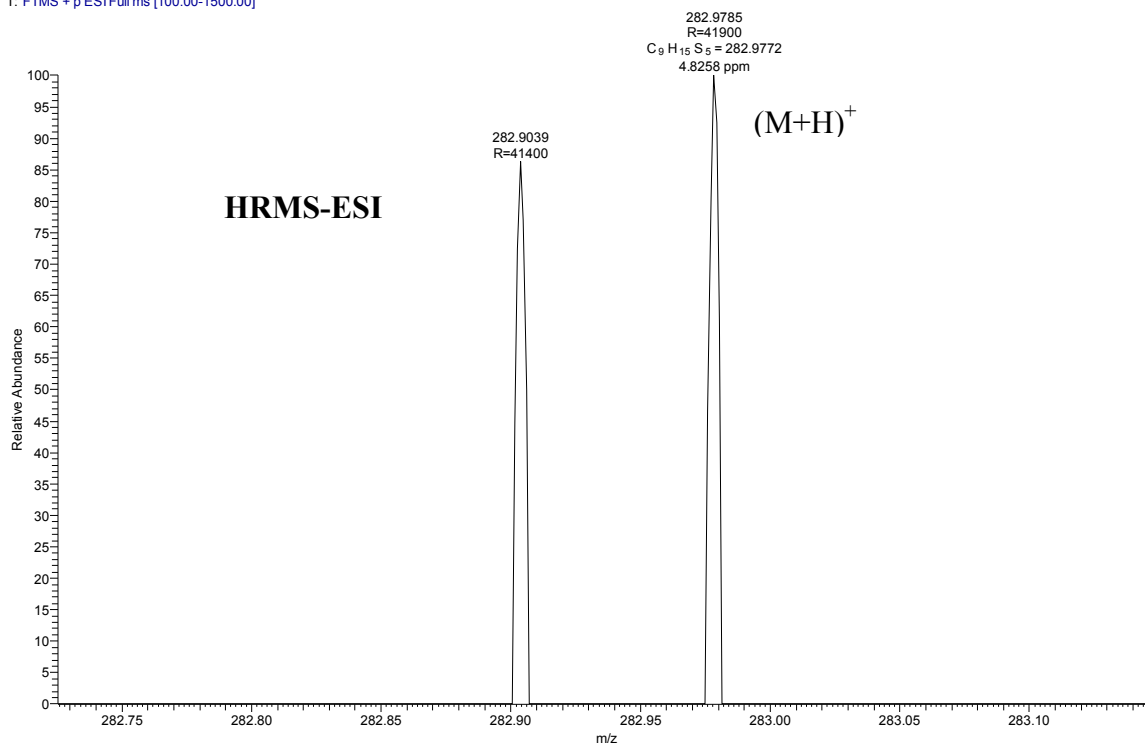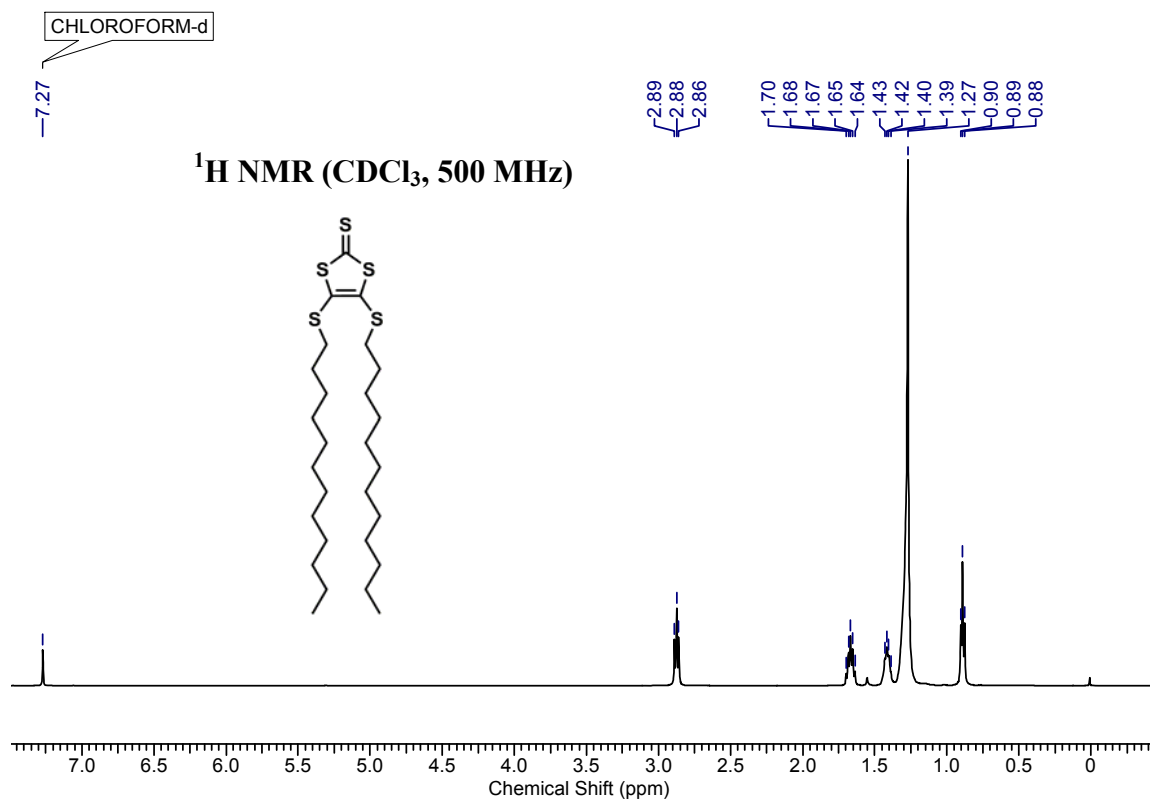

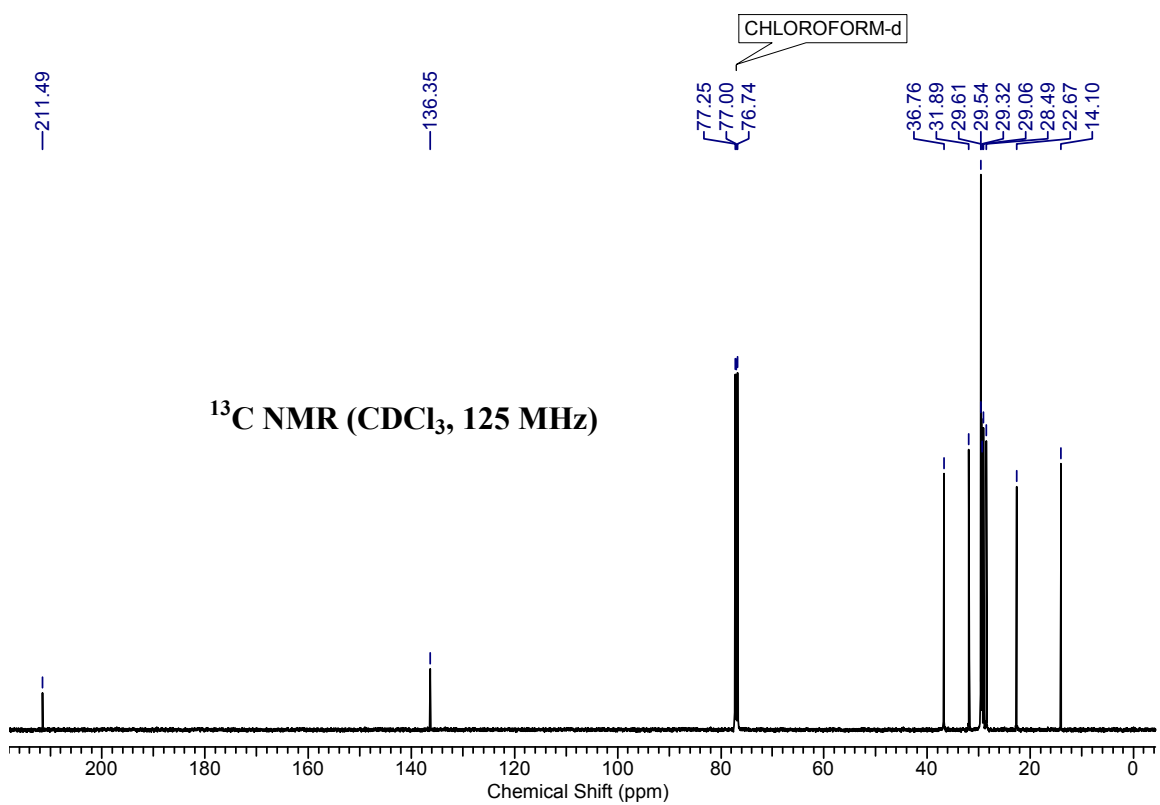## 4,5-bis(butylthio)-1,3-dithiole-2-thione (1c)
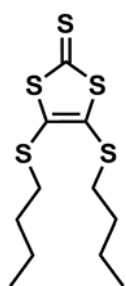
The compound **1c** was obtained following the same procedure employed for **1a** using TEA$_2$[Zn(DMIT)$_2$] (500 mg, 0.70 mmol) and butyl bromide (374 µL, 3.49 mmol). Column chromatography (eluent: petroleum ether, R$_f$ = 0.65) furnished compound **1c** as brown oil (421 mg, 97%); IR (CHCl$_3$) v (cm^{-1}): 2963, 2933, 2875, 1601, 1523, 1466, 1065, 929; ^{1}H NMR (400 MHz, chloroform-*d*) δ = 2.91 - 2.83 (m, 4H), 1.70 - 1.60 (m, 4H), 1.51 - 1.39 (m, 4H), 0.93 (t, *J* = 7.5 Hz, 6H); ^{13}C NMR (100 MHz, chloroform-*d*) δ = 211.5, 136.3, 36.4, 31.6, 21.6, 13.5; MALDI-TOF/TOF: 332.93 (M+Na)$^+$, 348.91 (M+K)$^+$.
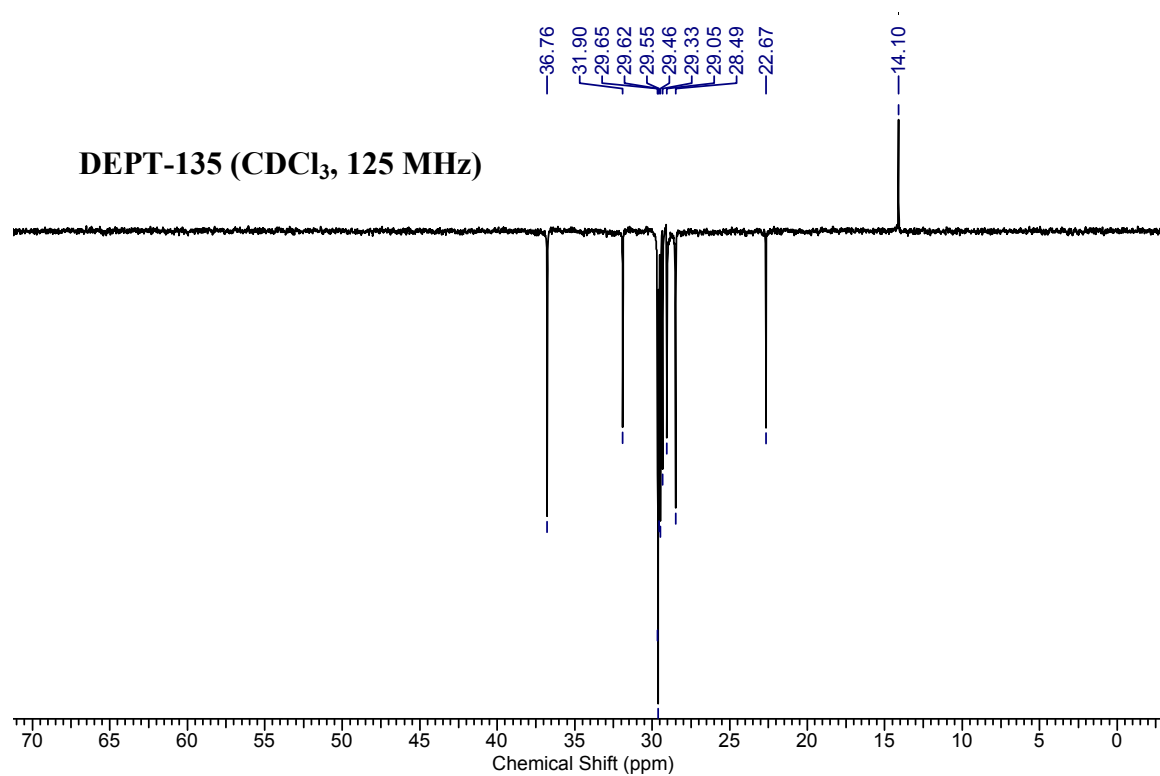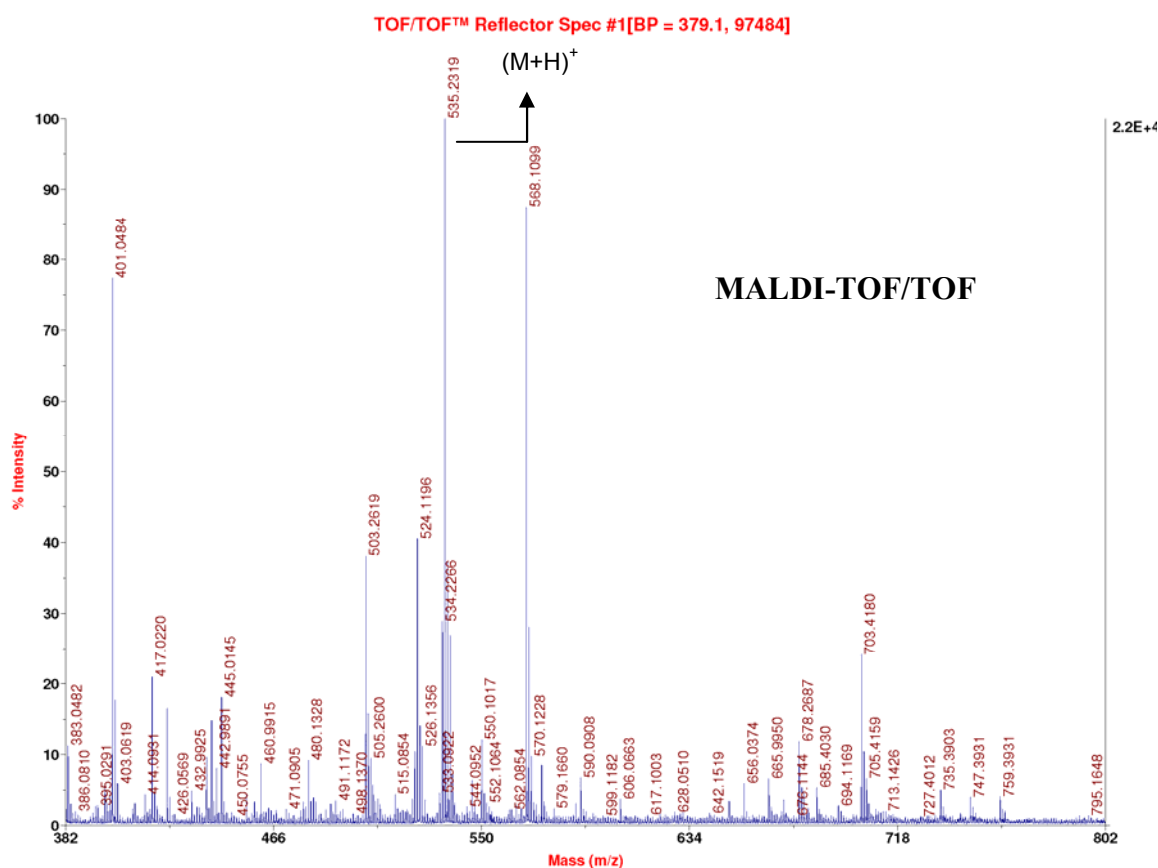
CHLOROFORM-d

—7.26

—2.89
—2.87
—2.85

1.67
1.65
1.64
1.63
1.61
1.47
1.45
1.44
1.42
0.95
0.93
0.91

—-0.01

¹H NMR (CDCl₃, 400 MHz)

7.0 6.5 6.0 5.5 5.0 4.5 4.0 3.5 3.0 2.5 2.0 1.5 1.0 0.5 0
Chemical Shift (ppm)

—36.42
—31.62
—21.62
—13.50

DEPT-135 (CDCl₃, 100 MHz)

200 180 160 140 120 100 80 60 40 20 0
Chemical Shift (ppm)
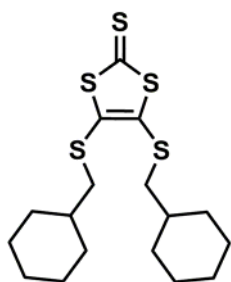
¹³C NMR (CDCl₃, 100 MHz)
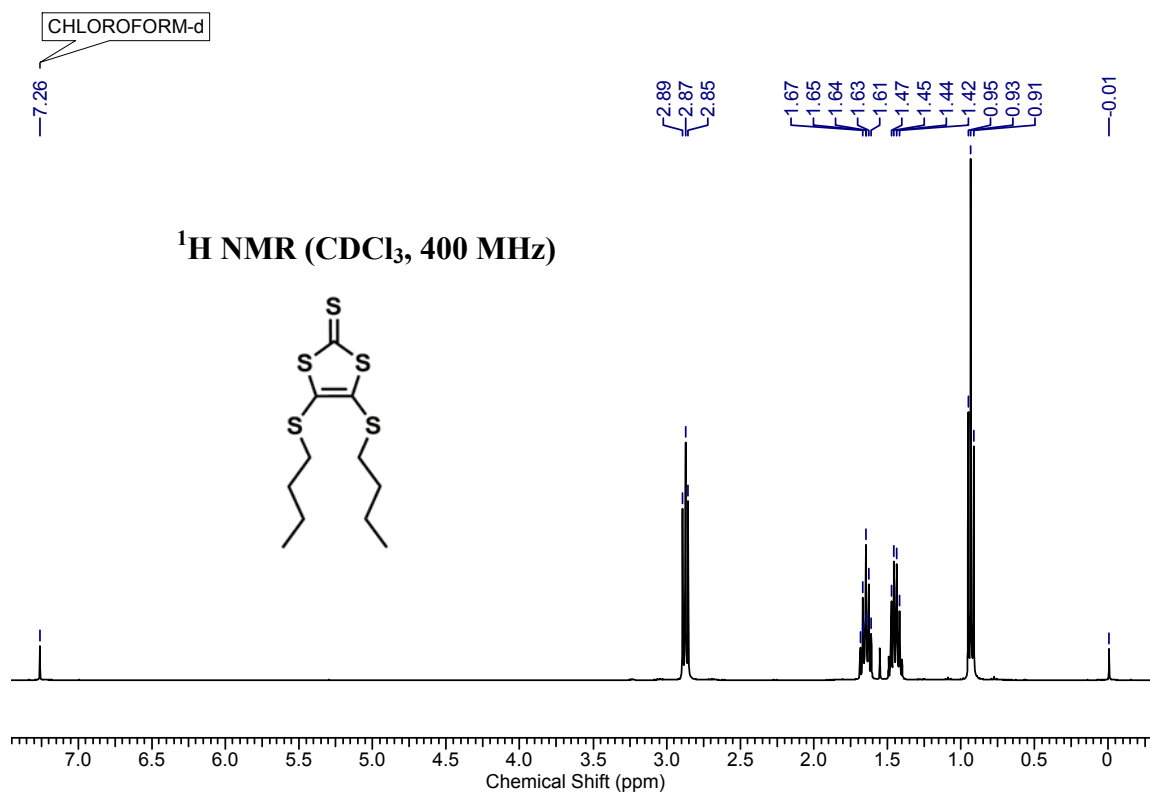
4,5-bis(dodecylthio)-1,3-dithiole-2-thione (1d)

The compound **1d** was obtained following the same procedure employed for **1a** using TEA$_2$[Zn(DMIT)$_2$] (500 mg, 0.70 mmol) and dodecyl bromide (835 µL, 3.48 mmol). Column chromatography (eluent: petroleum ether, R$_f$ = 0.65) furnished compound **1d** as yellow solid (698 mg, 94%); mp: 52-53 °C; IR (CHCl$_3$) ν (cm^{-1}): 2928, 2855, 1601, 1525, 1465, 1425, 1065, 929, 851; ^{1}H NMR (500 MHz, chloroform-*d*) δ = 2.87 (t, *J* = 7.4 Hz, 4H), 1.67 (quin, *J* = 7.4 Hz, 4H), 1.47 - 1.37 (m, 4H), 1.27 (br. s., 32H), 0.89 (t, *J* = 6.9 Hz, 6H); ^{13}C NMR (125 MHz, chloroform-*d*) δ = 211.5, 136.3, 36.8, 31.9, 29.6, 29.6, 29.5, 29.5, 29.3, 29.1, 28.5, 22.7, 14.1; MALDI-TOF/TOF: 535.23 (M+H)$^+$

^{1}H NMR (CDCl$_3$, 500 MHz)

DEPT-135 (CDCl₃, 125 MHz)

36.76 31.90 29.65 29.62 29.55 29.46 29.33 29.05 28.49 22.67   14.10

Chemical Shift (ppm)

211.49   136.35   CHLOROFORM-d   77.25 77.00 76.74   36.76 31.89 29.61 29.54 29.32 29.06 28.49 22.67 14.10
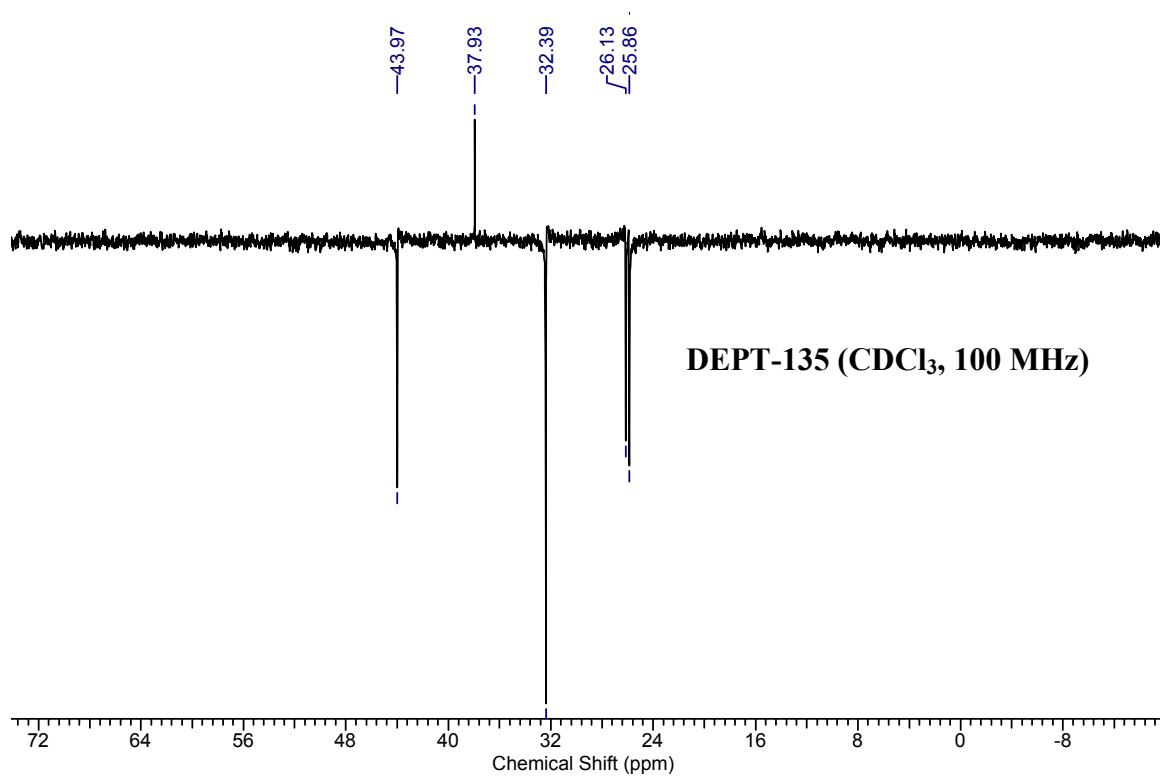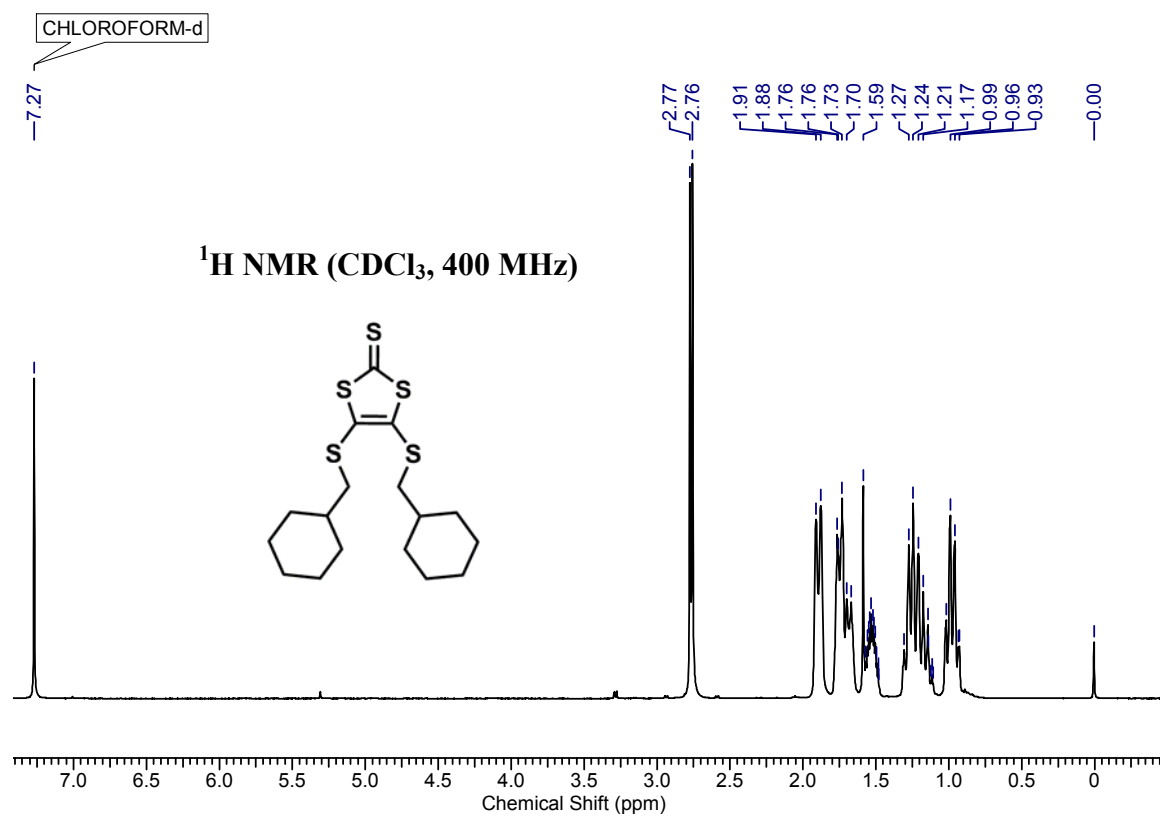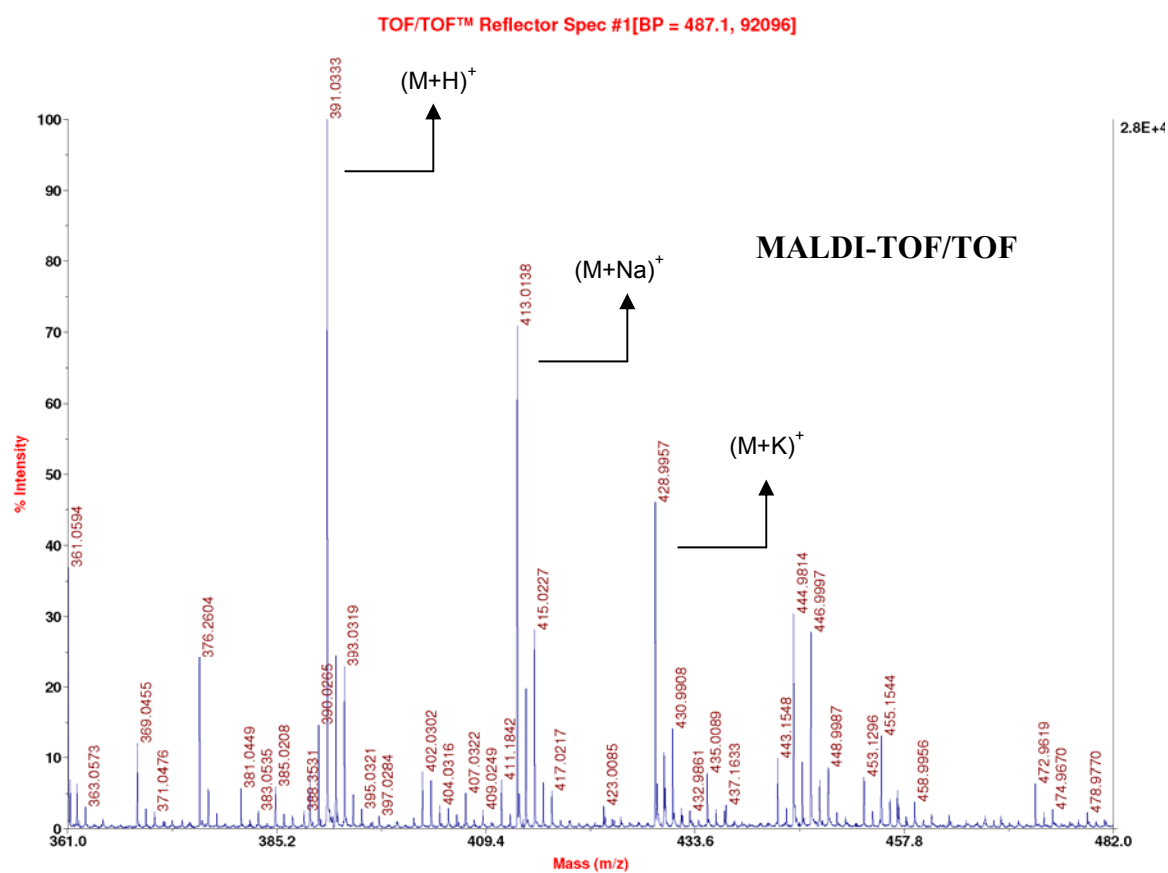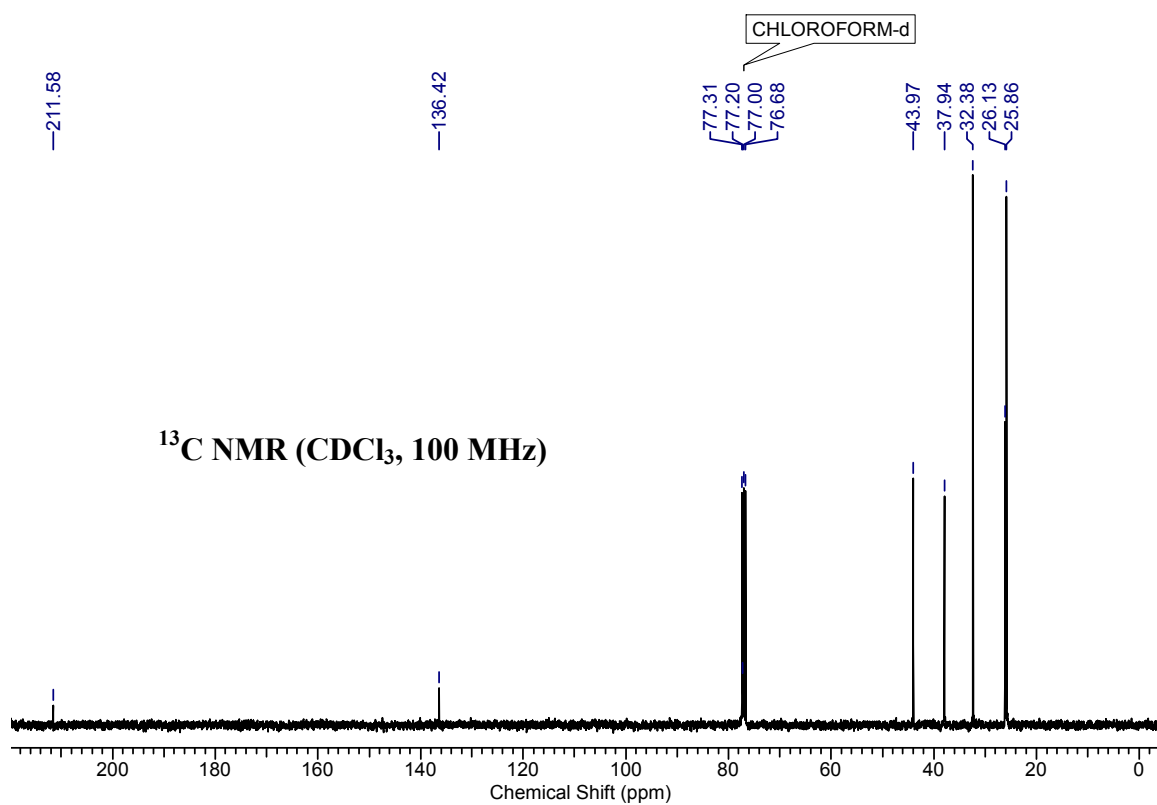
¹³C NMR (CDCl₃, 125 MHz)

Chemical Shift (ppm)

4,5-bis((cyclohexylmethyl)thio)-1,3-dithiole-2-thione (1e)

The compound **1e** was obtained following the same procedure employed for **1a** using TEA$_2$[Zn(DMIT)$_2$] (200 mg, 0.28 mmol) and cyclohexylmethyl bromide (296 mg, 1.67 mmol). Purification was carried out using column chromatography (eluent: petroleum ether, R$_f$ = 0.2) to furnish **1e** as brown oil (195 mg, 90%); IR (CHCl$_3$) ν (cm^{-1}): 2923, 2850, 1630, 1307, 1067, 1032, 961, 890; ^{1}H NMR (400MHz, chloroform -*d*) δ = 2.76 (d, *J* = 6.7 Hz, 4H), 1.89 (d, *J* = 12.2 Hz, 4H), 1.80 - 1.71 (m, 4H), 1.67 (br. s., 2H), 1.57 - 1.46 (m, 2H), 1.33 - 1.09 (m, 6H), 1.05 - 0.91 (m, 4H); ^{13}C NMR (100 MHz, chloroform-*d*) δ = 211.6, 136.4, 44.0, 37.9, 32.4, 26.1, 25.9; MALDI-TOF/TOF: 391.03 (M+H)$^+$, 413.01 (M+Na)$^+$, 428.99 (M+K)$^+$.
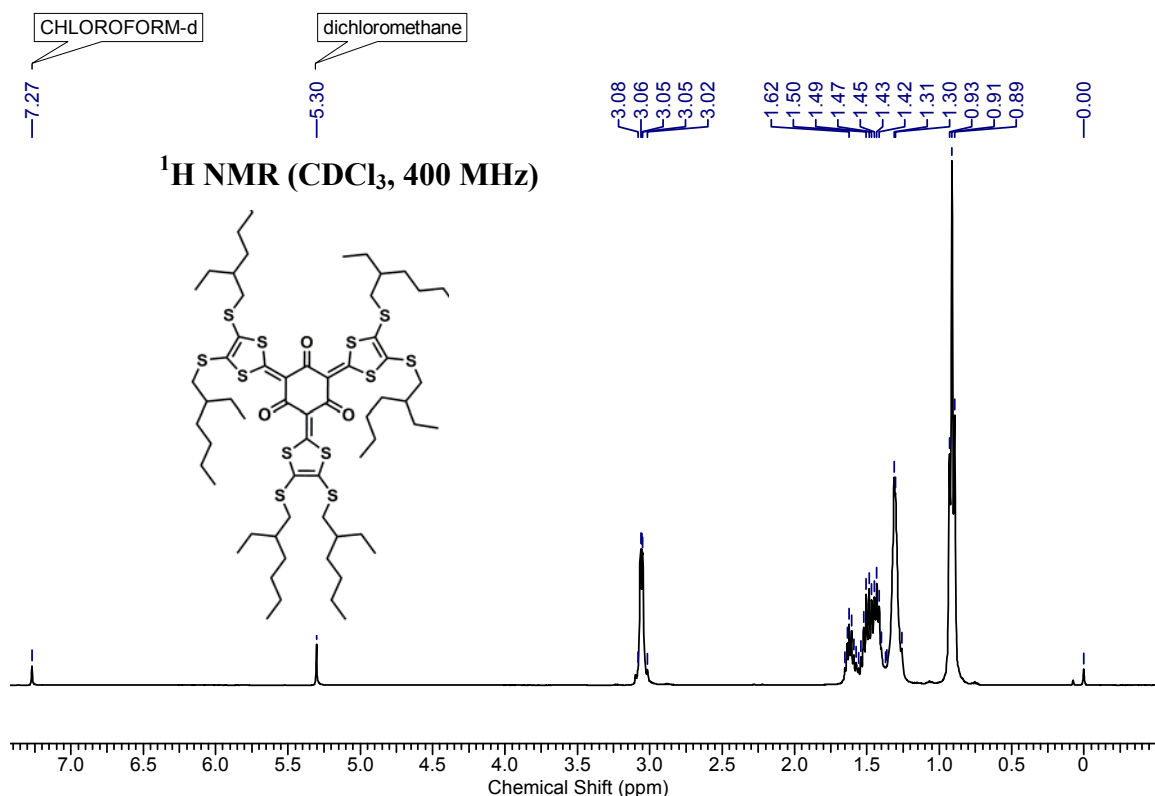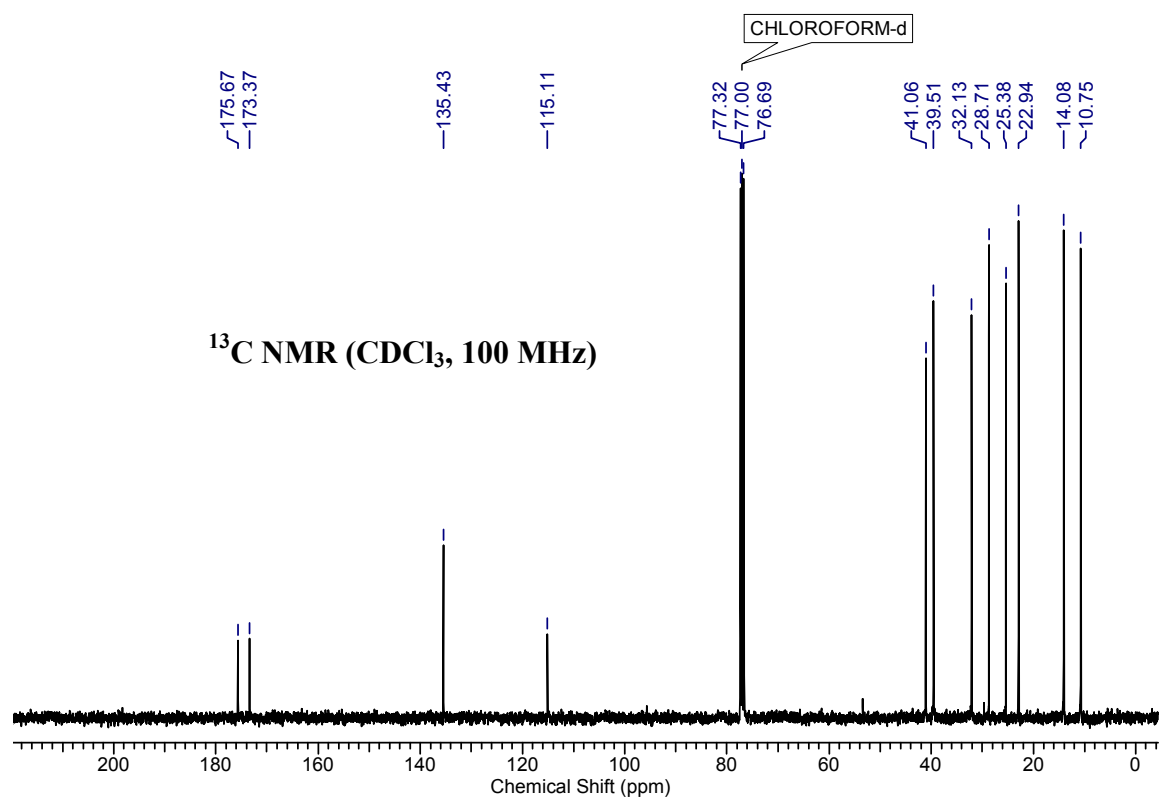
CHLOROFORM-d

7.27

2.77
2.76

1.91
1.88
1.76
1.76
1.73
1.70
1.59
1.27
1.24
1.21
1.17
0.99
0.96
0.93

0.00

¹H NMR (CDCl₃, 400 MHz)

7.0 6.5 6.0 5.5 5.0 4.5 4.0 3.5 3.0 2.5 2.0 1.5 1.0 0.5 0

Chemical Shift (ppm)

43.97

37.93

32.39

26.13
25.86

DEPT-135 (CDCl₃, 100 MHz)

72 64 56 48 40 32 24 16 8 0 -8

Chemical Shift (ppm)

CHLOROFORM-d

—211.58

—136.42

77.31
77.20
77.00
76.68

—43.97
—37.94
32.38
26.13
25.86

¹³C NMR (CDCl₃, 100 MHz)

200   180   160   140   120   100   80   60   40   20   0
Chemical Shift (ppm)

TOF/TOF™ Reflector Spec #1[BP = 487.1, 92096]

2.8E+4

$(M+H)^+$

$(M+Na)^+$

$(M+K)^+$

MALDI-TOF/TOF

% Intensity

391.0333
413.0138
428.9957
361.0594
376.2604
393.0319
390.0265
415.0227
444.9814
446.9997
369.0455
381.0449
402.0302
411.1842
430.9908
443.1548
453.1296
455.1544
363.0573
371.0476
383.0535
385.0208
388.3531
395.0321
397.0284
404.0316
407.0322
409.0249
417.0217
423.0085
432.9861
435.0089
437.1633
448.9987
458.9956
472.9619
474.9670
478.9770

361.0   385.2   409.4   433.6   457.8   482.0
Mass (m/z)

Synthesis of compounds 2,4,6-tris(4,5-bis(alkylthio)-1,3-dithiol-2-ylidene)cyclohexane-1,3,5-triones (2a-e)
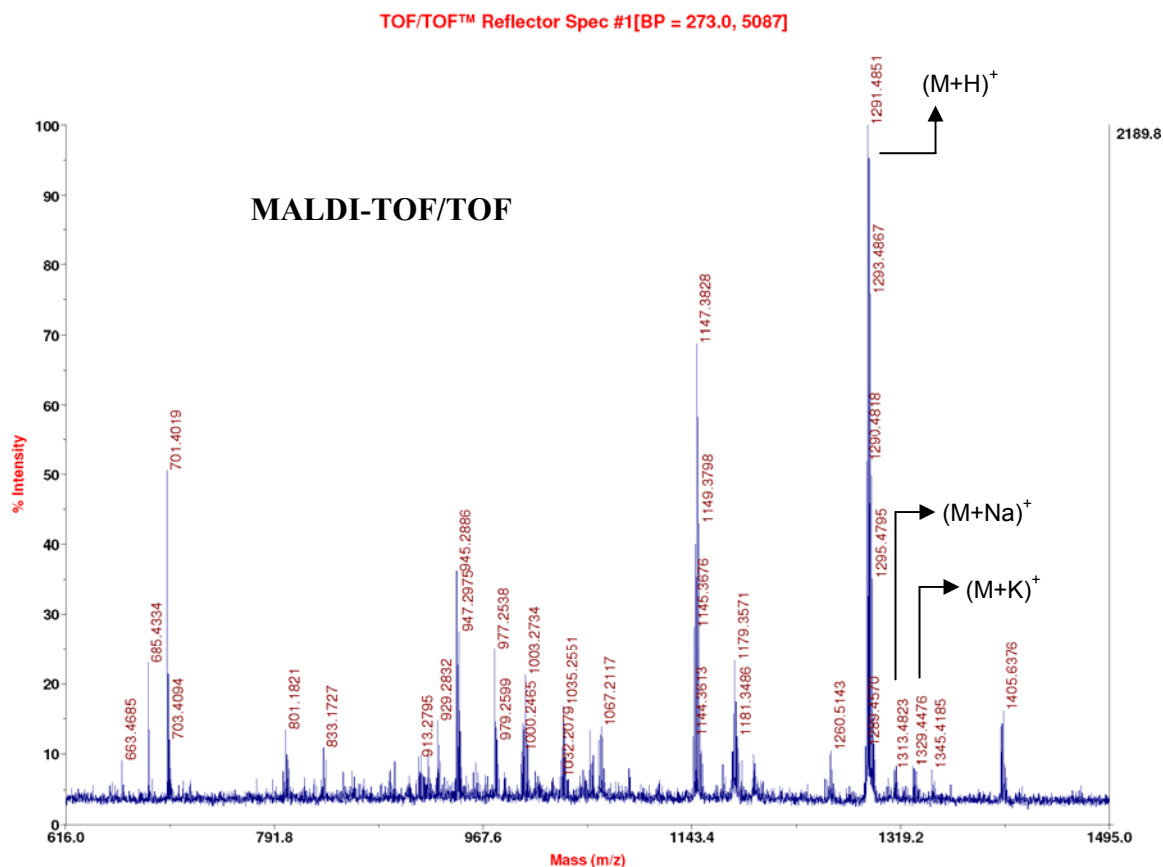
Representative procedure for **2,4,6-tris(4,5-bis((2-ethylhexyl)thio)-1,3-dithiol-2-ylidene)cyclohexane-1,3,5-trione (2a)**
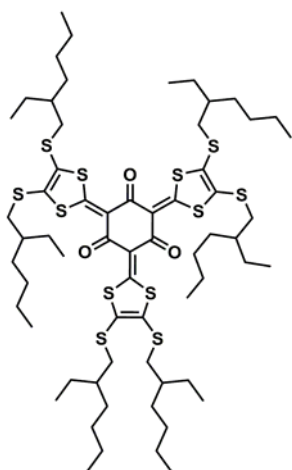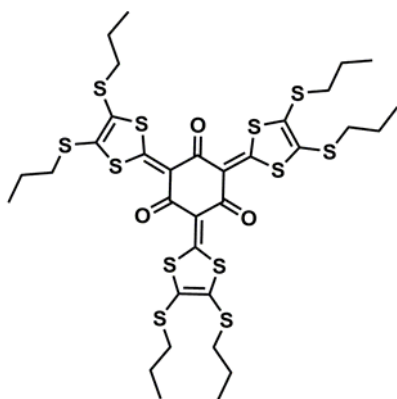

To the stirred solution of phloroglucinol (15.66 mg, 0.12 mmol) and **1a** (236.25 mg, 0.56 mmol) in anhydrous acetonitrile, triethylamine (104 μL, 0.75 mmol) was added dropwise followed by silver nitrate (47.08 mg, 0.27 mmol). The reaction mixture was heated to 75 °C for 12 h. The reaction mixture, after being cooled to room temperature, was filtered using celite®. The filtrate was concentrated *in vacuo* and purified by column chromatography (eluent: 50% dichloromethane: petroleum ether, R_f = 0.5) to furnish **2a** as dark orange oil (79 mg, 51%); IR (CHCl₃) v (cm⁻¹): 2958, 2925, 2857, 1537, 1462, 1411, 1030, 809; ¹H NMR (400 MHz, chloroform-*d*) δ = 3.12 - 3.00 (m, 12H), 1.68 - 1.55 (m, 6H), 1.55 - 1.38 (m, 24H), 1.37 - 1.21 (m, 24H), 0.91 (t, *J* = 7.3 Hz, 36H); ¹³C NMR (100 MHz, chloroform -*d*) δ = 175.7, 173.4, 135.4, 115.1, 41.1, 39.5, 32.1, 28.7, 25.4, 22.9, 14.1, 10.7; MALDI-TOF/TOF: 1291.48 (M+H)⁺, 1313.48 (M+Na)⁺, 1329.45 (M+K)⁺.
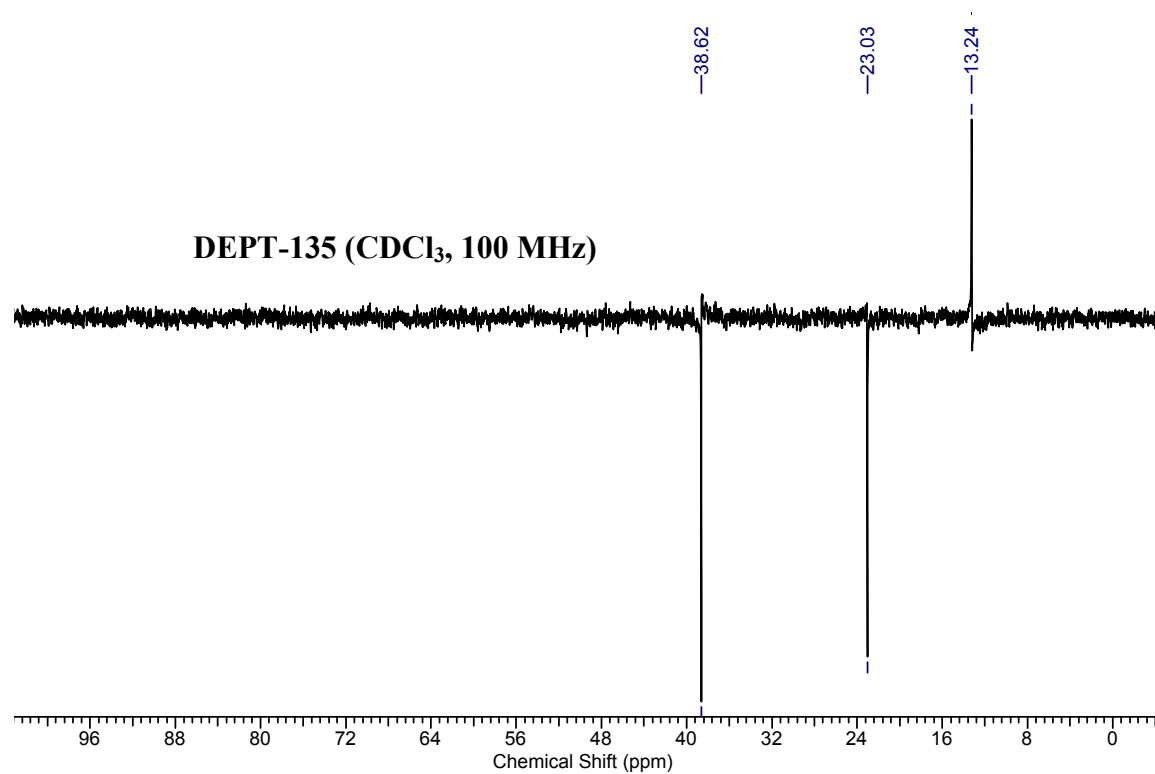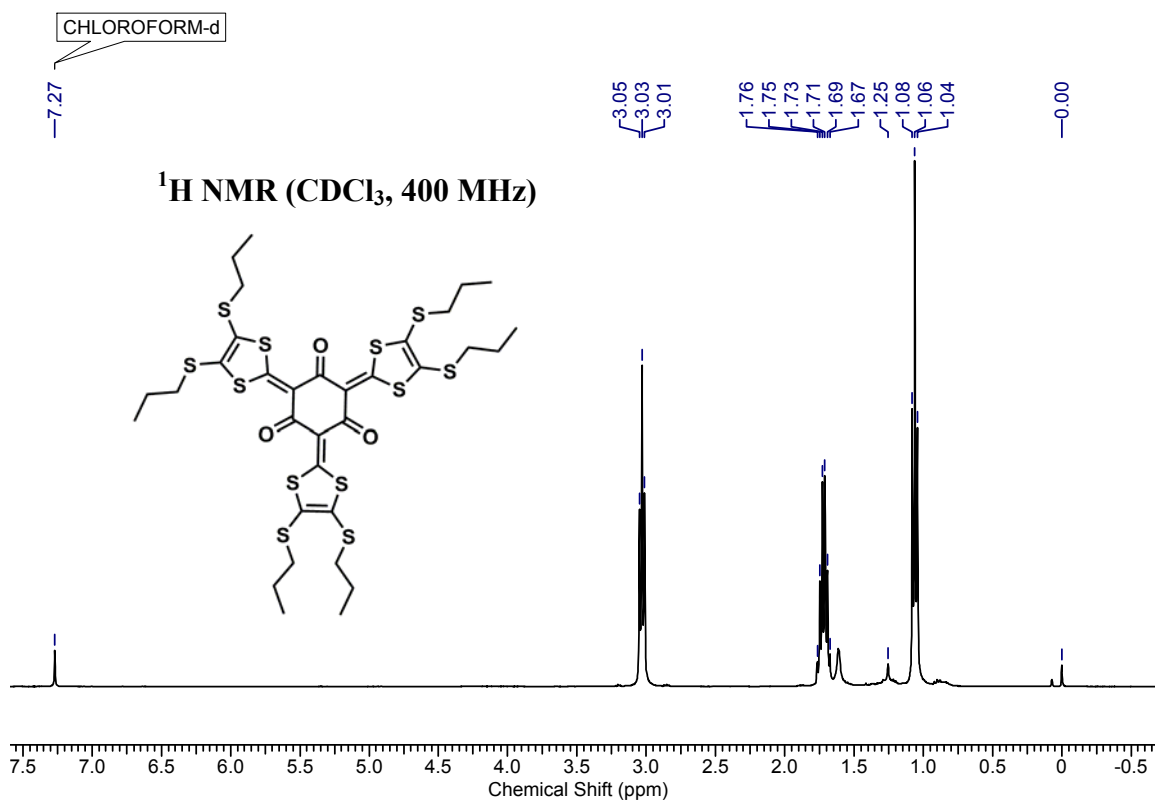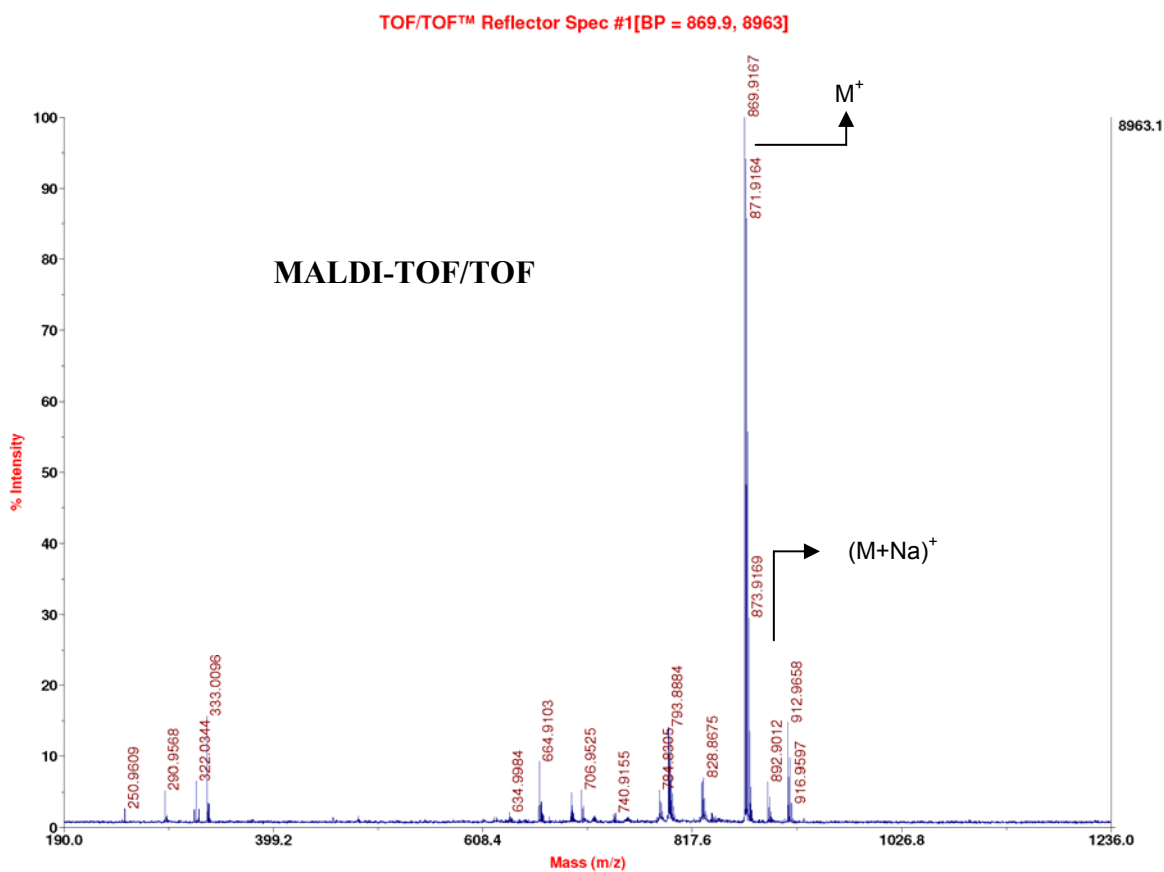
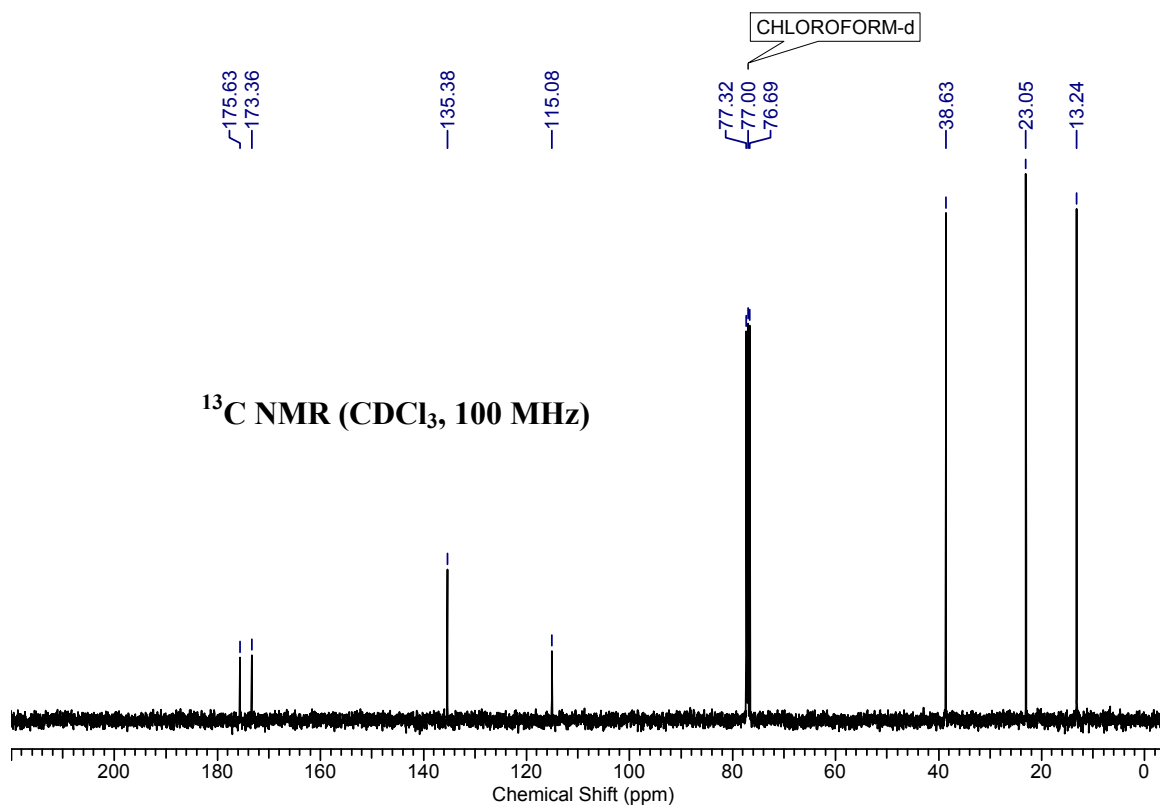**DEPT-135 (CDCl₃, 100 MHz)**

41.07
39.52
32.13
28.72
25.38
22.94
14.08
10.75

96   88   80   72   64   56   48   40   32   24   16   8   0   -8
Chemical Shift (ppm)

CHLOROFORM-d

175.67
173.37
135.43
115.11
77.32
77.00
76.69
41.06
39.51
32.13
28.71
25.38
22.94
14.08
10.75

¹³C NMR (CDCl₃, 100 MHz)

200   180   160   140   120   100   80   60   40   20   0
Chemical Shift (ppm)

TOF/TOF™ Reflector Spec #1[BP = 273.0, 5087]

MALDI-TOF/TOF
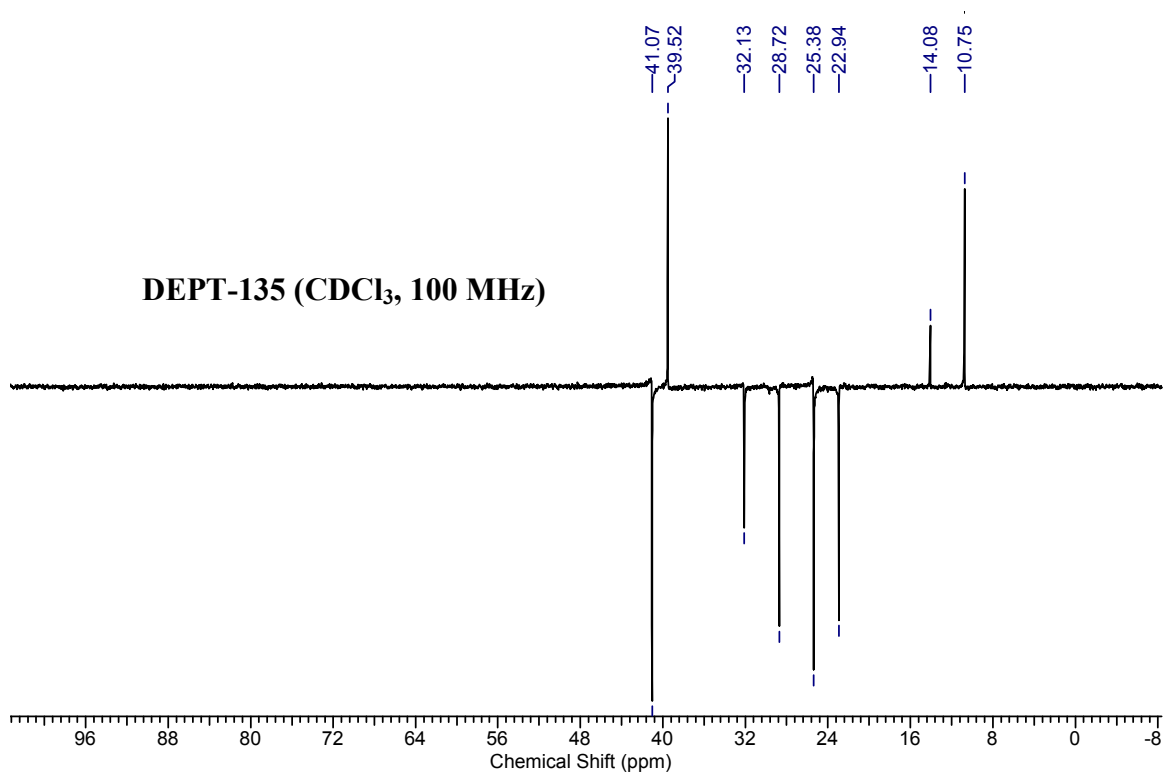
2,4,6-tris(4,5-bis(propylthio)-1,3-dithiol-2-ylidene)cyclohexane-1,3,5-trione (2b)
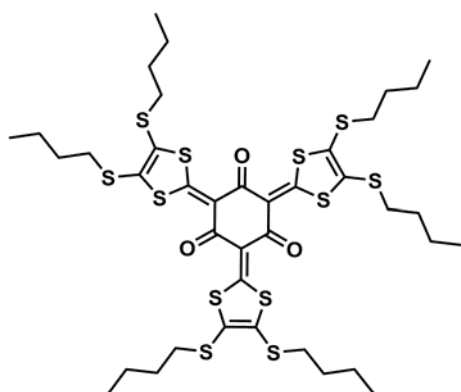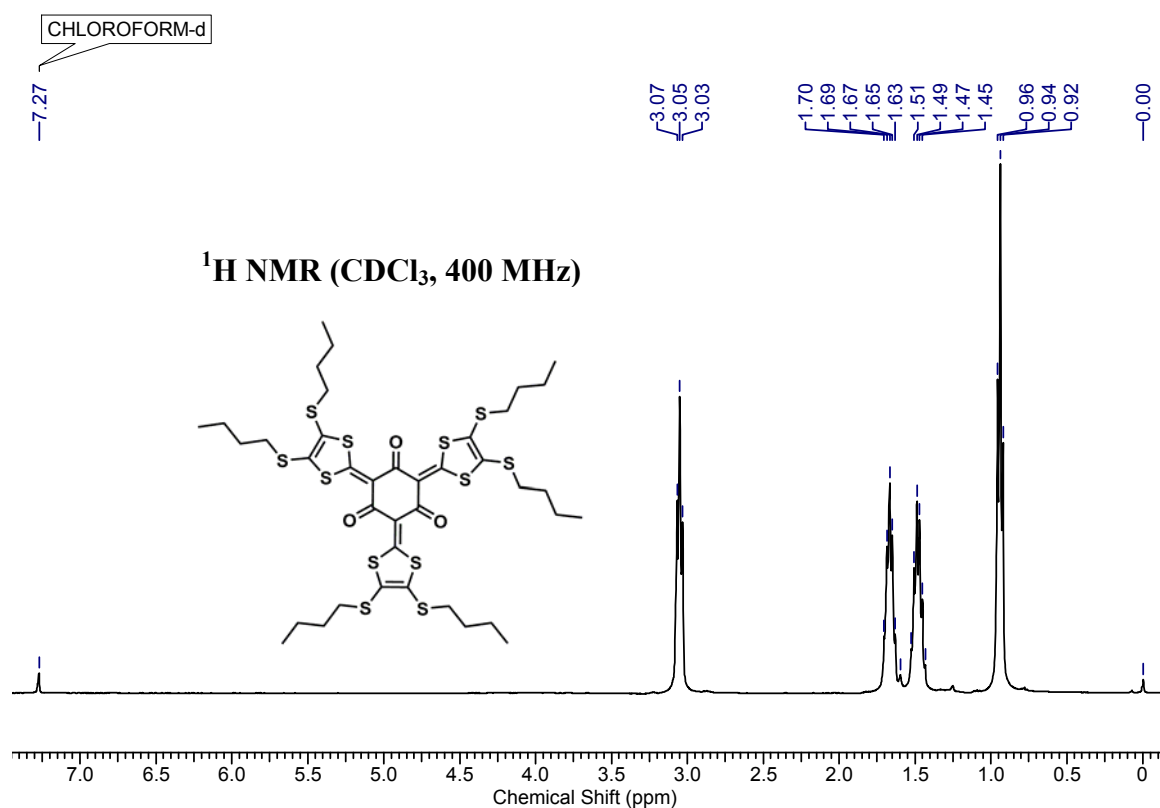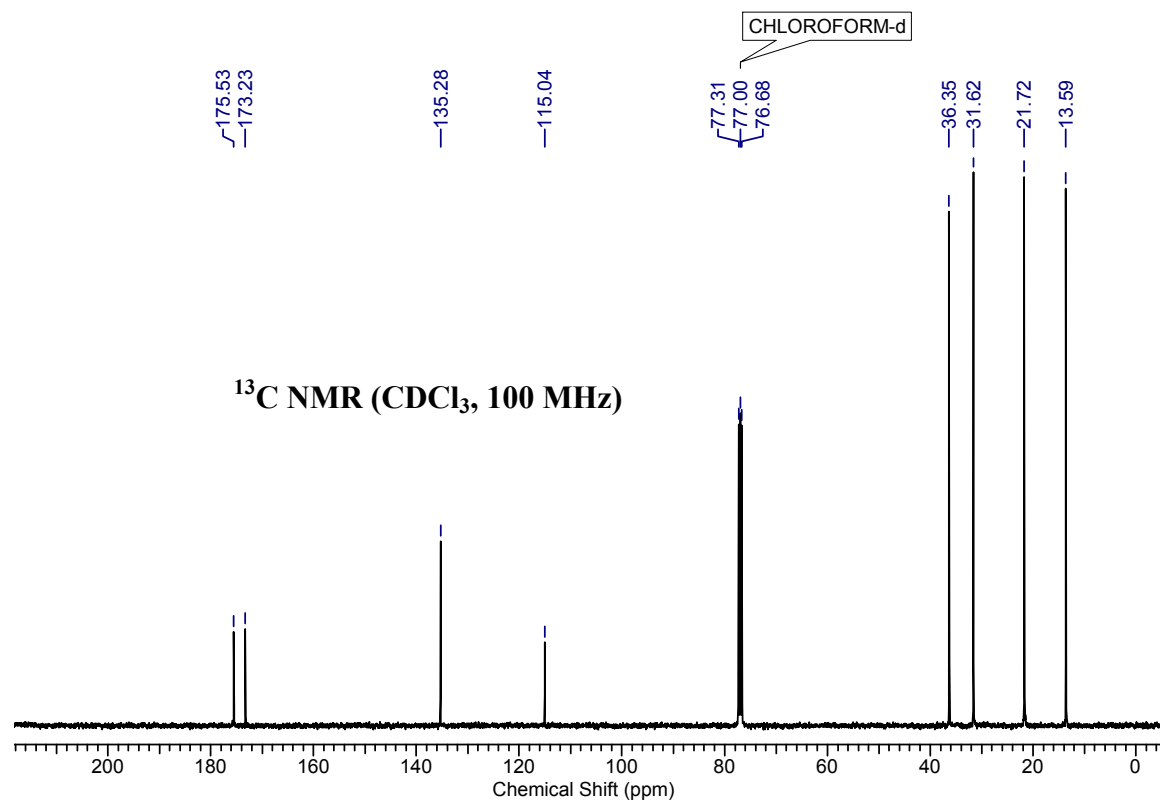

The compound **2b** was obtained following the same procedure employed for **2a** using phloroglucinol (7.8 mg, 0.06 mmol), **1b** (78.3 mg, 0.27 mmol), triethylamine (51.54 μL, 0.37 mmol) and silver nitrate (47.08 mg, 0.27 mmol). Purification was carried out using column chromatography (eluent: 30-40% dichloromethane: petroleum ether, R_f = 0.3) to furnish **2b** as orange solid (15 mg, 28%); mp: 224-225 °C; IR (CHCl₃) v (cm⁻¹):

1531, 1404, 1034, 928; ¹H NMR (400 MHz, chloroform -*d*) δ = 3.03 (t, *J* = 7.3 Hz, 12H), 1.72 (sxt, *J* = 7.3 Hz, 12H), 1.06 (t, *J* = 7.3 Hz, 18H); ¹³C NMR (100 MHz, chloroform -*d*) δ = 175.6, 173.4, 135.4, 115.1, 38.6, 23.0, 12.2; MALDI-TOF/TOF: 869.92 (M)⁺, 892.90 (M+Na)⁺.

¹H NMR (CDCl₃, 400 MHz)

DEPT-135 (CDCl₃, 100 MHz)

CHLOROFORM-d

175.63
173.36
135.38
115.08
77.32
77.00
76.69
38.63
23.05
13.24

¹³C NMR (CDCl₃, 100 MHz)

200   180   160   140   120   100   80   60   40   20   0
Chemical Shift (ppm)

TOF/TOF™ Reflector Spec #1[BP = 869.9, 8963]

869.9167   M⁺
871.9164
873.9169   (M+Na)⁺

MALDI-TOF/TOF

8963.1

250.9609   290.9568   322.0344   333.0096   634.9984   664.9103   706.9525   740.9155   794.8905   793.8884   828.8675   892.9012   912.9658   916.9597

% Intensity

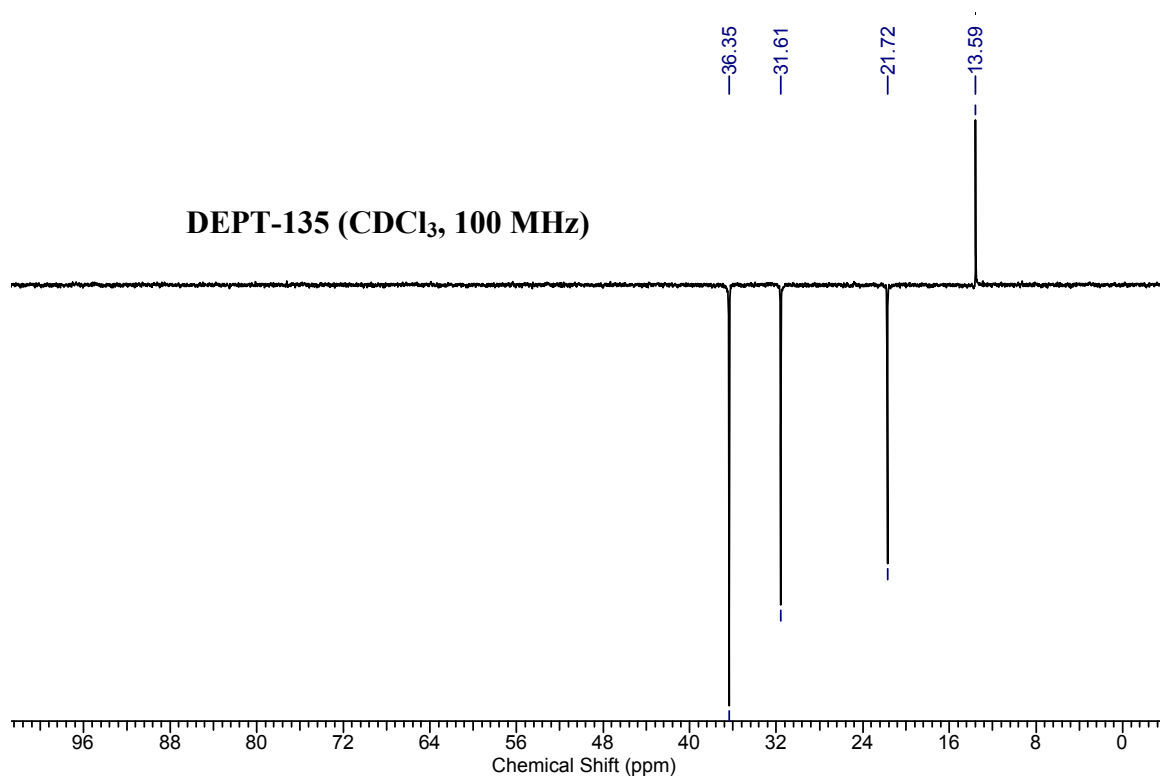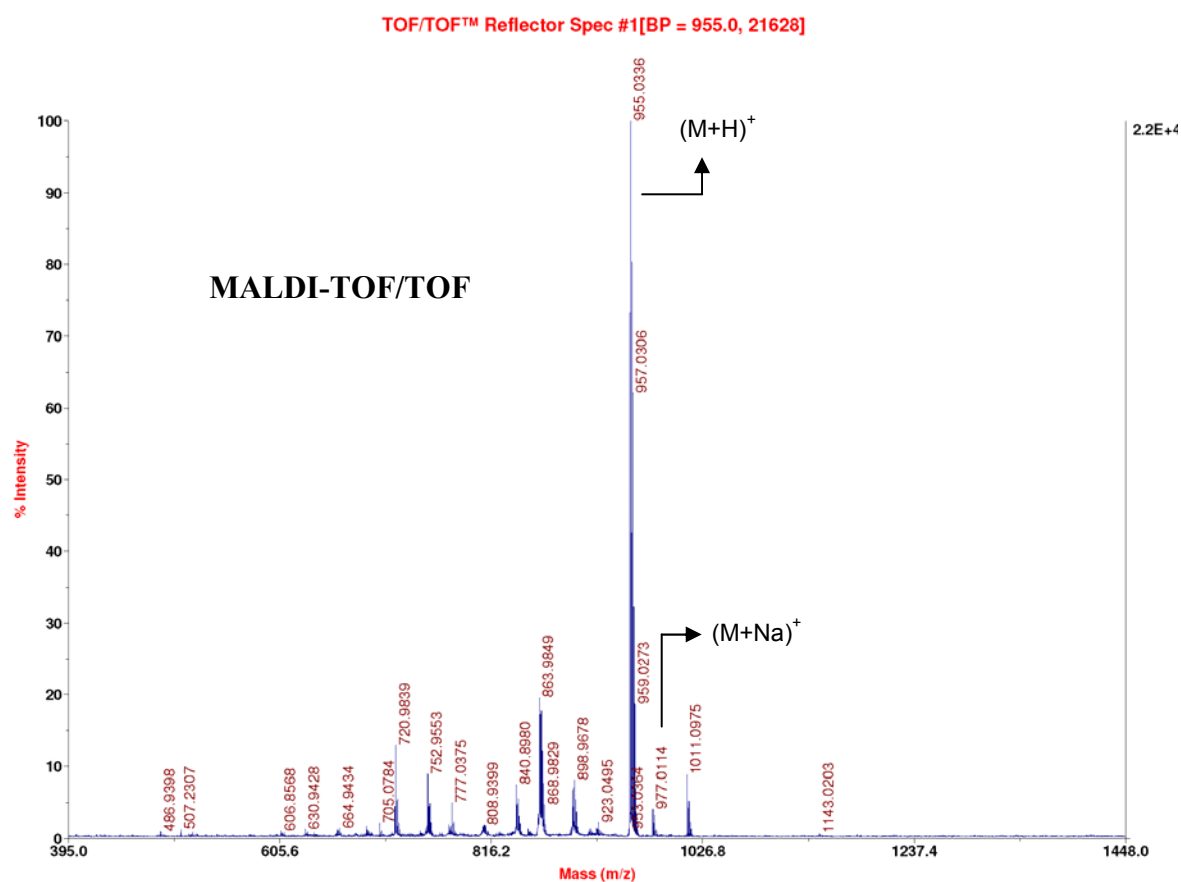190.0   399.2   608.4   817.6   1026.8   1236.0
Mass (m/z)

2,4,6-tris(4,5-bis(butylthio)-1,3-dithiol-2-ylidene)cyclohexane-1,3,5-trione (2c)

The compound **2c** was obtained following the same procedure employed for **2a** using phloroglucinol (7.61 mg, 0.06 mmol), **1c** (84.37 mg, 0.27 mmol), triethylamine (50.52 µL, 0.36 mmol) and silver nitrate (46.14 mg, 0.27 mmol). Purification was carried out using column chromatography (30-40% dichloromethane: petroleum ether, R_f = 0.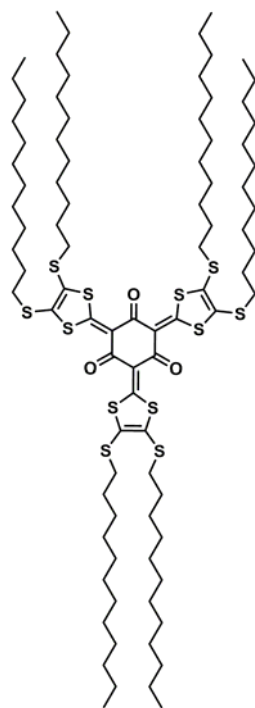3) to furnish **2c** as orange solid (34.3 mg, 60%); mp: 145 °C; IR (CHCl₃) v (cm^{-1}): 1532, 1405, 1037; ^{1}H NMR (400MHz, chloroform -*d*) δ = 3.05 (t, *J* = 7.3 Hz, 12H), 1.67 (quin, *J* = 7.3 Hz, 12H), 1.48 (sxt, *J* = 7.3 Hz, 12H), 0.94 (t, *J* = 7.3 Hz, 18H); ^{13}C NMR (100 MHz, chloroform-*d*) δ = 175.5, 173.2, 135.3, 115.0, 36.4, 31.6, 21.7, 13.6; MALDI-TOF/TOF: 955.03 (M+H)$^+$, 977.01 (M+Na)$^+$.

^{1}**H NMR (CDCl₃, 400 MHz)**
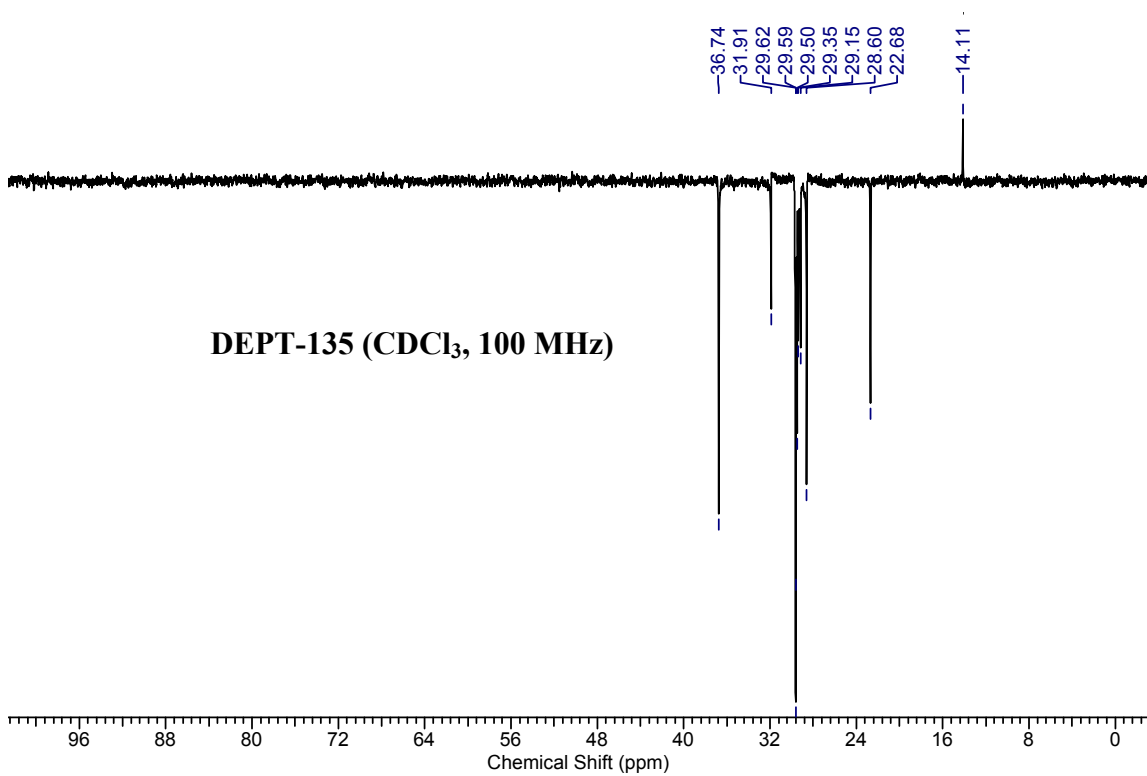
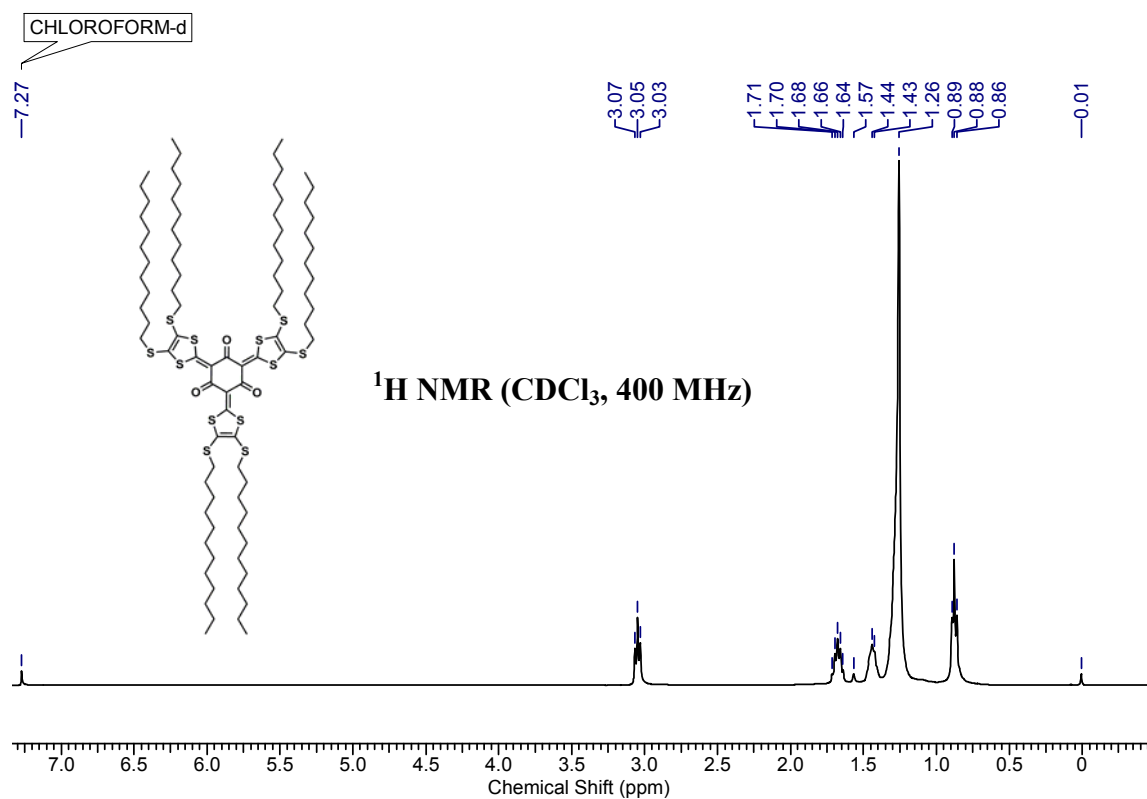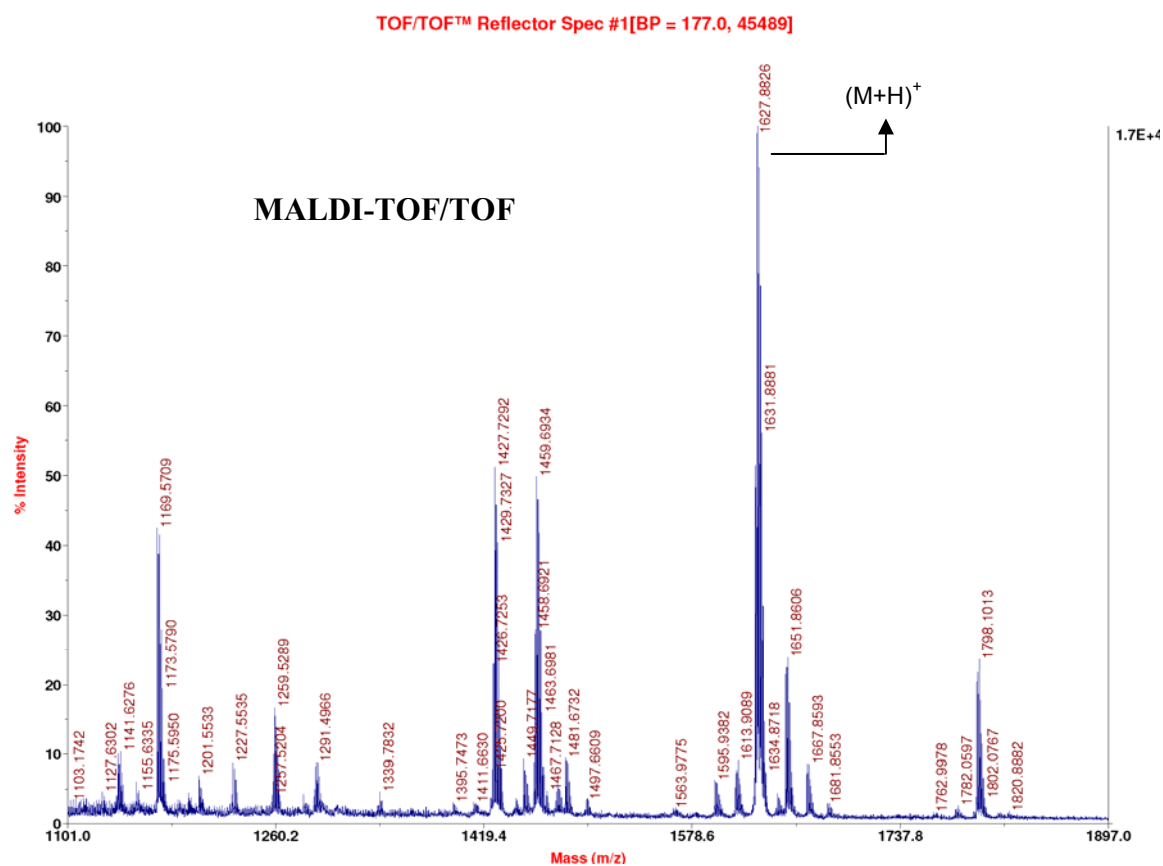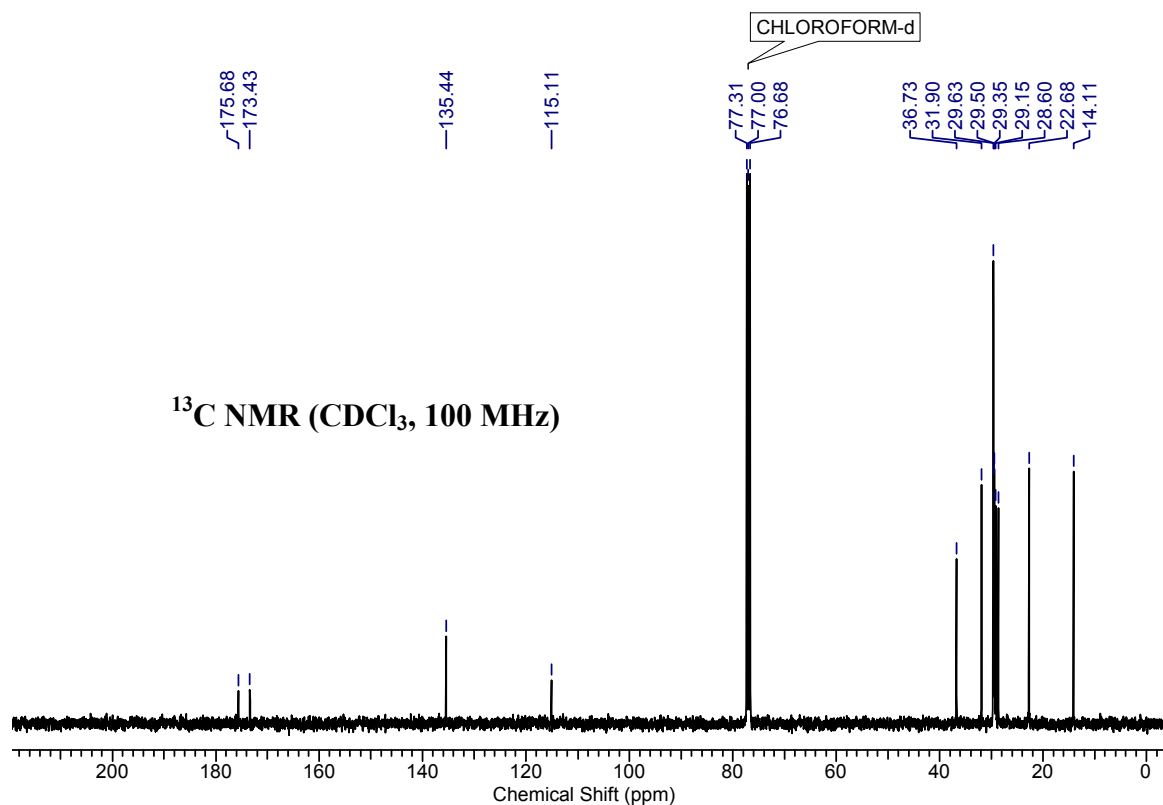**DEPT-135 (CDCl₃, 100 MHz)**

¹³C NMR (CDCl₃, 100 MHz)

2,4,6-tris(4,5-bis(dodecylthio)-1,3-dithiol-2-ylidene)cyclohexane-1,3,5-trione (2d)
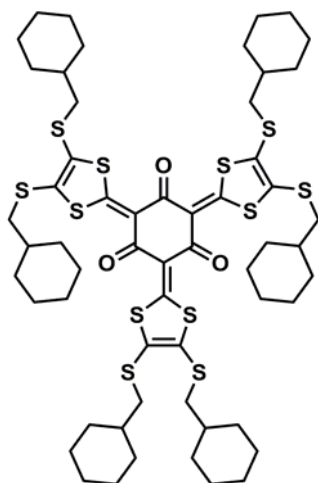

The compound **2d** was obtained following the same procedure employed for **2a** using phloroglucinol (2.98 mg, 0.02 mmol), **1d** (56.98 mg, 0.11 mmol), triethylamine (19.80 µL, 0.14 mmol) and silver nitrate (18.06 mg, 0.11 mmol). Purification was carried out using column chromatography (20% dichloromethane: petroleum ether, R_f = 0.3) to furnish **2d** as orange solid (34 mg, 88%); mp: 65 °C; IR (CHCl$_3$) v (cm^{-1}): 2928, 2855, 1530, 1475, 1405, 1023, 929, 850; ^{1}H NMR (400MHz, chloroform-d) δ = 3.05 (t, J = 7.3 Hz, 12H), 1.68 (quin, J = 7.3 Hz, 12H), 1.43 (d, J = 6.4 Hz, 12H), 1.26 (br. s., 96H), 0.88 (t, J = 6.4 Hz, 18H); ^{13}C NMR (100MHz, chloroform -d) δ = 175.7, 173.4, 135.4, 115.1, 36.7, 31.9, 29.6, 29.5, 29.4, 29.2, 28.6, 22.7, 14.1; MALDI-TOF/TOF: 1627.88 (M+H)$^+$.

CHLOROFORM-d

7.27

3.07
3.05
3.03

1.71
1.70
1.68
1.66
1.64
1.57
1.44
1.43
1.26
0.89
0.88
0.86

-0.01

¹H NMR (CDCl₃, 400 MHz)

7.0 6.5 6.0 5.5 5.0 4.5 4.0 3.5 3.0 2.5 2.0 1.5 1.0 0.5 0
Chemical Shift (ppm)

36.74
31.91
29.62
29.59
29.50
29.35
29.15
28.60
22.68

14.11

DEPT-135 (CDCl₃, 100 MHz)

96 88 80 72 64 56 48 40 32 24 16 8 0
Chemical Shift (ppm)

^{13}**C NMR (CDCl₃, 100 MHz)**

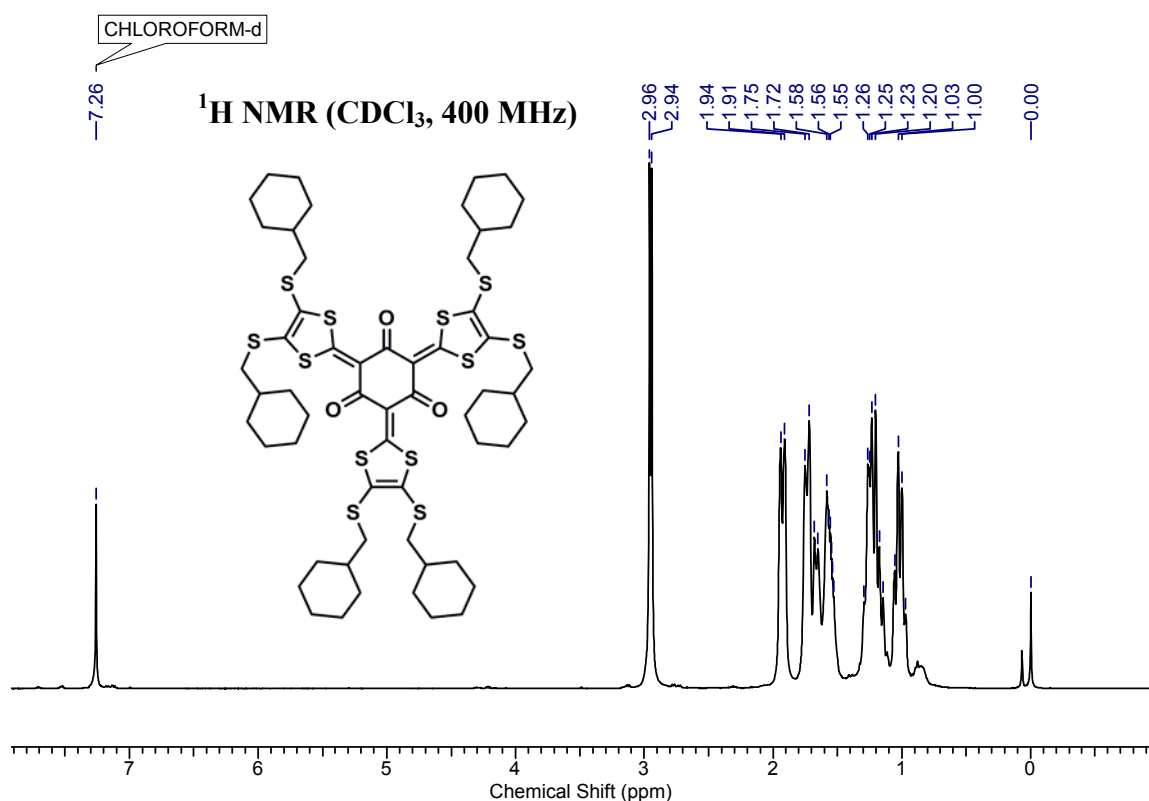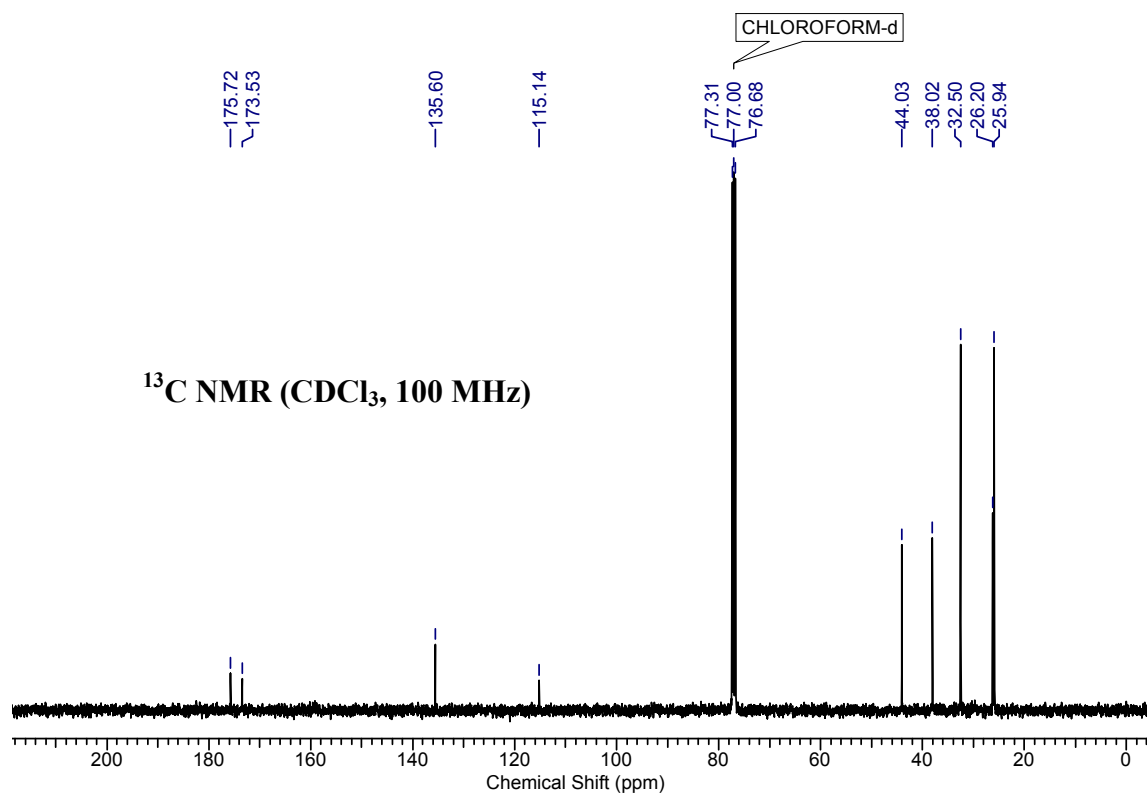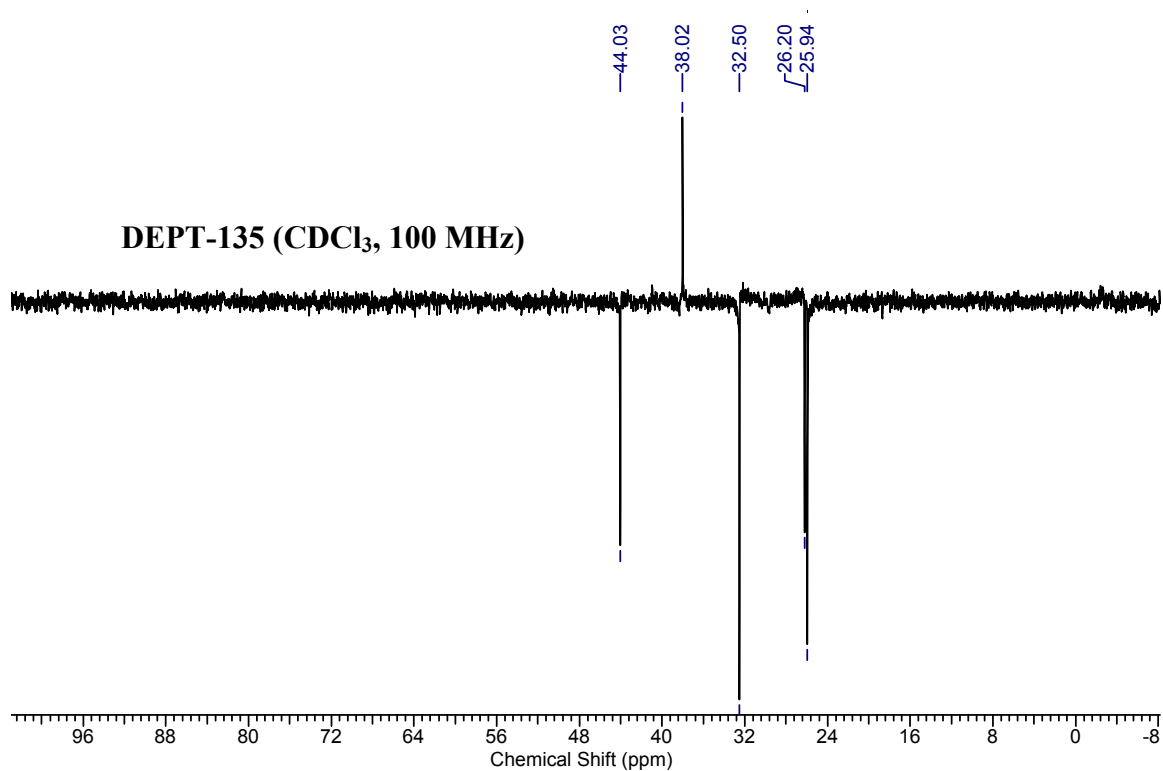TOF/TOF™ Reflector Spec #1[BP = 177.0, 45489]

MALDI-TOF/TOF

$(M+H)^+$

2,4,6-tris(4,5-bis((cyclohexylmethyl)thio)-1,3-dithiol-2-ylidene)cyclohexane-1,3,5-trione (2e)

The compound **2e** was obtained following the same procedure employed for **2a** using phloroglucinol (20.95 mg, 0.17 mmol), **1e** (146 mg, 0.75 mmol), triethylamine (139 μL, 1.00 mmol) and silver nitrate (126.99 mg, 0.75 mmol). Purification was carried out using column chromatography (2.5% ethyl acetate: petroleum ether, R_f = 0.4) to furnish **2e** as orange solid (12 mg, 6%); mp: 243-245 °C; IR (CHCl₃) v (cm⁻¹): 1533, 1404, 1035; ¹H NMR (400 MHz, chloroform-*d*) δ = 1.92 (d, *J* = 11.6 Hz, 12H), 1.82 - 1.48 (m, 36H), 1.35 - 1.10 (m, 18H), 1.09 - 0.94 (m, 12H); ¹³C NMR (100 MHz, chloroform-*d*) δ = 175.7, 173.5, 135.6, 115.1, 44.0, 38.0, 32.5, 26.2, 25.9; HRMS: $C_{57}H_{79}O_3S_{12}$ (M+H)⁺ calcd: 1195.2672, found: 1195.2706.

DEPT-135 (CDCl₃, 100 MHz)

44.03
38.02
32.50
26.20
25.94

Chemical Shift (ppm)

CHLOROFORM-d

175.72
173.53
135.60
115.14
77.31
77.00
76.68
44.03
38.02
32.50
26.20
25.94

¹³C NMR (CDCl₃, 100 MHz)

Chemical Shift (ppm)

CYCLO-HEX-HET-FINAL #189 RT: 0.84 AV: 1 NL: 7.26E4
T: FTMS + p ESI Full ms [100.00-1500.00]

1195.2706
R=20300
$C_{57} H_{79} O_3 S_{12}$ = 1195.2672
2.8518 ppm

$(M+H)^+$

HRMS-ESI
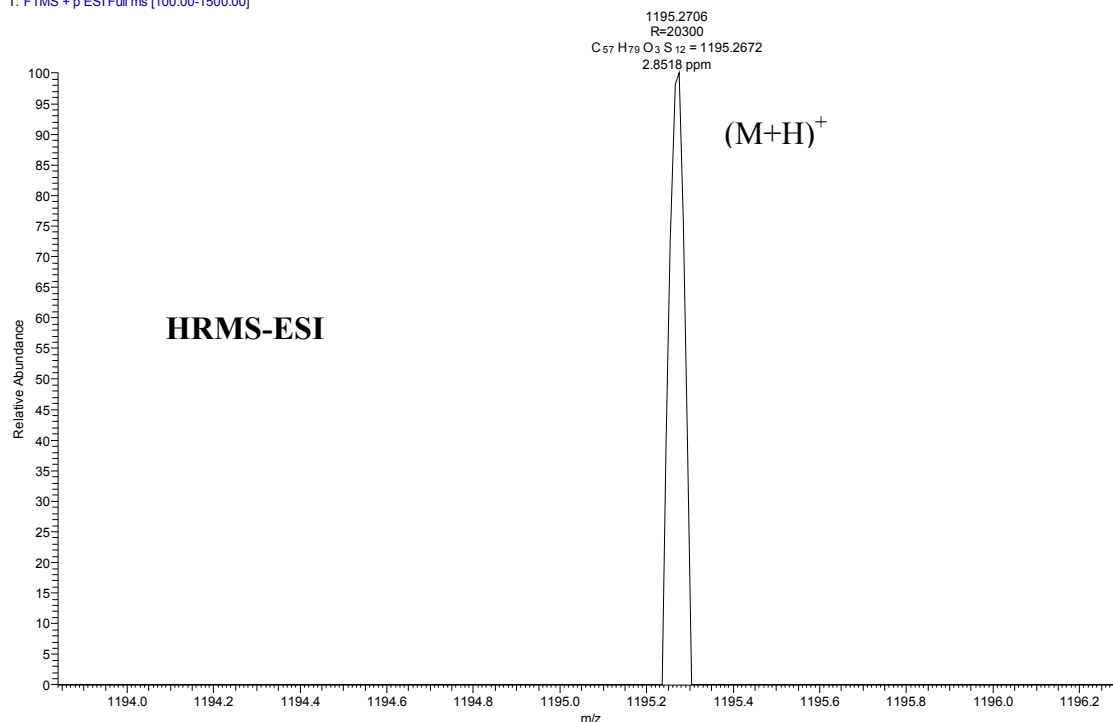
4.6 References

(1) a) Hasegawa, M.; Iyoda, M. *Chem. Soc. Rev.* **2010**, *39*, 2420; b) Hoeben, F. J.; Jonkheijm, P.; Meijer, E.; Schenning, A. P. *Chem. Rev.* **2005**, *105*, 1491; c) Batail, P. *Chem. Rev.* **2004**, *104*, 4887; d) Li, Y.; Liu, T.; Liu, H.; Tian, M.-Z.; Li, Y. *Acc. Chem. Res.* **2014**, *47*, 1186.

(2) a) Gomar-Nadal, E.; Puigmartí-Luis, J.; Amabilino, D. B. *Chem. Soc. Rev.* **2008**, *37*, 490; b) Li, C.; Bai, H.; Shi, G. *Chem. Soc. Rev.* **2009**, *38*, 2397; c) Nayak, S.; Lyon, L. A. *Angew. Chem. Int. Ed.* **2005**, *44*, 7686.

(3) a) Lehn, J.-M. *Science* **2002**, *295*, 2400; b) Whitesides, G. M.; Grzybowski, B. *Science* **2002**, *295*, 2418; c) Desiraju, G. R. *Angew. Chem. Int. Ed.* **1995**, *34*, 2311.

(4) Inokuchi, H.; Saito, G.; Wu, P.; Seki, K.; Tang, T. B.; Mori, T.; Imaeda, K.; Enoki, T.; Higuchi, Y.; Inaka, K. *Chem. Lett.* **1986**, *15*, 1263.

(5) a) Hill, J. P.; Jin, W.; Kosaka, A.; Fukushima, T.; Ichihara, H.; Shimomura, T.; Ito, K.; Hashizume, T.; Ishii, N.; Aida, T. *Science* **2004**, *304*, 1481; b) Yamamoto, Y.; Fukushima, T.; Jin, W.; Kosaka, A.; Hara, T.; Nakamura, T.; Saeki, A.; Seki, S.; Tagawa, S.; Aida, T. *Adv. Mater.* **2006**, *18*, 1297; c) Yamamoto, Y.; Fukushima, T.; Suna, Y.; Ishii, N.; Saeki, A.; Seki, S.; Tagawa, S.; Taniguchi, M.; Kawai, T.; Aida, T. *Science* **2006**, *314*, 1761.

(6) a) Joergensen, M.; Bechgaard, K.; Bjoernholm, T.; Sommer-Larsen, P.; Hansen, L. G.; Schaumburg, K. *J.Org. Chem.* **1994**, *59*, 5877; b) Kitahara, T.; Shirakawa, M.; Kawano, S.-i.; Beginn, U.; Fujita, N.; Shinkai, S. *J. Am. Chem. Soc.* **2005**, *127*, 14980; c) Wang, C.; Zhang, D.; Zhu, D. *J. Am. Chem. Soc.* **2005**, *127*, 16372.

(7) a) Kawano, S. i.; Fujita, N.; Shinkai, S. *Chem. Eur. J.* **2005**, *11*, 4735; b) Messmore, B. W.; Hulvat, J. F.; Sone, E. D.; Stupp, S. I. *J. Am. Chem. Soc.* **2004**, *126*, 14452; c) Schoonbeek, F. S.; van Esch, J. H.; Wegewijs, B.; Rep, D. B.; de Haas, M. P.; Klapwijk, T. M.; Kellogg, R. M.; Feringa, B. L. *Angew. Chem. Int. Ed.* **1999**, *38*, 1393.

(8) Che, Y.; Datar, A.; Yang, X.; Naddo, T.; Zhao, J.; Zang, L. *J. Am. Chem. Soc.* **2007**, *129*, 6354.

(9) Honna, Y.; Isomura, E.; Enozawa, H.; Hasegawa, M.; Takase, M.; Nishinaga, T.; Iyoda, M. *Tetrahedron Lett.* **2010**, *51*, 679.

(10) a) Puigmartí-Luis, J.; Laukhin, V.; Pérez del Pino, Á.; Vidal-Gancedo, J.; Rovira, C.; Laukhina, E.; Amabilino, D. B. *Angew. Chem. Int. Ed.* **2007**, *46*, 238; b) Puigmartí-Luis, J.; Minoia, A.; Pérez del Pino, Á.; Ujaque, G.; Rovira, C.; Lledós, A.; Lazzaroni, R.; Amabilino, D. B. *Chem. Eur. J.* **2006**, *12*, 9161; c) Kitamura, T.; Nakaso, S.; Mizoshita, N.; Tochigi, Y.; Shimomura, T.; Moriyama, M.; Ito, K.; Kato, T. *J. Am. Chem. Soc.* **2005**, *127*, 14769.

(11) a) Enozawa, H.; Hasegawa, M.; Isomura, E.; Nishinaga, T.; Kato, T.; Yamato, M.; Kimura, T.; Iyoda, M. *ChemPhysChem* **2009**, *10*, 2607; b) Enozawa, H.; Hasegawa, M.; Takamatsu, D.; Fukui, K.-i.; Iyoda, M. *Org. Lett.* **2006**, *8*, 1917.

(12) Hasegawa, M.; Enozawa, H.; Kawabata, Y.; Iyoda, M. *J. Am. Chem. Soc.* **2007**, *129*, 3072.

(13) Coffin, M. A.; Bryce, M. R.; Clegg, W. *J. Chem. Soc., Chem. Commun.* **1992**, 401.

(14) Dhindsa, A. S.; Bryce, M. R.; Petty, M. C.; Kobayashi, K.; Tukada, H. *Synth. Met.* **1989**, *31*, 379.

(15) Svenstrup, N.; Becher, J. *Synthesis* **1995**, *1995*, 215.

(16) Park, S. S.; Hontz, E. R.; Sun, L.; Hendon, C. H.; Walsh, A.; Van Voorhis, T.; Dincă, M. *J. Am. Chem. Soc* **2015**, *137*, 1774.

(17) Enozawa, H.; Takahashi, T.; Nishinaga, T.; Kato, T.; Hasegawa, M.; Iyoda, M. *Bull. Chem. Soc. Jpn.* **2012**, *85*, 1120.